New Type of Emerald
from Afghanistan

Irradiation of
Pink-to-Red Tourmaline

Discovery of Alexandrite
and Phenakite

Formation of the
'Matryoshka' Diamond

SSEF
SCHWEIZERISCHES GEMMOLOGISCHES INSTITUT
SWISS GEMMOLOGICAL INSTITUTE
INSTITUT SUISSE DE GEMMOLOGIE

Gem-A
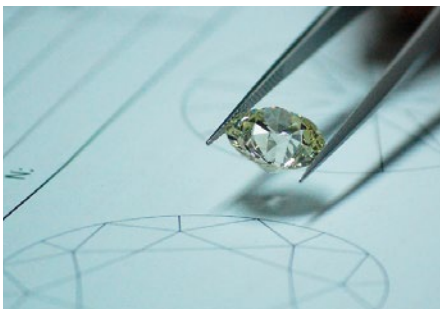THE GEMMOLOGICAL ASSOCIATION
OF GREAT BRITAIN

SSEF +

SCHWEIZERISCHES GEMMOLOGISCHES INSTITUT
SWISS GEMMOLOGICAL INSTITUTE
INSTITUT SUISSE DE GEMMOLOGIE

ORIGIN DETERMINATION · TREATMENT DETECTION

DIAMOND GRADING · PEARL TESTING

EDUCATION · RESEARCH

THE SCIENCE OF GEMSTONE TESTING™

The Journal of Gemmology

COLUMNS

Cover photo: A new type of emerald from Afghanistan's Panjshir Valley entered the market in 2017. These stones show some different properties from earlier production, as described in an article on pp. 474–495 of this issue. The older-type Panjshir emerald in the ring weighs 10.11 ct, while the loose stones are representative of newer material and weigh 1.94, 7.09 and 3.48 ct (from left to right). The emerald crystal is from earlier production and weighs 127 g (approximately 80 x 35 x 30 mm). The individual stones have been resized for aesthetic purposes in this photo composite by M. S. Krzemnicki (© SSEF).

ARTICLES

Photo by J. Štubňa

Photo by Tay Thye Sun

Photo by T. Sripoonjan

The Journal of Gemmology

Gem-A
THE GEMMOLOGICAL ASSOCIATION OF GREAT BRITAIN

CONTENT SUBMISSION

The Editor-in-Chief is glad to consider original articles, news items, conference reports, announcements and calendar entries on subjects of gemmological interest for publication in *The Journal of Gemmology*. A guide to the various sections and the preparation of manuscripts is given at https://gem-a.com/membership/journal-of-gemmology/submissions, or contact the Editor-in-Chief.

SUBSCRIPTIONS

Gem-A members receive *The Journal* as part of their membership package, full details of which are given at https://gem-a.com/membership. Laboratories, libraries, museums and similar institutions may become direct subscribers to *The Journal*; download the form from *The Journal*'s home page.

ADVERTISING

Enquiries about advertising in *The Journal* should be directed to advertising@gem-a.com.

COPYRIGHT AND REPRINT PERMISSION

For full details of copyright and reprint permission contact the Editor-in-Chief. *The Journal of Gemmology* is published quarterly by Gem-A, The Gemmological Association of Great Britain. Any opinions expressed in *The Journal* are understood to be the views of the contributors and not necessarily of the publisher.

DESIGN & PRODUCTION

Zest Design, London. www.zest-uk.com

PRINTER

DG3 Group (Holdings) Ltd, London. www.dg3.com

FSC Mixed Sources
Product group from well-managed forests and other controlled sources
www.fsc.org Cert no. TT-COC-002454
© 1996 Forest Stewardship Council

What's New

NEWS AND PUBLICATIONS

CIBJO Pearl Guide

In February 2021, the CIBJO Pearl Commission issued its *CIBJO Guide for Classifying Natural Pearls and Cultured Pearls*. This publication gives parameters for describing the quality of natural pearls from akoya species and cultured pearls from *Pinctada maxima*, and also provides general information on many other varieties of natural and cultured pearls. Descriptions and photographs are included of several types of saltwater and freshwater pearl-producing molluscs, including both nacreous and non-nacreous types. Terminology is provided for describing pearl quality factors of lustre, colour, surface appearance, shape, weight and size. This useful 62-page resource can be downloaded from www.cibjo.org/wp-content/uploads/2021/02/21-02-17-CIBJO-Pearl-Guide.pdf.
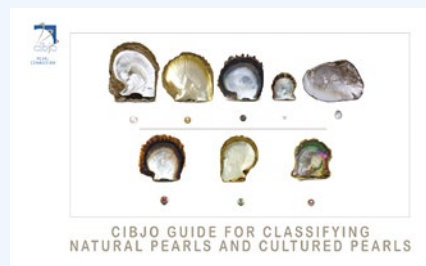
Consumer Surveys on Diamond and Coloured Stones

In January 2021, the Natural Diamond Council released a report titled *Consumer Insights Report on Diamond Desirability*, 'to increase understanding about the desira-bility, perceived values, and shopping habits for natural diamond jewelry among American Millennials (currently aged 25–39) and Generation Z (aged 18–24)'. The survey found that both groups place importance on the lasting value, uniqueness, emotional connection and versatility of diamond jewellery. They mostly plan to follow buying patterns seen in the past 2 years, although with increased involvement in the research and purchase decision. The report can be downloaded at https://tinyurl.com/3axwysvs. In February 2021, USA-based MVI Marketing LLC released *Colored Gemstones Capture More Consumer & Trade Attention*, which showed that '93% of U.S. jewelry consumers *Love* or *Like* ALL precious colored gemstones with sapphires being the most purchased colored gemstone by 46% of consumers followed by emerald (41%) and ruby (41%).' Download the report after filling out an online form at www.themveye.com/download-report.php?report=57.   *Brendan M. Laurs* FGA

Diamond, Coloured Stone and Jewellery Market Reports from GJEPC

The Gem & Jewellery Export Promotion Council (Mumbai, India) provides a Research & Statistics section of its website with summaries of global and Indian gem and jewellery information, as well as numerous reports on trade statistics and market analyses from 2019 to the present. Information is included on the export and import of gems and jewellery, marketing collaborations between India and other countries, the impact of COVID-19 on the gem and jewellery market, global economic trends and monthly trade updates. Visit https://gjepc.org/statistics.php.
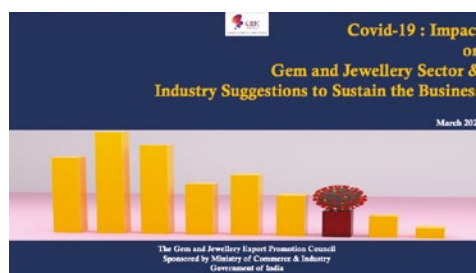
GemFair Annual Report

GemFair is a pilot project from De Beers Group that connects artisanal and small-scale diamond miners with the global market. Its annual report, *The GemFair Way 2019–2020*, was released in November 2020 with the subtitle 'Keeping people safe during a global pandemic, while continuing to raise the standards of artisanal miners'. The 17-page report includes highlights of the project's 'community response plan', implementation of the ASM Assurance Program, involvement with mining communities in Sierra Leone and plans for the future. Download the report at https://gemfair. com/static/files/End-of-year_report_2020_v2.pdf or visit https://gemfair.com to learn more about the programme.

Global Diamond Industry Report 2020–2021

The 10th annual report from the Antwerp World Diamond Centre and Bain & Co. was released in February 2021. It reviews the diamond industry's performance in 2019 and the effects of the COVID-19 pandemic in 2020, updates consumer preferences and attitudes, and examines key trends affecting the industry, including recovery scenarios for 2021. During the pandemic, the diamond industry performed better than the personal luxury market overall, with overall revenues down 15–33%. Rough diamond production fell to 111 million carats, with 2020 production declining 20% compared to 2019, and rough and polished prices decreased by 11% and 3%, respectively. Diamond jewellery sales fell 15% in 2020, but consumers continued to express a strong desire for the product. The report identifies the need for diamond jewellery marketing to evolve in the face of online sales growth. Early 2021 trends already show signs of economic recovery, promising a positive long-term outlook for the diamond market. Download the report at www.bain. com/insights/global-diamond-industry-2020-21.

The Journal's Cumulative Index and Bibliography Lists Updated

The Journal of Gemmology's cumulative index has been updated to cover all issues through 2020. The index is provided in electronic (PDF) format, so it can be searched for specific first authors as well as topics. In addition, the subject bibliographies covering articles and notes published in *The Journal* have been updated through 2020. These include the following topics: asterism and chatoyancy, biogenic gems, chrysoberyl and alexandrite, colour-change gems, corundum, diamond, emerald and other beryls, feldspar, garnet, historical gems and jewels, jades, opal, pearl, quartz, spinel and tourmaline. Download the index and bibliographies at https://gem-a.com/ news-publications/journal-of-gemmology.

OTHER RESOURCES

Webinars and Other Online Content for Gemmological Education

Various educational and gem industry organisations are providing webinars and other archived video and audio content of interest to gemmologists during the ongoing COVID-19 pandemic (in addition to those listed in several previous What's New sections).

- The **Gem Certification & Assurance Lab** (GCAL) launched their 'Diamond Profile' podcast series in July 2020. Available podcasts include an interview with Stuller executives and a discussion with industry leaders on the state of the diamond market. Visit www.gcalusa.com/blog/category/podcast.

- Since February 2019, **JCK** has offered a podcast series titled 'The Jewelry District'. The podcasts include interviews with jewellery and gem industry leaders, JCK show recaps and more. The latest one (16 February 2021) covers demantoid from Madagascar. Access the podcasts at www.jckonline.com/category/news-trends/podcasts.

- **Inhorgenta Trendfactory** was held on 22 October 2020 as an interactive online conference in lieu of the regular annual Inhorgenta Munich show. Recorded presentations and classes are available for a fee through the 'On Demand Content' link at www.inhorgenta.com/en/trendfactory/trendfactory-digital. While most of them cover industry trends, one topic of particular interest to *Journal* readers is 'The role of the gemmologist in the 21st century'.

- **NYC Jewelry Week 2020** celebrated its third year with a virtual event on 16–22 November, and videos of the presentations are now available at https://nycjewelryweek.com/events under the Talks/Tours/Panels tab. The videos cover an array of jewellery topics, including museum exhibitions, innovative designers, international trends and more. Participants include journalists, curators, gemmologists, designers and jewellers.

- The **Responsible Jewellery Council** now has a YouTube channel at www.youtube.com/c/ResponsibleJewelleryCouncil with archived recordings of various recent events, webinars and panel discussions, including 'Responsibility: A Critical Enabler of Survival in a Crisis', 'Building Consumer Confidence in Coloured Gemstone Trading in the New World', 'Lab-Grown Diamonds – The Importance of Detection and Disclosure' and more.

What's New provides announcements of new instruments/technology, publications, online resources and more. Inclusion in What's New does not imply recommendation or endorsement by Gem-A. Entries were prepared by Carol M. Stockton unless otherwise noted.

Gem Notes

COLOURED STONES

Horsetail-like Inclusions in a Colour-Change Garnet from Tanzania

Bundles of curved fibrous inclusions emerging from a common centre—commonly referred to as *horsetails*—are well-known internal features in demantoid from Russia. They are typically composed of chrysotile fibres, and have been noted in demantoid from various other serpentinite-hosted deposits such as in Val Malenco, Italy, and Baluchistan, Pakistan (Lewis 2018). However, to the author's knowledge, similar inclusions have not previously been found in colour-change garnet.

In November 2020, a few pieces of garnet rough were sent to the author for cutting by Alexander Buggisch, who had obtained the material from Roughstore24 in Germany, which reported that the stones came from Tunduru, Tanzania. Two of the pieces were eye clean, with only some tiny, thin, straight needles inside. However, one of the samples contained conspicuous radiating inclusions resembling horsetails. In this case, however, the fibres were straight rather than curved.

Faceting of this garnet yielded a 3.43 ct stone, which had an RI of 1.772. The stone was brownish yellow under cool-white illumination (i.e. a mixture of 5500 K and 6500 K fluorescent bulbs) and showed a colour change to orangey red in warm-white lighting (approximately 2500 K from a mixture of fluorescent and LED bulbs; Figure 1). Raman micro-spectroscopy identified the core of the horsetail-like feature (Figure 2) as rutile, but the fibres could only tentatively be identified as anatase and, in places, other titanium oxides. A clear identification was not possible because of the narrow dimension of the fibres.

Chemical analysis of the stone was done with laser ablation inductively coupled plasma mass spectrometry (LA-ICP-MS), using a Teledyne Cetac LSX-213 G2+ laser ablation system connected to a Thermo Fisher Scientific XSeries 2 ICP-MS, as described in Bindereif *et al.* (2020). The data were normalised to a Si concentration of 17 wt.% (as would be the case for spessartine). Also, Mg, Ca, Mn and Fe were summed to 3 formula units, and Al was assumed to be the only trivalent cation. The analyses yielded an average formula of $Mn_{1.30}Mg_{0.88}Ca_{0.71}Fe_{0.11}Al_2(SiO_4)_3$, corresponding mainly to a spessartine-pyrope-grossular composition (see data for the Tunduru sample in Table I). This garnet mixture is consistent with other (mostly blue-green) colour-change garnets from Kenya and Tanzania in the author's reference collection (again, see Table I). However, the trace-element content of the present garnet with the horsetail-like inclusions showed some differences
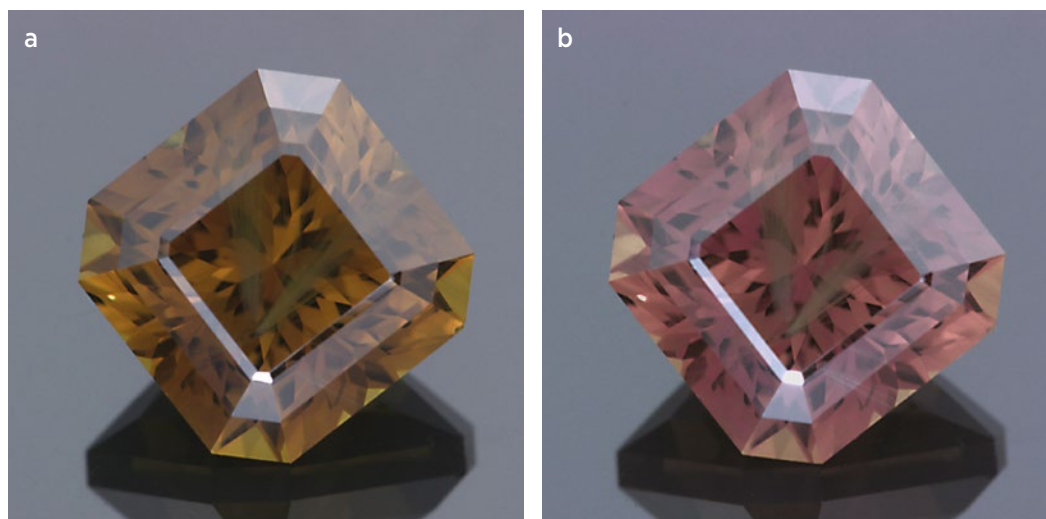
Figure 1: This 3.43 ct colour-change garnet, reportedly from Tunduru, Tanzania, is shown under cool-white (left) and warm-white (right) illumination. Photos by C. Schwarzinger.
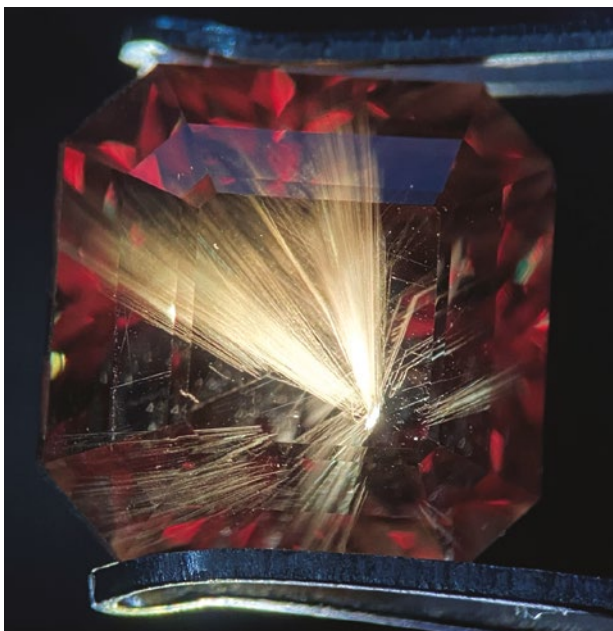
Figure 2: The horsetail-like inclusion in the 3.43 ct garnet in Figure 1 consists of white fibres of titanium oxides emerging from a rutile crystal. Photomicrograph by C. Schwarzinger; image width 8.8 mm.

compared to those reference samples (Table II), with lower amounts of V (2400 ppm vs 4950–8210 ppm) and rare-earth elements (14.3 ppm vs 142–273 ppm), and higher amounts of Ti (1910 ppm vs 170–1000 ppm).

Needles of rutile have been previously documented in garnets from the Umba Valley in Tanzania (i.e. Gübelin & Koivula 2005), but they consisted of crystallographically oriented intersecting networks or star patterns rather than radiating sprays. White acicular inclusions with a somewhat similar appearance to those seen in the present stone were documented by Gübelin and Koivula (2005) in an almandine from Sri Lanka, but those were identified as sillimanite.

Dr Clemens Schwarzinger
(Clemens.Schwarzinger@jku.at)
Johannes Kepler University Linz, Austria

References

Bindereif, S.G., Rüll, F., Schwarzinger, S. & Schwarzinger, C. 2020. Chemometric modeling of trace element data for origin determination of demantoid garnets. *Minerals*, **10**, article 1046 (15 pp.), https://doi.org/10.3390/min10121046.

Gübelin, E.J. & Koivula, J.I. 2005. *Photoatlas of Inclusions in Gemstones*, Vol. 2. Opinio Publishers, Basel, Switzerland.

Lewis, Z. 2018. Beyond 'horse tails' in demantoid garnet. *Gems&Jewellery*, **27**(4), 32–35.

Table I: Average end-member composition determined by LA-ICP-MS of some colour-change garnets from East Africa.

Locality	Spessartine	Pyrope	Grossular	Almandine
Tunduru, Tanzania	43.4	29.3	23.8	3.5
Lindi, Tanzania[1]	50.2	36.1	8.6	5.1
Lindi, Tanzania[1]	51.4	35.7	8.5	4.4
Lindi, Tanzania[1]	39.1	35.0	21.9	4.0
Kenya[2]	38.6	31.8	25.6	4.0

[1] Samples obtained from New Era Gems, Grass Valley, California, USA.

[2] Sample obtained from Gichuchu Okeno, Voi, Kenya.

Table II: Trace-element composition by LA-ICP-MS of some colour-change garnets from East Africa.

Element (ppmw)	Tunduru, Tanzania	Lindi, Tanzania	Lindi, Tanzania	Lindi, Tanzania	Kenya
Ti	1910	170	200	566	1000
V	2400	7210	7350	4950	8210
Cr	1000	1530	1330	320	1020
Ga	12.5	10.5	11.2	18.6	2.61
Ge	4.61	11.1	10.7	7.69	2.10
Y	15.1	718	437	259	441
Zr	17.2	16.9	17.1	16.1	20.1
Ce	0.216	0.022	0.046	0.248	0.408
Pr	0.177	0.061	0.075	0.208	0.216
Nd	3.05	1.03	1.01	3.33	3.61
Sm	1.97	2.32	2.25	5.74	6.59
Eu	1.31	0.566	0.504	0.749	1.75
Gd	2.12	14.2	12.4	15.7	22.0
Tb	0.318	5.40	4.21	4.10	5.74
Dy	1.85	63.3	44.6	35.4	51.8
Ho	0.381	19.7	12.6	8.23	14.3
Er	1.17	71.8	40.3	27.1	51.3
Tm	0.169	11.0	5.95	4.31	8.12
Yb	1.36	72.4	37.9	32.2	59.0
Lu	0.207	10.8	5.49	4.66	10.0
Sum REE*	14.3	235	273	167	142

* Sum of rare-earth elements calculated for Ce through Lu.

A Rare Ruby Showing an Interesting Sheen Effect

In early 2019, a unique orange sapphire with a golden sheen effect—reportedly from Kenya—was described by one of the present authors (Sripoonjan *et al.* 2019). It was found to be distinct from orange sapphires from other sources such as Songea in Tanzania. In addition, it showed features in common with 'Gold Sheen' sapphires from Kenya (e.g. Bui *et al.* 2015), which are known for their shimmering appearance caused by oriented inclusions of Fe-Ti oxides (i.e. hematite, ilmenite and magnetite).

Recently, we had the opportunity to examine a 1.86 ct ruby with a remarkable golden sheen effect (Figure 3),

Figure 3: This 1.86 ct ruby shows a sheen effect throughout the table facet and across some crown facets when illuminated at an oblique angle. Photo by T. Sripoonjan.
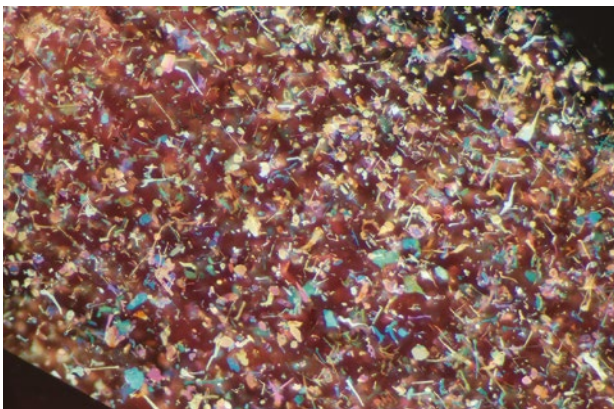
Figure 4: Numerous iridescent platelets of hematite are responsible for the sheen effect in the ruby. Photomicrograph by T. Sripoonjan; image width 3.2 mm.
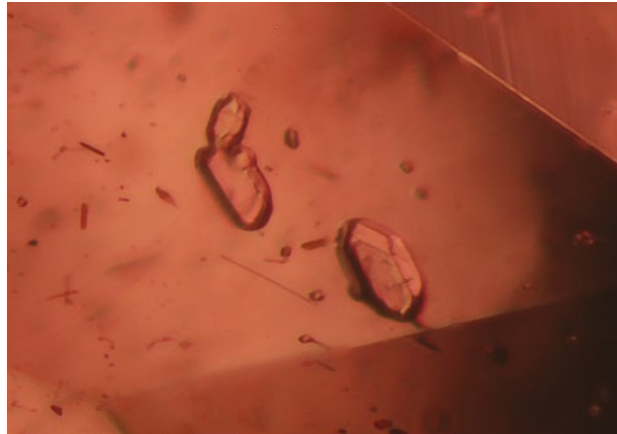
Figure 5: The ruby also contains zircon inclusions, which are seen here as a cluster of transparent crystals. Photomicrograph by T. Sripoonjan; image width 0.5 mm.

also reportedly from Kenya. Its RIs were 1.768–1.778 and its hydrostatic SG value was 4.00. The sample was inert to long- and short-wave UV radiation. Microscopic observation revealed locally dense arrays of iridescent platelets of hematite-ilmenite (identified by Raman micro-spectroscopy) that caused the sheen effect when viewed with oblique illumination at just the right angle (Figure 4). In addition, transparent inclusions, confirmed by Raman analysis as zircon, were observed as euhedral, slightly elongated forms or clusters of rounded crystals (e.g. Figure 5).

Ultraviolet-visible-near infrared (UV-Vis-NIR) spectroscopy (Figure 6) showed that the sample's colour was mainly due to Cr^{3+}, which produced an absorption at 555 nm and a luminescence peak at 693 nm. A strong Fe^{3+}-related feature at 450 nm contributed a yellowish tint (Ferguson & Fielding 1972). The combination of
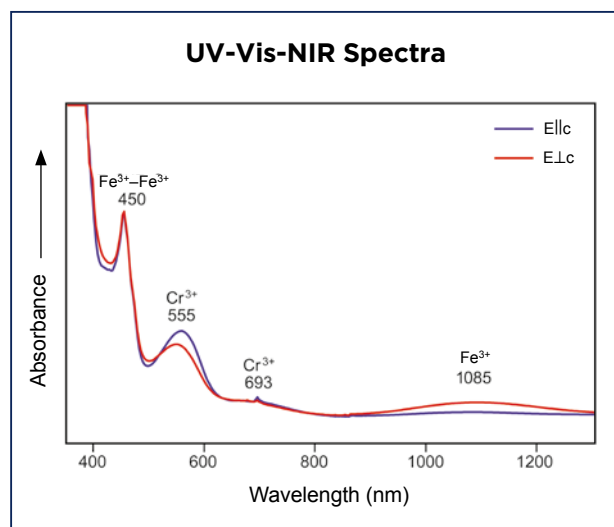
Figure 6: The UV-Vis-NIR spectra of the sheen-type ruby show Fe^{3+}- and Cr^{3+}-related absorption features.

Table III: EDXRF chemical composition of sheen-type gem corundum.*

Oxides (wt.%)	Ruby (this study)	Orange sapphire (Sripoonjan et al. 2019)	'Gold Sheen' sapphire (Narudeesombat et al. 2016)
TiO$_2$	0.02	0.04	0.01–0.02
V$_2$O$_5$	0.01	0.01	nd–0.01
Cr$_2$O$_3$	0.12	0.05	nd–0.01
Fe$_2$O$_3$	1.96	1.94	1.00–1.50
Ga$_2$O$_3$	0.01	0.01	0.02–0.05

* Abbreviation: nd = not detected.

these chromophores resulted in the sample's orangey red colouration. Also recorded was a weak but broad band in the NIR region at around 1085 nm that occurs only in corundum with high Fe^{3+} concentrations (Dubinsky et al. 2020).

Energy-dispersive X-ray fluorescence (EDXRF) analysis of the ruby showed a distinct amount of Fe (1.96 wt.% Fe$_2$O$_3$) and relatively high Cr (0.12 wt.% Cr$_2$O$_3$) compared to previous data for sheen-bearing sapphires (Table III). Its composition was only slightly different from that of the orange sapphire with a golden sheen reported by Sripoonjan et al. (2019), except for the higher Cr content that is consistent with the redder colour of the current sample. The chemical data indicate a similar magmatic source for (1) typical 'Gold Sheen' sapphires, (2) the previously documented orange sapphire with sheen and (3) this sheen-type ruby. Indeed, it seems plausible that all of these stones were derived from the same deposit.

Tasnara Sripoonjan (tasnara@hotmail.com)
G-ID Laboratories, Bangkok, Thailand

Papawarin Ounorn
GIT Gem Testing Laboratory
Bangkok, Thailand

References

Bui, T.N., Deliousi, K., Malik, T.K. & De Corte, K. 2015. From exsolution to 'Gold Sheen': A new variety of corundum. *Journal of Gemmology*, **34**(8), 678–691, https://doi.org/10.15506/JoG.2015.34.8.678.

Dubinsky, E.V., Stone-Sundberg, J. & Emmett, J.L. 2020. A quantitative description of the causes of color in corundum. *Gems & Gemology*, **56**(1), 2–28, https://doi.org/10.5741/gems.56.1.2.

Ferguson, J. & Fielding, P.E. 1972. The origins of the colours of natural yellow, blue, and green sapphires. *Australian Journal of Chemistry*, **25**(7), 1371–1385, https://doi.org/10.1071/ch9721371.

Narudeesombat, N., Saengbuangamlam, S., Lhuaamporn, T. & Leelawatanasuk, T. 2016. Golden sheen and non-sheen sapphires from Kenya. *The 5th GIT International Gem and Jewelry Conference (GIT 2016)*, Pattaya, Thailand, 14–15 November, 284–290.

Sripoonjan, T., Saengbuangamlam, S. & Maneekrajangsaeng, M. 2019. Gem News International: Unique orange sapphire with golden sheen effect reportedly from Kenya. *Gems & Gemology*, **55**(1), 152–155.

Spectroscopic Study of Serendibite from Sri Lanka

The mineral serendibite was discovered in 1902 near Gangapitiya, Kandy District, Central Province, Sri Lanka, and its name is derived from *serendib*, an old Arabic term for the country's original name of Ceylon (Prior & Coomáraswámy 1903). Gem-quality serendibite has appeared on the market only rarely (Reinitz & Johnson 1997; Schmetzer et al. 2002). The present study provides a spectroscopic investigation of a gemmy serendibite specimen, and was motivated mainly by the lack of reliable, appropriate-quality reference Raman spectra for this mineral in the published literature and in online databases.

The studied specimen originated from Kolonna (Ratnapura District, Sabaragamuwa Province, southern Sri Lanka). It was tested previously by Crystals Gallery – Gem Lab, Ratnapura (report 1423 issued in October 2012) and the Gemological Institute of America (report 7328158318 issued in March 2019). The rough piece weighs 0.052 g and has been polished on one side. It is strongly pleochroic, ranging from vivid greenish blue to nearly colourless (Figure 7). The RIs are 1.697–1.702 and the SG (here reported as mass density) is ~3.43 g/cm³.

Chemical composition was determined by means of an electron probe micro-analyser (EPMA) operated at 15 kV and 10 nA, except for boron (*K*α), which was measured at 5 kV and 150 nA. More EPMA details are described elsewhere (Zeug et al. 2018) or can be obtained from the authors upon request. Assuming 40 oxygen ions per
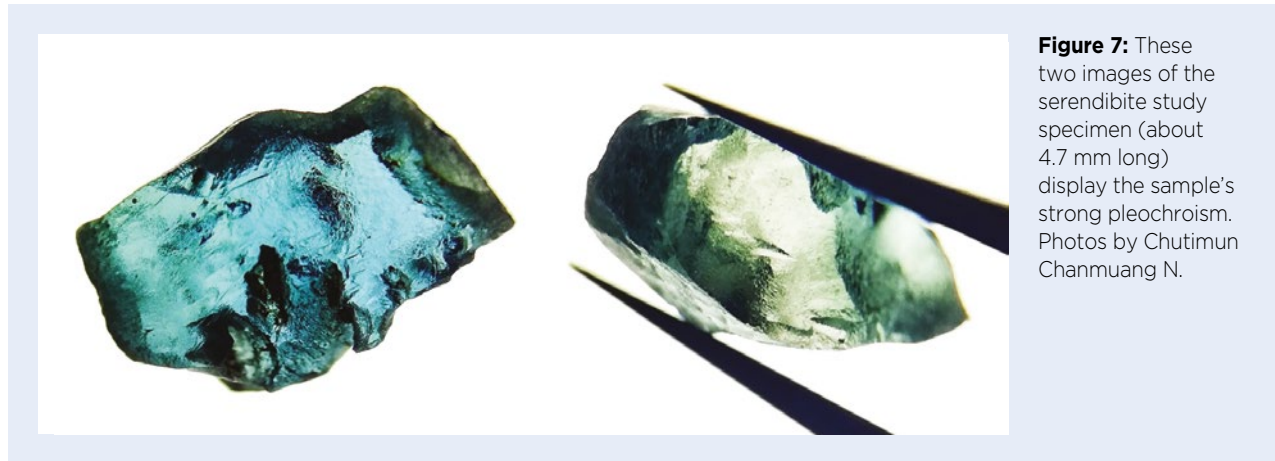
Figure 7: These two images of the serendibite study specimen (about 4.7 mm long) display the sample's strong pleochroism. Photos by Chutimun Chanmuang N.

formula unit, the chemical formula was calculated as $Ca_{3.47}Na_{0.59}(Al_{6.24}Mg_{5.53}Fe_{0.19})(Si_{6.25}Al_{3.16}B_{2.59})O_{40}$. Slight dominance of Al^{3+} over Mg^{2+} at the octahedral cation sites agrees with results of previous studies (Schmetzer *et al.* 2002; Grice *et al.* 2014 and references therein) and thus seems to be a general feature of serendibite.

Optical absorption and photoluminescence (PL) spectra (Figure 8; for analytical details see Zeug *et al.* 2018) correspond to those reported by Schmetzer *et al.* (2002). The absorption in the visible range is dominated by an intense, broad band at about 14,300 cm^{-1} (or ~700 nm wavelength), which is presumably caused by Fe^{2+}–Fe^{3+} intervalence charge transfer. Reliable assignment of this and additional low-intensity bands near 21,500 cm^{-1}

(~465 nm) and 24,100 cm^{-1} (~415 nm) to Fe^{3+}-related absorption would only be possible with information on the valence state(s) of iron—obtainable by Mössbauer and/or electronic paramagnetic resonance spectroscopy—but is beyond the scope of this study. The PL electronic emission is dominated by a fairly narrow doublet band in the red range, at 14,425 and 14,490 cm^{-1} (~693 and ~690 nm, respectively), superimposed on a broad emission feature in the range of 11,500–15,000 cm^{-1} (~870–667 nm). The doublet is assigned to the split, spin-forbidden $^2E \rightarrow {}^4A_2$ transition of Cr^{3+}, the trace concentration of which is, however, below the EPMA detection limit. The asymmetric broad hump consists of the spin-allowed $^4T_2 \rightarrow {}^4A_2$ transition of Cr^{3+} and vibronic coupling (for
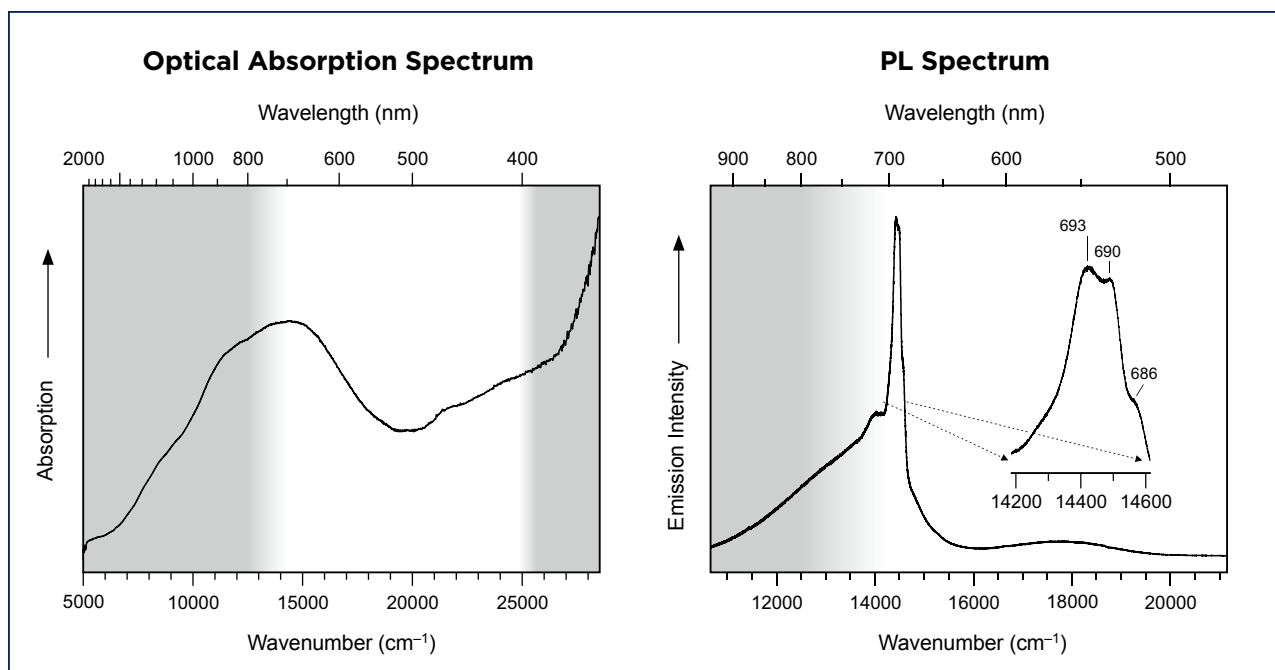
Figure 8: Shown here are the optical absorption spectrum (left, recorded in the greenish blue direction; sample thickness about 1.9–2.3 mm) and PL spectrum (right, obtained with 473 nm excitation) of the serendibite specimen. Spectral ranges that are invisible to the human eye are shaded grey.
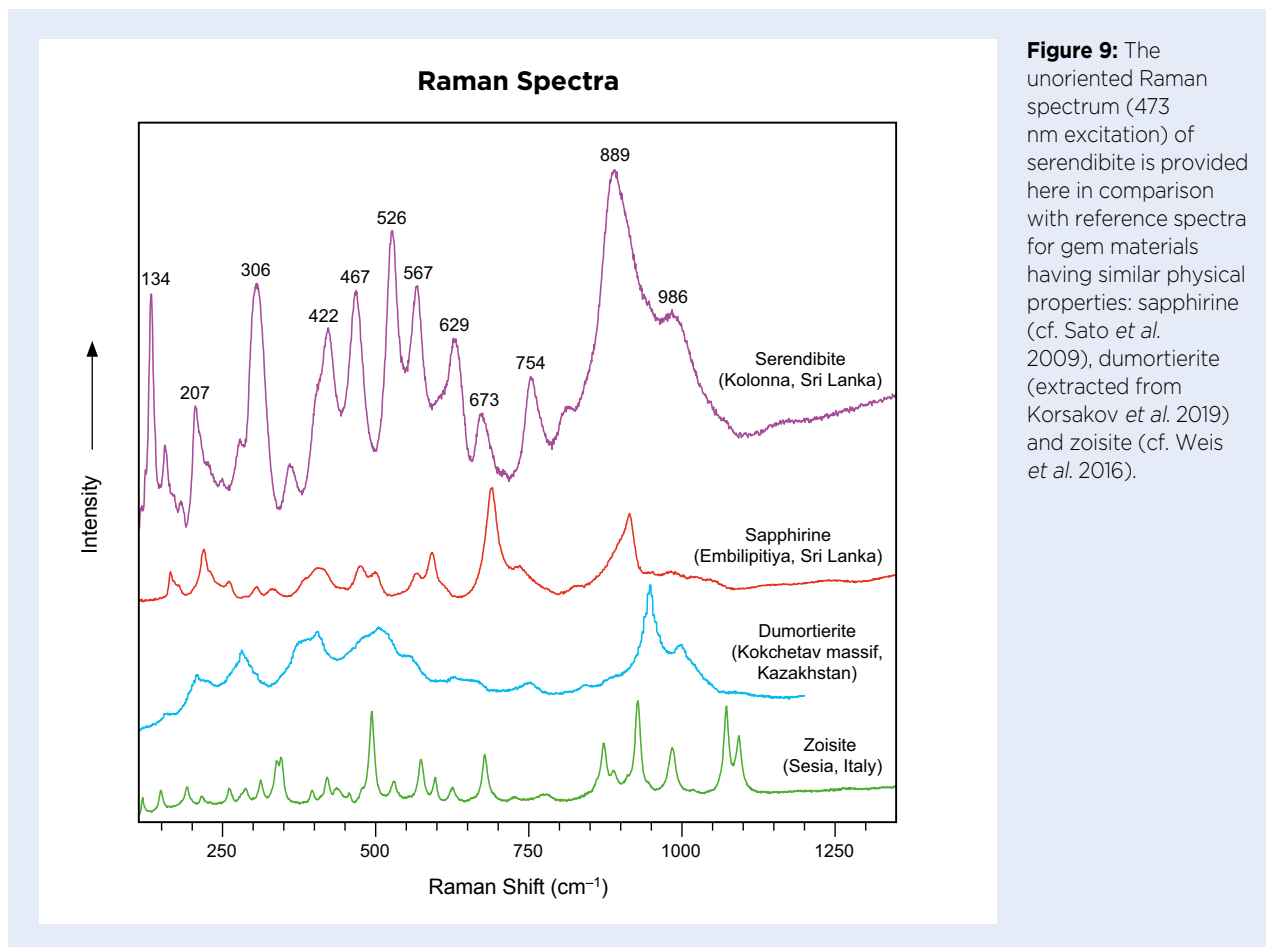
Figure 9: The unoriented Raman spectrum (473 nm excitation) of serendibite is provided here in comparison with reference spectra for gem materials having similar physical properties: sapphirine (cf. Sato *et al.* 2009), dumortierite (extracted from Korsakov *et al.* 2019) and zoisite (cf. Weis *et al.* 2016).

the analogous assignment of constituents of the Cr^{3+} emission of topaz, see Tarashchan *et al.* 2006). The cause of the weak, broad emission near 17,850 cm^{-1} (~560 nm) remains unclear.

The Raman spectrum (for analytical details, see Zeug *et al.* 2018) of the specimen is presented in Figure 9, and the raw x,y data are available in *The Journal*'s online data depository. Serendibite is a relatively weak Raman scatterer and, therefore, Raman analysis is hampered considerably by background luminescence if present. In particular with 633 nm (He-Ne laser) excitation, the Raman spectrum was heavily obscured by laser-induced PL. The least disturbing PL effects were observed when using blue (473 nm) laser excitation. The principal fingerprint Raman pattern of serendibite is clearly distinct from those of other gem minerals with similar physical properties, in particular sapphirine, dumortierite and zoisite/tanzanite (Reinitz & Johnson 1997; Schmetzer *et al.* 2002; Heo & Kwak 2016). In conclusion, as long as disturbance by laser-induced PL is avoided (by choosing a short-wavelength excitation source), Raman spectroscopy provides a reliable and straightforward means of non-destructively identifying serendibite.

Dr Chutimun Chanmuang N.
(chutimun.chanmuang@univie.ac.at),
Prof. Dr Lutz Nasdala and Prof. Dr Manfred Wildner
University of Vienna, Austria

Dr Radek Škoda
Masaryk University, Brno, Czech Republic

E. Gamini Zoysa FGA
Mincraft Co., Mount Lavinia, Sri Lanka

References

Grice, J.D., Belley, P.M. & Fayek, M. 2014. Serendibite, a complex borosilicate mineral from Pontiac, Quebec: Description, chemical composition, and crystallographic data. *Canadian Mineralogist*, **52**(1), 1–14, https://doi.org/10.3749/canmin.52.1.1.

Heo, M. & Kwak, K.-W. 2016. Two rare gems with similar appearance: Serendibite and sapphirine. *ICGL Newsletter*, No. 3, 4–5.

Korsakov, A.V., Rezvukhina, O.V., Rezvukhin, D.I., Greshnyakov, E.D. & Shur, V.Y. 2019. Dumortierite and tourmaline from the Barchi-Kol diamond-bearing kyanite gneisses (Kokchetav massif): A Raman spectroscopic study and petrological implications. *Journal of Raman Spectroscopy*, **51**(9), 1839–1848, https://doi.org/10.1002/jrs.5699.

Prior, G.T. & Coomáraswámy, A.K. 1903. Serendibite, a new borosilicate from Ceylon. *Mineralogical Magazine and Journal of the Mineralogical Society*, **13**(61), 224–227, https://doi.org/10.1180/minmag.1903.13.61.04.

Reinitz, I. & Johnson, M.L. 1997. Gem Trade Lab Notes: Serendibite, a rare gemstone. *Gems & Gemology*, **33**(2), 140–141.

Sato, K., Santosh, M. & Tsunogae, T. 2009. A petrologic and laser Raman spectroscopic study of sapphirine–spinel–quartz–Mg-staurolite inclusions in garnet from Kumiloothu, southern India: Implications for extreme metamorphism in a collisional orogen. *Journal of Geodynamics*, **47**(2–3), 107–118, https://doi.org/10.1016/j.jog.2008.07.003.

Schmetzer, K., Bosshart, G., Bernhardt, H.-J., Gübelin, E.J. & Smith, C.P. 2002. Serendibite from Sri Lanka. *Gems & Gemology*, **38**(1), 73–79, https://doi.org/10.5741/gems.38.1.73.

Tarashchan, A.N., Taran, M.N., Rager, H. & Iwanuch, W. 2006. Luminescence spectroscopic study of Cr^{3+} in Brazilian topazes from Ouro Preto. *Physics and Chemistry of Minerals*, **32**, 679–690, https://doi.org/10.1007/s00269-005-0042-1.

Weis, F.A., Lazor, P., Skogby, H., Stalder, R. & Eriksson, L. 2016. Polarized IR and Raman spectra of zoisite: Insights into OH-dipole orientation and the luminescence. *European Journal of Mineralogy*, **28**(3), 537–543, https://doi.org/10.1127/ejm/2016/0028-2528.

Zeug, M., Nasdala, L., Wanthanachaisaeng, B., Balmer, W.A., Corfu, F. & Wildner, M. 2018. Blue zircon from Ratanakiri, Cambodia. *Journal of Gemmology*, **36**(2), 112–132, https://doi.org/10.15506/JoG.2018.36.2.112.

Turquoise from Armenia

Turquoise is probably the oldest-known gem material to have been extracted on a large scale. The mineral turquoise—$CuAl_6(PO_4)_4(OH)_8 \bullet 4H_2O$—is a member of the turquoise group. Turquoise is global in its distribution and most of the deposits have been developed to produce material for lapidary work. Within the Middle East, those in Iran are thought to be extensive, whereas the turquoise mines of the Sinai Peninsula in Egypt are no longer economic (King 2002).

According to Kievlenko (2003), in Armenia turquoise was discovered in 1974 at the Tekhut porphyry copper-molybdenum deposit, located 12 km east of Alaverdy on the western slope of the Panskar Range. The Tekhut deposit is associated with Early Cretaceous granitoids of the Shnokh Kokhb massif, which intrude Middle Jurassic extrusive and sedimentary rocks. Turquoise occurs in the oxidation zone of the deposit as nodules up to 5 cm in dimension, and as lenses that are typically 10–20 m long and from 1 to 30 mm thick. It is mainly concentrated in a kaolinised area, which is locally mineralised with several kilograms of turquoise per cubic metre of host rock. Most of the turquoise is intensely altered and requires treatment.

Mineralogical research on turquoise from Armenia has been performed in detail by various Russian scientists (e.g. Suchkova & Akhmetova 1985). Three main varieties have been identified, which differ in colour, SG,

Figure 10: Cabochons of turquoise from Armenia examined for this report include these 3.24 ct treated (13.4 × 10.0 mm), 10.48 ct treated (17.8 × 13.4 mm) and 14.68 ct untreated (24.0 × 17.0 mm) samples, shown from left to right. Photo by J. Štubňa.

composition of accessory minerals and microstructure of the turquoise aggregates (Kievlenko 2003).

During the March 2019 Vicenzaoro show in Vicenza, Italy, one dealer had some interesting rough samples of blue turquoise recently mined from the Tekhut deposit. Some of the samples were untreated, while others were claimed by the dealer to have been treated with beeswax. Author AA cut and polished 100 cabochons (2–34 ct) from the treated rough material and five cabochons (8–15 ct) from the untreated Armenian turquoise. For this study, we examined 10 representative cabochons that ranged from 13.4 to 24.0 mm in maximum dimension (e.g. Figure 10). The untreated samples had RIs of 1.610–1.650 and hydrostatic SG values of 2.70–2.73, while the stabilised
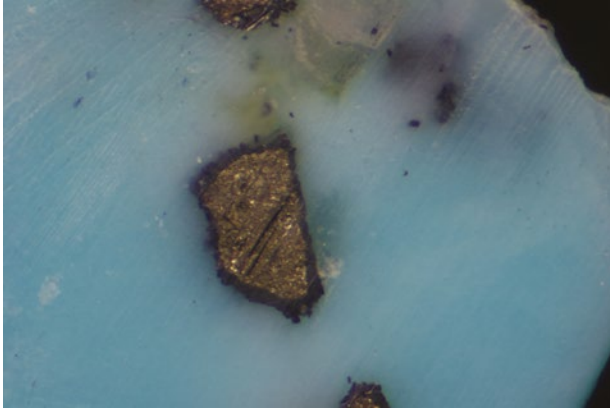
Figure 11: Armenian turquoise commonly contains inclusions of pyrite. Photomicrograph by J. Štubňa; magnified 20×.
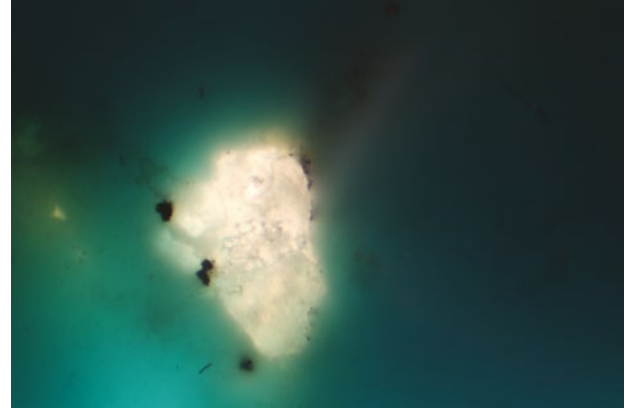
Figure 12: A cavity in one of the treated cabochons is filled with a colourless material used to stabilise the turquoise. Photomicrograph by J. Štubňa; magnified 10×.

turquoise had much lower RIs of 1.435–1.485 and SG values of 2.11–2.40. Small inclusions of pyrite were common (Figure 11). In addition, we observed a colourless organic substance in the stabilised turquoise (Figure 12).

The samples' identity as turquoise was confirmed by Raman spectroscopy (Figure 13). For all samples, we recorded bands at 230, 334, 420, 472, 550, 593, 642, 815, 1000, 1040, 1094, 1160, 3473 and 3508 cm^{-1}; the last two bands are due to OH-stretching vibrations (Čejka *et al.* 2015). In the treated samples, bands characteristic of impregnation were also observed at 1453 cm^{-1} (CH$_3$ bending), 1726 cm^{-1} (C=O stretching), 2947 cm^{-1} and 3003 cm^{-1} (cf. Miliani *et al.* 2002). The bands in the 2800–3100 cm^{-1} region are due to C-H stretching; their intensity is related to the alkyl group (Miliani *et al.* 2002). Although we could not identify the specific substance used for the treatment, Raman spectra did

not reveal evidence of paraffin or beeswax, which show prominent bands of antisymmetric and symmetric stretching vibrations of methylene groups at 2881 and 2847 cm^{-1} (Špaldoňová *et al.* 2021).

Information in the local media indicates that in 2019 most of the Armenian turquoise reserves were mined and are awaiting processing. Armenian turquoise is generally not of high quality, and due to its porosity it needs to be treated to achieve an appealing appearance and to avoid susceptibility to discolouration from wear.

Dr Ján Štubňa (janstubna@gmail.com)
Gemmological Laboratory, Constantine the
Philosopher University, Nitra, Slovakia

Alžbeta Andrášiová
Atelier GemmaAnima, Kremnica, Slovakia
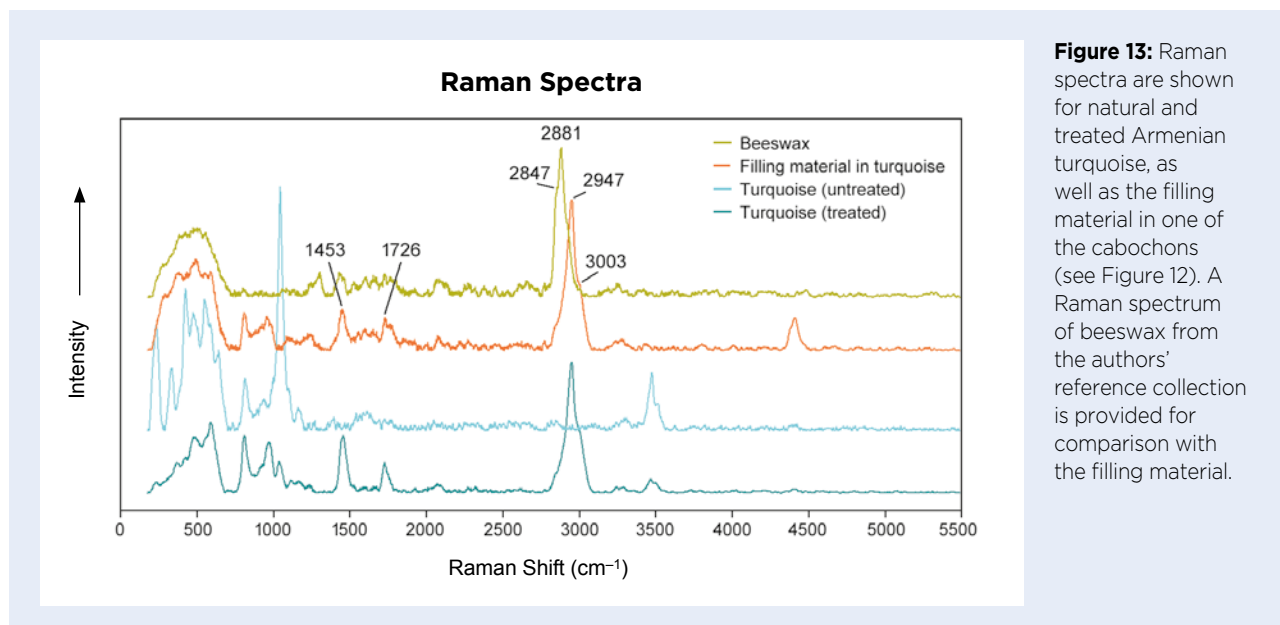
Figure 13: Raman spectra are shown for natural and treated Armenian turquoise, as well as the filling material in one of the cabochons (see Figure 12). A Raman spectrum of beeswax from the authors' reference collection is provided for comparison with the filling material.

References

Čejka, J., Sejkora, J., Macek, I., Malíková, R., Wang, L., Scholz, R., Xi, Y. & Frost, R.L. 2015. Raman and infrared spectroscopic study of turquoise minerals. *Spectrochimica Acta Part A: Molecular and Biomolecular Spectroscopy*, **149**, 173–182, https://doi.org/10.1016/j.saa.2015.04.029.

Kievlenko, E.Y. 2003. *Geology of Gems*. Ocean Pictures Ltd, Littleton, Colorado, USA, 468 pp.

King, R.J. 2002. Turquoise. *Geology Today*, **18**(3), 110–114, https://doi.org/10.1046/j.1365-2451.2002.00345.x.

Miliani, C., Ombelli, M., Morresi, A. & Romani, A. 2002. Spectroscopic study of acrylic resins in solid matrices.

Surface and Coatings Technology, **151–152**, 276–280, https://doi.org/10.1016/s0257-8972(01)01606-1.

Špaldoňová, A., Havelcová, M., Lapčák, L., Machovič, V. & Titěra, D. 2021. Analysis of beeswax adulteration with paraffin using GC/MS, FTIR-ATR and Raman spectroscopy. *Journal of Apicultural Research*, **60**, 73–83, https://doi.org/10.1080/00218839.2020.1774152.

Suchkova, E.M. & Akhmetova, G.L. 1985. Relation of the turquoise structure, composition, and properties with 1st jewelry-decorative quality. *The First Gemological Conference Gemology-1*, Chernogolovka, Russia, 15–17 October, 87–88.

Turquoise from Mongolia

Gem-quality turquoise is known from several localities, including Iran, USA, Egypt, China, Tajikistan, Uzbekistan and Armenia (Kievlenko 2003). However, during a mineral show that took place in May 2018 in Brno, Czech Republic, dealer Ivan Doležal had some interesting untreated rough samples of turquoise from the Erdenetiin Ovoo deposit (also known as Erdenet or Precious Hill) in northern Mongolia. To the authors' knowledge, the gemmological characteristics of Mongolian turquoise have not been reported previously.

Erdenet is the largest porphyry copper-molybdenum mine in Mongolia and is located 240 km north-west of the capital, Ulaanbaatar. According to Gerel *et al.* (2006), the deposit was discovered (by Czech geologists) in 1964 and mining has taken place since 1978. The mineralisation is associated with the Erdenet pluton, which forms part of the Selenge Intrusive Complex of Permo-Triassic age, which intruded the Orkhon-Selenge volcano-sedimentary assemblage. The mineralisation and associated alteration are related to shallow-level porphyritic intrusions (i.e. stocks and dykes). According to Kavalieris *et al.* (2017), the primary ore contains chalcopyrite, chalcocite, covellite, bornite, sphalerite and molybdenite, together with K-feldspar, muscovite, magnetite, clay, gypsum and fluorite. The secondary ore consists of an assemblage of clay, chalcocite, covellite, turquoise and chrysocolla. An oxidised zone originally exposed by erosion at the top of the deposit was 50–100 m thick (before it was removed by mining), and consisted of supergene malachite, azurite, turquoise and powellite.

We cut and polished 10 greenish blue cabochons of the Mongolian turquoise ranging from 5.50 × 5.06 mm to 9.27 × 8.47 mm (e.g. Figure 14). They had RIs of 1.612–1.626 and hydrostatic SG values of 2.71–2.75. Some of the samples contained pyrite, which is commonly found in turquoise from various localities. EDXRF spectroscopy with a Delta Classic Plus handheld spectrometer (configured for analysing metal alloys) detected Cu as a major element, along with some minor Fe, Zn and As. The material's identity as turquoise was confirmed by Raman spectroscopy (e.g. Figure 15a) of three of the cabochons. Interestingly, a recognisable

Figure 14: This rough sample (3.48 g) and cabochon (3.17 ct) of untreated turquoise are from the Erdenet mine in northern Mongolia. The slightly mottled appearance of the cabochon is due to the local presence of matrix material. Photo by J. Štubňa.
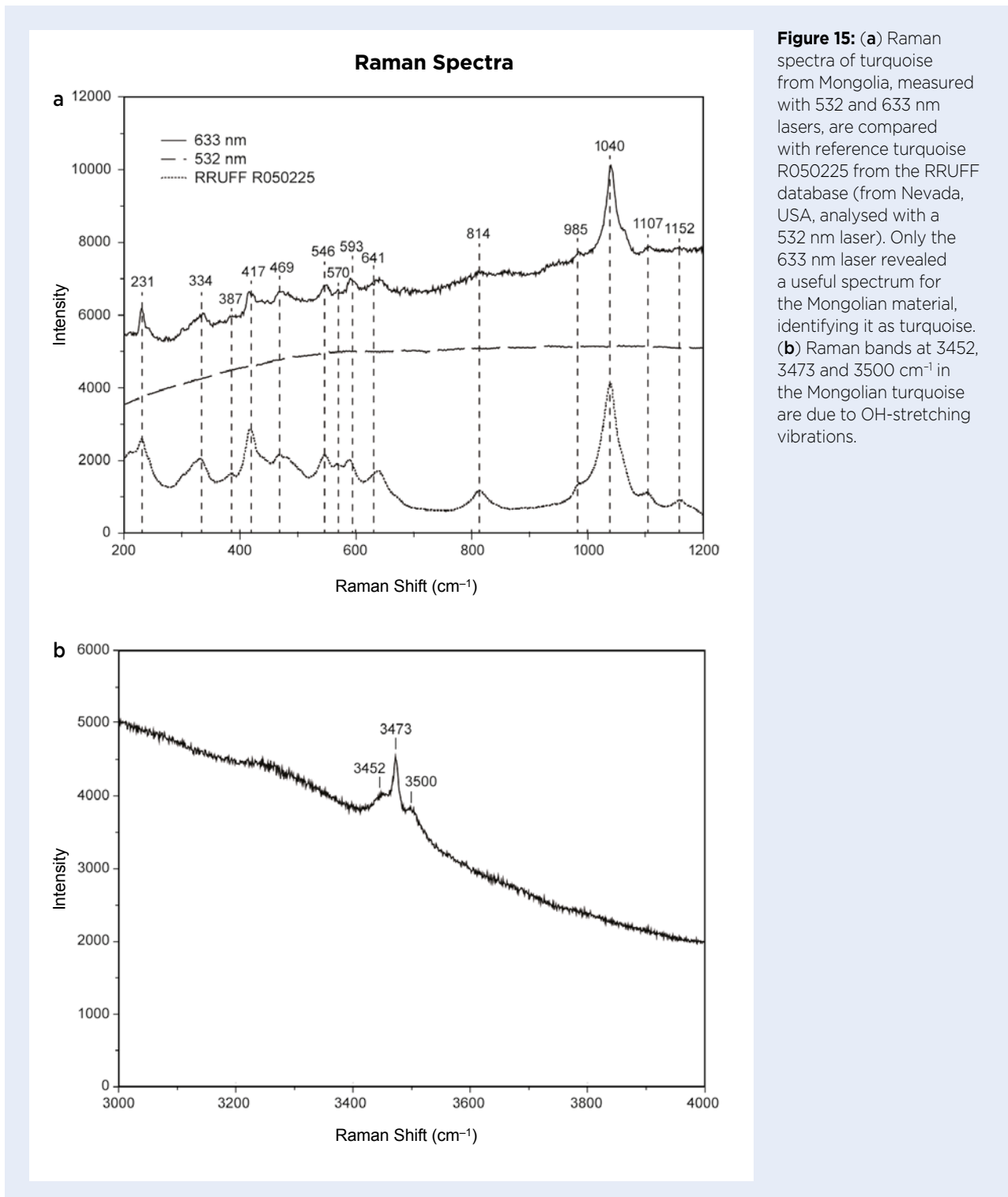
Figure 15: (**a**) Raman spectra of turquoise from Mongolia, measured with 532 and 633 nm lasers, are compared with reference turquoise R050225 from the RRUFF database (from Nevada, USA, analysed with a 532 nm laser). Only the 633 nm laser revealed a useful spectrum for the Mongolian material, identifying it as turquoise. (**b**) Raman bands at 3452, 3473 and 3500 cm⁻¹ in the Mongolian turquoise are due to OH-stretching vibrations.

Raman spectrum was obtained only when using a laser wavelength of 633 nm; analyses with 532 and 473 nm lasers did not produce any Raman scattering. In addition, Figure 15b shows the Raman spectral region of OH-stretching vibrations, which displays bands at 3452, 3473 and 3500 cm⁻¹; these are assigned to hydrogen-bonded, symmetrically distinct hydroxyl groups

(Čejka *et al*. 2015). Powder X-ray diffraction (Figure 16) also confirmed the identification as turquoise, and the following unit-cell parameters were calculated: $a = 7.422(3)$ Å, $b = 7.645(2)$ Å, $c = 9.920(3)$ Å, $\alpha = 68.59(2)°$, $\beta = 69.52(2)°$, $\gamma = 65.02(2)°$ and $V = 462.1(2)$ Å³. Deviations from published unit-cell parameters for turquoise are probably due to substitution of Cu and P
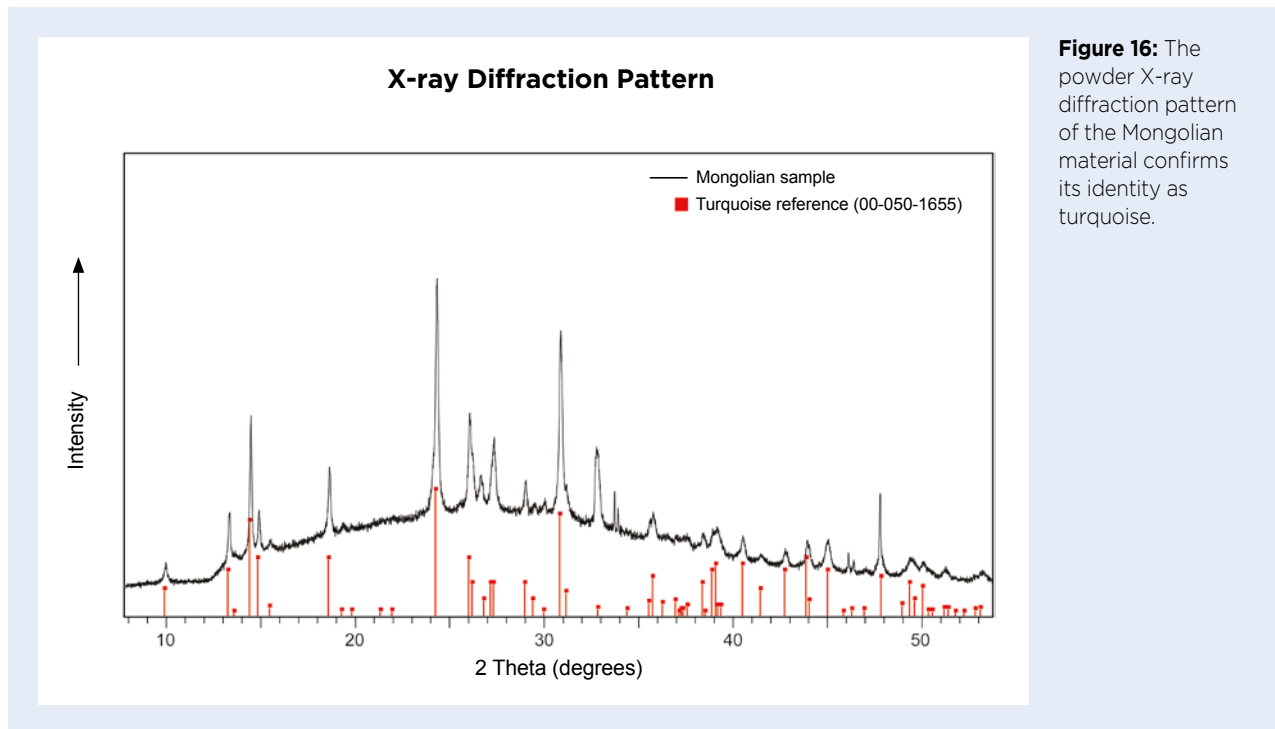
Figure 16: The powder X-ray diffraction pattern of the Mongolian material confirms its identity as turquoise.

by Fe and As, which were detected by EDXRF and have larger ionic radii than Cu ($^{VI}Fe^{2+}$ = 0.78 Å vs $^{VI}Cu^{2+}$ = 0.73 Å) and P ($^{IV}As^{5+}$ = 0.34 Å vs $^{IV}P^{5+}$ = 0.17 Å).

Rough turquoise from Mongolia is available on the domestic market, where it is being sold by the company that is mining the deposit (Erdenet Mining Corp.).

Dr Ján Štubňa (janstubna@gmail.com)
Gemmological Laboratory, Constantine the
Philosopher University, Nitra, Slovakia

Dr Peter Bačík and Dr Jana Fridrichová
Comenius University, Bratislava, Slovakia

Dr Radek Hanus
Gemological Laboratory of e-gems.cz
Prague, Czech Republic

References

Čejka, J., Sejkora, J., Macek, I., Malíková, R., Wang, L., Scholz, R., Xi, Y. & Frost, R.L. 2015. Raman and infrared spectroscopic study of turquoise minerals. *Spectrochimica Acta Part A: Molecular and Biomolecular Spectroscopy*, **149**, 173–182, https://doi.org/10.1016/j.saa.2015.04.029.

Gerel O., Dandar, S., Myagmarsuren, S. & Soyolmaa, B. 2006. Cu-Mo porphyry deposit of the Erdenetiin Ovoo: An environmental study. *Atlantic Geology*, **42**(1), 86.

Kavalieris, I., Khashgerel, B.-E., Morgan, L.E., Undrakhtamir, A. & Borohul, A. 2017. Characteristics and $^{40}Ar/^{39}Ar$ geochronology of the Erdenet Cu-Mo deposit, Mongolia. *Economic Geology*, **112**(5), 1033–1054, https://doi.org/10.5382/econgeo.2017.4500.

Kievlenko, E.Y. 2003. *Geology of Gems*. Ocean Pictures Ltd, Littleton, Colorado, USA, 468 pp.

PEARLS

Molluscs Artificially Filled with Cultured Pearls of Various Colours

In recent years, cultured pearls of various colours have become widespread in online marketplaces and social media sales channels—in some cases via streaming to a live audience. Recently, some sellers began offering pearl-producing molluscs in vacuum-sealed packages, which buyers unseal and open themselves to reveal cultured pearls of various colours. In most cases, these products are advertised as saltwater oysters containing pearls with more than 50 possible colours.

We purchased 23 of these molluscs from various
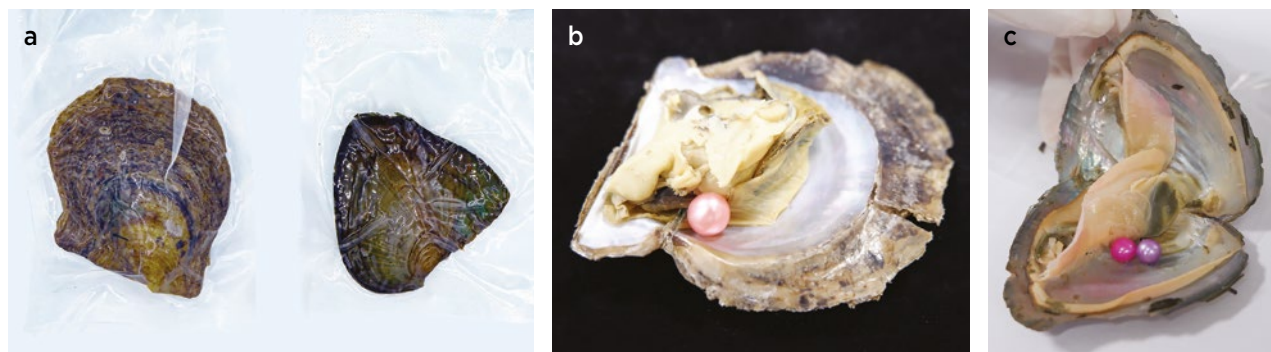
Figure 17: (**a**) A saltwater *Pinctada* sp. mollusc (left) and freshwater *Hyriopsis* sp. mussel (right) are shown here in vacuum-sealed packages that are representative of such products being sold online. A newly opened saltwater mollusc (**b**) and freshwater mussel (**c**) reveal that the cultured pearls they contain are not implanted in the gonad or mantle, respectively, but appear to have been placed in the shells after being previously harvested. Note also the artificial colour appearance of the cultured pearls and the lack of corresponding colouration in the nacre of the shells. Each shell measures approximately 5 × 6 cm; photos by M. Seneewong-Na-Ayutthaya.

e-commerce platforms based in China. They turned out to consist of 16 saltwater molluscs and seven freshwater mussels (e.g. Figure 17a). Upon opening them, we found a total of 28 cultured pearls measuring 6.20–8.10 mm in diameter and weighing 1.80–3.50 ct. They showed various colours: white, cream, yellow, orange, pink, purple, brown and blue (e.g. Figure 18). Most of the colours were quite unnatural and indicated a dyed origin, and this was supported by microscopic evidence (e.g. uneven colouration and residues concentrated along surface-reaching fractures).

Pearls typically grow in either the gonad (saltwater mollusc) or mantle (freshwater mussel) tissues, regardless of whether they form naturally or are cultivated with human intervention (Cartier *et al.* 2012). However, in the mollusc samples we acquired, they were not found in either the gonad or mantle areas. Instead, it was clear they had been placed into the shells after being previously harvested (Figure 17b, c).

X-radiography revealed that all of our samples (from both the freshwater and saltwater molluscs) were non-beaded freshwater cultured pearls (e.g. Figure 19). EDXRF analyses yielded 0.12–0.52 wt.% MnO and 0.32–0.70 wt.% SrO; the SrO/MnO ratios of 0.35–3.50 were consistent with a freshwater origin for these cultured pearls (cf. Abduriyim 2018).

Raman spectroscopy showed peaks at 1085 and 706 cm^{-1}, which indicate that aragonite/calcite is the major constituent of these cultured pearls. Natural-colour cultured pearls of freshwater origin with orange, pink and purple colouration often show Raman bands at 1532 and 1134 cm^{-1} related to their organic pigments (Otter *et al.* 2017). By comparison, the present cultured pearl samples (which showed brighter, unnatural colours) did not produce any such Raman bands, consistent with being artificially dyed. In addition, UV-Vis reflectance spectroscopy of our yellow, blue, pink and purple samples also showed evidence of dyeing (Figure 20). Only the yellow sample possessed a colour that could be found naturally, but it displayed a prominent absorption band at around 450 nm that is known to occur in dyed deep yellow to golden coloured cultured pearls (Kwak *et al.* 2016).

Figure 18: Various colours—some of them quite artificial in appearance—are exhibited by these selected cultured pearls (6.20–8.10 mm in diameter) that were recovered from the mollusc samples acquired from online sellers. Photo by M. Seneewong-Na-Ayutthaya.
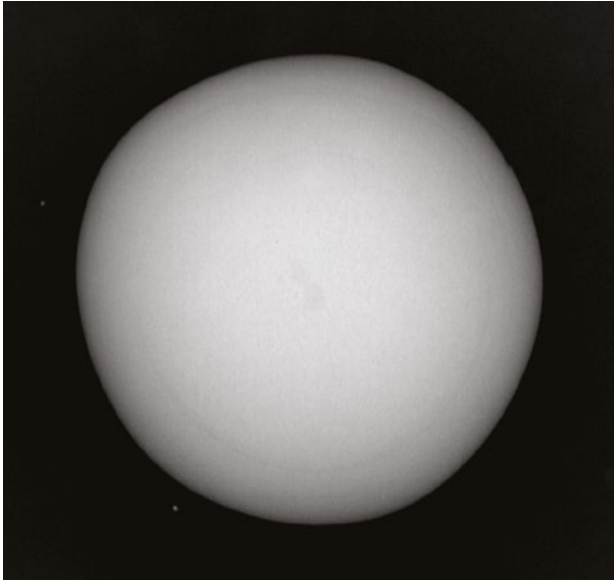
Figure 19: X-radiography of the samples obtained in this investigation showed that they all were non-beaded freshwater cultured pearls, as shown by this 6.55-mm-diameter example. Image by M. Seneewong-Na-Ayutthaya.

strategy of these products gives a misleading impression to the consumer that they are saltwater cultured pearls which were produced by the molluscs containing them. Even though the cultured pearls can be personally 'collected' from these molluscs, this clearly does not preclude them from being dyed (or natural-coloured) products that were inserted into the shells after being previously harvested.

Dr Montira Seneewong-Na-Ayutthaya
(smontira@git.or.th)
and Wassana Chongraktrakul
Gem and Jewelry Institute of Thailand
Bangkok, Thailand

Yadawadee Kowinthaweewat
Srinakharinwirot University
Bangkok, Thailand

Regardless of the saltwater or freshwater origin of the mollusc samples obtained for this study, they were all found to contain non-beaded freshwater cultured pearls, most of which were dyed. The marketing
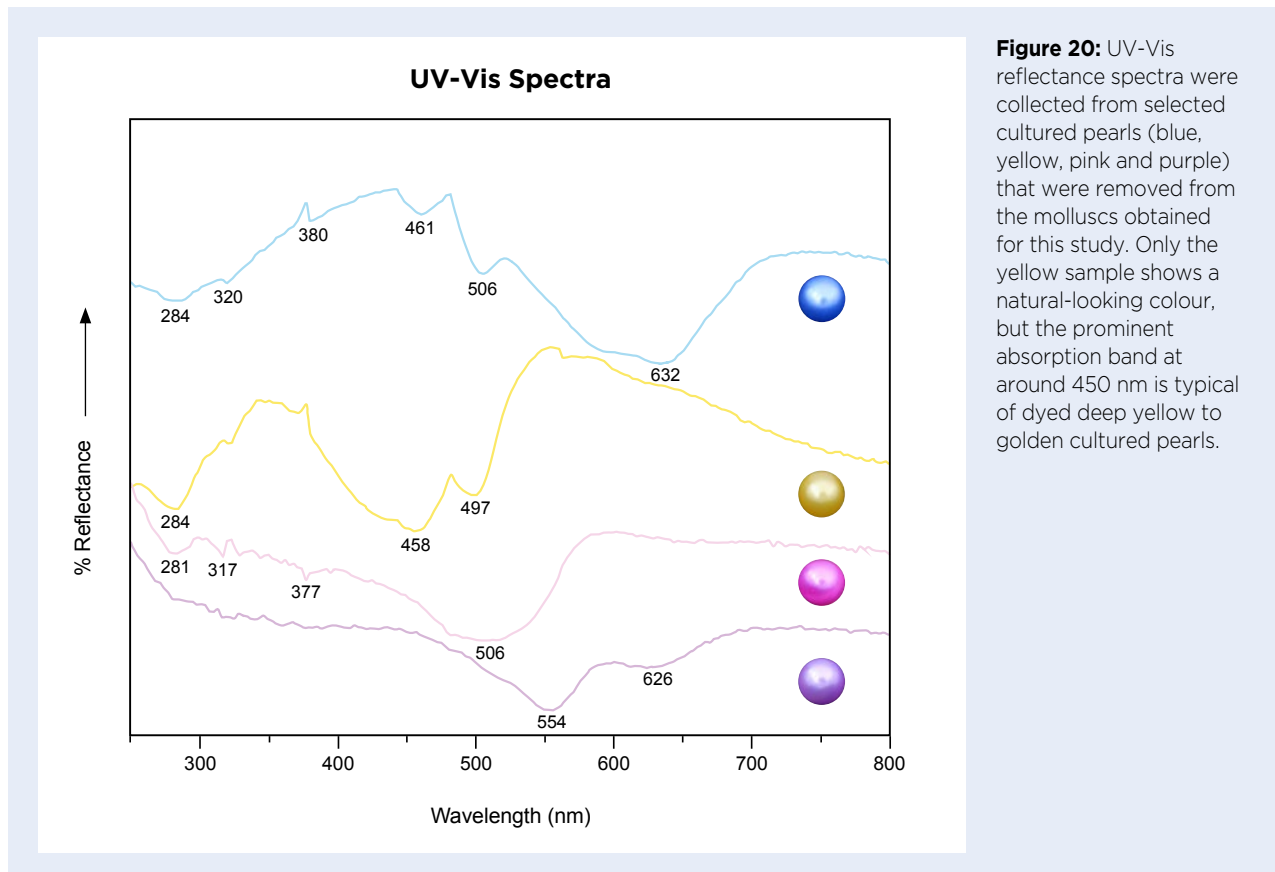
Figure 20: UV-Vis reflectance spectra were collected from selected cultured pearls (blue, yellow, pink and purple) that were removed from the molluscs obtained for this study. Only the yellow sample shows a natural-looking colour, but the prominent absorption band at around 450 nm is typical of dyed deep yellow to golden cultured pearls.

References

Abduriyim, A. 2018. Cultured pearls from Lake Kasumigaura: Production and gemological characteristics. *Gems & Gemology*, **54**(2), 166–183, https://doi.org/10.5741/GEMS.54.2.166.

Cartier, L.E., Krzemnicki, M.S. & Ito, M. 2012. Cultured pearl farming and production in the Federated States of Micronesia. *Gems & Gemology*, **48**(2), 108–122, https://doi.org/10.5741/gems.48.2.108.

Kwak, K.-W., Lee, J.-K. & Jeong, E.-A. 2016. Identification of dyed golden South Sea pearls using UV-Vis and PL tests. *Journal of the Gemmological Association of Hong Kong*, **37**, 58–61.

Otter, L.M., Agbaje, O.B.A., Huong, L.T.-T., Hager, T. & Jacob, D.E. 2017. Akoya cultured pearl farming in eastern Australia. *Gems & Gemology*, **53**(4), 423–437, https://doi.org/10.5741/gems.53.4.423.

An Unusual Black Natural Pearl from Mytilidae

In October 2020, the Netherlands Gemmological Laboratory received a pendant for testing from a client who wanted to auction the jewellery. The pendant was set with Old European brilliant-cut, eight-cut and small rose-cut diamonds with a dark brown-to-black, button-shaped pearl that hung next to a pendant diamond (about 1 ct; Figure 21a). The diameter of the pearl measured about 7.0 mm and its height was approximately 5 mm (Figure 21b).

Under a standard daylight-equivalent lamp the pearl appeared very dark brown to almost black. However, when viewed with a microscope using focused fibre-optic illumination, the pearl showed a reddish brown overtone, with slightly transparent areas near the surface. The pearl's surface showed a classic nacreous structure with overlapping layers (Figure 22). It fluoresced very weak, slightly reddish brown to long-wave UV radiation, and weak brown to short-wave UV.

An X-radiograph of the pearl showed some concentric layers, indicating a natural structure, along with some thin cracks near the drill hole. EDXRF analysis showed a Mn content close to the detection limit and about 0.7 wt.% SrO, indicating a saltwater origin.

Raman analysis using a 532 nm laser (Figure 23) revealed a sharp, intense band at about 1086 cm^{-1} and a doublet at 701 and 706 cm^{-1} associated with the v_1 symmetric mode and v_4 in-plane mode, respectively, along with some lattice modes below 400 cm^{-1}, all typical for carbonate ions in aragonite (cf. Urmos *et al.* 1991). The Raman spectrum also displayed two prominent bands at around 1100 and 1485 cm^{-1}, along with weak bands at about 1015 and 1295 cm^{-1} indicating the presence of pigments with polyenic chains (i.e. one or more sequences of alternating double and single carbon bonds), thus confirming the colour was natural. Polyenic molecules generate two main characteristic vibrations (v_1 and v_2).

Figure 21: This antique diamond-set pendant contains an unusual dark pearl (7.0 mm in diameter). (**a**) From the front, the pearl looks perfectly round, but (**b**) from the side the button shape can be seen. Photos by (a) Dirk van der Marel and (b) J. C. Zwaan.
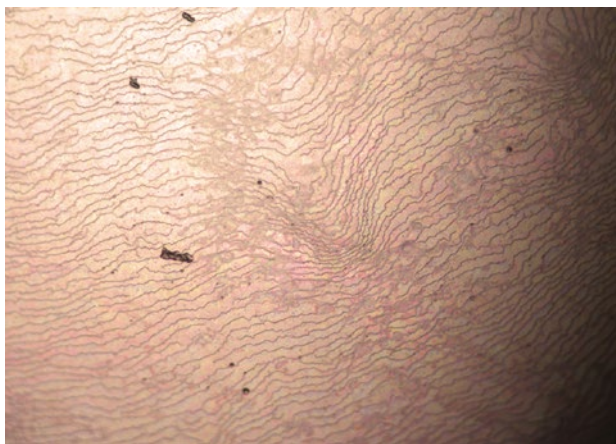
Figure 22: With magnification, the classic nacreous structure (overlapping layers) can be seen on the surface of the pearl. Photomicrograph by J. C. Zwaan; image width 0.6 mm.

In the 1450–1600 cm^{-1} range the ν_1 vibration occurs due to stretching of C=C double bonds, and in the 1100–1200 cm^{-1} range the ν_2 vibration is due to stretching of C-C single bonds (coupled with C–H in-plane bending modes when four methyl groups are attached to the chain). The positions of these bands depend strongly on the exact number of C=C bonds in the polyenic chain; longer chains yield vibrations at shorter wavenumbers (e.g. Karampelas *et al.* 2019).

However, the present Raman spectrum is unusual because the colour of most black nacreous saltwater pearls (such as those from the molluscs *Pinctada margaritifera* or *Pteria* sp.) is caused by tetrapyroles (porphyrin pigments), not by polyenes, which present different spectral features (e.g. Kiefert *et al.* 2004; Karampelas *et al.* 2019). Raman bands due to polyenic pigments (partially methylated polyenes) can be present in pearls from various mollusc species, but these pigments are rarely found in nacreous saltwater pearls; to date, only those coming from *P. radiata*, *P. fucata* and Mytilidae are known (see again Karampelas *et al.* 2019). The position of the polyenic Raman bands (shifted towards lower wavenumbers) indicates the presence of a polyenic pigment with an unusually long chain (with around 14 C=C double bonds). So far, this particular pigment has only been observed in Mytilidae pearls (Karampelas & Erel 2009; Karampelas *et al.* 2019). Species of Mytilidae bivalves are found worldwide, but they are more abundant in colder seas. Natural pearls, mostly small (<5 mm) and of blue colour, are found in *Mytilus* sp. which largely occur in North America and in the coastal waters of north and north-west Europe (Fernandes & Seed 1983). However, Mytilidae pearls of darker colour and larger sizes have been described, presumably from *Modiolus* sp. fished off the Philippines (Laurs 2016). The authors are not aware of any pearl cultivation using Mytilidae bivalves. Regardless of the bivalve species, this pearl is a truly unique item because Mytilidae pearls of this colour and size are rarely encountered.

Dr J. C. (Hanco) Zwaan FGA
(hanco.zwaan@naturalis.nl)
Netherlands Gemmological Laboratory
Naturalis Biodiversity Center
Leiden, The Netherlands

Dr Stefanos Karampelas
Laboratoire Français de Gemmologie
Paris, France

References

Fernandes, F.C. & Seed, R. 1983. The incidence of pearls in populations of the blue mussel, *Mytilus edulis* L., from North Wales. *Journal of Molluscan Studies*, **49**(2), 107–115, https://doi.org/10.1093/oxfordjournals.mollus.a065700.

Karampelas, S. & Erel, E. 2009. Gem News International: Rare necklace made of natural pearls from different mollusks. *Gems & Gemology*, **45**(2), 149–150.

Karampelas, S., Fritsch, E., Makhlooq, F., Mohamed, F. & Al-Alawi, A. 2019. Raman spectroscopy of natural and cultured pearls and pearl producing mollusc shells. *Journal of Raman Spectroscopy*, **51**(9), 1813–1821, https://doi.org/10.1002/jrs.5670.

Figure 23: The Raman spectrum of the pearl shows bands typical for aragonite (i.e. below 400 cm^{-1} and at 701–706 and 1086 cm^{-1}), as well as bands associated with molecules containing long, partially methylated, polyenic chains causing the dark colour (1015, 1100, 1295 and 1485 cm^{-1}).

Kiefert, L., Moreno, D.M., Arizmendi, E., Hänni, H.A. & Elen, S. 2004. Cultured pearls from the Gulf of California, Mexico. *Gems & Gemology*, **40**(1), 26–38, https://doi.org/10.5741/gems.40.1.26.

Laurs, B.M. 2016. Gem Notes: Natural mussel pearls from the Philippines. *Journal of Gemmology*, **35**(1), 25.

Urmos, J., Sharma, S.K. & Mackenzie, R.T. 1991. Characterization of some biogenic carbonates with Raman spectroscopy. *American Mineralogist*, **76**(3–4), 641–646.

Visit to a Gold-Lipped Cultured Pearl Farm in Myanmar

Figure 24: These silver and golden Myanmar cultured pearls were harvested in February 2020 and range from 9.25 to 13.92 mm in diameter. They are shown resting on a *P. maxima* shell. Photo by Tay Thye Sun.

Cultured pearls from Myanmar are famous for their silver to golden colour (e.g. Figure 24). Pearl cultivation takes place in the Mergui (or Myeik) Archipelago in the Andaman Sea off southern Myanmar. The Myanmar pearl-farming industry started in 1954 as a joint venture between the Burma Pearl Fishing and Culture Syndicate and the Japanese pearl farmer Kichiro Takashima, under the name South Sea Pearl Co. The industry has expanded to a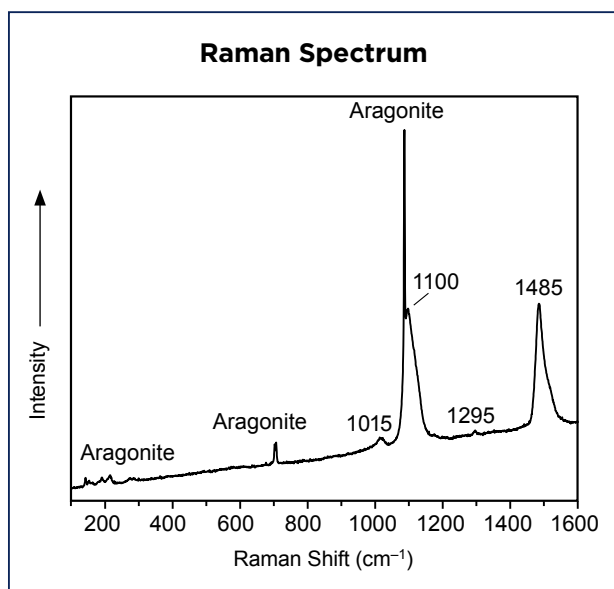bout 11 joint-venture companies with operations distributed across various islands of the Mergui Archipelago (Sze Man 2018, 2019). Based on an economic report by Khin Chaw Myint (2009), at that time the pearl-culturing industry employed about 30% of the local population.

In February 2020, the authors visited a pearl farm at Pa Lel Kyun (formerly known as Sir J. Malcolm Island) or, as it is called by the locals, Pearl Island. We began our journey in Myeik (the capital city of Tanintharyi Region) and travelled for nearly five hours by speedboat to reach the island. The pearl farm was operated by Myanmar Pearl Enterprise (MPE), and it occupied an area of about 10.3 × 3.9 km, extending to about 12.6 km offshore. The mollusc used for pearl cultivation was *Pinctada maxima*, or the South Sea gold-lipped oyster (Tint Tun 1998; Strack 2006).

The pearl farm's office and operation centre were situated in a small bay on the island (Figure 25). MPE deputy general manager Myo Lwin and his staff guided us through the areas where the oyster spat cultivation took place. MPE established the original hatchery hall in the 1980s, but in 1998 they added a modern facility to increase spat production. A temperature-controlled room (kept at 20°C) is used for cultivating phytoplankton to feed the oyster spat. The spat grow in tanks where they hang on strings for about 28 days, with about 200 spat on each string and 96–160 strings in each tank. After the spat have grown to about 12 mm (or about 60 days), they are transferred to small frames surrounded by netting, with each frame holding only 12 spat to encourage their growth. The frames are suspended in the ocean for approximately two months and then the spat are transferred to new frames. After 18 months

Figure 25: This view of the pearl farm at Pa Lel Kyun (or Pearl Island) shows office buildings and hatchery halls used for oyster spat cultivation (left), as well as floating huts where the spat and implanted oysters are cleaned (right). Photo by Tay Zar Linn.

Figure 26: A staff member at the pearl farm demonstrates insertion of a bead nucleus into an oyster. Implantation is done when the oysters reach about 12 mm in size. Photo by Tay Thye Sun.

Figure 27: The seeded oysters are placed in a panel net, which is suspended in the ocean (with regular tending) for two years before harvesting. Photo by Tay Thye Sun.

the oysters reach about 12 cm in size, and then each one is implanted with a bead nucleus (Figure 26). The bead is made of shell (4.5–7.0 mm in diameter) and is inserted along with a piece of mantle issue from a donor mollusc. The seeded oysters are then placed in panel nets (Figure 27) and returned to the ocean for two years before harvesting. During this period the oysters receive monthly cleaning by hand and pressure washer to remove parasites such as barnacles, sponges and burrowing worms.

All of the cultured pearls are sent to MPE's headquarters in Nay Pyi Daw. They are sold through auctions in Nay Pyi Daw (hosted by Myanma Gem Enterprise) and in Hong Kong. MPE managing director Min Min Oo indicated that Myanmar's South Sea cultured pearls have gained global attention since they were first auctioned in Hong Kong in 2013. Myanmar's cultured pearl production rose to 568,320 momme in 2018–2019, up from 424,628 momme in 2014–2015. Since 2014, Myanmar has produced nearly four million cultured pearls equivalent to 2.5 million momme (Sto. Domingo 2020). According to MPE, from 2019 to 2020 about 1.3 million cultured pearls were produced that weighed 764,151 momme.

Dr Tay Thye Sun (tay@gem.com.sg)
Far East Gem Lab, Singapore

Dr Thet Tin Nyunt
Department of Geological Survey
and Mineral Exploration
Ministry of Natural Resources and
Environmental Conservation
Myanma Gems Museum, Nay Pyi Taw, Myanmar

Myo Lwin
Myanmar Pearl Enterprise
Ministry of Natural Resources and
Environmental Conservation
Myeik, Myanmar

Tay Zar Linn
Myanmar Pearl Enterprise
Ministry of Natural Resources and
Environmental Conservation
Myanma Gems Museum, Nay Pyi Taw, Myanmar

References

Khin Chaw Myint 2009. Pearl culturing industry and regional employment generation. *Yangon Institute of Economics Research Journal*, **1**(1), 88–97.

Sto. Domingo, B. 2020. Myanmar eyes solid footing in global pearl market. *JNA*, No. 419, 60–61.

Strack, E. 2006. *Pearls*. Ruhle-Diebener-Verlag, Stuttgart, Germany, 696 pp.

Sze Man, Y. 2018. Myanmar pearl dealer eyes Asia. *JNA*, No. 404, 46–47.

Sze Man, Y. 2019. Myanmar finds footing in global pearl sector. *Pearl Report 2019*. Informa Markets, Hong Kong, 36–38.

Tint Tun 1998. Myanmar pearling: Past, present and future. *SPC Pearl Oyster Information Bulletin*, No. 12, 3–7.

SYNTHETICS AND SIMULANTS

Near-Colourless CVD Synthetic Diamond with Uncompensated Boron

Gem-quality synthetic diamonds produced by chemical vapour deposition (CVD) began to appear on the Chinese gem market in around 2012 (e.g. Lu *et al.* 2019). Most colourless to near-colourless CVD-grown samples are type IIa. Gem-quality type IIb CVD synthetics are quite rare, and the few reported samples have been distinctly blue or brown (Martineau *et al.* 2004; Wang & Moses 2008; Eaton-Magaña 2012). Recently, however, the National Gemstone Testing Center's Beijing laboratory examined a near-colourless type IIb CVD synthetic diamond that showed some unusual properties.

The sample consisted of a round brilliant weighing 0.66 ct and measuring 5.48–5.54 × 3.45 mm, with a colour grade of J (slight brown hue) and clarity of SI_1. With magnification, it showed strong graining and contained some black non-diamond carbon inclusions (Figure 28). Viewed with crossed polarisers, it displayed strong anomalous birefringence with low- to high-order interference colours (Figure 29). The strain patterns were linear or grid-like, rather than the tatami structure typical of type IIa natural diamonds (e.g. Howell 2012). The sample fluoresced very weak yellow to long-wave UV radiation and weak orange to short-wave UV. No phosphorescence or electrical conductivity was observed.

Figure 29: Strong birefringence is displayed by the CVD synthetic diamond when observed between crossed polarisers. Photomicrograph by Z. Song; magnified 32×.

The DiamondView showed moderately strong orangey red fluorescence with a grid-like pattern of blue fluorescence (Figure 30a). The images demonstrate that the sample had a rather inhomogeneous defect composition. In addition, parallel banding was seen on the pavilion (Figure 30b), indicating that interruptions occurred during the CVD growth process (Eaton-Magaña & Shigley 2016). A moderately strong bluish green phosphorescence was also observed (Figure 30c, d).

The infrared spectrum revealed no detectable nitrogen, but distinct absorption features were recorded at 4090, 2925 and 2800 cm^{-1} due to uncompensated boron (Gaillou *et al.* 2015). The concentration of the uncompensated boron was calculated at about 0.005 ppm (cf. Collins 2010). We also observed weak absorptions related to hydrogen at 7353, 6855, 6425 and 5565 cm^{-1} in the near-infrared region (Martineau *et al.* 2004).

The UV-Vis-NIR spectrum, collected at liquid-nitrogen temperature, showed a smooth, gradual increase in absorption from long to short wavelengths in the visible region. Also observed was a strong, broad band due to isolated nitrogen centred at about 270 nm, as well as a weak absorption from the $Si-V^-$ defect at 737 nm.

PL spectra were collected at liquid-nitrogen temperature with 532 nm (green) and 473 nm (blue) laser excitation.

Figure 28: Non-diamond carbon inclusions are present in the CVD synthetic diamond described here. Photomicrograph by H. Dai; magnified 25×.
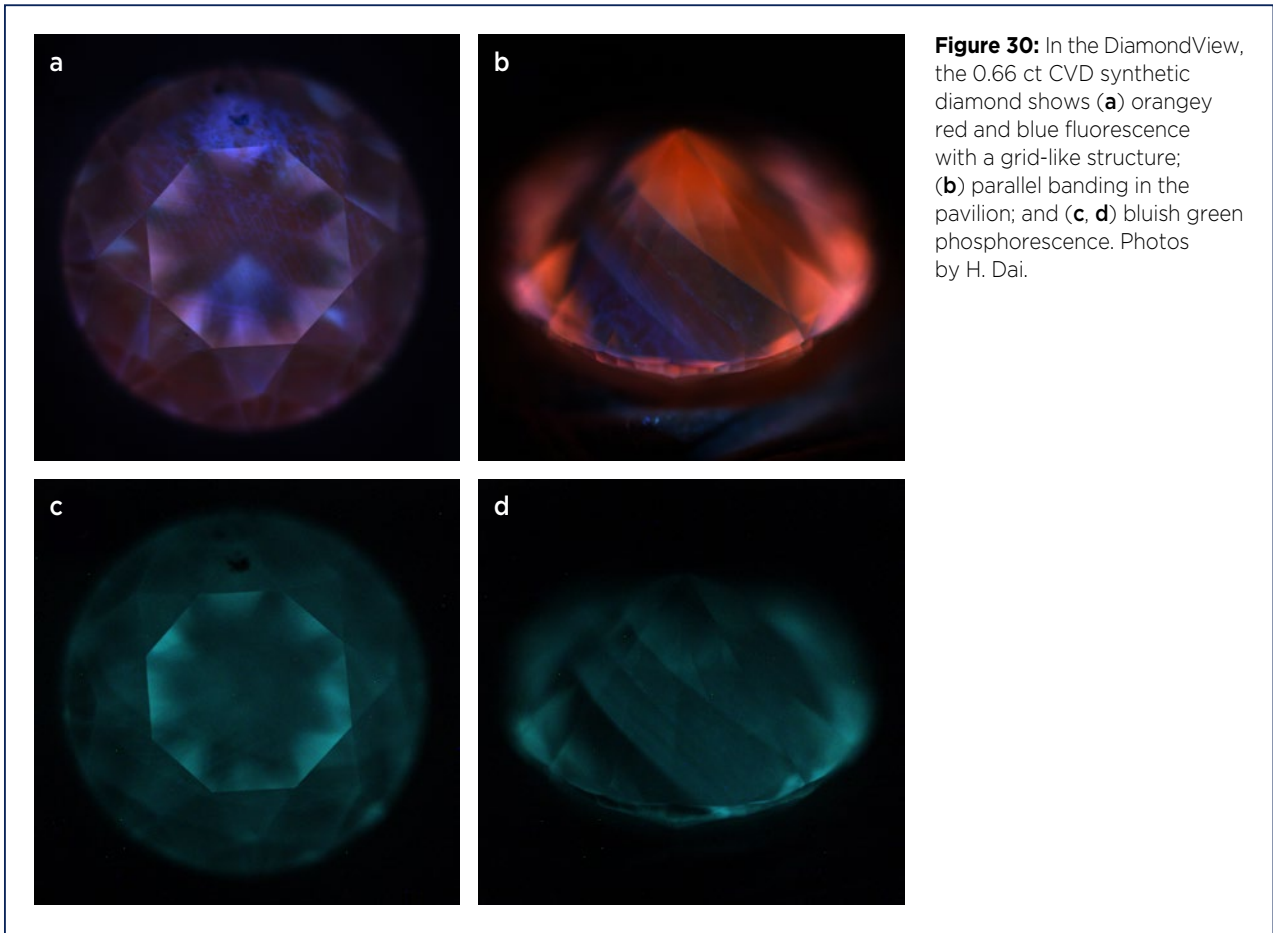
Figure 30: In the DiamondView, the 0.66 ct CVD synthetic diamond shows (**a**) orangey red and blue fluorescence with a grid-like structure; (**b**) parallel banding in the pavilion; and (**c**, **d**) bluish green phosphorescence. Photos by H. Dai.

With the green laser (Figure 31), the sample displayed very strong emission from the Si-V⁻ defect at 736.6/736.9 nm, as well as strong and moderate emissions due to N-V⁰ and N-V⁻ centres (zero-phonon lines at 575 and 637 nm, respectively). Clear emissions at 596.5 and 597.0 nm were also recorded, indicating that the sample had not
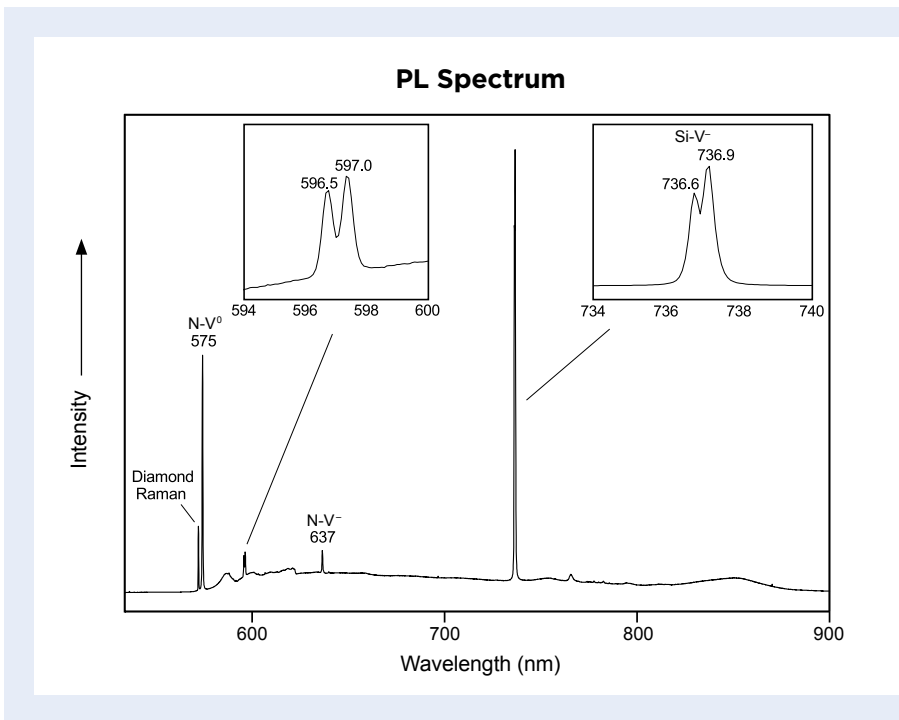
Figure 31: With green laser (532 nm) excitation, the PL spectrum of the synthetic diamond exhibits features consistent with an extremely high concentration of Si-V⁻ defects, abundant N-V⁰ centres and a moderate amount of N-V⁻ centres. In addition, emissions at 596.5 and 597.0 nm indicate the sample has not been subjected to post-growth HPHT processing.

been subjected to post-growth high-pressure, high-temperature (HPHT) processing (Eaton-Magaña & Shigley 2016). The PL spectrum collected with the blue laser revealed sharp peaks at 477.0 and 482.0 nm, as well as weak but sharp peaks at 479.5, 485.6 and 489.4 nm.

The gemmological and spectroscopic features confirmed this was an as-grown type IIb CVD synthetic diamond containing a very small amount of isolated nitrogen. The relatively good (near-colourless) colour grade combined

with its boron content is unusual. In addition, its distinctive DiamondView pattern and extremely high concentration of Si-V⁻ defects are also anomalous compared to CVD synthetic diamonds documented previously.

Huiru Dai (478202834@qq.com), Zhonghua Song,
Dr Taijin Lu and Yongwang Ma
National Gemstone Testing Center
Beijing, China

References

Collins, A.T. 2010. Determination of the boron concentration in diamond using optical spectroscopy. *61st Diamond Conference*, University of Warwick, 13–16 July 2010, abstract P5 (unpublished).

Eaton-Magaña, S. 2012. Lab Notes: Type IIb CVD synthetic diamond. *Gems & Gemology*, **48**(3), 213.

Eaton-Magaña, S. & Shigley, J.E. 2016. Observations on CVD-grown synthetic diamonds: A review. *Gems & Gemology*, **52**(3), 222–245, https://doi.org/10.5741/gems.52.3.222.

Gaillou, E., Post, J.E., Byrne, K.S. & Butler, J.E. 2015. Study of the Blue Moon diamond. *Gems & Gemology*, **50**(4), 280–286, https://doi.org/10.5741/gems.50.4.280.

Howell, D. 2012. Strain-induced birefringence in natural diamond: A review. *European Journal of Mineralogy*, **24**(4), 575–585, https://doi.org/10.1127/0935-1221/2012/0024-2205.

Lu, T., Ke, J., Lan, Y., Song, Z., Zhang, J., Tang, S., Su, J., Dai, H. *et al.* 2019. Current status of Chinese synthetic diamonds. *Journal of Gemmology*, **36**(8), 748–757, https://doi.org/10.15506/JoG.2019.36.8.748.

Martineau, P.M., Lawson, S.C., Taylor, A.J., Quinn, S.J., Evans, D.J.F. & Crowder, M.J. 2004. Identification of synthetic diamond grown using chemical vapor deposition (CVD). *Gems & Gemology*, **40**(1), 2–25, https://doi.org/10.5741/gems.40.1.2.

Wang, W. & Moses, T.M. 2008. Lab Notes: Gem-quality CVD synthetic diamond with traces of boron. *Gems & Gemology*, **44**(2), 158–159.

HPHT-Grown Near-Colourless Synthetic Diamond with Detectable GR1 Defect

Recently, NGTC's Beijing laboratory received a 1.00 ct round brilliant with a very pale blue tinge that was mounted in a ring (Figure 32). Magnification revealed

clusters of dark inclusions (probably graphite; Figure 33). The mid-infrared absorption spectrum (5500–500 cm⁻¹ range, 4.0 cm⁻¹ resolution) recorded at room temperature
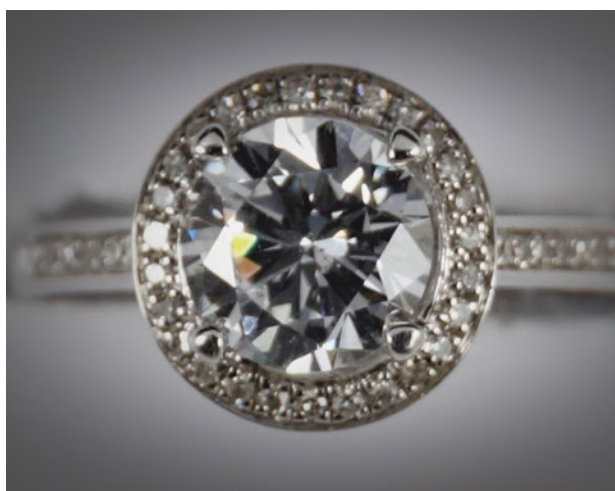
Figure 32: The 1.00 ct round brilliant in this ring was identified as a type IIb HPHT-grown synthetic diamond containing GR1 defects. Photo by B. Gao.
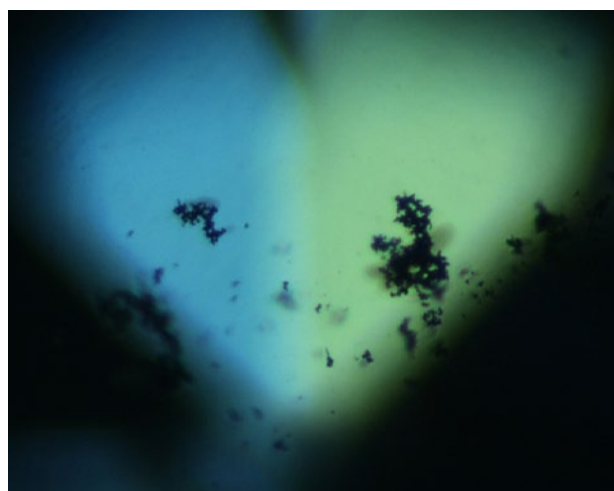
Figure 33: Dark inclusions (probably graphite) are visible through the table facet of the synthetic diamond. Photomicrograph by Z. Song; magnified 50×.
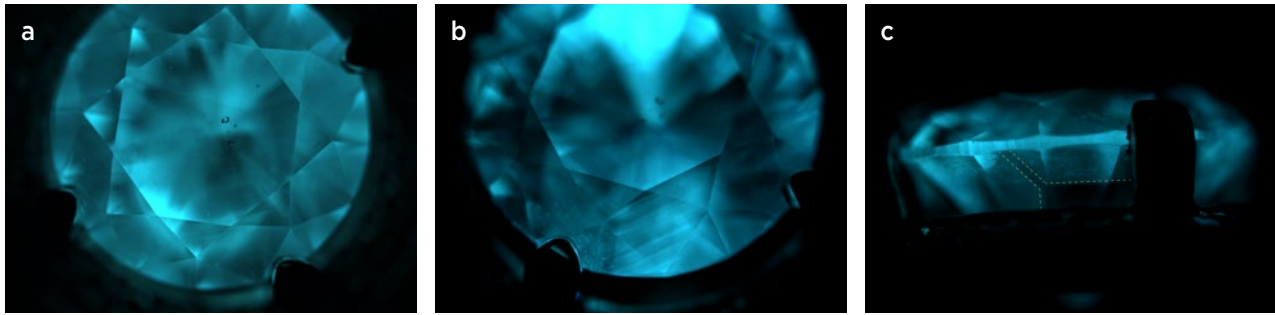
Figure 34: Examination of the 1.00 ct synthetic diamond with the DiamondView reveals (**a**) greenish blue luminescence and a very faint growth pattern visible through the table facet; (**b**) slightly more distinct growth zoning seen through some crown facets when viewed at an angle; and (**c**) a cuboctahedral growth pattern (marked with dashed lines) in the pavilion when observed from the side. Photos by Z. Song.

showed distinct bands at 4090 and 2800 cm^{-1}, which indicated that it was a type IIb diamond with uncompensated boron (cf. D'Haenens-Johansson *et al.* 2014).

In the DiamondView (Figure 34), the sample showed greenish blue fluorescence, with nearly invisible growth sectors under the table facet. Since the sample was mounted, we could not observe it from the pavilion direction. Nevertheless, careful observation from various angles showed the presence of very faint cuboctahedral growth sectors, indicating that it was a synthetic diamond. It also displayed very strong and long-lasting blue phosphorescence, consistent with an HPHT-grown origin.

PL spectra obtained at liquid-nitrogen temperature with 473 and 532 nm excitation showed some unusual features. The 473 nm laser (Figure 35a) produced peaks at 489.5 and 489.8 nm (related to radiation; Song *et al.* 2020), as well as the 3H centre at 503.5 nm (related to interstitial

carbon atoms and radiation; Wang & Moses 2005). The 532 nm laser (Figure 35b) yielded a distinct peak at 575 (NV^0), as well as weak peaks at 637 (NV$^-$) and 741 nm (GR1). We also detected a doublet emission at 883 and 884 nm (related to Ni; Eaton-Magaña *et al.* 2017).

Most HPHT-grown colourless to near-colourless synthetic diamonds are type IIa or IIa+IIb with greenish blue fluorescence, moderate to strong long-lasting phosphorescence and a cuboctahedral growth pattern. They can usually be distinguished from natural diamonds based on their fluorescence colour and growth pattern. The synthetic diamond described here is unusual due to its faint growth pattern and the presence of the GR1 defect detected with PL spectroscopy. The GR1 centre is often found in untreated natural type IIa diamonds, but this is the first time that this defect has been found in an as-grown HPHT synthetic diamond submitted to

Figure 35: (**a**) The PL spectrum of the synthetic diamond obtained with 473 nm excitation shows peaks at 489.5 and 489.8 nm related to radiation, as well as the 3H centre at 503.5 nm that is due to interstitial carbon atoms and radiation. (**b**) Excitation with the 532 nm laser shows peaks at 575 (NV^0), 637 (NV$^-$) and 741 nm (GR1).
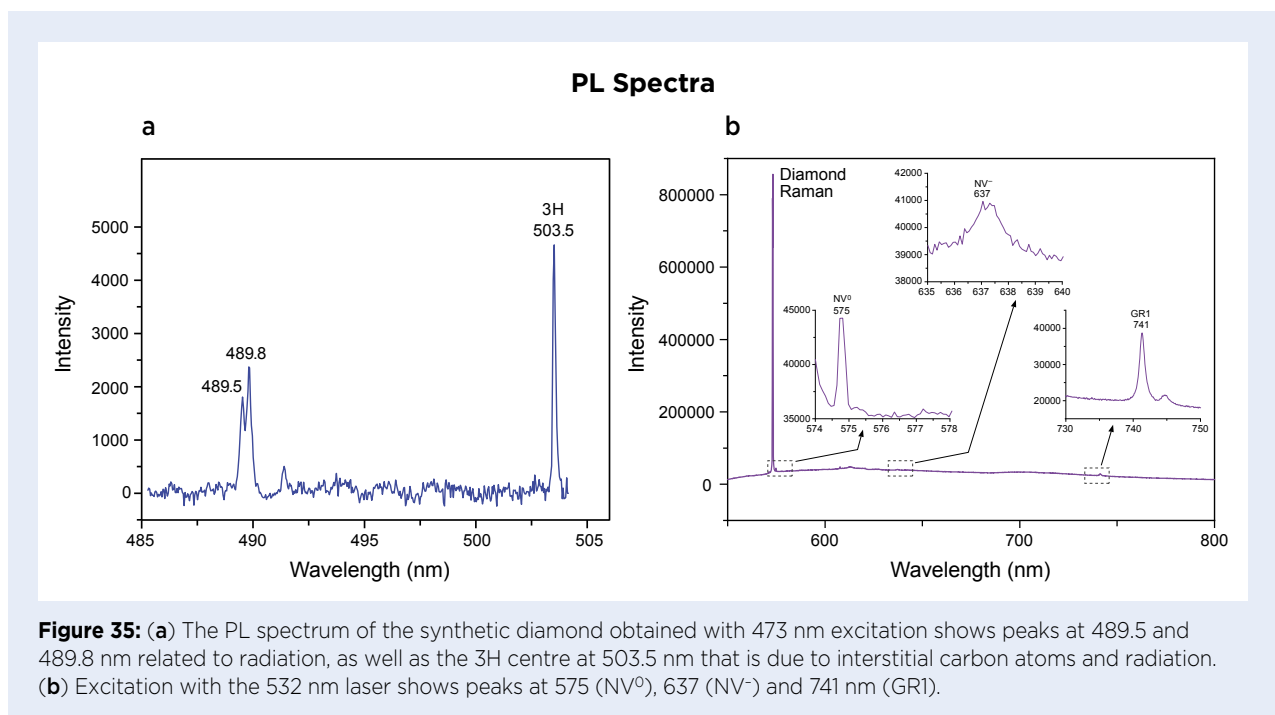
NGTC's Beijing laboratory. Therefore, we propose that the GR1 defect was intentionally introduced by artificial irradiation in order to complicate the sample's identification by making it appear more spectroscopically natural. The possible use of multi-treatment processes for this purpose was also mentioned by Eaton-Magaña and Breeding (2016).

Bo Gao (gaobo@mayoyo.com), Zhonghua Song,
Dr Taijin Lu and Yongwang Ma
National Gemstone Testing Center
Beijing, China

References

D'Haenens-Johansson, U.F.S., Moe, K.S., Johnson, P., Wong, S.Y., Lu, R. & Wang, W. 2014. Near-colorless HPHT synthetic diamonds from AOTC Group. *Gems & Gemology*, **50**(1), 30–45, https://doi.org/10.5741/gems.50.1.30.

Eaton-Magaña, S. & Breeding, C.M. 2016. An introduction to photoluminescence spectroscopy for diamond and its applications in gemology. *Gems & Gemology*, **52**(1), 2–17, https://doi.org/10.5741/gems.52.1.2.

Eaton-Magaña, S., Shigley, J.E. & Breeding, C.M. 2017. Observations on HPHT-grown synthetic diamonds: A review. *Gems & Gemology*, **53**(3), 262–284, https://doi.org/10.5741/gems.53.3.262.

Song, Z., Lu, T., Dai, H., Ke, J., Zhang, J., Liu, H. & Zhu, W. 2020. Identification of type IIa blue CVD synthetic diamonds from Huzhou SinoC Semiconductor Co. in China. *Journal of Gemmology*, **37**(3), 306–313, https://doi.org/10.15506/JoG.2020.37.3.306.

Wang, W. & Moses, T. 2005. Lab Notes: Diamond with bodycolor possibly affected by the 3H defect. *Gems & Gemology*, **41**(1), 42–43.

Large Faceted Synthetic Forsterite and Synthetic Tephroite

Because of the ubiquity of iron in the earth and in extraterrestrial bodies, the occurrence of colourless olivine (forsterite: Mg_2SiO_4) is very unusual because iron imparts a green colouration. In fact, there is complete solid solution between forsterite and the Fe-rich olivine end member, fayalite (Fe_2SiO_4). Another member of the olivine group is tephroite (Mn_2SiO_4). This Mn-dominant species is quite rare, and it also forms a complete solid solution with forsterite (Francis 1985). As with Fe, even a small amount of Mn imparts colour in olivine.

Olivine of the forsterite–fayalite series is the dominant mineral in the earth's upper mantle, and there is much scientific interest in its physical properties for the interpretation of seismic data in order to better understand the structure and chemistry of the mantle. To elucidate the properties of olivines, especially their shear and bulk moduli and their propagation of acoustic waves, Asst. Prof. Kazuhiko Ito of Kyoto Gakuen University (Kameoka, Japan) and colleagues have grown large single crystals of synthetic forsterite, tephroite and other olivine compositions (Ito *et al.* 2003a, b). Produced by the Czochralski-pulling method, they are very difficult to synthesise, but large crystals are necessary for the desired acoustic-wave measurements. When boules of the appropriate size and quality are created, they are cut into oriented slabs for experimental measurements.
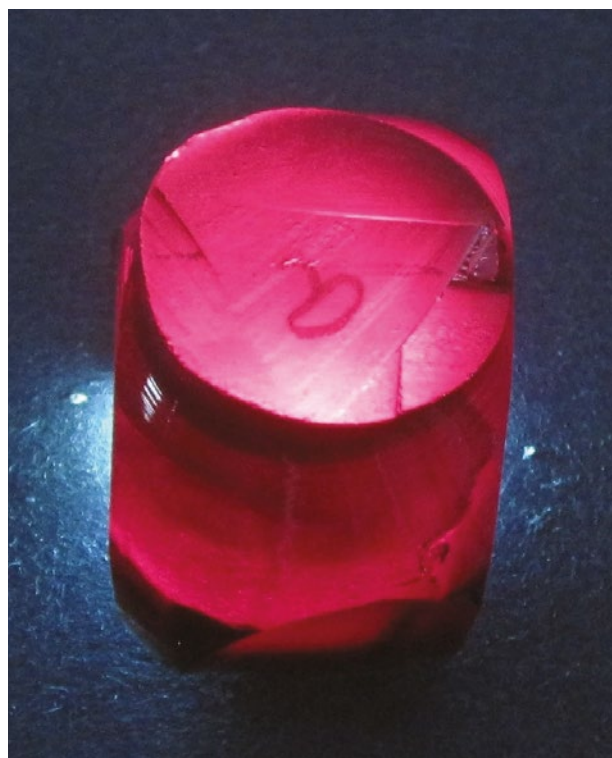
Figure 36: This 4-cm-tall remnant of a synthetic tephroite boule was used to facet three samples that weighed 14.5, 23.6 and 35 ct. Photo by J. Rakovan.

Some interesting samples have been faceted from unused portions of such boules. For example, a piece of synthetic tephroite (Figure 36) was faceted into three gems that weighed 14.5, 23.6 and 35 ct (e.g. Figure 37), and five samples were cut from synthetic forsterite that

Figure 37: One of three faceted specimens cut from the boule fragment in Figure 36 is this 35 ct (1.85 cm across) synthetic tephroite. The colour is due to the presence of Mn in the tephroite structure. Photo by J. Rakovan.

Figure 38: This 30 ct (2.1 cm diameter) synthetic forsterite is one of five faceted samples cut from a colourless boule. Colourless forsterite is extremely rare in nature because Fe is usually present to impart green colouration. Photo by J. Rakovan.

each weighed about 30 ct (e.g. Figure 38). The synthetic tephroite displays a deep pink-red colour similar to that of some rhodochrosite (also coloured by Mn), while the pure end-member forsterite contains no Fe or Mn and is therefore colourless. While this isn't the first time that synthetic forsterite has been faceted for gem use (Nassau 1994 illustrated a cut, light blue Cr-doped synthetic forsterite), it might the first time that colourless material has been faceted.

Dr John Rakovan (rakovajf@miamioh.edu)
Miami University, Oxford, Ohio, USA

References

Francis, C.A. 1985. New data on the forsterite–tephroite series. *American Mineralogist*, **70**(5–6), 568–575.

Ito, K., Sato, H., Kanazawa, H., Kawame, N., Tamada, O., Miyazaki, K., Uehara, S., Iio, Y. *et al.* 2003a. First synthesis of olivine single crystal as large as 250 carats. *Journal of Crystal Growth*, **253**(1–4), 557–561, https://doi.org/10.1016/s0022-0248(03)01029-7.

Ito, K., Sato, H., Takei, H., Tamada, O. & Kitazawa, T. 2003b. Synthesis of large high-quality forsterite single crystals to 200 mm length and its significance. *Geochemistry, Geophysics, Geosystems*, **4**(1), article 273 (4 pp.), https://doi.org/10.1029/2001gc000273.

Nassau, K. 1994. Synthetic forsterite and synthetic peridot. *Gems & Gemology*, **30**(2), 102–108, https://doi.org/10.5741/gems.30.2.102.

New Variation on Artificial Glass Imitating Tanzanite

A retail jeweller recently submitted five faceted violetish blue specimens ranging from 8.04 to 14.96 ct (e.g. Figure 39) to Stone Group Laboratories. Their individual containers were all labelled 'tanzanite'. While they lacked the strong violet colouration seen in most tanzanite, their colour was plausible for such material cut to show its blue axis direction.

No dichroism or dispersion was observed in any of

Figure 39: The tanzanite imitations described in this study included these 8.04 ct round and 14.96 ct oval faceted artificial glass samples. Photo by B. Williams.

Figure 40: Tiny, round gas bubbles such as these were present in all of the glass imitations of tanzanite. Photomicrograph by B. Williams; image width 5.2 mm.

the samples, and they were all inert to long- and short-wave UV radiation. No RI reading could be obtained, indicating they were probably a high-RI material that was over the limit of a standard refractometer. The hydrostatic SG value was 4.17 for all the samples. Between crossed polarisers, cross-like anomalous extinction effects were seen in some specimens, while in others the extinction appeared as a dark shadow crossing the sample four times upon a 360° rotation, which might be interpreted by a less cautious observer as anisotropy. Under darkfield microscopic observation, a faint, swirling optical effect was seen in most of the samples, and all of them contained tiny, isolated, round gas bubbles (Figure 40); they were otherwise free of inclusions. Their polish was poor and one specimen exhibited a scratch across the table.

Our Enwave Optronics 785 nm Raman spectrometer provided PL readings partially matching those of artificial glass, but they were not conclusive. Thermal resistance was extremely low, consistent with a low-hardness material such as glass. Chemical analysis with an Amptek X123-SDD EDXRF spectrometer showed high concentrations of Zr and Ba. (Although Si was not detected, our instrument is not configured to analyse for this element.) Barium is known to be an ingredient of high-RI artificial glasses that imitate a number of gem materials (Hainschwang 2009) and these are often stabilised with zirconium oxide. Thus, the chemical analysis, in combination with the other properties, conclusively identified these samples as artificial glass. Their violetish blue colour might be due to rare-earth elements, Zn and/or Cu, which were also detected. UV-Vis-NIR spectroscopy showed no distinguishing characteristics. Fourier-transform infrared (FTIR) spectra (e.g. Figure 41) showed features that differed slightly from those previously reported for a green Ba-rich glass with very low Si (Hainschwang 2009). The present samples differed in colour and SG from that particular green glass, but otherwise they showed similar properties. Moreover, the present samples differed from a piece of blue high-RI artificial glass documented by Koivula *et al*. (1993) that had a higher SG value (4.44), and also contrasted with a manufactured glass imitation of tanzanite reported by Quinn (2003) that had a lower RI (1.700).

Although tanzanite remains widely available and comparatively affordable, imitations are not infrequently
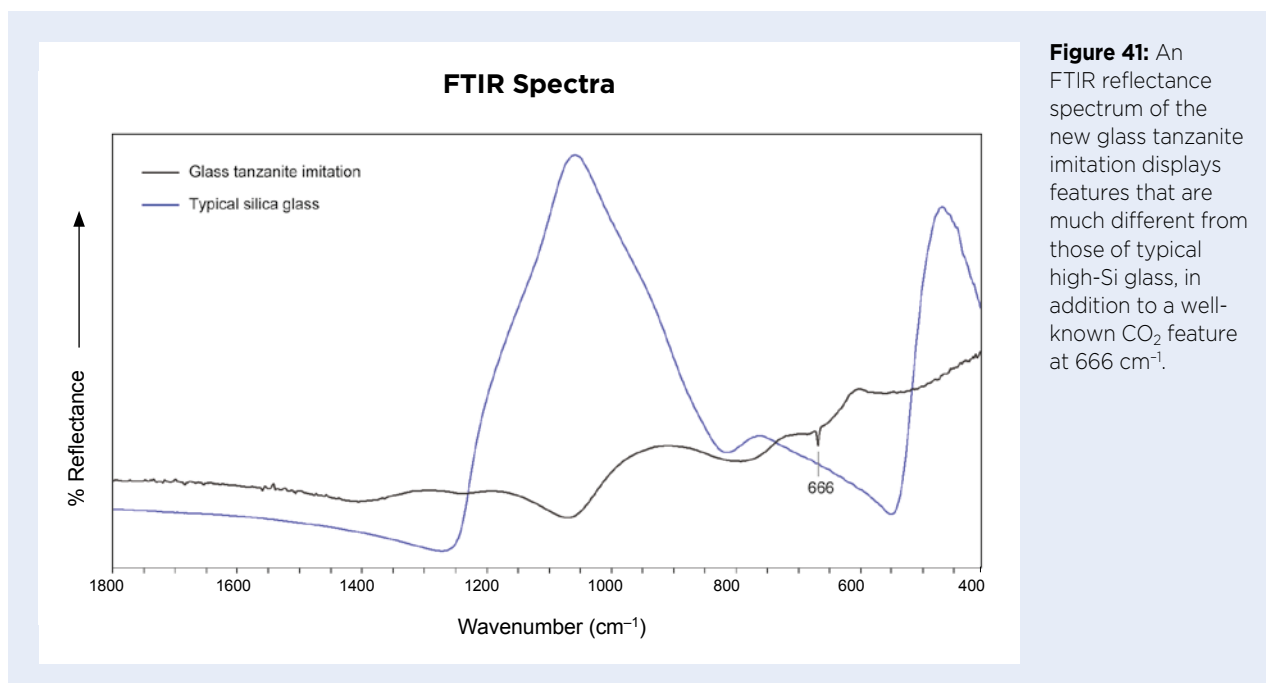
Figure 41: An FTIR reflectance spectrum of the new glass tanzanite imitation displays features that are much different from those of typical high-Si glass, in addition to a well-known CO_2 feature at 666 cm^{-1}.

encountered (e.g. Kiefert & Schmidt 1996). However, most are readily identifiable with standard desktop gemmological equipment. High-RI glasses in a variety of colours continue to challenge labs that are not equipped with advanced instruments.

Cara Williams FGA and Bear Williams FGA
(info@stonegrouplabs.com)
Stone Group Laboratories
Jefferson City, Missouri, USA

Brendan M. Laurs FGA

References

Hainschwang, T. 2009. Gem News International: High-RI barium-zirconium glass imitation of peridot and other gems. *Gems & Gemology*, **45**(4), 307–308.

Kiefert, L. & Schmidt, S.T. 1996. Some tanzanite imitations. *Gems & Gemology*, **32**(4), 270–276, https://doi.org/10.5741/gems.32.4.270.

Koivula, J.I., Kammerling, R.C. & Fritsch, E. (eds) 1993. Gem News: Artificial glass with high R.I. and S.G. *Gems & Gemology*, **32**(4), 289.

Quinn, E. 2003. Lab Notes: High-R.I. glass imitation of tanzanite. *Gems & Gemology*, **39**(4), 317–318.

TREATMENTS

Rough Jadeite with an Artificial Coating to Imitate a Weathered Crust

A natural crust typically forms on rough alluvial jadeite due to weathering and abrasion during transport. Jadeite traders often attempt to judge the internal quality of alluvial jadeite based on characteristics of this crust, with certain features such as a waxy appearance suggestive of valuable rough material. However, artificial coatings may be applied by unscrupulous traders to imitate high-quality jadeite, as recently noted in Ruili, Yunnan, China, where rough material is sold on the direct-broadcast online market.

In September 2020, we obtained a 631.68 g sample sold in Ruili as natural rough jadeite, which was coated with a deceptive artificial crust. The piece was mostly brown with some dark green areas and had a waxy lustre (Figure 42). However, the outer layer was quite soft and could be scratched with a fingernail. When the

Figure 43: When exposed to long-wave UV radiation, the sample in Figure 42 shows a mottled blue and white fluorescence in areas corresponding to the artificial coating and no fluorescence where the coating has been deeply scratched or peeled off. Photomicrograph by W. Lu; magnified 15×.

sample was observed under a long-wave UV lamp, it showed mottled blue and white fluorescence, except for inert areas where the outer layer had peeled off or was deeply scratched (Figure 43). Slicing the sample revealed an abrupt boundary between the crust and the underlying rock material, rather than the expected gradual transition between weathered crust and adjacent jadeite. The crust actually consisted of two distinct layers: a waxy exterior and an underlying green powdery layer (Figure 44).

FTIR spectra were recorded in attenuated total reflectance (ATR) and diffuse reflectance modes using a Thermo Nicolet 6700 infrared spectrometer (Figure 45). The ATR-FTIR spectra of a peeled-off piece of the crust

Figure 42: The 'crust' of this 631.68 g jadeite sample was identified as consisting of an artificial green powdery layer overlain by a brown mixture of wax and epoxy. Photo by W. Lu.

Figure 44: Slicing the sample reveals that the artificial crust consists of a waxy-looking exterior and an underlying green layer. Photomicrograph by W. Lu; magnified 15×.

showed absorption bands in the range of 1500–2000 cm⁻¹ that are characteristic of wax (Ling & Chen 2014), and additional bands at 2852, 2919, 2962, 3035 and 3095 cm⁻¹ that are associated with epoxy (Fritsch *et al.* 1992). By contrast, reflectance FTIR spectroscopy of an area of the underlying sample exposed after flaking off the crust revealed bands at approximately 744 and 1050 cm⁻¹, in addition to four bands between 400 and 600 cm⁻¹, which are generally consistent with jadeite (Li *et al.* 2015).

We infer that this sample was manufactured by first grinding a piece of low-grade jadeite into a cobble, then coating it with a green powder to impart the colouration of high-grade rough jadeite, and finally applying a brown mixture of wax and epoxy to the surface to give it a smooth and partially translucent appearance. The availability of such material on the market is an important reminder that a waxy-looking crust is not necessary indicative of high-quality jadeite, even if it appears very natural. Such an artificial crust can be distinguished by its low hardness (and corresponding scratching or peeling), anomalous UV fluorescence and diagnostic IR spectral features.

Wenting Lu (330107881@qq.com)
National Gemstone Testing Center
(NGTC), Yunnan, China

Lei Zhang
Kunming University of Science
and Technology
Yunnan, China

Qiusheng Zhang
NGTC, Yunnan, China

Zhonghua Song and Dr Taijin Lu
NGTC, Beijing, China
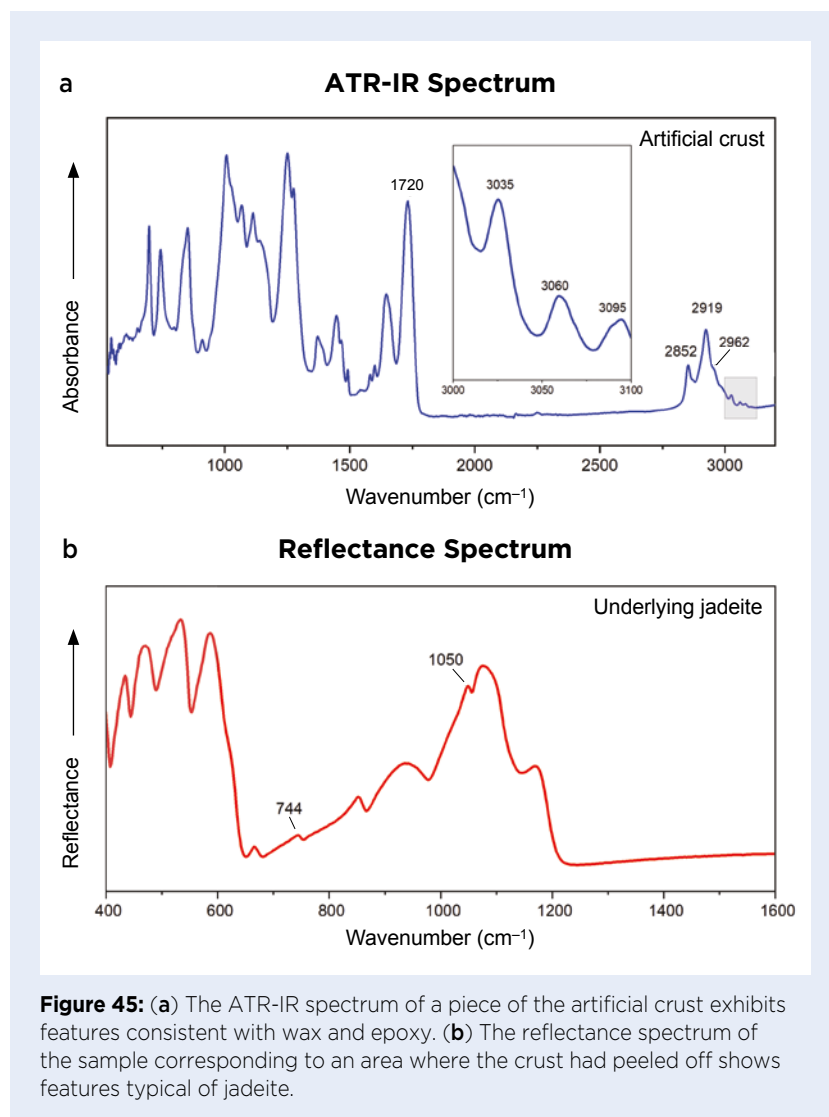
Figure 45: (**a**) The ATR-IR spectrum of a piece of the artificial crust exhibits features consistent with wax and epoxy. (**b**) The reflectance spectrum of the sample corresponding to an area where the crust had peeled off shows features typical of jadeite.

References

Fritsch, E., Wu, S.-T.T., Moses, T., McClure, S.F. & Moon, M. 1992. Identification of bleached and polymer-impregnated jadeite. *Gems & Gemology*, **28**(3), 176–187, https://doi.org/10.5741/gems.28.3.176.

Li, J., Luo, Y., Liu, X., Yu, X., Li, G., Fan, C. & Ye, H. 2015. Gem News International: Jadeite with high albite content. *Gems & Gemology*, **51**(1), 102–103.

Ling, A.J. & Chen, Z.Q. 2014. Gambling jadeite and characteristics of an inner filled gambling jadeite. *Acta Petrologica et Mineralogica*, **33**(Supp.), 97–100.

A New Type of Emerald from Afghanistan's Panjshir Valley

Michael S. Krzemnicki, Hao A. O. Wang and Susanne Büche

ABSTRACT: Since 2017, a new type of emerald from the Panjshir Valley, Afghanistan, has entered the gem trade. This material is commonly of excellent quality and compares with the finest emeralds from Colombia, not only visually, but also with respect to inclusions, spectral features and chemical composition. As a result, some of these stones have entered the market as Colombian emeralds. This study presents detailed microscopic, spectral and trace-element data for these recently produced Afghan emeralds and compares them to 'classic' emeralds from the Panjshir Valley and from Laghman Province in Afghanistan. The samples from each of the three Afghan occurrences showed differences in their UV-Vis-NIR spectra and water-related features in their Raman spectra, and they could also be distinguished from one another—as well as those from other important emerald deposits worldwide— by their trace-element composition. A distinctly higher Fe concentration is the main criterion that separates the recent Panjshir production from Colombian emeralds. This study further shows that it is possible to clearly differentiate emeralds from different localities based on trace-element data using t-SNE statistical processing, which is an unsupervised machine-learning method.

Emerald, the green chromium-bearing variety of beryl (Be$_3$Al$_2$Si$_6$O$_{18}$), has been one of the most sought-after gem materials throughout history. Since the 17th century, emeralds from Colombia have gained the highest reputation and market importance, but other sources have also emerged in recent decades, such as Zambia (e.g. Kafubu), Madagascar (e.g. Mananjary) and Ethiopia (Shakiso) in Africa, as well as Pakistan (Swat Valley), Afghanistan (Panjshir [Panjsher] Valley) and China (Davdar in the Xinjiang Uyghur Autonomous Region) in Asia. Stones from the Panjshir Valley in Afghanistan are commonly described as resembling Colombian emeralds in terms of colour, quality and even inclusion features (Bowersox *et al.* 1991; Schwarz & Pardieu 2009). Their reputation is underscored by the fact that a 10 ct Afghan emerald was sold at auction in 2015 for USD2.275 million (Christie's 2015)—equivalent to the highest recorded per-carat price for any emerald from a non-Colombian locality.

The Swiss Gemmological Institute SSEF regularly receives emeralds from Afghanistan for testing, quite often in impressive layouts and settings. In the past, determining their geographic origin was in most cases quite straightforward. However, in early 2017 this changed, and since then we have analysed more than 100 samples of an apparently new type of emerald from the Panjshir Valley in Afghanistan. (Hereafter in this article these stones will be referred to as 'Panjshir type II' emeralds.) They have been submitted to SSEF by reliable sources for research and testing, and currently

Authors' note (added December 2021): At least some of the new 'Panjshir type II' emerald samples characterised in this article are now believed to be from Musakashi in the Solwezi District of Zambia. This is based on new LA-ICP-MS data (obtained in November 2021) acquired on Musakashi emeralds. For more information, see M. S. Krzemnicki *et al.*, 'Gem Notes: New emeralds from Musakashi, Zambia, appear on the market', *Journal of Gemmology*, **37**(8), 2021, pp. 769–771.

we do not have any further information on the specific mining area in the Panjshir Valley that produced them. However, based on their uniform appearance and exceptional quality, as well as their consistent inclusion features and very homogeneous chemical composition, the authors assume that they originated from a specific Panjshir location (or gem 'pocket') and not from various mining sites within the area. The stones more closely resemble Colombian emeralds in terms of inclusion features, physical properties and trace-element concentrations (Krzemnicki 2018), as compared to the previously known material from Afghanistan (hereafter referred to as 'Panjshir type I' emeralds). Because the Panjshir type II stones are often of very high quality—matching the best Colombian emeralds from Muzo and other famous Colombian mines—this makes accurate origin attribution even more important.

In this study, we present detailed gemmological data for Panjshir type II emeralds and compare them to previously known emeralds from Afghanistan (from Panjshir and Laghman Province; Figure 1). In addition, we compare the Panjshir type II emeralds to those from other deposits, including Colombia, with the aim of providing reliable criteria for origin determination.

LOCATION AND GEOLOGY

Emeralds from Afghanistan's Panjshir Valley have been traded for an unknown period of time. Theophrastus's *Treatise on Stones* (314 BC; see Forestier & Piat 1998) and Pliny the Elder's *Naturalis* (77 AD; see Bowersox *et al.* 1991) both mentioned *smaragdus* from Bactria, much of which lay in modern-day Afghanistan. However, *smaragdus* was also used in antiquity to describe a wide range of green gems, so it is uncertain whether these reports refer to emeralds from Afghanistan. Interestingly, oxygen isotope analysis of a historic emerald from the treasure of Nizam in Hyderabad (India) revealed that the Panjshir Valley was its likely origin (Giuliani *et al.* 2000). This evidence supports Panjshir as a (sporadic) source of gem-quality emeralds at least as early as the 18th century.

In the modern gem market, Panjshir emeralds have been known since the 1970s (Bariand & Poullen 1978). Systematic surveys were done by Russian and Afghan geologists (Rossovskiy *et al.* 1976; Abdullah *et al.* 1977; Rossovskiy 1981; Chmyriov *et al.* 1982), and the deposits were also described in a few gemmological publications (Bowersox 1985; Bowersox *et al.* 1991). Years later, emeralds were also discovered in neighbouring Laghman Province, including some gem-quality material near the village of Korgun (about 100 km east of Kabul) and semi-transparent stones near Lamonda (Laurs 2001; Henn & Schmitz 2014; Groat *et al.* 2014).

Today, the mines of the Panjshir Valley (literally 'Valley of the Five Lions') are the main source of gem-quality emeralds in Afghanistan. The largest specimens reported in the literature are an 8 g crystal (Sultan & Aria 2018) and a 15 ct faceted stone (Schwarz & Giuliani 2002). However, in the past two decades, the authors have seen and tested fine-quality Afghan emerald crystals larger than 120 g and faceted stones over 85 ct. Nevertheless, based on our lab experience, most gem-quality faceted emeralds from Afghanistan are less than 5 ct. By comparison, the Panjshir type II emeralds that emerged since 2017 are generally rather small (median about 2.5 ct), but in rare cases they reach up to 20 ct.

The Panjshir Valley is located about 150 km north-east of Kabul in the Hindu Kush mountain range and follows the Panjshir River north-east to south-west (Figure 2).

Figure 1: The three types of emeralds from Afghanistan discussed in this article are illustrated here: a 10.11 ct Panjshir type I emerald of very fine quality that was also set in the ring shown on the cover of this issue (left), a 2.42 ct Panjshir type II emerald of excellent quality (centre) and an 18.58 ct Laghman-type emerald (right). Photos by Luc Phan; composited by M. S. Krzemnicki, © SSEF.

Figure 2: The map on the left (© USAID) shows the location of the emerald deposits in the Panjshir Valley and near Korgun (Laghman Province) in north-east Afghanistan. The three-dimensional block map on the right (courtesy of WikiCommons) is looking into the Panjshir Valley, which extends about 100 km towards the north-east. The Panjshir emerald mining area is located upstream of Khenj village, which is about 115 km from Kabul.

The emerald mines are located in a zone approximately 16 km long and 3 km wide extending north-east along the Panjshir River from Khenj village (Bowersox *et al.* 1991; Giard 1998), at elevations of about 2000–4000 m (DeWitt *et al.* 2020).

The Panjshir Valley follows a continental collision zone—the Herat-Panjshir suture (Chmyriov *et al.* 1982; Kazmi & Snee 1989; Giuliani *et al.* 2019)—which divides platform-derived sedimentary rocks in northern Afghanistan from southern structural blocks of various origins (Bowersox 2015) that also contain metamorphosed relics of the Paleo-Tethys Ocean (Bowersox *et al.* 1991; Snee *et al.* 2005).

The emerald deposits are found in Proterozoic metamorphic basement rocks consisting of migmatite, gneiss, schist, marble and amphibolite. They are classified as type IIC (tectonic-metamorphic-related deposits, and hosted in metamorphic rocks; Giuliani *et al.* 2019). The emeralds formed within vugs and quartz veins, and are associated with muscovite, tourmaline, albite, pyrite, rutile, dolomite and chlorapatite in schists that were affected by intense fracturing, fluid circulation and hydrothermal alteration (Sabot *et al.* 2000; Groat *et al.*

2014; Giuliani *et al.* 2019). Similar to Colombian emeralds, Panjshir material contains fluid inclusions of high salinity, which indicates (as in Colombia) a leaching of evaporite sequences (Giuliani *et al.* 1997, 2017; Sabot *et al.* 2000) by hydrothermal alteration during the Himalayan orogeny. In contrast to Colombian emeralds, however, they formed at a distinctly higher metamorphic grade, at around 400°C (Schwarz & Giuliani 2002) during Oligocene time. (^{40}Ar-^{39}Ar dating of muscovite in an emerald-bearing quartz vein indicated 23 ± 1 million years; Sabot *et al.* 2001.)

By contrast, very little is known about the emerald deposits in Laghman Province (Laurs 2001; Henn & Schmitz 2014), especially the geological setting of the gem-quality emerald occurrence near Korgun. Based on the inclusions (biotite and tremolite) and chemical composition (rich in alkalis and alkaline earths), these emeralds appear to have a distinctly different formation environment than those of the Panjshir Valley. Due to their similar properties and trace-element content compared to emeralds from Zambia (Kafubu) and Ethiopia (Shakiso), we speculate that their formation might be similarly linked to metabasites that were metasomatically altered by Be-bearing fluids from

nearby granitoid intrusions. To our knowledge, the emerald occurrence near Korgun has produced only a limited amount of gem-quality emeralds (Laurs 2001), which are only rarely encountered in the gem trade.

For a more detailed description of the geology of emerald deposits in Afghanistan, readers are referred to Groat *et al.* (2014), Giuliani *et al.* (2019) and references therein.

MATERIALS & METHODS

We analysed 113 emeralds from Afghanistan (summarised in Table I), ranging from 0.12 to 21.22 ct: 51 showing properties consistent with Panjshir type I, 54 Panjshir type II and eight from Laghman Province (hereafter referred to as 'Laghman type' and assumed to be from the Korgun locality). Most were faceted stones (e.g. Figure 3), with only a few crystal fragments, and all of the Panjshir samples were of fine gem quality, showing good to excellent clarity and a well-saturated green colour. A detailed list of all samples is available in *The Journal*'s online data depository at https://gem-a.com/the-journal-of-gemmology-data-depository.

All samples were meticulously investigated with a microscope (System Eickhorst Gemmaster, 10–70× magnification) and analysed by standard gemmological methods, including RI, hydrostatic SG and UV fluorescence (254 and 365 nm). Ultraviolet-visible-near infrared (UV-Vis-NIR) absorption spectra (polarised o-ray) of all samples were recorded with either: (1) an Agilent Cary 5000 instrument in absorption mode (normalised path length) at 290–900 nm, with a step size of 0.35 nm and a scan rate of 0.5 s per step; or (2) our in-house-developed portable UV-Vis-NIR spectrometer equipped with an Avantes high-resolution spectrometer and using a xenon flash and halogen lamp as excitation sources.

Raman micro-spectroscopy of selected emeralds and their inclusions was performed using a Renishaw inVia spectrometer attached to a Leica DM2500 M microscope.

The system utilised an argon-ion laser (514.5 nm) and had a spectral resolution of 1.5 cm^{-1}. All analyses were carried out in confocal mode using a 20× objective to focus on the surface or within the samples (for inclusions and filler identification). For the analysis of water molecule orientation in the emeralds, the *c*-axis was oriented perpendicular to the vibrational direction of the polarised Raman laser (cf. Huong *et al.* 2010). Due to the strong Cr-related fluorescence of emerald, the laser intensity had to be reduced in some cases to prevent saturation of the Peltier detector.

Polarised Fourier-transform infrared absorption spectroscopy was carried out on all samples using a Thermo Nicolet iS50 spectrometer in the 400–4000 cm^{-1} range at a resolution of 4 cm^{-1}, primarily to detect any fissure fillings (mainly oil type) that were present occasionally in these samples.

For chemical analysis we used both energy-dispersive X-ray fluorescence (EDXRF) and laser ablation inductively coupled plasma time-of-flight mass spectrometry (LA-ICP-TOF-MS) to fully characterise the trace-element contents of the emerald samples. When summarising the range of elements present, we chose the median instead of the arithmetic average, as it is more robust to outliers and thus better represents the average concentration. EDXRF analyses of 88 selected samples (40 Panjshir type I, 43 Panjshir type II and five Laghman type) were carried out under vacuum with a Thermo Scientific ARL Quant'X instrument using our in-house-developed standard procedure with six excitation energies (4, 8, 12, 16, 20 and 40 kV) for optimised sensitivity to the full range of elements detectable by this technique. For LA-ICP-TOF-MS analyses we used our GemTOF setup consisting of a 193 nm ArF excimer laser equipped with a TwoVol2 ablation chamber (NWR193UC, Elemental Scientific Lasers, USA) coupled with a commercial ICP-TOF-MS unit (*icp*TOF, Tofwerk AG, Switzerland) that was modified from an optimised ICP-Q-MS unit (iCAP Q from Thermo Fisher Scientific). On each of 55 selected

Table I: Emerald samples from Afghanistan examined for this study.

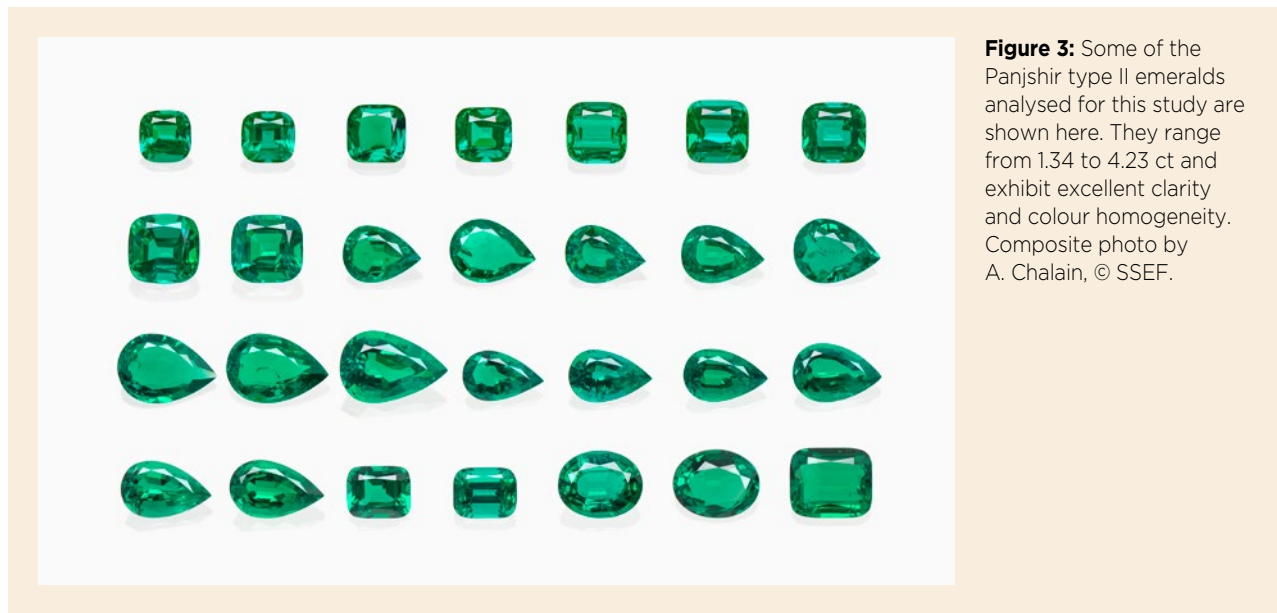| Afghan origin	Designation	Number of samples	Weight (ct)	Average SG	Average RIs	Long-wave UV fluorescence
Panjshir Valley—'classic'	Panjshir type I	51	0.43–13.79	2.74	1.581–1.589	Inert
Panjshir Valley—'new'	Panjshir type II	54	0.12–21.22	2.72	1.575–1.582	Weak to moderate red
Korgun, Laghman Province	Laghman type	8	3.17–18.58	2.74	1.580–1.588	Inert

Figure 3: Some of the Panjshir type II emeralds analysed for this study are shown here. They range from 1.34 to 4.23 ct and exhibit excellent clarity and colour homogeneity. Composite photo by A. Chalain, © SSEF.

samples (11 Panjshir type I, 36 Panjshir type II and eight Laghman type) we analysed 3–4 spots (ablation diameter 100 µm) on visually inclusion-free areas. All spots were ablated at 20 Hz and with a fluence of 5.6 J·cm^{-2} using helium as the carrier gas (0.8–0.9 L/min). Five pre-cleaning laser shots were fired at the beginning of each measurement (30 s ablation time). We used NIST 610 and NIST 612 glasses as external standards, and ^{29}Si$^+$ (for ideal beryl) as an internal standard.

TOF-MS (compared to more conventional quadru-pole-MS) has the advantage of simultaneous acquisition of the full mass spectrum. It allows the operator to first measure almost the entire composition of the sample and then determine which elements are of interest. This approach is ideal to detect unusual trace elements or to monitor elemental variations (e.g. due to growth zoning), or to detect and chemically charac-terise accidentally ablated (sub-microscopic) inclusions. Detailed information about instrumental parameters, analytical conditions and data processing can be found in Wang *et al*. (2016) and Wang & Krzemnicki (2021).

For data interpretation and discussion, the analysed elemental concentrations were plotted in two-dimen-sional (2D) and three-dimensional (3D) diagrams, combining our analyses for the investigated Afghan emeralds with SSEF's reference database for emerald samples from other origins (92 from Colombia, 26 from Ethiopia, two from Nigeria, 23 from Pakistan and 104 from Zambia). We further evaluated the chemical data using t-distributed stochastic neighbour embedding (t-SNE), a statistical method for dimension reduction. This machine-learning algorithm has proven to be a versatile method for the non-linear transformation of high-dimensional datasets (e.g. multi-element concentrations from mass spectrometry) into a low-dimensional space (van der Maaten & Hinton 2008). The unsupervised algorithm used by this technique means that the data input into the statistical calculation are not labelled with their origin *a priori*. The t-SNE scatter points are colour-coded according to their respective origins only after t-SNE analysis, and the clustering or grouping of data points is purely due to their elemental similarity. This method allows us to better visualise sample relationships and place separate mineral data sets into various subgroups. A detailed description of this statistical methodology for an emerald case study is provided in Wang & Krzemnicki (2021). In the present study, we calculated the t-SNE plot using concentrations of 56 elements from more than 1,100 spot analyses of 360 emerald samples. A list of the 56 elements used for this process is provided in the data depository.

RESULTS

The analysed Panjshir type II emeralds were mostly of excellent quality (e.g. Figure 3), with few fissures and a homogeneous and well-saturated green colour, reminiscent of the best-quality Colombian emeralds. As such, these stones can be considered mostly superior to the average quality of Panjshir type I emeralds and definitively more attractive than the rather included and moderately saturated Laghman-type emeralds.

Standard gemmological testing revealed rather low RI (1.575–1.582) and SG (2.72) values for the Panjshir type II material, similar to Colombian emeralds, and distinctly lower values than those of Panjshir type I and

Laghman-type emeralds (see Table I). In addition, only the Panjshir type II emeralds showed a reddish fluorescent reaction to long-wave UV radiation, whereas all the studied Panjshir type I and Laghman-type emeralds were inert (consistent with their distinctly higher Fe concentrations; see below).

Internal Features

Careful and meticulous microscopic observation is the basis for robust gemmological research and expertise—particularly when studying material from different origins or mines—as was the case for the three different types of Afghan emeralds examined in this study. Surprisingly, there are few detailed published descriptions of microscopic features in Panjshir emeralds (Bowersox *et al.* 1991; Schwarz & Pardieu 2009). Table II summarises the microscopic characteristics reported in the literature alongside those we observed in our Panjshir type I, Panjshir type II and Laghman-type samples.

In Panjshir type I emeralds (Figure 4a), spiky-to-tubular

Table II: Inclusion features in the Afghan emeralds.[a]

Feature	Panjshir type I	Panjshir type II	Laghman type
General appearance	Mostly included	Often rather clean	Often highly included
Colour zoning	Occasional hexagonal colour zoning	—	Occasional colourless hexagonal zones
Growth structures	Dense growth lines || to *c*-axis	Dense growth lines || to *c*-axis; occasional swirled to chevron-like structures	Dense growth lines || to *c*-axis
Main fluid inclusions	Spiky and tubular multiphase	Small, spiky to tubular and 'sawtooth' multiphase	Small, irregular to slightly rectangular two-phase and multiphase
Hollow channels || to *c*-axis	Coarse to fine, partly filled with FeO(OH)	Fine and often densely arranged; partly kinked or slightly curved	Coarse, partly filled with graphite
Etch tubes	Coarse, often filled with FeO(OH)	Fine, irregular to curved; partially filled with FeO(OH)	—
Platelets/cavities	—	Occasional flat, semicircular surface cavities partially filled with FeO(OH)	Numerous tiny platelets ⊥ to *c*-axis
Fine particles	Not common	—	Dispersed in zones or in 'dust' lines
Solid inclusions:			
Feldspar (microcline and albite)	Occasional	Rare	—
Quartz[b]	Occasional	—	—
Phlogopite	—	—	Very common
Tremolite	—	—	Very common
Tourmaline[b]	Occasional	—	—
Dolomite	Occasional	—	—
Rhombic carbonate (ankerite)[b]	Occasional	—	—
Apatite	—	Rare	—
Phosphate (monazite/eosphorite)[b]	Rare	—	—
Rutile	Rare	Rare	—
Pyrite	Rare	—	—

[a] Abbreviations: — = not observed, \|\| = parallel and ⊥ = perpendicular.
[b] From the literature: Bowersox *et al.* (1991), Schwarz and Pardieu (2009), and Henn and Schmitz (2014).

(along the *c*-axis) halite-sylvite-bearing multiphase fluid inclusions are typically seen (Giuliani *et al.* 2018; see Figures 4b and 4c). Occasionally we observed distinct hexagonal colour zoning—with a lighter core and a darker green rim—when looking along the *c*-axis (Figure 4d), and in some cases dense growth lines parallel to the *c*-axis. Other common features were fine (Figure 4e, f) to rather coarse (Figure 4g, h) hollow tubes parallel to the *c*-axis, which were often partially filled with brownish

Fe-hydroxide (identified by Raman micro-spectroscopy) and some black foreign substance (presumably residue of the cutting process). Fe-hydroxide was commonly present in the fissures and cavities of most of the Panjshir type I emeralds (cf. Bowersox *et al.* 1991), as also observed on the outer surface of one crystal (Figure 4i). In our samples we found only a few solid inclusions, among them octahedral pyrite, rhombic dolomite, rutile and small grains of microcline (K-feldspar), which were
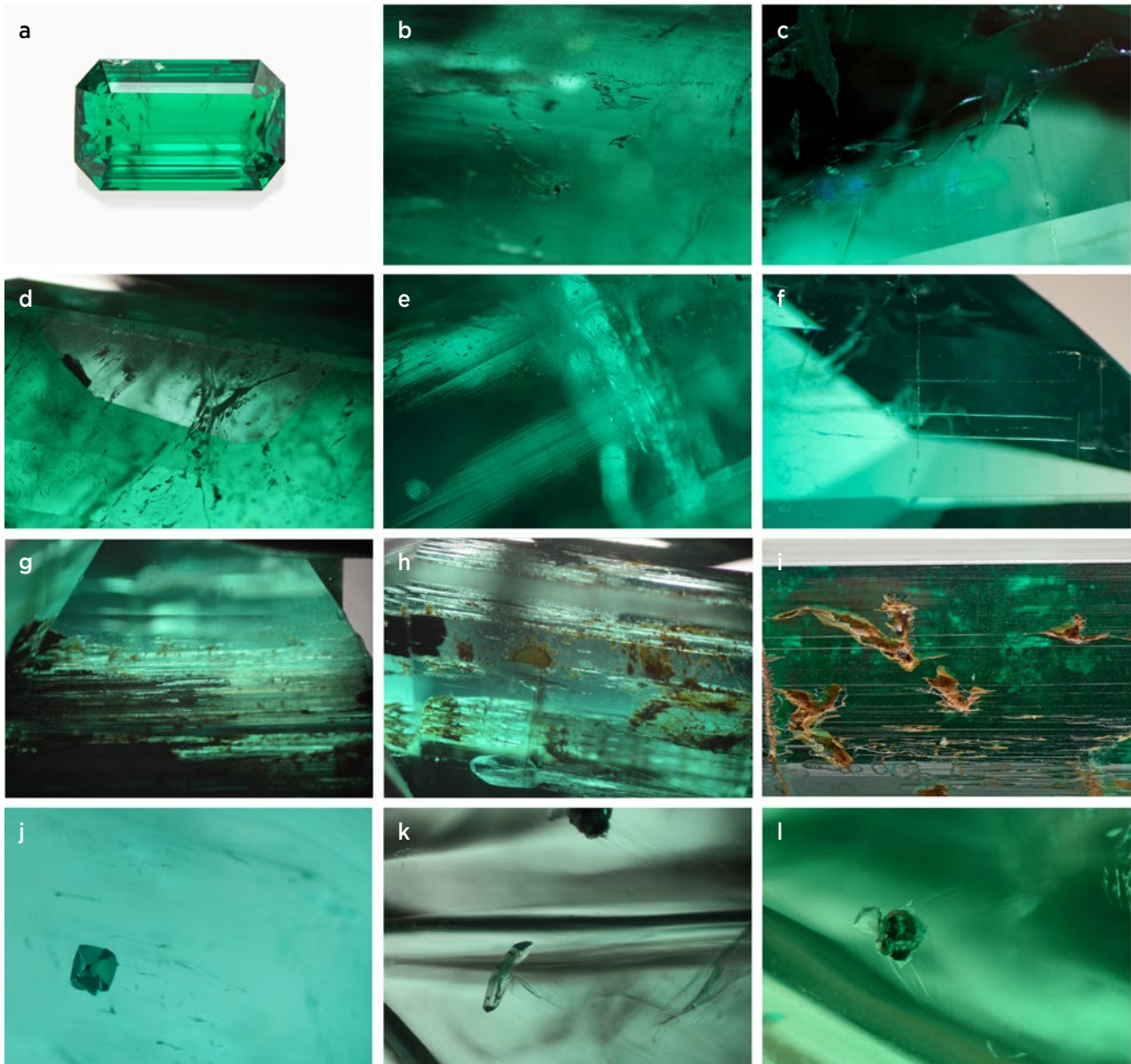
Figure 4: (**a**) This fine-quality 4.82 ct Panjshir type I emerald is typical of the material in which the inclusions shown here were observed. Features seen in Panjshir type I emeralds include: (**b**) and (**c**) spiky and tubular (along the *c*-axis) halite-sylvite-bearing multiphase fluid inclusions (both magnified 50×); (**d**) hexagonal colour zoning seen looking down the *c*-axis (magnified 30×); (**e**) fine and dense growth lines parallel to the *c*-axis (magnified 40×); (**f**) fine hollow channels parallel to the *c*-axis (magnified 30×); (**g**) a dense pattern of coarse hollow tubes oriented along the *c*-axis, partially filled with Fe-hydroxide and a black foreign substance, presumably residue from the cutting process (magnified 20×); (**h**) coarse hollow channels filled with brownish aggregates of Fe-hydroxide (magnified 20×); (**i**) etch features lined with Fe-hydroxide on the surface of an emerald crystal (magnified 10×); (**j**) a pyrite octahedron (magnified 70×); (**k**) a flat rhombic dolomite crystal (magnified 50×); and (**l**) microcline accompanied by pyrite (magnified 70×). Photomicrographs by M. S. Krzemnicki, © SSEF.

all identified by Raman micro-spectroscopy (Figures 4j–l). Other inclusions—such as ankerite, tourmaline and a phosphate—have been mentioned in the literature (Bowersox *et al.* 1991; Schwarz & Pardieu 2009) but were not observed in our samples.

The internal features in the Panjshir type II emeralds showed some resemblance to those in the type I stones, but we also observed notable differences. The most intriguing characteristic was fewer inclusions overall, resulting in a number of fine-quality eye-clean stones

(e.g. Figure 5a). Occasionally, the Panjshir type II emeralds showed fine growth features such as zones of swirly structures (Figure 5b) or chevron-like shapes (Figure 5c), and occasionally dense growth lines parallel to the *c*-axis. However, we did not observe the columnar honeycomb pattern (also known as *gota de aceite*) that is seen in some Colombian emeralds. Some irregular-to-curved etch channels were present (Figure 5d), often filled partially with Fe-hydroxide. In some cases, flat semicircular cavities occurred at the surface
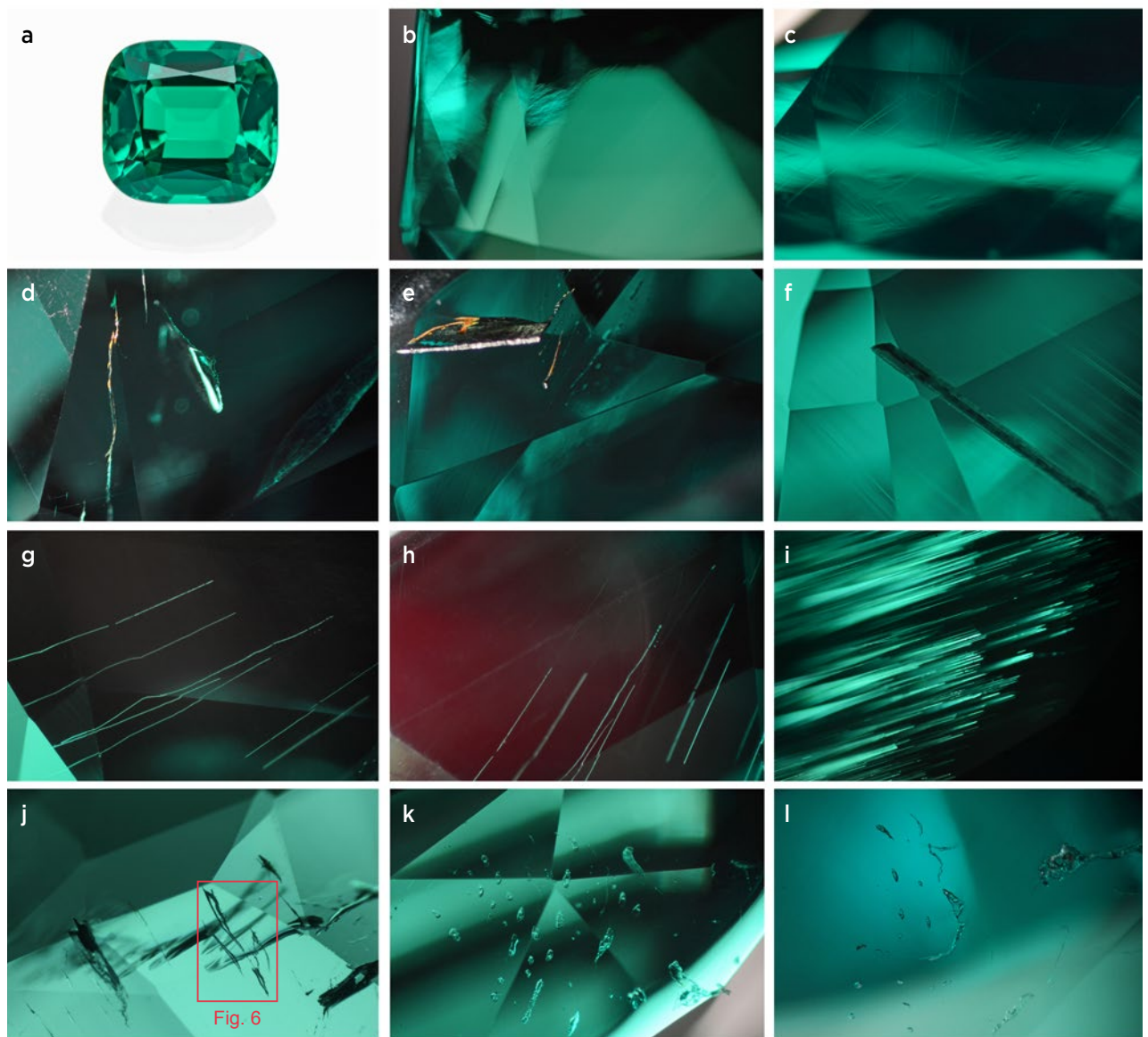
Figure 5: (**a**) A 2.42 ct Panjshir type II emerald displays the excellent quality of some of this relatively new material from Afghanistan. Inclusions in such Panjshir type II emeralds can consist of: (**b**) occasional fine, swirly to (**c**) chevron-like growth zoning (both magnified 50×); (**d**) irregular-to-curved, fine etch channels partially filled with Fe-hydroxide (magnified 60×); (**e**) a flat semicircular cavity at the surface, along with etch channels partially filled with Fe-hydroxide (magnified 50×); (**f**) a flat hollow channel parallel to the *c*-axis filled with epigenetic material (magnified 30×); (**g**) a few slightly irregular and kinked hollow channels parallel to the *c*-axis (magnified 50×); (**h**) reddish visible fluorescence together with a few hollow channels (magnified 50×); (**i**) a dense pattern of fine hollow channels parallel to the *c*-axis (magnified 50×); (**j**) tubular multiphase fluid inclusions with 'sawtooth' outlines (magnified 30×); (**k**) a group of irregularly shaped multiphase fluid inclusions (magnified 30×); and (**l**) tiny spiky multiphase fluid inclusions (magnified 70×). Photomicrographs by M. S. Krzemnicki, © SSEF.

(Figure 5e), presumably relict of a dissolved primary phase (possibly tabular calcite crystals). Solid inclusions were rather rarely observed and consistently very small in the Panjshir type II samples. These consisted of albite, rutile and a tiny prismatic apatite crystal (all identified by Raman micro-spectroscopy).

Also, like Panjshir type I emeralds, the type II stones additionally contained both hollow channels along the *c*-axis (e.g. Figure 5f) and spiky-to-tubular multiphase fluid inclusions (Krzemnicki 2018). However, the hollow channels were mostly very thin and slightly curved or locally bent, and usually did not contain Fe-hydroxide (Figures 5g and 5h). These hollow channels were the dominant inclusion feature in some samples (Figure 5i), and were much more apparent than in Colombian emeralds, where similar channels are even thinner. The multiphase fluid inclusions in the Panjshir type II emeralds were often very small and tubular to irregular or spiky in shape (Figure 5j–l). Interestingly, some of these primary fluid inclusions showed a distinct 'sawtooth' outline (Figures 5j–k and 6; see also Hughes 2021), which in our opinion is unique to Panjshir type II material.

The Laghman-type emeralds showed very different inclusion features and therefore cannot be misinterpreted as Panjshir emeralds. They tended to be quite included and often showed rather low colour saturation (Figure 7a; see also Henn & Schmitz 2014), at least compared to Panjshir emeralds. All of our Laghman-type
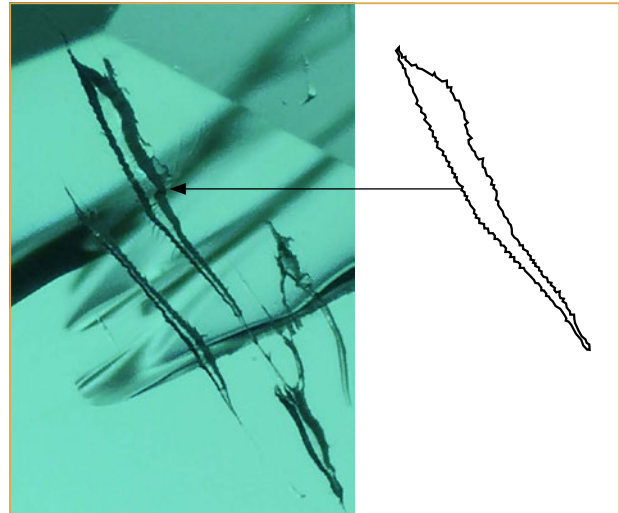
Figure 6: Tubular fluid inclusions with a distinct sawtooth outline were observed in Panjshir type II emeralds. Photo by M. S. Krzemnicki, © SSEF; magnified 70×.

samples were characterised by the presence of tremolite (Figure 7b), often as randomly oriented, slightly curved needles (Figure 7c). In addition, they all contained numerous slightly brownish phlogopite flakes (Figure 7d). Both tremolite and phlogopite were identified by Raman micro-spectroscopy. The Laghman-type emeralds also contained two-phase fluid inclusions with irregular to slightly rectangular shapes (Figure 7e), as well as fine platelets dispersed in zones or aligned as 'dust
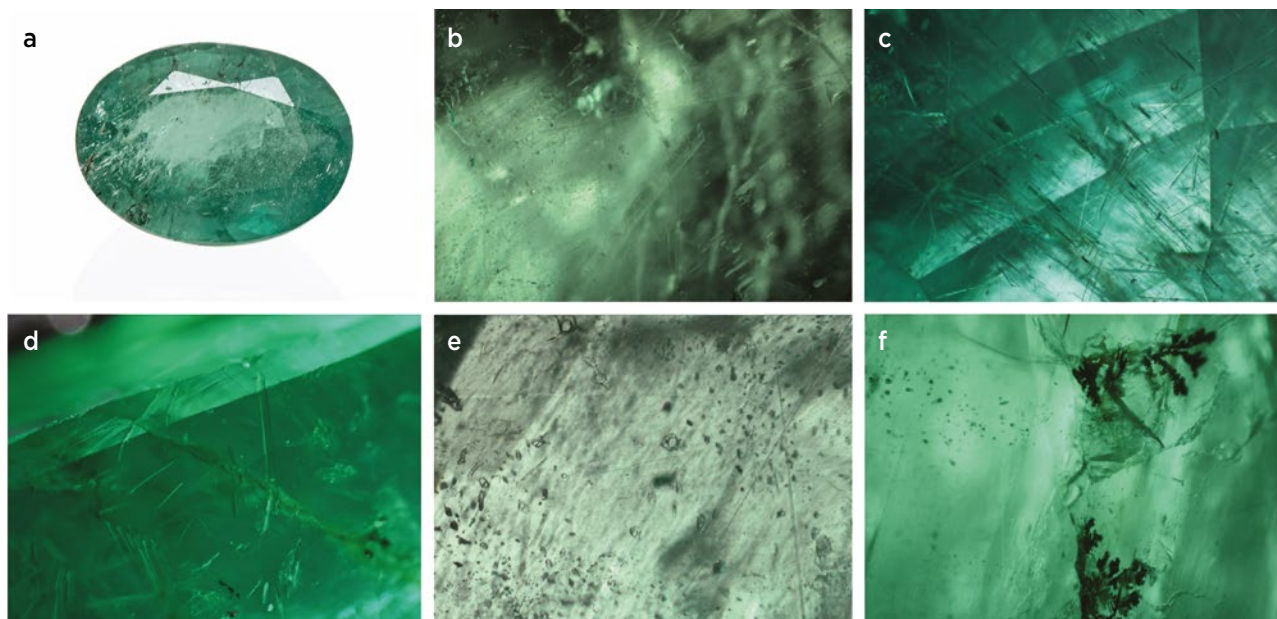
Figure 7: (**a**) A typical 3.17 ct Laghman-type emerald shows the generally included appearance and lower colour saturation of this material. Typical internal features in Laghman-type emeralds include: (**b**) near-colourless tremolite needles (magnified 40×); (**c**) dense patterns of randomly oriented and slightly curved tremolite needles (magnified 30×); (**d**) many slightly brownish flakes of phlogopite (magnified 40×); (**e**) tiny irregular to slightly rectangular two-phase fluid inclusions (magnified 50×); and (**f**) fissures containing graphite dendrites (magnified 50×). Photomicrographs by M. S. Krzemnicki, © SSEF.

lines'. Open fissures and cavities were often filled with secondary black dendritic material (Figure 7f), which was identified by Raman analysis as graphite (of rather low crystallinity).

UV-Vis-NIR Spectroscopy

The green colour of emerald is well known to be linked not to the presence of Cr alone, but to a complex interplay of the transition metals Cr, V and Fe in the beryl structure (Wood & Nassau 1968), and this was also shown by the Afghan emeralds in this study. Their UV-Vis-NIR spectra (for the ordinary ray, equivalent to E⊥c) could be separated into two groups: (1) Panjshir type I and Panjshir type II, and (2) Laghman type (Figure 8).

The spectra of the Panjshir emeralds were mostly dominated by broad absorption bands centred at approximately 435 and 605 nm due to octahedrally coordinated Cr^{3+} and V^{3+}, and by small, sharp, spin-forbidden Cr bands in the 600–700 nm range (Wood & Nassau 1968; Schmetzer 2014 and references therein). In the Panjshir type I emeralds, the band at approximately 435 nm was occasionally superimposed by a shoulder at about 390 nm attributed to V^{3+} at the octahedrally coordinated Al^{3+} site of the beryl structure (Schmetzer et al. 2006), consistent with the considerable V concentrations in those samples. In addition, a small feature at about 375 nm related to octahedrally coordinated Fe^{3+} was occasionally present. A common feature of all Panjshir
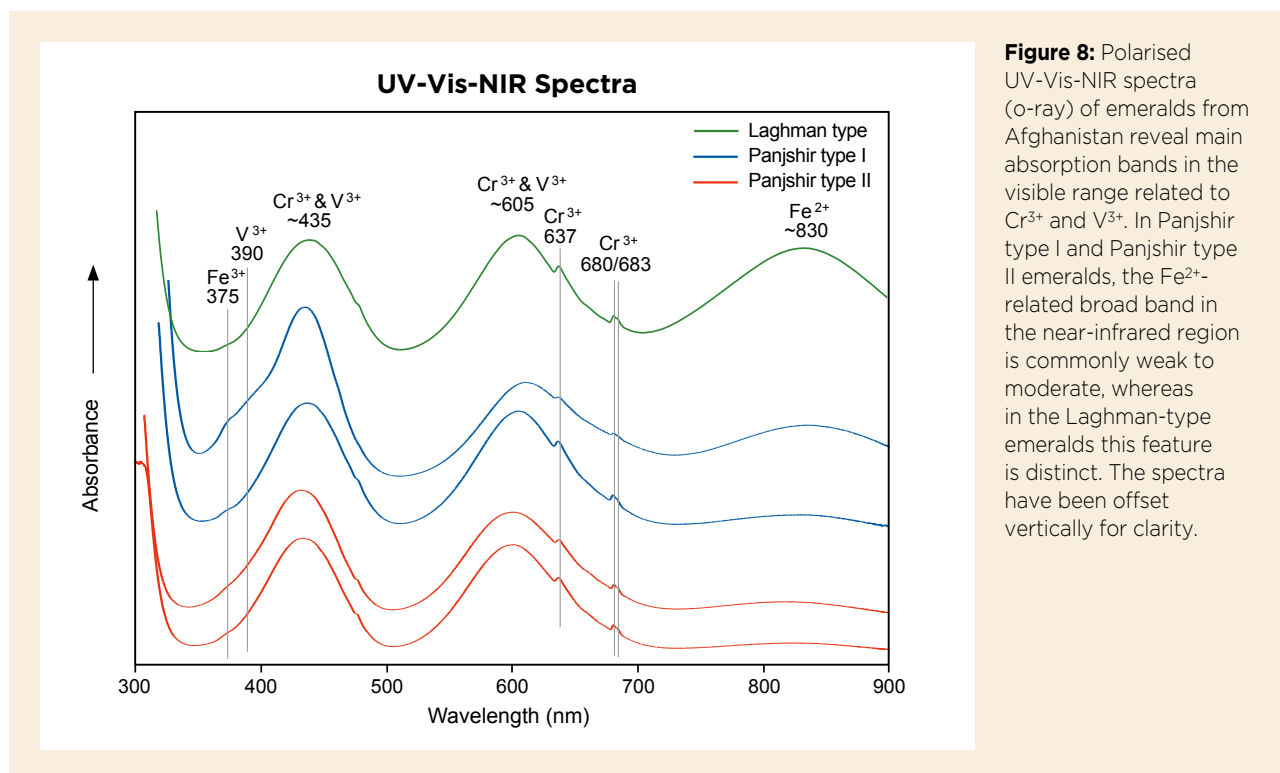
emeralds is a broad absorption band in the near-infrared region at about 830 nm, which is related to octahedrally coordinated Fe^{2+} (Wood & Nassau 1968; Taran & Rossman 2001). The intensity of this band can vary from very weak to moderate in Panjshir emeralds. By contrast, the spectra of the relatively Fe-rich Laghman-type emeralds were distinctive in showing a significantly stronger Fe^{2+} absorption band at about 830 nm; this is among the features that are sometimes described as the 'aquamarine component' in such Fe-rich emeralds.

Raman Spectroscopy: Type I and Type II H_2O

Raman micro-spectroscopy was used to determine the average orientation of H_2O molecules in the beryl channel structure (cf. Huong 2008; Huong et al. 2010), based on the relative intensity of the bands at 3608 cm^{-1} (type I H_2O) and 3598 cm^{-1} (type II H_2O). Interestingly, the three types of Afghan emeralds in this study revealed distinct differences in the patterns of these bands (Figure 9).

For the Panjshir type II emeralds, type I H_2O clearly dominated over type II H_2O, indicating that the axis of the water molecules in these emeralds is predominately perpendicular to the c-axis (and channel axis; see Wood & Nassau 1968; Huong et al. 2010). This is consistent with their low concentration of alkali elements, as determined by the chemical analyses (see below).

By contrast, the Panjshir type I emeralds generally

Figure 8: Polarised UV-Vis-NIR spectra (o-ray) of emeralds from Afghanistan reveal main absorption bands in the visible range related to Cr^{3+} and V^{3+}. In Panjshir type I and Panjshir type II emeralds, the Fe^{2+}-related broad band in the near-infrared region is commonly weak to moderate, whereas in the Laghman-type emeralds this feature is distinct. The spectra have been offset vertically for clarity.
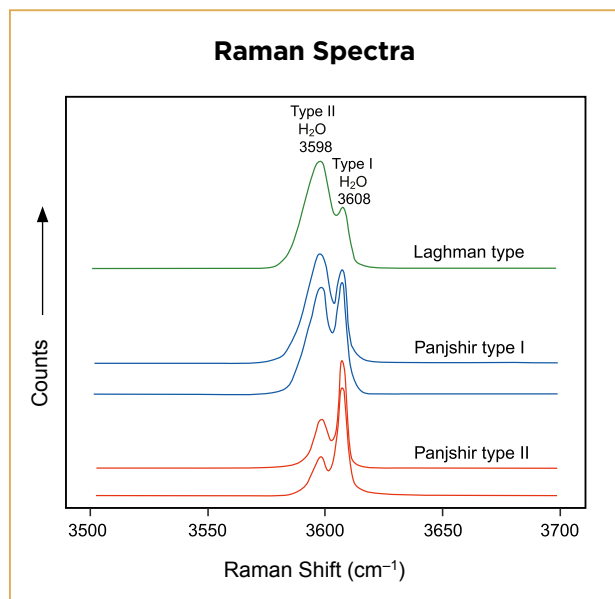
Figure 9: Raman spectra show variable band intensities corresponding to the different orientations of the water molecules in the channel structure (i.e. type I and type II H_2O; after Huong *et al.* 2010) for emeralds from the three studied occurrences in Afghanistan. The spectra have been offset vertically for clarity.

showed essentially equal intensities of both H_2O bands, thus indicating no particular abundance of the water-molecule orientation parallel or perpendicular to the *c*-axis.

Interestingly, the Laghman-type emeralds were distinct from both types of Panjshir emeralds by the predominance of type II H_2O. This indicates that the axis of most water molecules in these emeralds is oriented parallel to the *c*-axis. This is characteristic of emeralds hosted in mafic to ultramafic host rocks (i.e. deposit types IA and IIA; Giuliani *et al.* 2019), which typically contain notable amounts of alkali elements (Na, K, Rb and Cs) in the channels of the beryl structure.

EDXRF Chemical Analysis

EDXRF spectroscopy is for many gem laboratories the standard method to obtain chemical data from gems, and this technique can sometimes provide important information about the origin and geological context of a sample—particularly for emeralds, with their extensive possibilities for chemical substitutions in the different lattice sites and the channel structure of beryl (Groat *et al.* 2014). Table III summarises the results for selected elements as determined by EDXRF spectroscopy for the Afghan emeralds and for samples from SSEF's reference collection. As with the water-related Raman spectra described above, the trace-element compositions of the three types of emeralds were quite distinct from each other.

Although the Mg concentrations in our samples varied considerably, the Panjshir type I and Laghman-type emeralds generally contained distinct amounts of this element (Panjshir type I median = 0.70 wt.% MgO and Laghman-type median = 1.41 wt.% MgO). By contrast, Mg was not detectable in any of the Panjshir type II emeralds with our EDXRF spectrometer.

The average concentrations of the chromophores V, Cr and Fe also showed distinct trends for all three types

Table III: Chemical composition by EDXRF of the Afghan emeralds compared to those from other sources.*

Oxides (wt.%)	Panjshir type I (40 samples)	Panjshir type II (43 samples)	Laghman type (5 samples)	Muzo, Colombia	Muzo, Colombia (high Sc)	Kafubu, Zambia
MgO	0.11–1.76 (0.70)	bdl	0.84–1.92 (1.41)	bdl	bdl	1.98
Sc_2O_3	0.04–0.64 (0.31)	bdl–0.14 (0.04)	0.02–0.06 (0.02)	0.04	0.35	bdl
V_2O_3	0.10–1.61 (0.93)	0.15–0.42 (0.31)	0.02–0.05 (0.03)	0.83	0.73	0.04
Cr_2O_3	0.16–0.72 (0.31)	0.32–0.86 (0.54)	0.41–0.85 (0.69)	0.64	0.10	0.43
Fe_2O_3	0.47–2.84 (0.89)	0.20–0.42 (0.28)	0.43–0.67 (0.48)	0.10	0.13	2.86
Cs_2O	bdl	bdl	0.08–0.13 (0.10)	bdl	bdl	0.14

* Numbers in parentheses are median values. Representative analyses of Colombian and Zambian emeralds were selected from SSEF's database. Abbreviation: bdl = below detection limit (commonly 0.002 wt.% for heavy elements and 0.1–0.5 wt.% for light elements).
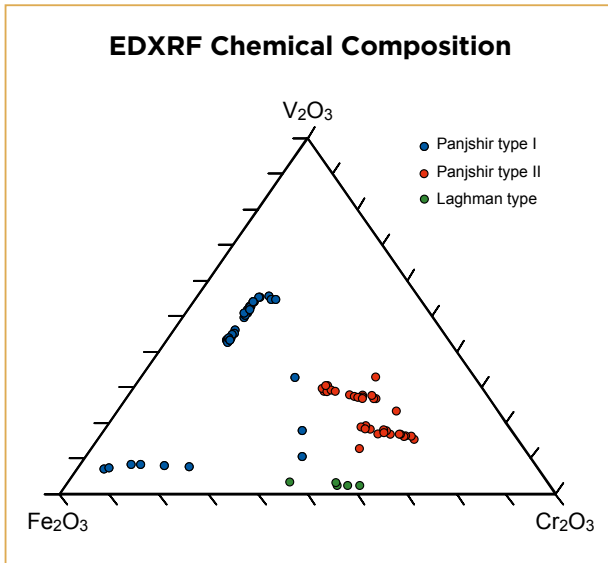
Figure 10: EDXRF chemical data for the chromophores V, Cr and Fe are plotted in this ternary diagram (after Graham & Midgley 2000) for the three different emerald types from Afghanistan.

of Afghan emeralds (Figure 10). Panjshir type I emeralds generally had the greatest amount of V (up to 1.61 wt.% V_2O_3). The V-rich emeralds also commonly showed the highest Sc concentrations (up to 0.64 wt.% Sc_2O_3) of all the samples we tested, indicating a positive correlation trend for V and Sc in Panjshir emeralds.

In general, the Cr concentration of our Panjshir type I emeralds was lower (median 0.31 wt.% Cr_2O_3) than the amount of Fe (median 0.89 wt.% Fe_2O_3). By contrast, the Cr concentration of the Panjshir type II emeralds (up to 0.86 wt.% Cr_2O_3) was distinctly higher than Fe (median of only 0.28 wt.% Fe_2O_3), with V values equal to or lower than those of Cr.

The Laghman-type emeralds were very poor in V and Sc but contained appreciable amounts of Cr (median = 0.69 wt.% Cr_2O_3) and Fe (median = 0.48 wt.% Fe_2O_3). The alkali metal Cs (residing in the beryl channel structure) was detected by EDXRF only in the Laghman-type emeralds (see also Henn & Schmitz 2014).

Comparing our Afghan emeralds with selected samples from other important sources, the chemical composition of the Laghman-type samples was consistent with those from schist-hosted deposits (i.e. types IA and IIA after Giuliani *et al.* 2019), such as Kafubu, Zambia. The Panjshir type II material was similar in composition to emeralds from Colombia (including those with high Sc; again, see Table III).

LA-ICP-TOF-MS Chemical Analysis

Table IV summarises the results of LA-ICP-TOF-MS analyses of our Afghan emerald samples. The data

show that, similar to our EDXRF results, the three types of Afghan emeralds can be conclusively distinguished by their trace-element compositions. However, mass spectrometry is sensitive to a much larger range of elements, so it provides data not accessible by EDXRF, specifically regarding light elements (e.g. Li, Be and B) and ultra-trace elements (in this case, Ge, Sr and Tl).

The Laghman-type emeralds generally contained more chemical impurities than the Panjshir emeralds. Specifically, they showed distinctly higher concentrations of Li, B, Mn, Co, Ni, Zn, Sn, Cs and Tl. The distribution of chromophores (V, Cr and Fe) clearly underscores the difference in the geological setting and formation of Laghman-type emeralds compared to both types of Panjshir emeralds. The Panjshir type I and Panjshir type II samples both had distinctly higher concentrations of V than the Laghman-type emeralds. In addition, some of the Panjshir type II emeralds showed distinctly higher V concentrations (up to 3105 ppm) than Panjshir type I stones—which is opposite to our EDXRF results. This might be related to chemical zoning in these emeralds, which cannot be resolved by EDXRF due to the rather large area analysed by this method. The trends in Sc concentration, however, were consistent with the EDXRF results, revealing that the highest Sc concentrations occurred in the Panjshir type I emeralds.

Plotting V vs Sc shows a distinct linear correlation, with the three types of Afghan emeralds falling into discrete groups (Figure 11a). A non-logarithmic plot (Figure 11b) reveals further correlation trends within the Panjshir type II samples.

It is well known that the incorporation of alkaline earth metals (specifically Mg^{2+} and Ca^{2+}) in the octahedrally coordinated Al^{3+} site in beryl is charge-balanced by alkali metals (specifically Na^+, K^+, Rb^+ and Cs^+) in the channel structure: $Al^{3+} \rightarrow (Mg, Ca)^{2+} + (Na, K, Rb, Cs)^+_{channel}$ (see Groat *et al.* 2014 and references therein). A plot of (Mg + Ca) vs Na (Figure 12a) shows a near-perfect positive correlation for Panjshir emeralds, in two well-discernible groups (Panjshir type I and Panjshir type II). Therefore, in these emeralds the alkaline earths (Mg and Ca) are almost completely charge balanced by Na only. By contrast, the Laghman-type emeralds are slightly offset from the r = 1 correlation line in Figure 12a. However, by taking into account all additional alkalis (K, Rb and Cs) present in the channel structure, they plot more closely to the correlation line (Figure 12b). Interestingly, in this second figure we also see that the Panjshir type I (and some type II) emeralds are slightly offset below the r = 1 correlation line, possibly indicating that some of the alkali

Table IV: Chemical composition by LA-ICP-TOF-MS of Afghan emeralds.*

Elements (ppm)	Panjshir type I (20 samples)	Panjshir type II (44 samples)	Laghman type (8 samples)
Li	81.12–212.6 (91.54)	73.36–108.7 (93.13)	216.6–371.6 (313.4)
B	bdl–1.959 (0.794)	bdl–1.171 (0.383)	2.225–5.561 (3.078)
Na	6730–11690 (9997)	3130–6210 (4141)	10920–13340 (12680)
Mg	5860–11720 (9914)	2565–5620 (3624)	12960–15050 (14300)
K	242.0–870.4 (696.2)	22.46–77.20 (33.28)	526.1–770.0 (654.6)
Ca	236.2–610.6 (385.4)	278.6–714.4 (567.8)	563.2–995.4 (829.6)
Sc	130.3–1083 (708.4)	36.83–767.3 (71.75)	36.19–111.2 (100.2)
Ti	9.87–59.91 (24.19)	4.49–17.69 (10.85)	12.51–24.20 (17.90)
V	447.6–990.7 (862.5)	595.5–3105 (824.5)	117.6–188.3 (176.3)
Cr	239.8–2979 (1223)	1878–4875 (2625)	1710–5317 (4669)
Mn	1.434–3.526 (2.212)	0.336–0.952 (0.503)	6.628–9.955 (8.128)
Fe	3963–11330 (8000)	1100–2057 (1308)	1925–2317 (2116)
Co	bdl–0.102 (0.043)	bdl–0.110 (bdl)	1.471–1.646 (1.538)
Ni	0.298–3.128 (0.644)	0.630–2.952 (1.138)	9.79–15.94 (10.88)
Zn	bdl–0.760 (0.285)	0.333–0.964 (0.627)	13.90–18.64 (15.11)
Ga	17.74–36.74 (32.14)	13.94–31.53 (17.30)	7.65–8.94 (8.06)
Ge	0.831–1.969 (1.339)	0.202–0.654 (0.295)	0.511–0.909 (0.694)
Rb	19.72–68.46 (51.92)	1.929–4.316 (2.554)	33.55–46.79 (37.78)
Sr	bdl–0.163 (bdl)	bdl–0.209 (bdl)	0.036–0.166 (0.056)
Sn	0.097–1.432 (0.349)	bdl–0.120 (0.050)	1.498–4.560 (3.827)
Cs	30.84–70.37 (45.75)	6.916–9.993 (8.725)	612.4–1334 (769.3)
Tl	0.009–0.036 (0.023)	bdl–0.014 (bdl)	0.127–0.273 (0.197)

* Numbers in parentheses are median values; bdl = below detection limit (commonly a few ppb for heavy elements to hundreds of ppb for light elements).
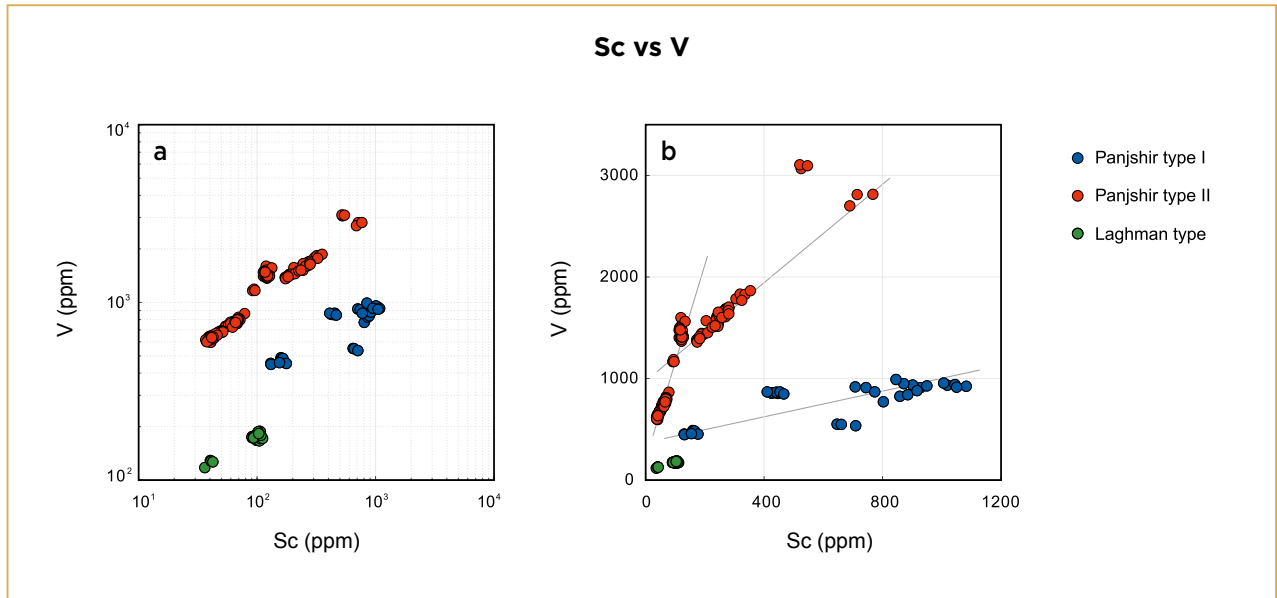
Sc vs V

Figure 11: A positive correlation between Sc and V in Afghan emeralds is shown on these scatter plots with (**a**) logarithmic axis scales and (**b**) linear axis scales. The analyses for each of the three localities also cluster into distinct groups.
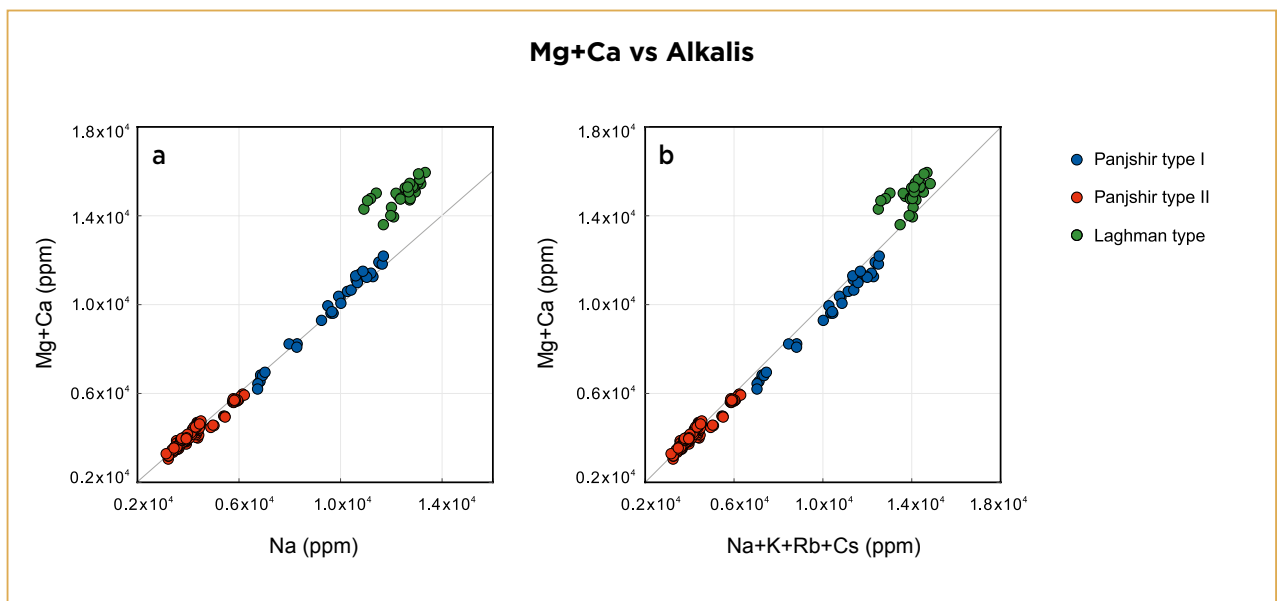
Mg+Ca vs Alkalis

Figure 12: These scatter diagrams plot octahedrally coordinated Ca + Mg vs alkali elements in the channel sites—that is, (**a**) Na and (**b**) Na + K + Rb + Cs. They reveal a distinct positive correlation—with data points falling along the r = 1 correlation line—as a result of charge-balanced substitution processes. In both diagrams, the emeralds from the three studied occurrences in Afghanistan are clearly distinct from each other along the correlation lines.

metals in the channel structure are charge-balanced by Fe^{2+} replacing Al^{3+} in the octahedral site: $Al^{3+} \rightarrow Fe^{2+} + (Na, K, Rb, Cs)^{+}_{channel}$. The distinct presence of Fe^{2+} in Panjshir type I emeralds was confirmed by UV-Vis-NIR spectroscopy, which revealed a weak-to-moderate broad band in the NIR attributed to octahedrally coordinated Fe^{2+} (see Figure 8).

It has been documented previously in the literature that Al substitution by alkalis and alkaline-earth metals also directly affects the physical properties of beryl,

namely SG and RI values (e.g. Winchell & Winchell 1951; Sosedko 1957; Černý & Hawthorne 1976; Hänni 1980). These correlations can also be observed in the three different types of emeralds from Afghanistan. The Panjshir type II stones, with only minor concentrations of alkalis and alkaline earths, showed the lowest SG and RI values (average SG = 2.72 and RI = 1.575–1.582), whereas the Panjshir type I and Laghman-type emeralds, with distinctly higher amounts of these elements, had greater SG and RI values (see Table I).

DISCUSSION

The three types of emeralds from Afghanistan investigated in this study can be clearly separated from each other based on their trace-element composition (as well as spectral features for Panjshir- vs Laghman-type samples). More challenging, however, is the separation of Afghan emeralds from those of other important deposits, notably from Colombia. This is specifically important for the Panjshir type II emeralds, which in many aspects are very similar to top-quality emeralds from Muzo and other famous sources in Colombia. It is therefore not surprising that a number of these Panjshir type II emeralds have been (and still are) mislabelled as Colombian stones.

Panjshir Type I vs Colombia and Davdar (China)

Panjshir type I emeralds are to some extent similar to Colombian emeralds but are still quite straightforward to identify. The spiky (jagged) halite-sylvite-bearing multiphase fluid inclusions in Panjshir type I emeralds are considered characteristic (Figure 4b, c) and help to separate them from Colombian emeralds, which contain mainly three-phase inclusions (Schwarz & Pardieu 2009; Saeseaw *et al.* 2014; Giuliani *et al.* 2018). In addition, Panjshir type I emeralds show a characteristic weak-to-moderate absorption band in the near-infrared region (Figure 13; see also Schwarz & Pardieu 2009; Karampelas *et al.* 2019), which is absent from most Colombian emeralds and only rarely encountered in some Fe-rich ones. In addition, Fe normally dominates the concentration of other colouring elements (V ± Cr) in Panjshir type I emeralds, which is distinctly different from Colombian emeralds. The visual appearance and internal features (i.e. jagged fluid inclusions) of Davdar emeralds (Schwarz & Pardieu 2009; Cui *et al.* 2020) might seem similar to Panjshir type I stones, but the Davdar emeralds can generally be distinguished by their much stronger absorption in the near-infrared region and differences in trace-element concentrations (see below).

Laghman Type (Korgun) vs Other Sources

The internal features of Laghman-type stones are similar to those found in schist-hosted emeralds related to mafic and ultramafic host rocks (i.e. types IA and IIA of Giuliani *et al.* 2019), such as from deposits in Zambia, Ethiopia and Russia, and can only be separated from those by careful examination. Their similarity is also expressed by a distinct Fe^{2+}-related absorption band in the near-infrared region (Figures 8 and 13; see also Henn & Schmitz

2014; Karampelas *et al.* 2019) and by the dominance of type II water in the beryl channel structure (more intense 3598 cm^{-1} band in Raman spectra; see Figure 9). Both of these features are highly characteristic of emeralds from deposits related to mafic and ultramafic host rocks. However, a fundamental difference is that the Laghman-type emeralds we investigated contained rather low Fe concentrations, in many cases even lower than Cr (see EDXRF data in Table III), whereas Fe is generally much higher than Cr in schist-hosted emeralds.

Panjshir Type II vs Colombia

Although Panjshir type II emeralds are challenging for origin determination, there are still various ways to make a clear and unambiguous separation from Colombian emeralds.

Meticulous microscopic observation will often reveal characteristic features of Panjshir type II emeralds, such as dense patterns of hollow channels (parallel to the *c*-axis) that are partially filled with brownish Fe-hydroxide. This is in contrast to Colombian emeralds, which sometimes show similar hollow channels, but these are extremely fine and without similar secondary
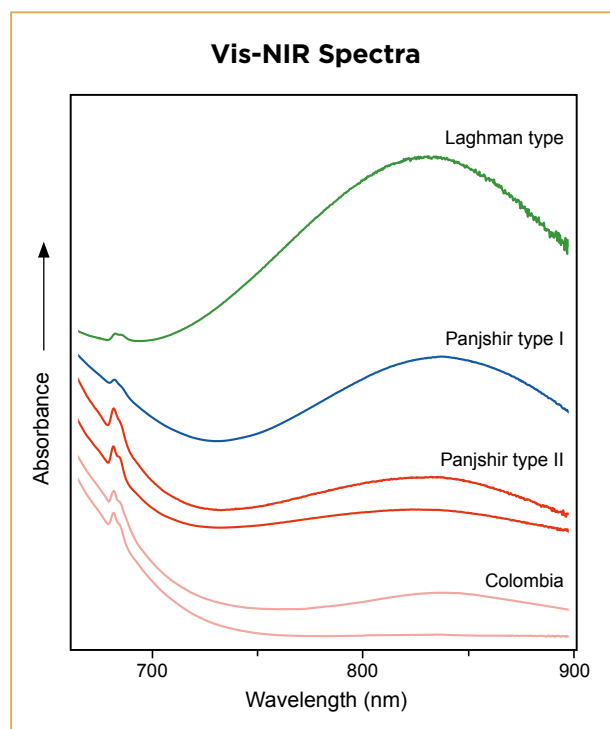
Figure 13: Polarised absorption spectra (o-ray) for the three Afghan emerald types in the red to near-infrared range show variations in the strength of the absorption band at about 830 nm, which is related to octahedrally coordinated Fe^{2+}. Panjshir type I and Panjshir type II emeralds show weak-to-moderate absorption, whereas stones from Colombia typically exhibit no such absorption feature. The spectra have been offset vertically for clarity.
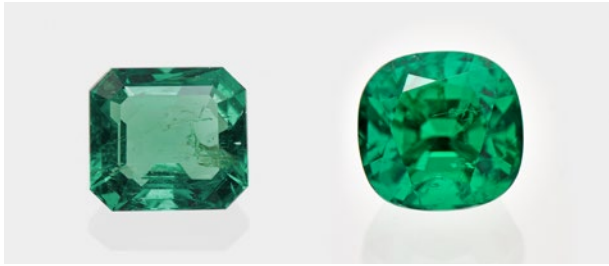
Figure 14: The appearance of an unusual Fe-rich emerald from Colombia (left, 5.77 ct) that shows a weak absorption band in the near-infrared region at about 830 nm is compared to a vibrant green Panjshir type II emerald (right, 4.50 ct). Composite photo by Luc Phan, © SSEF.

natural residue. Although swirled patterns were seen occasionally in the Panjshir type II emeralds, we have not observed the distinct *gota de aceite* graining pattern seen in some Colombian emeralds.

In addition, Panjshir type II emeralds always show a weak Fe^{2+}-related absorption band at about 830 nm (Figure 13), similar to or even weaker than the Panjshir type I emeralds. This is in contrast to Colombian emeralds of high quality, which in most cases show no such absorption in the near-infrared range. Occasionally, Fe-rich Colombian emeralds may show a weak absorption in the near-infrared similar to Afghan emeralds, however those Colombian stones are usually characterised by a slightly greyish green colour of rather low saturation as compared to the vibrant green colour of Panjshir type II emeralds (Figure 14).

Raman analysis of both Panjshir type II and Colombian emeralds show a prevalence of type I H_2O (i.e. the 3608 cm^{-1} band is clearly dominant over the 3598 cm^{-1} band), indicating a low concentration of alkali elements (Na, K, Rb and Cs) in the beryl channel structure. Therefore it is not possible to separate samples from these two origins based on this criterion.

Trace-element data provide the best option for clearly distinguishing Panjshir type II emeralds from those of Colombia. Notably, the concentration of Fe is usually distinctly higher in the Panjshir type II emeralds (Figure 15). In rare cases, gem-quality emeralds from Colombia can also show high Fe concentrations (up to 2000 ppm, according to SSEF's database, and also reported by Saeseaw *et al.* 2014 and Karampelas *et al.* 2019). However, when plotting the V/Cr ratio vs Fe, all of the Colombian emeralds in SSEF's database—including the so-called Fe-rich samples—can be clearly separated from Panjshir type II, and even more so from Panjshir type I and Laghman-type emeralds (again, see Figure 15). This was also evident from our EDXRF analyses, which showed 0.20–0.42 wt.% Fe_2O_3 in the Panjshir type II samples and generally only about 0.10 wt.% Fe_2O_3 in Colombian stones (see, e.g., Table III). In many cases, the differences between Panjshir type II and Colombian emeralds can be detected by comparing the peak ratios of V, Cr and Fe in EDXRF spectra (Figure 16). Based on this, we propose that EDXRF spectroscopy—a commonly available technique in gem labs—can be helpful for separating emeralds from these two sources. Nevertheless, this approach may not be valid for Fe-rich Colombian emeralds, and always requires further (i.e. microscopic) investigations to draw a reliable conclusion.
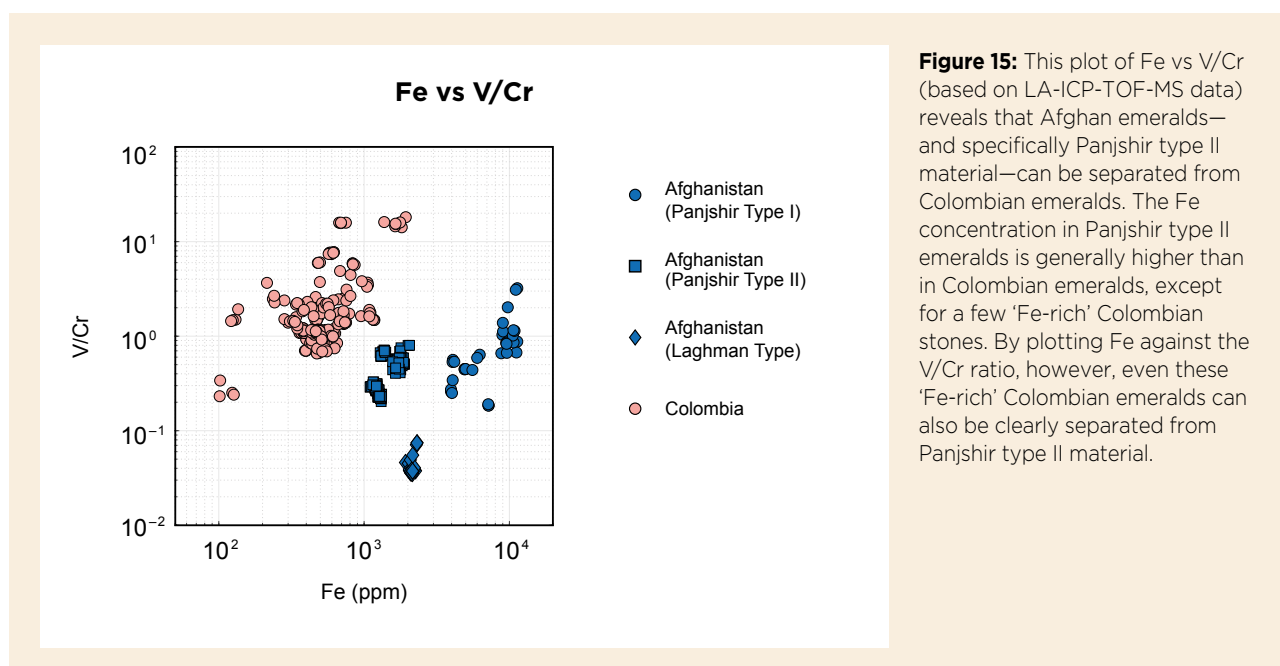

Figure 15: This plot of Fe vs V/Cr (based on LA-ICP-TOF-MS data) reveals that Afghan emeralds—and specifically Panjshir type II material—can be separated from Colombian emeralds. The Fe concentration in Panjshir type II emeralds is generally higher than in Colombian emeralds, except for a few 'Fe-rich' Colombian stones. By plotting Fe against the V/Cr ratio, however, even these 'Fe-rich' Colombian emeralds can also be clearly separated from Panjshir type II material.
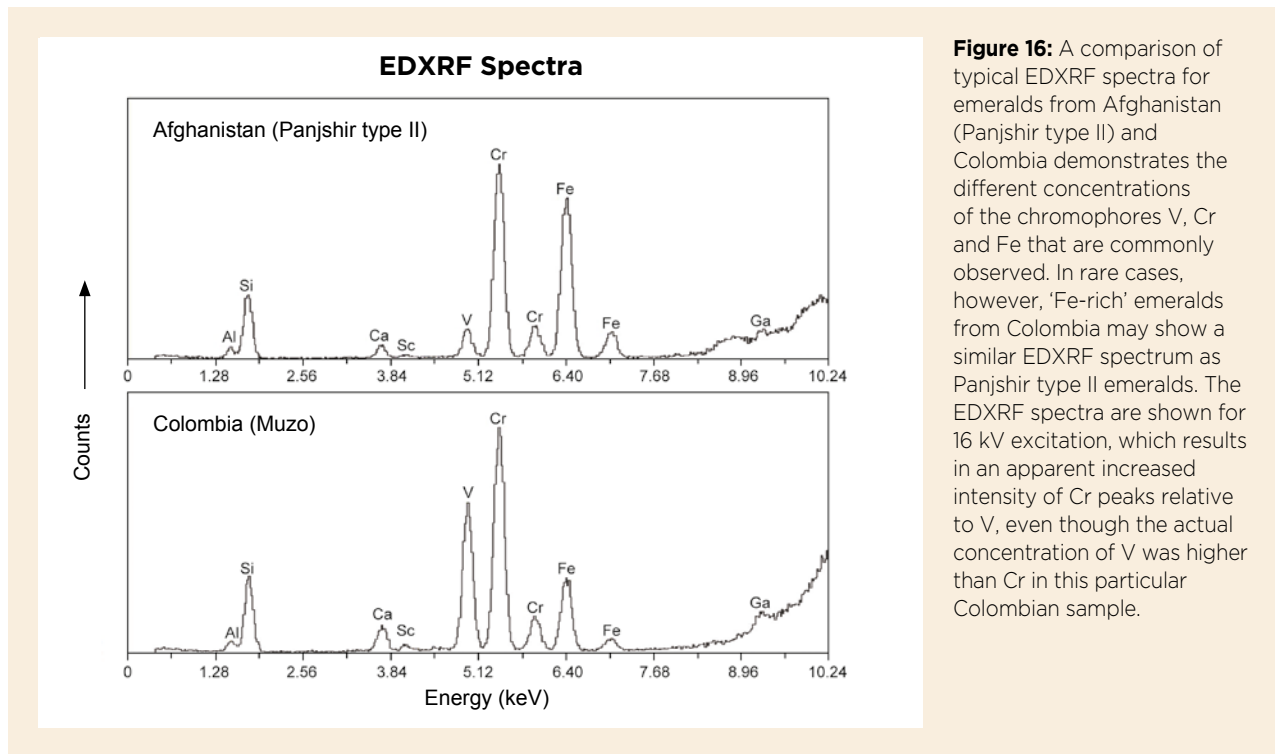
Figure 16: A comparison of typical EDXRF spectra for emeralds from Afghanistan (Panjshir type II) and Colombia demonstrates the different concentrations of the chromophores V, Cr and Fe that are commonly observed. In rare cases, however, 'Fe-rich' emeralds from Colombia may show a similar EDXRF spectrum as Panjshir type II emeralds. The EDXRF spectra are shown for 16 kV excitation, which results in an apparent increased intensity of Cr peaks relative to V, even though the actual concentration of V was higher than Cr in this particular Colombian sample.

Summary: Emeralds from Afghanistan vs Other Sources

Emeralds from different origins reveal a large chemical variability as a result of the beryl structure, which offers multiple sites for element substitutions, including a large channel structure. As such, emeralds (and beryl in general) are very susceptible indicators of the geological environment in which they formed and can be classified into different deposit/formation types (see Giuliani *et al.* 2019 and references therein).

LA-ICP-MS trace-element data can be very helpful for separating gems from different provenances (e.g. Guillong & Günther 2001; Abduriyim & Kitawaki 2006) and specifically emeralds (Cronin & Rendle 2012; Schwarz & Klemm 2012; Saeseaw *et al.* 2014; Aurisicchio *et al.* 2018; Karampelas *et al.* 2019). However, visualising trends in a large multi-element data set is often challenging and requires evaluation of multiple 2D and 3D scatter plots.

Figure 17 demonstrates how the Panjshir type I and Panjshir type II emeralds are quite similar to Colombian emeralds, whereas Laghman-type stones plot close to those from Zambia, Ethiopia and the Swat Valley in Pakistan. As seen in the Li-Cs 2D scatter plot (Figure 17a) and, even better, in the Rb-Tl-Cs 3D diagram (Figure 17d), our Panjshir type II emeralds significantly overlap Colombian emeralds, whereas in the other 2D and 3D scatter plots these data clusters are more distinct.

Emeralds from Davdar (China) are in many aspects quite similar to stones from Panjshir (Schwarz & Pardieu 2009) and even Colombian emeralds. Cui *et al.* (2020) discussed the difficulty of chemically separating Davdar emeralds from Panjshir material due to overlapping elemental concentrations. However, by plotting their data together with our LA-ICP-TOF-MS analyses, we can see a clear chemical distinction based on Ni, Rb and Cs (see Figure 18 and the rotational video clip in the data depository).

Plotting elemental ratios in a 2D diagram is another option for distinguishing emeralds from different origins based on trace elements. Figure 19 plots the ratios Cs/Ga vs Na/Li for emeralds from Colombia, Pakistan (Swat Valley), Brazil (Santa Terezinha), Austria (Habachtal), Nigeria and Russia (from Schwarz 2015 and Giuliani *et al.* 2019). Adding our data from Afghanistan and other sources (Colombia, Ethiopia, Nigeria, Pakistan and Zambia) results in significant overlaps between the various localities. Notably, the Panjshir type II emeralds plot completely within the Colombian field, and the Laghman-type emeralds overlap those from Russia and Zambia. Consequently, this ratio diagram is of only limited use for separating Afghan emeralds from those of other sources, although it is helpful for geochemical studies since it groups together emeralds of similar geological contexts.

As an alternative, we used an automated statistical algorithm (t-SNE) to visualise data clusters and sample relationships within the multi-element data set. For
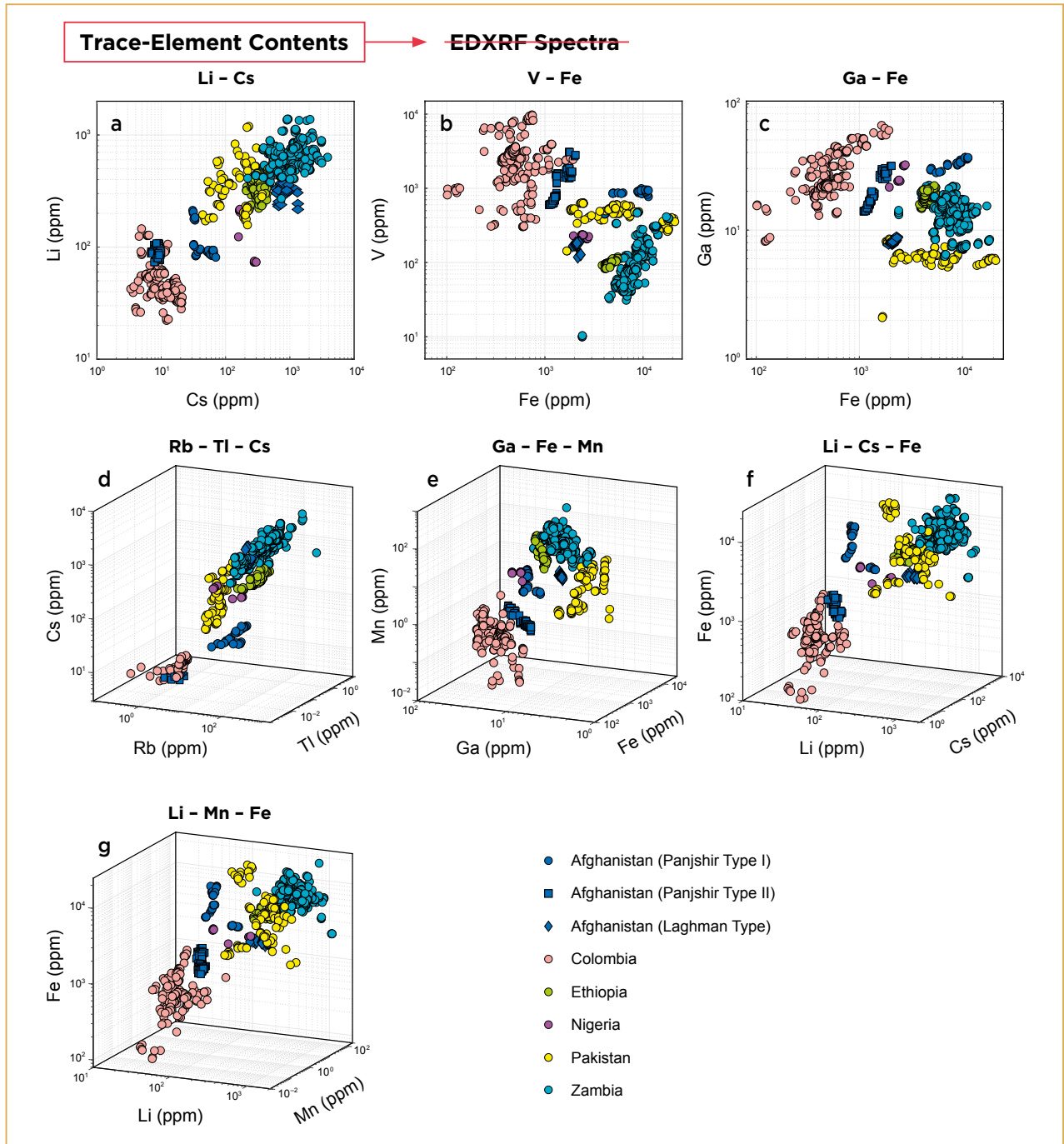
Figure 17: Scatter plots for various elements compare the three types of emeralds from Afghanistan with those from other important deposits, based on data collected at SSEF using LA-ICP-TOF-MS. Rotational video clips for each of the 3D scatter plots are available in *The Journal*'s data depository.

a detailed description of this new and versatile data processing method, see Wang and Krzemnicki (2021). The 3D t-SNE plot in Figure 20 shows that this approach is effective for distinguishing emeralds from different localities, including all three types from Afghanistan. The Panjshir type II emeralds plot in a cluster that is clearly separate from Colombian emeralds, and also from all other selected sources, including Zambia, Ethiopia, Pakistan and Nigeria. For simplicity, we have omitted from this plot some emerald deposits (mainly schist type)—such as those in Brazil (e.g. Itabira-Nova Era), Madagascar (e.g. Mananjary) and China (e.g. Yunnan)—which are easily separated from those of Afghanistan and Colombia (i.e. hydrothermal type).

For all the 3D scatter plots in Figures 17 and 20, rotational video clips are available in the data depository to better visualise the relationships between the analytical clusters for emeralds from different provenances.
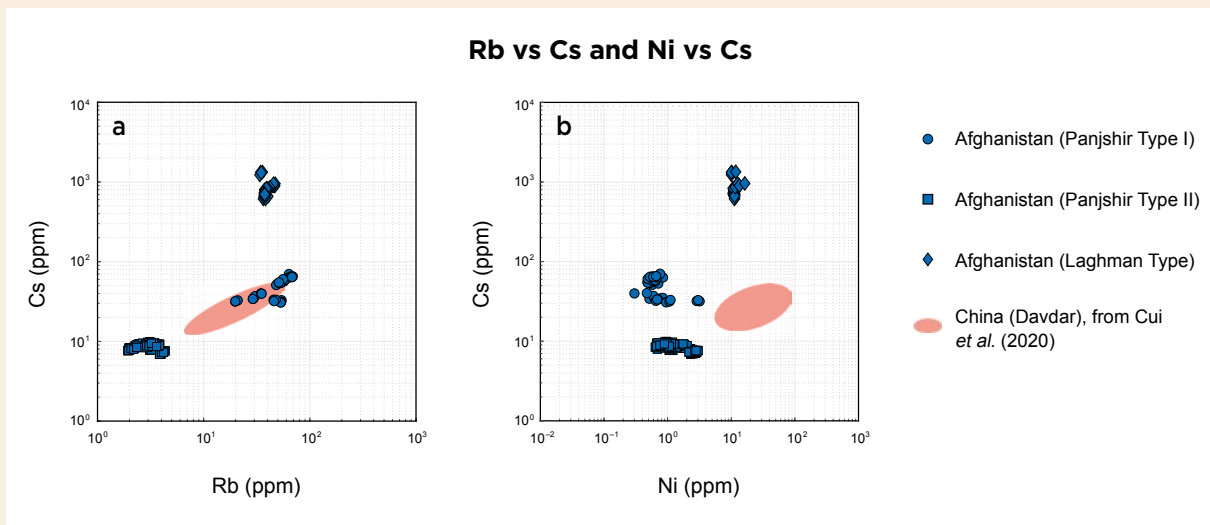
Rb vs Cs and Ni vs Cs

Figure 18: Trace-element data for Davdar emeralds (from Cui *et al.* 2020) are plotted together with analyses obtained in this study for the three types of Afghan emeralds. (**a**) A plot of Rb vs Cs shows a distinct positive correlation for both Davdar and Panjshir type I emeralds, with some overlap, whereas Panjshir type II and Laghman-type samples are clearly distinct. (**b**) A plot of Ni vs Cs clearly separates all three Afghanistan occurrences from Davdar emeralds.
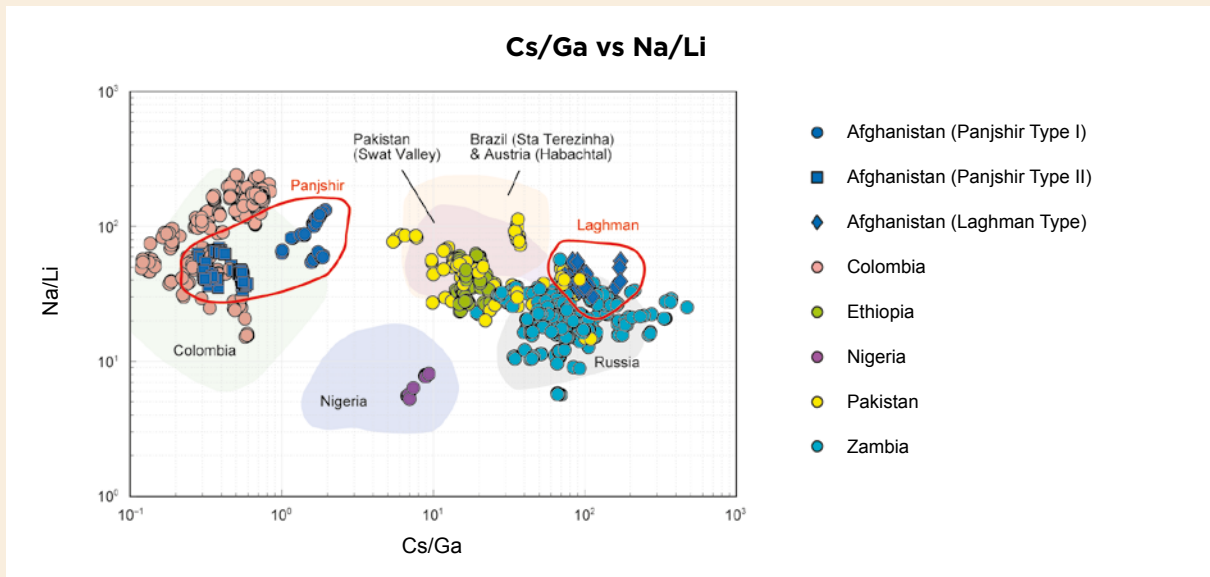
Cs/Ga vs Na/Li

t-SNE Plot

Figure 19: A plot of the ratios of Cs/Ga vs Na/Li, as proposed by Schwarz (2015) for showing genetic relationships between various types of emerald deposits, reveals that stones from Panjshir (specifically type II) and Laghman overlap with different emerald population fields. The coloured fields are from Schwarz (2015) and Giuliani *et al.* (2019).
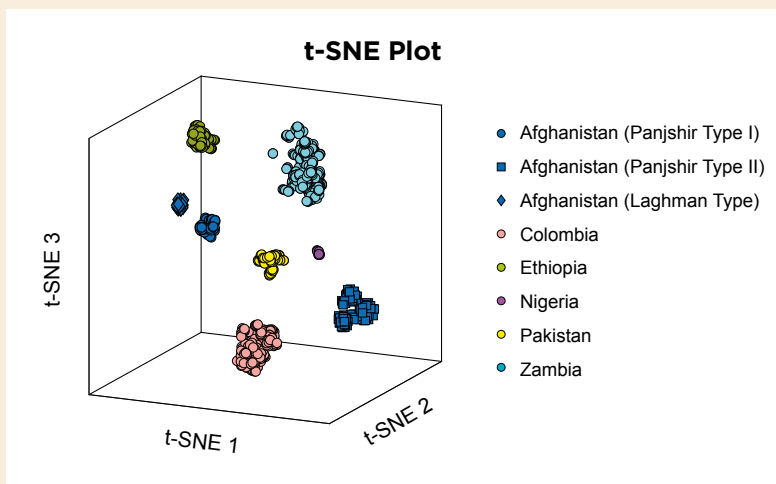
Figure 20: A 3D t-SNE scatter plot shows that data clusters for the three emerald occurrences in Afghanistan can be distinguished from each other and from other selected worldwide sources.

CONCLUSIONS

Fine-quality emeralds from Afghanistan have been known in the trade for decades, with the main source being the Panjshir Valley (providing what is referred to in this article as Panjshir type I emeralds) and a few stones coming from Laghman Province near Korgun. This study focused on relatively new emerald production from the Panjshir Valley—referred to here as Panjshir type II—which emerged on the market in 2017. This newer Afghan material is in many aspects equal to the best-quality Colombian emeralds, including some similar microscopic and chemical features. Nevertheless, we have shown that Panjshir type II emeralds can be clearly separated from their Colombian counterparts by standard gemmological techniques (e.g. microscopy) and more sophisticated analytical methods (e.g. UV-Vis-NIR, Raman and EDXRF spectroscopy, and LA-ICP-TOF-MS). A statistical dimension-reduction algorithm (t-SNE) applied to the trace-element data from our samples provided an effective, unambiguous way to distinguish emeralds from various localities compared to typical concentration plots and element-ratio diagrams.

This study demonstrates how combining a standard gemmological approach with advanced analytical and statistical methods is useful for characterising gem materials from new sources emerging in the trade. Our research also illustrates how a new type of material can emerge from a well-known gem locality—in this case, emerald from Afghanistan's Panjshir Valley—that possesses quite different properties and trace-element concentrations as a result of local, small-scale variations in geological conditions.

REFERENCES

Abdullah, S., Chmyriov, V.M., Stazhilo-Alekseev, K.F., Dronov, V.I., Gannon, P.J., Lubemov, B.K., Kafarskiy, A.K. & Malyarov, E.P. 1977. *Mineral Resources of Afghanistan*, 2nd edn. Ministry of Mines and Industries, Afghan Geological and Mines Survey, Kabul, Afghanistan, 419 pp.

Abduriyim, A. & Kitawaki, H. 2006. Applications of laser ablation–inductively coupled plasma–mass spectrometry (LA-ICP-MS) to gemology. *Gems & Gemology*, **42**(2), 98–118, https://doi.org/10.5741/gems.42.2.98.

Aurisicchio, C., Conte, A.M., Medeghini, L., Ottolini, L. & De Vito, C. 2018. Major and trace element geochemistry of emerald from several deposits: Implications for genetic models and classification schemes. *Ore Geology Reviews*, **94**, 351–366, https://doi.org/10.1016/j.oregeorev.2018.02.001.

Bariand, P. & Poullen, J.F. 1978. Famous mineral localities: The pegmatites of Laghman, Nuristan, Afghanistan. *Mineralogical Record*, **9**(5), 301–308.

Bowersox, G.W. 1985. A status report on gemstones from Afghanistan. *Gems & Gemology*, **21**(4), 192–204, https://doi.org/10.5741/gems.21.4.192.

Bowersox, G.W. 2015. The emerald mines of the Panjshir Valley, Afghanistan. *InColor*, December, Special Issue: World Emerald Update, 70–77.

Bowersox, G., Snee, L.W., Foord, E.E. & Seal, R.R. 1991. Emeralds of the Panjshir Valley, Afghanistan. *Gems & Gemology*, **27**(1), 26–39, https://doi.org/10.5741/gems.27.1.26.

Černý, P. & Hawthorne, F.C. 1976. Refractive indices versus alkali contents in beryl: General limitations and applications to some pegmatite types. *Canadian Mineralogist*, **14**(4), 491–497.

Chmyriov, V.M., Kafarskiy, A.K., Abdullah, D., Dronov, V.I. & Stazhilo-Alekseev, K.F. 1982. Tectonic zoning of Afghanistan. *Miscellaneous Publication – Geological Survey of India*, **41**(3), 317–329.

Christie's 2015. Hong Kong Magnificent Jewels: An exceptional emerald ring. Christie's, Hong Kong, www.christies.com/lot/lot-an-exceptional-emerald-ring-5952358, accessed December 2020.

Cronin, D.P. & Rendle, A.M. 2012. Determining the geographical origins of natural emeralds through nondestructive chemical fingerprinting. *Journal of Gemmology*, **33**(1–4), 1–13, https://doi.org/10.15506/JoG.2012.33.1.1.

Cui, D., Liao, Z., Qi, L., Zhong, Q. & Zhou, Z. 2020. A study of emeralds from Davdar, north-western China. *Journal of Gemmology*, **37**(4), 374–392, https://doi.org/10.15506/JoG.2020.37.4.374.

DeWitt, J.D., Chirico, P.G., O'Pry, K.E. & Bergstresser, S.E. 2020. Mapping the extent and methods of small-scale emerald mining in the Panjshir Valley, Afghanistan. *Geocarto International*, article 1716394 (23 pp.), https://doi.org/10.1080/10106049.2020.1716394.

Forestier, F.H. & Piat, D.H. 1998. Emeraudes de Bactriane: Mythe ou réalité, La vallée du Panjshir (Afghanistan). *In*: Giard, D., Giuliani, G., Cheilletz, A., Fritsch, E. & Gonthier, E. (eds) *L'émeraude : Connaissances Actuelles et Prospectives*. Association Française de Gemmologie, Paris, France, 139–146.

Giard, D. 1998. Le Bouzkachi des émeraudes. Les émeraudes de la Vallée du Panjshir. *In*: Giard, D., Giuliani, G., Cheilletz, A., Fritsch, E. & Gonthier, E. (eds) *L'émeraude : Connaissances Actuelles et Prospectives*. Association Française de Gemmologie, Paris, France, 177–184.

Giuliani, G., France-Lanord, C., Zimmermann, J.L., Cheilletz, A., Arboleda, C., Charoy, B., Coget, P. *et al.* 1997. Fluid composition, δD of channel H_2O, and $δ^{18}O$ of lattice oxygen in beryls: Genetic implications for Brazilian, Colombian, and Afghanistani emerald deposits. *International Geology Review*, **39**(5), 400–424, https://doi.org/10.1080/00206819709465280.

Giuliani, G., Chaussidon, M., Schubnel, H.-J., Piat, D.H., Rollion-Bard, C., France-Lanord, C., Giard, D. *et al.* 2000. Oxygen isotopes and emerald trade routes since antiquity. *Science*, **287**(5453), 631–633, https://doi.org/10.1126/science.287.5453.631.

Giuliani, G., Dubessy, J., Ohnenstetter, D., Banks, D., Branquet, Y., Feneyrol, J., Fallick, A.E. & Martelat, J.-E. 2017. The role of evaporites in the formation of gems during metamorphism of carbonate platforms: A review. *Mineralium Deposita*, **53**(1), 1–20, https://doi.org/10.1007/s00126-017-0738-4.

Giuliani, G., Groat, L.A. & Marshall, D.D. 2018. Emerald deposits in the 21st century: Then, now and beyond. *InColor*, No. 40, 22–32.

Giuliani, G., Groat, L.A., Marshall, D., Fallick, A.E. & Branquet, Y. 2019. Emerald deposits: A review and enhanced classification. *Minerals*, **9**(2), article 105 (63 pp.), https://doi.org/10.3390/min9020105.

Graham, D.J. & Midgley, N.G. 2000. Graphical representation of particle shape using triangular diagrams: An Excel spreadsheet method. *Earth Surface Processes and Landforms*, **25**(13), 1473–1477, https://doi.org/10.1002/1096-9837(200012)25:13%3C1473::aid-esp158%3E3.0.co;2-c.

Groat, L., Giuliani, G., Marshall, D. & Turner, D. 2014. Emerald. *In*: Groat, L.A. (ed) *Geology of Gem Deposits*, 2nd edn. Mineralogical Association of Canada Short Course Series, **44**, Québec City, Québec, Canada, 135–174.

Guillong, M. & Günther, D. 2001. Quasi 'non-destructive' laser ablation-inductively coupled plasma-mass spectrometry fingerprinting of sapphires. *Spectrochimica Acta Part B: Atomic Spectroscopy*, **56**(7), 1219–1231, https://doi.org/10.1016/s0584-8547(01)00185-9.

Hänni, H.A. 1980. *Mineralogische und mineralchemische Untersuchungen an Beryll aus alpinen Zerrklüften*. PhD thesis, University of Basel, Switzerland, 112 pp.

Henn, U. & Schmitz, F. 2014. Smaragde aus der Provinz Laghman, Afghanistan; ein Vergleich mit Smaragden aus dem Panjshir-Tal (Emeralds from Laghman Province, Afghanistan; a comparison with emeralds from Panjshir Valley). *Gemmologie: Zeitschrift der Deutsche Gemmologische Gesellschaft*, **63**(3–4), 105–110.

Hughes, R.W. 2021. Hyperion: The Lotus Gemology inclusion search engine. Lotus Gemology, Bangkok, Thailand, www.lotusgemology.com/index.php/library/inclusion-gallery, accessed December 2020.

Huong, L.T.-T. 2008. *Microscopic, chemical and spectroscopic investigations on emeralds of various origins*. PhD thesis, Johannes Gutenberg-Universität Mainz, Germany, 226 pp., https://doi.org/10.25358/openscience-2607.

Huong, L.T.-T., Häger, T. & Hofmeister, W. 2010. Confocal micro-Raman spectroscopy: A powerful tool to identify natural and synthetic emeralds. *Gems & Gemology*, **46**(1), 36–41, https://doi.org/10.5741/gems.46.1.36.

Karampelas, S., Al-Shaybani, B., Mohamed, F., Sangsawong, S. & Al-Alawi, A. 2019. Emeralds from the most important occurrences: Chemical and spectroscopic data. *Minerals*, **9**(9), article 561 (29 pp.), https://doi.org/10.3390/min9090561.

Kazmi, A.H. & Snee, L.W. (eds) 1989. *Emeralds of Pakistan: Geology, Gemology, and Genesis*. Van Nostrand Reinhold, New York, New York, USA, xii + 269 pp.

Krzemnicki, M.S. 2018. New emeralds from Afghanistan. *SSEF Facette*, No. 24, 12–13, www.ssef.ch/wp-content/uploads/2018/03/2018_SSEF_Facette_24.pdf.

Laurs, B.L. 2001. Gem News International: Emeralds from Laghman, Afghanistan. *Gems & Gemology*, **37**(1), 68.

Rossovskiy, L.N. 1981. Rare metal pegmatites with precious stones and conditions for their formation (Hindu Kush). *International Geology Review*, **23**, 1312–1320.

Rossovskiy, L.N., Chmyrev, V.M. & Salakh, A.S. 1976. New fields and belts of rare-metal pegmatites in the Hindu Kush (eastern Afghanistan). *International Geology Review*, **18**(11), 1339–1342, https://doi.org/10.1080/00206817609471351.

Sabot, B., Cheilletz, A., de Donato, P., Banks, D., Levresse, G. & Barrès, O. 2000. Afghan emeralds face Colombian cousins. *Chronique de la Recherche Minière*, No. 541, 111–114.

Sabot, B., Cheilletz, A., de Donato, P., Banks, D., Levresse, G. & Barrès, O. 2001. The Panjsher-Afghanistan emerald deposit: New field and geochemical evidence for Colombian style mineralisation. *European Union Geoscience XI, Strasbourg*, France, 8–13 April, 548.

Saeseaw, S., Pardieu, V. & Sangsawong, S. 2014. Three-phase inclusions in emerald and their impact on origin determination. *Gems & Gemology*, 114–132, https://doi.org/10.5741/gems.50.2.114.

Schmetzer, K. 2014. Letters: Analysis of three-phase inclusions in emerald. *Gems & Gemology*, **50**(4), 316–319.

Schmetzer, K., Schwarz, D., Bernhardt, H.-J. & Häger, T. 2006. A new type of Tairus hydrothermally-grown synthetic emerald, coloured by vanadium and copper. *Journal of Gemmology*, **30**(1/2), 59–74, https://doi.org/10.15506/jog.2006.30.1.59.

Schwarz, D. 2015. The geographic origin determination of emeralds. *InColor*, December, Special Issue: World Emerald Update, 98–105.

Schwarz, D. & Giuliani, G. 2002. Emeralds from Asia. *In*: Giuliani, G., Jarnot, M., Neumeier, G., Ottaway, T. & Sinkankas, J. (eds) *Emeralds of the World*. extraLapis English No. 2, Lapis International, East Hampton, Connecticut, USA, 60–63.

Schwarz, D. & Pardieu, V. 2009. Emeralds from the Silk Road countries: A comparison with emeralds from Colombia. *InColor*, No. 12, 38–43.

Schwarz, D. & Klemm, L. 2012. Chemical signature of emerald. *34th International Geological Congress*, Brisbane, Australia, 5–10 August, 2812.

Snee, L.W., Lindsay, C.R., Bohannon, R.G., Turner, K.J., Wasay, A., Omar, M., Seal, R.R., Wilds, S.R. *et al.* 2005. *Emerald Deposits of the Panjsher Valley, Afghanistan—Preliminary Assessment of Geologic Setting and Origin of the Deposits*. USGS Administrative Report 2005, Afghanistan Project Product No. 038, U.S. Geological Survey, Washington DC, USA, 97 pp.

Sosedko, T.A. 1957. The change of structure and properties of beryl with increasing amounts of alkalis. *Memoirs of the All-Union Mineralogical Society*, **86**, 495–499.

Sultan, M. & Aria, T. 2018. Afghanistan's emeralds: Hidden treasures. *InColor*, No. 40, 85–87.

Taran, M.N. & Rossman, G.R. 2001. Optical spectroscopic study of tuhualite and a re-examination of the beryl, cordierite, and osumilite spectra. *American Mineralogist*, **86**(9), 973–980, https://doi.org/10.2138/am-2001-8-903.

van der Maaten, L. & Hinton, G. 2008. Visualizing data using t-SNE. *Journal of Machine Learning Research*, **9**, 2579–2605.

Wang, H.A.O. & Krzemnicki, M.S. 2021. Multi-element analysis of minerals using laser ablation inductively coupled plasma time of flight mass spectrometry and geochemical data visualization using t-distributed stochastic neighbor embedding: Case study on emeralds. *Journal of Analytical Atomic Spectrometry*, preprint (10 pp.), https://doi.org/10.1039/d0ja00484g.

Wang, H.A.O., Krzemnicki, M.S., Chalain, J.-P., Lefèvre, P., Zhou, W. & Cartier, L. 2016. Simultaneous high sensitivity trace-element and isotopic analysis of gemstones using laser ablation inductively coupled plasma time-of-flight mass spectrometry. *Journal of Gemmology*, **35**(3), 212–223, https://doi.org/10.15506/JoG.2016.35.3.212.

Winchell, A.N. & Winchell, H. 1951. *Elements of Optical Mineralogy*, Part 2. John Wiley & Sons Inc., New York, New York, USA, 551 pp.

Wood, D.L. & Nassau, K. 1968. Characterization of beryl and emerald by visible and infrared absorption spectroscopy. *American Mineralogist*, **53**(5–6), 777–800.

The Authors

Dr Michael S. Krzemnicki FGA[1,2],
Dr Hao A. O. Wang[1] and Susanne Büche[1]
[1] Swiss Gemmological Institute SSEF, Aeschengraben 26, 4051 Basel, Switzerland
[2] Department of Environmental Sciences, University of Basel, Switzerland
Email: michael.krzemnicki@ssef.ch

The Discovery and Naming of Alexandrite and Phenakite: Separating Fact from Fiction

Karl Schmetzer and Evgenii Vladimirovich Burlakov

ABSTRACT: Alexandrite was discovered in 1833 in the emerald mines of the Ural Mountains, Russia. Since then, numerous legends have been told about the discovery and naming of this first colour-change gem material. Key figures in these stories were L. A. Perovskii, vice president of the appanage department of the Russian Tsar and minister of Internal Affairs of the Russian Empire, and N. G. Nordenskiöld, superintendent of mines in Finland. Phenakite was also discovered in the Uralian emerald mines in the early 1830s, with the same two people involved. Based upon extant letters written by both individuals—Perovskii and Nordenskiöld—as well as the published literature, this article critically evaluates the facts about the discoveries and the initial descriptions of alexandrite and phenakite. Our research shows that a third individual, Y. V. Kokovin, who at that time was director of the Ekaterinburg lapidary works, actually discovered both gem materials, and soon after samples of each were distributed via Perovskii to various mineralogists for examination. The name *phenakite* was suggested by Nordenskiöld in late 1832 or early 1833, ignoring the local use of the already-existing name *kokovinite*. Nordenskiöld suggested the name *alexandrite*, in honour of the Russian Crown Prince, almost a decade later—in 1842—after Kokovin's death.

Russian alexandrite from the Uralian emerald mines is prized for its attractive twinned crystals (e.g. Figure 1) and for occasionally being facetable into gemstones showing remarkable colour change behaviour. Not surprisingly, since the discovery of alexandrite in the 1830s, legends surrounding the naming and discovery of this rare gem material have appeared in the literature—and, especially nowadays, on the internet. Numerous publications (e.g. Bautsch 2014) lack any primary references and typically refer mainly to secondary literature.

Common to the legends are the key roles played by a Russian aristocrat, Lev Alekseevich Perovskii, and the mineralogist Nils Gustaf Nordenskiöld (from Helsingfors, Finland, but also a Russian citizen), who worked together for more than two decades. One of these legends, which is found frequently with small variations, attributes the discovery of alexandrite to Nordenskiöld and the presentation of the new gem material to the Tsarevich (the Russian Crown Prince) in 1834 to Perovskii, as described here from an online source ('Alexandrite or… Diaphanite?', www.planetgemstones.com/pages/about-alexandrite-page-2):

According to a widely popular but controversial story, alexandrite was discovered by the Finnish mineralogist Nils Gustaf Nordenskjold, (1792–1866) on the Tsarevich Alexander's sixteenth birthday on April 17, 1834 and named Alexandrite in honor of the future Tsar of the Russian Empire.

Nordenskjold described and discovered a number of minerals, some new and some previously unknown in Russia. He also published a number of articles in foreign journals and later went on to discover and name green andradite as demantoid (like a Diamond). His reputation was established well beyond Russia and Scandinavia and there was no one who could compete with Nordenskjold's knowledge of mineralogy. It was to Nordenskjold that Perovskii turned,
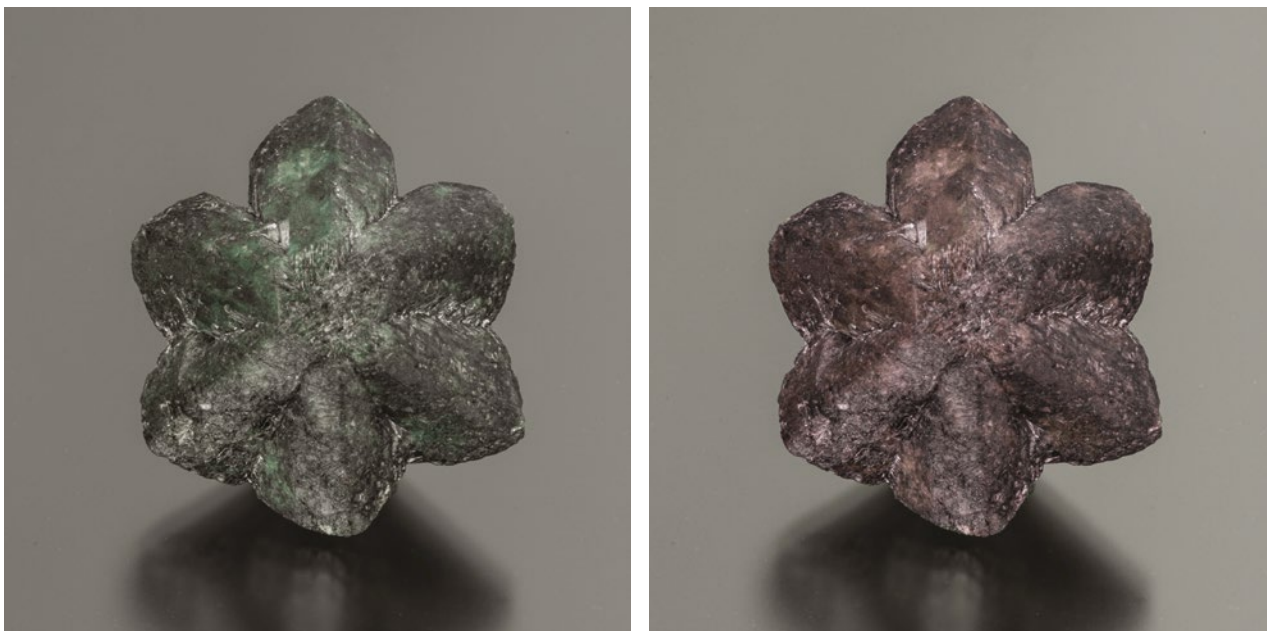
Figure 1: This cyclic twin (or trilling) of Russian alexandrite is shown as seen in daylight (left) and incandescent light (right). The crystal measures 3.5 × 3.4 × 2.0 cm. Photos by Mia Dixon, Pala International.

when he needed someone with a comprehensive knowledge of gemstones.

Although it was Nordenskjold who discovered alexandrite, he could not possibly have discovered and named it on Alexander's birthday. Nordensljold's [*sic*] initial discovery occurred as a result [of] an examination of a newly found mineral sample he had received from Perovskii, which he identified it [*sic*] as emerald at first. Confused with the high hardness, he decided to continue his examinations. Later that evening, while looking at the specimen under candlelight, he was surprised to see that the color of the stone had changed to raspberry-red instead of green. Later, he confirmed the discovery of a new variety of chrysoberyl, and suggested the name "diaphanite" (from the Greek "di" - two and "aphanes", - unseen or "phan", to appear, or show).

Perovskii however had his own plans and used the rare specimen to ingratiate himself with the Imperial family by presenting it to the future Tsar and naming it Alexandrite in his honor on April 17, 1834.

There is no question that alexandrite was discovered in the early 1830s in the Russian emerald mines of the Ural Mountains (Figure 2), and in this era a second new gem material was also discovered and described as a new mineral—phenakite. Both individuals, Perovskii and Nordenskiöld, were involved in examining and naming them. Nevertheless, as we shall see in this article, the history of their discovery and naming involves far more

than the sequence of events and personages mentioned in the passage quoted above.

Biographies of L. A. Perovskii and N. G. Nordenskiöld

The history and present status of the Russian emerald deposits in the Ural Mountains were summarised by Burlakov and Burlakov (2018, 2019). Exploitation activities for these emeralds (e.g. Figure 3) started in January 1831. During this time, Lev Alekseevich Perovskii[1] (Лев Алексе́евич Перо́вский, 1792–1856; Figure 4) was vice president of the appanage department, part of the Russian imperial cabinet. Perovskii was the illegitimate son of Count A. K. Razumovsky, and therefore had to struggle for his position in society rather than attaining his status by birth into nobility. He studied at Moscow University, and then started his career in the Russian army before changing to civil service in 1826 when he joined the appanage department of Tsar Nicholas I (or Tsar Nikolay I), which managed the imperial family's estates and income. In 1828, he became vice president of this department, a position that he still held when emerald exploitation commenced. During the initial mining the appanage department received all emeralds that were produced from the area near Takowaja
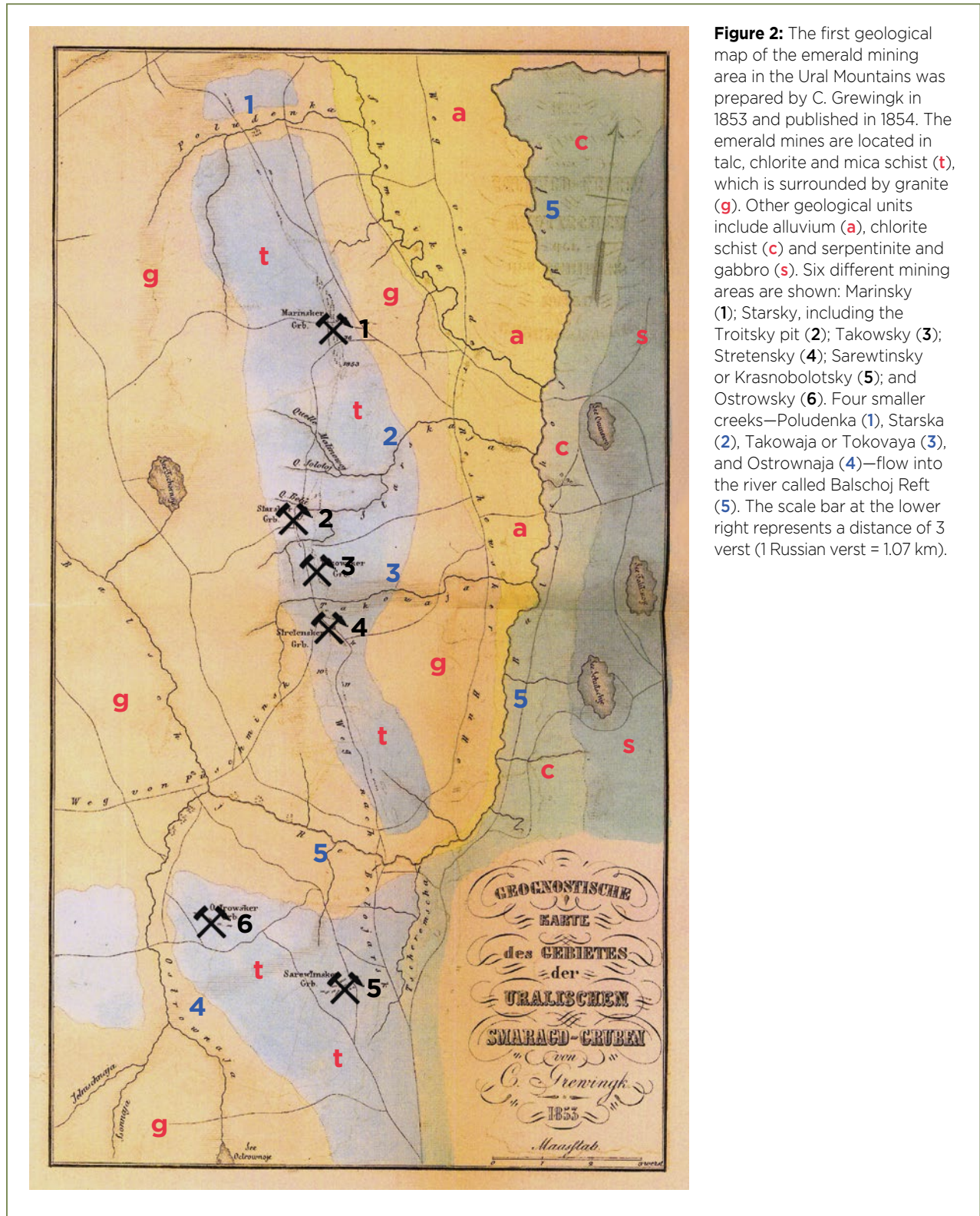

Figure 2: The first geological map of the emerald mining area in the Ural Mountains was prepared by C. Grewingk in 1853 and published in 1854. The emerald mines are located in talc, chlorite and mica schist (t), which is surrounded by granite (g). Other geological units include alluvium (a), chlorite schist (c) and serpentinite and gabbro (s). Six different mining areas are shown: Marinsky (1); Starsky, including the Troitsky pit (2); Takowsky (3); Stretensky (4); Sarewtinsky or Krasnobolotsky (5); and Ostrowsky (6). Four smaller creeks—Poludenka (1), Starska (2), Takowaja or Tokovaya (3), and Ostrownaja (4)—flow into the river called Balschoj Reft (5). The scale bar at the lower right represents a distance of 3 verst (1 Russian verst = 1.07 km).

(or Tokovaya) creek in the Ural Mountains. In 1841, Perovskii became minister of the internal affairs department, and in 1852 he became minister of the appanage department and also president of the imperial cabinet. As a passionate mineral collector, Perovskii was not only interested in filling his own collection with extraordinary samples, but also in finding new species and getting samples scientifically examined. To achieve this goal, Perovskii distributed new finds from the Ural Mountains to various mineralogists in St Petersburg and elsewhere.

Perovskii cooperated for more than two decades with Nils Gustaf Nordenskiöld (1792–1866; Figure 5),

Figure 3: (**a**) Russian emeralds commonly form aggregates of hexagonal prisms. This sample (6 × 4 × 4 cm) contains numerous crystals that are up to 23 mm long and 8 mm wide. Private collection; photo by K. Schmetzer. (**b**) This 7.19 ct emerald was faceted from a specimen mined in the Ural Mountains. Stone and photo courtesy of Peter Lyckberg.

Figure 4: Count Lev Alekseevich Perovskii (1792–1856) travelled to Ekaterinburg in 1832 to inspect the emerald mines in the Ural Mountains. During this trip, he obtained the first samples of a new mineral which became known as phenakite. In 1833 and 1834, he received the first samples of the colour-change chrysoberyl variety, later named alexandrite, from the emerald mines.

NILS GUSTAF NORDENSKIÖLD.

Figure 5: Nils Gustaf Nordenskiöld (1792–1866) received from Perovskii in 1832 some samples of an unknown mineral resembling quartz. This mineral was described in 1833 and 1834 and named phenakite. In 1834, he received the first fragments and, later, larger crystals of the colour-change variety of chrysoberyl that was named alexandrite in 1842 to honour the Crown Prince, later Tsar Alexander II.

superintendent of mines in Helsingfors (now Helsinki), Finland, which from 1809 to 1917 was part of the Russian Empire. In the 1810s and 1820s, Nordenskiöld[2] spent several lengthy periods in the laboratory of Prof. J. J. Berzelius in Stockholm to study newly developed techniques in mineral analysis. Travelling within Europe in the early 1820s, he met numerous scientists in Berlin, Paris, London and Edinburgh. Nordenskiöld devoted his work to the development of the mining industry in Finland and to the study of minerals from his home country. In wintertime he frequently travelled to St Petersburg to discuss mineralogical and mining problems with colleagues. Although he had worked on numerous minerals from the Ural Mountains since the early 1830s, he was finally able to travel there himself for the first time in 1849, a trip he made again in 1854.

Biography of Y. V. Kokovin

Yakov Vasilievich Kokovin (1784–1840) was director of the Ekaterinburg lapidary works since 1818. He was the son of Vasily Evstafievich Kokovin (1760–1818), a well-known lapidary from Ekaterinburg. At the age of 15, Y. V. Kokovin was sent to St Petersburg, where he spent seven years (1799–1806) on a scholarship at the Academy of Arts. Later, after returning to Ekaterinburg, he became a master lapidary. In 1818, he succeeded his father as head of the Ekaterinburg lapidary plant. Both members of the Kokovin family developed and invented several machines for lapidary work, such as tools for cutting and polishing large vases from decorative minerals or rocks. In the 1820s, Y. V. Kokovin was awarded several medals and received bonuses in recognition of his work as a master lapidary craftsman.

Between 1831 and 1835, Kokovin guided the mining and exploitation activities of the Uralian emerald deposits, especially in the area of the Stretensky mine (again, see Figure 2). In 1835, he was accused of misusing his position and of stealing emeralds and other valuable gems, apparently because only small quantities of stones were being sent to St Petersburg. Before this, the relationship between Perovskii and Kokovin was already tense[3]. In June 1835, Perovskii initiated an inspection of Kokovin's work, including his private home and office. After numerous 'hidden' stones were found, Kokovin lost his position and was imprisoned from December 1835 to August 1839. After his release, he tried to reopen his case, but he died in 1840. For further details of Kokovin's unfortunate situation, especially the events related to a stolen emerald crystal of high quality, see, for example, Semyonov and Timofeev (2005) and Schmetzer (2010).

Initial Descriptions of Alexandrite

The first details of the discovery and naming of alexandrite are reported in an 1842 book describing the history and scientific activities of the Russian Imperial Mineralogical Society, which was titled *Russisch—Kaiserliche Gesellschaft für die Gesammte Mineralogie*, in German, meaning '*Russian—Imperial Society for the Complete Mineralogy*' (Schmetzer 2010). This book (Figure 6), a special 25th anniversary volume of the Russian Imperial Mineralogical Society, was edited by H. A. G. von Pott, the first Secretary of that society, which was founded 1817.

In this treatise, it is recorded that in 1833 Perovskii submitted four samples of a mineral that had been discovered in the Uralian emerald mines to the Society in St Petersburg for investigation. It is further stated that these crystals were identified as chrysoberyl by Franz von Wörth[4] based on the measurement of crystal angles and blowpipe examination. After receiving further samples of the mineral from the emerald mines in 1834, Perovskii submitted more of them to von Wörth, who confirmed his initial identification as chrysoberyl. The treatise also indicated that Perovskii mentioned a 'special dichroism' that led to the discovery of what we now call *colour change* between daylight and incandescent light.

It was also recorded in the 1842 book that Nordenskiöld made the same observations and concluded that the mineral 'deserves the first rank among the gemstones' because of its particular optical properties. He suggested naming this colour-change variety of chrysoberyl *alexandrite* in honour of Tsarevich (Crown Prince) Alexander Nikolayevich, the future Tsar Alexander II (1818–1881, reigning 1855–1881), who reportedly celebrated his coming of age on the

---

[2] Several transliterations of his name are used (e.g. Nordensjöld).

[3] In 1829, Perovskii suggested starting a special 'relationship' with Kokovin (through the director of the Peterhof lapidary facility in St Petersburg) in order to have first access to the best stones found in the Ural Mountains and to get them illegally for his own collection, thus bypassing established rules and procedures. Kokovin rejected this offer, for which Perovskii never forgave him (Fersman 1923).

[4] Franz Iwanowitsch von Wörth (1786–1856) was one of the founding members of the Russian Imperial Mineralogical Society and served as its second secretary until 1856. He performed numerous identifications and analyses of minerals.

Figure 6: (**a**) The 25-year anniversary volume of the Russian Imperial Mineralogical Society, published in 1842, contains a summary of the mineralogical properties of colour-change chrysoberyl and indicates that the first samples were found in 1833 and 1834. The treatise also mentions a suggestion by Nordenskiöld to name the new gem material alexandrite in honour of the Russian Crown Prince. (**b**) The book contains this illustration of an alexandrite specimen composed of two trillings. The painting is hand-coloured and small mica flakes are glued to the paper in areas corresponding to the schist matrix. The caption (translated from German by one of the present authors) reads: 'Siberian chrysoberyl from the emerald mines 180 verst from Ekaterinburg in normal colour in daylight'.

day the mineral was discovered in the Ural Mountains. The Tsarevich's 16th birthday was later celebrated in April 1834 in a public ceremony in St Petersburg. It was—already in 1842—evident to readers of the book that this connection of the discovery date with the date of the public ceremony in St Petersburg was concocted to please the Imperial family, especially because the same book also mentioned that the first alexandrites had already been discovered the year before, in 1833. However, the legend described in the 1842 book is still considered by some authors to be factual (Damaschun 2019). It should be emphasised that it was never directly stated in 19th century literature that Perovskii either influenced the naming (as suggested by Nordenskiöld) or presented the new gem material to the Tsarevich in 1834 or later.

The first description of colour-change chrysoberyl was published by David Brewster[5] in February 1835, after he had received a sample from Nordenskiöld. This piece had been sent from Helsingfors to Edinburgh on 12 December 1834. Nordenskiöld wrote that he had obtained it from Perovskii in the spring of that year. Brewster called it 'a variety of cymophane' in his article. At that time, the term *cymophane*—used, for example, by the French mineralogist René-Just Haüy—was a synonym for chrysoberyl. Only a few other publications before 1842 are available

---

[5] Sir David Brewster (1781–1868) was based in Scotland and devoted a great part of his scientific life to the examination of the optical properties of materials. He was also the editor of various scientific journals.

that describe the colour-change samples from the Uralian emerald deposits. These are found in a book by Sokolov[6] (1838) and in articles by Rose[7] (1839), who published the first crystallographic description of the cyclic twins that are also known as *trillings*. These publications referred to the mineral as chrysoberyl, cymophane or—when the focus was on optical properties—chrysoberyl with special optical properties.

The 25-year anniversary book of 1842 did not specifically mention who discovered the colour-change chrysoberyl from the Ural Mountains, nor who provided the samples that Perovskii distributed in 1833. However, the present authors recently found a short note about Uralian chrysoberyl in a book by Sokolov (1832) that predates Brewster (1835), which was previously regarded as the first-known description of alexandrite. Sokolov attributed the discovery of chrysoberyl from the Ural Mountains to Perovskii. To further evaluate this, the present authors examined extant documents from the early 1830s pertaining to the discovery and naming of alexandrite, as well as phenakite, which was found at approximately the same time.

SOURCES OF INFORMATION

Letters and Reports

The Nordenskiöld family archive is housed in the National Library of Finland at the University of Helsinki. Of relevance for the present investigation are eight letters from Perovskii that were written (in French) to Nordenskiöld before 1835.

The archive also contains a letter (written in English) from Nordenskiöld to Brewster in December 1834, which accompanied the alexandrite sample that was sent to Brewster for examination. Also relevant are letters between Nordenskiöld and his former teacher, J. J. Berzelius[8], in Stockholm, who became one of his closest friends. This correspondence (in Swedish) was edited by Söderbaum (1927).

In addition, a letter from Y. V. Kokovin to Prince Gagarin[9] revealed information about the discovery of alexandrite. This correspondence was found by V. B. Semyonov in the archives in Ekaterinburg during his research on the history of the Tokovaya emerald deposits. An English translation was published by Kozlov (2005), and a transcription of the letter (in Russian) was supplied by Semyonov to one of the authors (KS) in 2009.

A report from the inspector Yaroshevitsky[10] who searched Kokovin's home and office in 1835 was published, with comments, by Fersman (1923).

Publications Before 1842

As indicated above, the first mention of chrysoberyl from the Ural Mountains was published in Sokolov's treatise on mineralogy (1832), and the first publication about colour-change chrysoberyl by Brewster dated to February 1835. Brewster's article was briefly reviewed in 1835 and 1836 in German journals, but it was not cited later by other scientists (e.g. Rose 1839; Haidinger 1849; von Kokscharow 1862). Further publications describing the properties of colour-change chrysoberyl were written in Russian by Sokolov (1838) and in German by Rose (1839, translated into Russian and published in 1840).

The first note about the new mineral phenakite was published in Swedish by Berzelius (1833). The following year, Nordenskiöld's detailed description of phenakite was published in both German and Swedish (Nordenskiöld 1834a, b). A description in Russian was also published in 1834 in the Russian mining journal *Gornyi Zhurnal* (Anonymous 1834). A description of how the first samples of phenakite proceeded from Kokovin to Nordenskiöld via Perovskii was provided by Tankow (1842).

---

[6] Dmitrii Ivanovich Sokolov (1788–1852) was professor at St Petersburg University and founder of *Gornyi Zhurnal*, the first Russian journal on mineralogy, geology, mining and ore processing.

[7] Gustav Rose (1798–1873) was professor of mineralogy at Berlin University, Germany. He was one of the companions of Alexander von Humboldt on his journey through Russia in 1829 (Rose 1837, 1842). Rose discovered several new Russian minerals, four of which are still known as accepted species (e.g. perovskite, which was first described in 1839 and named in honour of L. A. Perovskii).

[8] Jöns Jacob Berzelius (1779–1848) was professor of chemistry in Stockholm. He is considered to be the founder of modern chemical analysis, especially of minerals. In the 1820s, Nordenskiöld spent several periods of study and research at Berzelius' laboratory.

[9] Prince Nikolai Sergeevich Gagarin (1784–1842) was, since October 1833, vice president of the Russian imperial cabinet.

[10] This inspector was referred to as Khroshevitsky (Хрошевицкий) by Fersman (1923), but most recent literature describes him as Yaroshevitsky (Ярошевицкий). It is documented that Councilor of State Leonty Yaroshevitsky was rewarded with the Order of St Ann by Tsar Nicholas I in 1832 (www.liveauctioneers.com/item/3622911_10-czar-of-russia-nicholas-i-signed-document). This is consistent with several Russian references mentioning a Councilor of State Leonty Fedorovich Yaroshevitsky (статский советник Леонтий Федорович Ярошевицкий), beginning around 1787. In addition to investigating Kokovin's work, Yaroshevitsky also examined cases of corruption in the appanage department under the reign of Tsar Nicholas I (Krasnikova 2010).
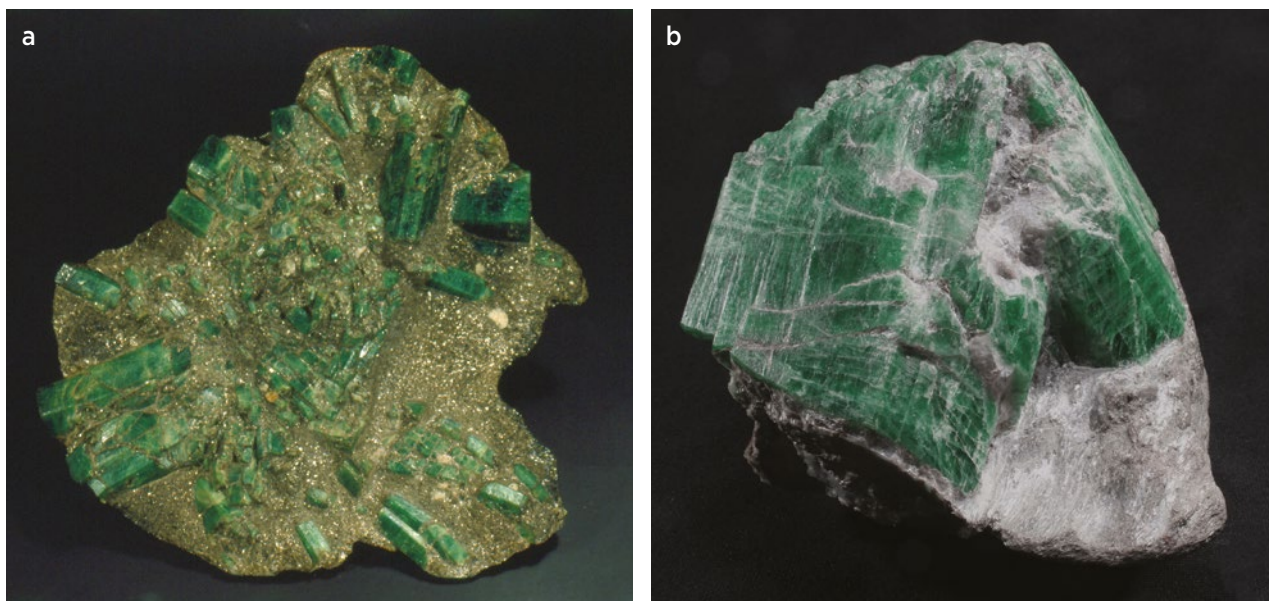

Figure 7: Emerald mining in the Ural Mountains started in January 1831. Some sizeable crystals were found that were locally transparent and of gem quality. (**a**) A large cluster of emerald crystals in matrix, known as the Leuchtenberg emerald druse (32 × 31 cm; 6.27 kg), was found in 1831 and came into the cabinet of Tsar Nicholas I. Later it was presented to his son-in-law, Maximilian von Leuchtenberg, as a birthday present. Specimen and photo courtesy of Mineralogische Staatssammlung, Munich, Germany. (**b**) This large emerald crystal in matrix (15 × 10 × 10 cm) resides in the Ural Geological Museum, Ekaterinburg. Photo by E. V. Burlakov.

CHRONOLOGY OF EVENTS

From the first letter Perovskii sent to Nordenskiöld on 22 November 1831, it is obvious that their cooperation, maybe by verbal agreement, had started shortly before. Emeralds in mica schist (e.g. Figure 7) had been exchanged or were exchanged again with another letter, dated 2 January 1832, in which Perovskii mentioned that he intended to visit the emerald mines during that year. In a subsequent letter, dated 4 June 1832, Perovskii indicated he was on leave for summer holidays at the Black Sea. After these holidays, he travelled to the Ural Mountains and visited the mines in the late summer or fall of 1832 (Semyonov & Timofeev 2005).

Chrysoberyl

Perovskii's trip to the Uralian emerald mines was successful because he was able to collect or receive samples that were until then unknown from these deposits: chrysoberyl (e.g. Figure 8) and a new mineral species that was later named phenakite (e.g. Figure 9). In a letter dated 7 December 1832, Perovskii informed his research partner in Helsingfors about this chrysoberyl, which was found in mica schist at a place some distance from the main emerald deposit.[11] He noted that, at the time, only one crystal was available. This find was briefly mentioned by Sokolov (1832), who indicated that the large chrysoberyl sample was found in the emerald pits, but no information about its colour was given.[12] Since the sample showed a typical crystal habit and other properties for chrysoberyl, there was no problem identifying it in St Petersburg.

Phenakite

A second mineral obtained during Perovskii's 1832 trip to the Ural Mountains proved more interesting. Before Perovskii informed Nordenskiöld about the new chrysoberyl find, he had already sent him samples of a

---

[11] Perovskii mentioned in his 1832 letter that the chrysoberyl was found about 50 versts from the emerald mines (1 Russian verst equals about 1.07 km), but this seems to be a mistake. In 1831, only those deposits in the central part of the Uralian emerald belt (e.g. the Stretensky mine) had been discovered and were being exploited. In 1832, deposits in the Starsky-Troitsky area were discovered and mining activities commenced there. In addition, exploration was also being done in other areas. If we assume that the chrysoberyl originated from an exploration pit north or south of the Stretensky mines in the central part of the emerald belt, the distance given is not reasonable (see Figure 2).

[12] Both volumes of Sokolov's book passed the censor in March 1832. Since Perovskii was in the Ural Mountains in the late summer or fall of that year, the Appendix must have been added later, after the book was already in press.
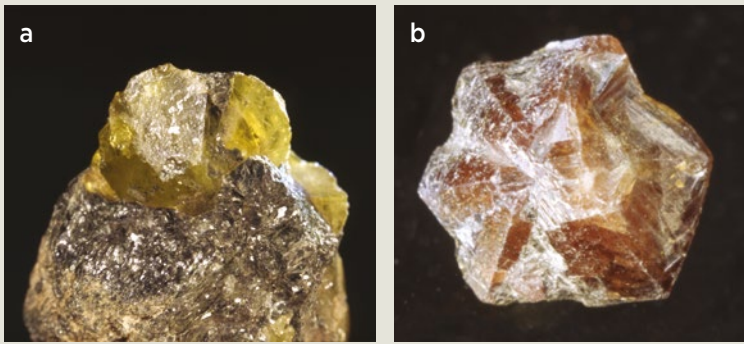
Figure 8: In the Uralian emerald deposits, Cr-free or almost Cr-free chrysoberyl is also found, in the form of (**a**) single crystals and (**b**) twinned crystals such as this trilling. The Fe-bearing yellow, greenish yellow, yellowish brown or brown samples do not show a distinct colour change between daylight and incandescent light, as seen for Cr-bearing alexandrite. These samples are courtesy of the Ural Geological Museum in Ekaterinburg and measure (a) about 5 cm wide and (b) 2.5 × 2.5 × 1.5 cm. Photos by E. V. Burlakov.

Figure 9: Phenakite was first discovered in the emerald mines of the Ural Mountains. (**a**) In this well-formed crystal group of Russian phenakite on matrix, the largest crystal measures 1.9 cm wide. Specimen and photo courtesy of Peter Lyckberg. (**b**) This large Russian phenakite crystal measures 7 × 7 × 7 cm and the faceted stones are between 6 and 18 ct. Courtesy of the Ural Geological Museum, Ekaterinburg; photos by E. V. Burlakov. (**c**) This faceted colourless Russian phenakite weighs 2.32 ct. Photo by Mia Dixon, Pala International.

mineral resembling quartz in visual appearance. The correspondence accompanying these 'quartz' samples is not preserved, but Nordenskiöld informed Berzelius in a letter dated 8 February 1833 that he had received this 'quartz' in autumn 1832 (here translated from Swedish by Peter Lyckberg):

> Vice president Peroffsky, with whom I have been in correspondence, sent me last autumn a specimen under the name 'Quartz which one has found in the mine of emeralds in the Urals'. It was crystal-lised in large, very flat rhombohedrons (like the flat calcite crystals, which occur at Freiberg). In the blowpipe this material did not behave like quartz […]. Hartwall[13] has now at my place analysed this material and found it to consist of beryllium earths bi silicate Be Si^2. We have in regard to the external appearance of this material, a surprising similarity to quartz, named it phenakite […]. I am waiting to know from St Petersburg, if crystals measurable with reflexion[14] could be obtained.

Nordenskiöld did not know who gave the quartz-like samples to Perovskii, but some information is found in a treatise by Tankow (1842) about the origins of gems, especially from Russia. Tankow[15] reported that the mining engineer V. V. Ljubarsky[16] brought samples from Ekaterinburg to St Petersburg and showed them to

[13] Victor Hartwall (1800–1857) studied mineralogy and chemistry in Åbo (Turku, Finland) and in Stockholm (with Berzelius). He was commissioner of mines in Helsingfors, and analysed various minerals from Finland and elsewhere.

[14] Nordenskiöld was awaiting crystals to measure angles between crystal faces with a goniometer. This was, at that time, the standard method used to identify mineral species.

[15] Alexander Dimitrievich Tankow was a member of the Russian Imperial Mineralogical Society, residing in St Petersburg.

some mineralogists and collectors, and that Kokovin also showed samples of the same mineral to Perovskii. He further reported that samples of the quartz-like mineral were sent by Perovskii to Nordenskiöld and Hartwall for examination and analysis.

Perovskii referred to this work in further letters to Nordenskiöld on 7 December 1832 and again on 16 February 1833, when he sent the first matrix specimen to measure crystal faces by goniometric examination. At that time, he already referred to 'phenakite' as the name of the new mineral, as had previously been suggested by Nordenskiöld. The name is derived from the Greek word for 'deceiver', in allusion to its similarity to quartz. In his annual report to the Swedish Academy of Sciences, submitted 31 March 1833, Berzelius mentioned Nordenskiöld's find. He reported that Nordenskiöld examined the new mineral and named it phenakite. This short report (in Swedish) was briefly reviewed in 1833 in German and Russian, and was fully translated into German in 1834. Several further letters in 1833 between Berzelius and Nordenskiöld discussed the properties and composition of phenakite. With the mineralogical and chemical examination finished, the detailed description of the new species was published in 1834 by Nordenskiöld, in both German (Figure 10) and Swedish journals (Nordenskiöld 1834a, b).

An additional description of phenakite as a new mineral was also published in 1834. This anonymous Russian text was presented, but not authored, by Perovskii and was, most likely, a translation or summary of Nordenskiöld's full article or similar information given to Perovskii.[17] A footnote was added to the article by the publication's editor (here translated from Russian by one of the present authors): 'Phenakite is the same quartz-like mineral that was discovered on the Tokovaya River (in the Ekaterinburg district) and was named (after the discoverer) kokovinite'.

From this, it is obvious that the new mineral had already been named, at least locally, in honour of its discoverer, but this was ignored by Perovskii. In the letters between Perovskii, Nordenskiöld and Berzelius, the former name of the mineral was not addressed, and neither the name Kokovin nor 'kokovinite' are found. By contrast, the 1835 report (included in Fersman 1923) of the examiner of Kokovin's house, Yaroshevitsky, mentioned that in addition to other gems—mainly emerald, aquamarine, amethyst and topaz—several rough and faceted specimens of 'kokovinite' were found ('phenakite' was not used in this report). Furthermore, a report by Planer[18] (1840) on new and re-examined minerals found in Russia since 1832 briefly mentioned
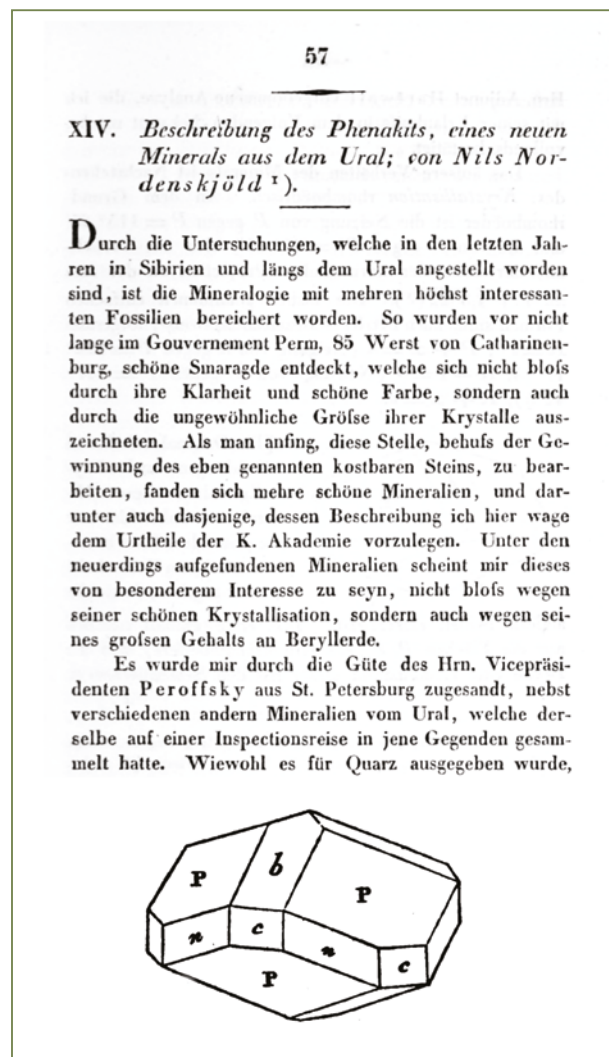

Figure 10: The first detailed description of the new mineral phenakite was published by N. G. Nordenskiöld in *Annalen der Physik und Chemie* in 1834. The top of this figure shows the first page of the publication (p. 57) and below it is a crystal drawing found on page 58.

[16] Vasilii Vasilevich Ljubarsky (1795–1852) was a mining engineer, mining inspector and metallurgist.

[17] The translation was performed by Alexander Dimitrievich Osersky (1813–1880), a mining engineer in St Petersburg. The text gives the exact chemical composition and crystallographic data (angles of crystal faces etc.) as published in Nordenskiöld's 1834 papers. This issue of *Gornyi Zhurnal* passed the censor on 23 June 1833. This indicates that Perovskii submitted a report or preliminary draft, written by Nordenskiöld in a foreign language (such as French, German or Swedish) to the editors of the Russian journal, but without mentioning Nordenskiöld as author.

[18] Dimitrii Ivanovich Planer (1821–1882) was a mining engineer who published numerous articles and a book (in 1867) about Russian minerals. In 1862, R. Hermann (see footnote 23) discovered a mineral in the Ural Mountains belonging to the turquoise group and named it planerite.

the original name 'kokovinite'. However, this name is not found in any later articles, such as the detailed description of phenakite by von Kokscharow (1859).

At the international level, the name *phenakite* was accepted and used in the description of a second locality for the mineral at Framont, north-west of Besançon, France (Beirich 1835), and later by authors describing other occurrences.

Alexandrite

The first crystals of alexandrite were found in 1833 in the Uralian emerald mines and submitted by Kokovin to Perovskii, who distributed the samples for identification. The initial find was reviewed in a letter from Kokovin to Prince Gagarin, dated 16 June 1834. Some of the samples were given by Perovskii to von Wörth in St Petersburg for examination. In addition, he sent two fragments to Nordenskiöld on 23 January 1834. Perovskii's accompanying letter mentioned that the material resembled chrysoberyl (here translated from French by Gérard Martayan):

> The emerald mine has not provided any new material except the 2 small crystal fragments that I am sending to you. I would like to know your opinion about this mineral, which according to its hardness and the crystallisation has some resemblance with chrysoberyl.

In this letter Perovskii did not refer to the chrysoberyl found previously in the Ural Mountains (as mentioned by Sokolov 1832).

A second series of larger crystals was given to Perovskii in April 1834, which was also mentioned in the letter from Kokovin to Gagarin dated 16 June 1834 (see above). Five crystals from this new find were sent by Perovskii to Nordenskiöld on 24 May 1834, accompanied by the following (here translated from French by Gérard Martayan):

> I have the honour in sending you a mineral that I just received from Siberia, it was found in the Ural emerald mine. The two numbered samples are part of my private collection; as for the two others, they are for your collection; with the exception of the first two samples, these are the best specimens sent to me; besides I am also sending a small piece for analysis. After completion of your analyses, I would be grateful if you could send me the first two samples, with your opinion on this mineral; its uncommon tabular crystallisation, which consist of 3 prisms that cut

each other crosswise by the middle; its hardness close to that of sapphire; its property to appear dark green in daylight and red when observed under the [candle]light, makes me think that this is a new mineral. Moreover, we can observe its red colour even in daylight, but it is not as intense as under the [candle]light and is seen only in certain parts of the stone while the rest keeps its green colour.

In both letters from June and May 1834 cited above (i.e. from Kokovin to Gagarin and from Perovskii to Nordenskiöld), the special habit of the cyclic twins (i.e. trillings; e.g. Figure 11), the high hardness and the peculiar colouration of the specimens were mentioned. We now describe the last as a colour change between daylight and incandescent light (Figures 1 and 12–14). Perovskii's letter to Nordenskiöld also mentioned that the properties led him to think that the samples represented a new mineral. However, Nordenskiöld's investigations proved that they were instead a new variety of chrysoberyl. Nordenskiöld summarised these results in a letter to Berzelius on 24 August 1834 (here translated from Swedish by Peter Lyckberg):

> Peroffsky sent to me two or three months ago for investigation a rock specimen from the [emerald mines] of the Urals. Although the mineral is not a new species as Peroffsky believed, it is, however, very remarkable. It is chrysoberyl but occurs as large distinct crystals, partly as simple crystals, partly as trillings about 1 to 2 inches in diameter and they

Figure 11: Large alexandrite crystals in the form of trillings were found in the Uralian emerald deposits; in general, such large crystals were not transparent. Shown here is the largest group of alexandrite crystals (20 × 14 cm; 5.38 kg) found in Russia, which was discovered in 1840. Designated Kochubei's druse, it consists of 22 alexandrite trillings. The largest crystal (in the centre of the specimen) measures about 7 cm in diameter. Specimen courtesy of the Fersman Mineralogical Museum, Russian Academy of Sciences, Moscow; photo by K. Schmetzer.
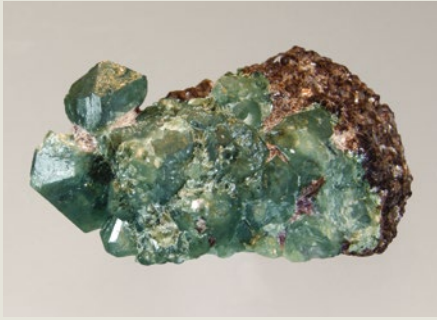
Figure 12: This crystal group (5.5 × 2.5 × 4.0 cm) with two Russian alexandrite twins (16 and 11 mm wide) in phlogopite matrix shows a distinct colour change between daylight (left) and incandescent light (right). Private collection; photos by K. Schmetzer.

Figure 13: Alexandrite crystals from the Ural Mountains are occasionally transparent, as demonstrated by this trilling (1.8 × 1.5 × 1.0 cm), which is seen in daylight (left) and incandescent light (right). Private collection; photos by E. V. Burlakov.

Figure 14: This faceted Russian alexandrite weighs 0.85 ct and is shown in daylight (left) and incandescent light (right). Photos by Mia Dixon, Pala International.

are already in that point of view uncommon, but the remarkable thing is that they are in daylight grass-green resembling emerald in colour and are weakly transparent; in candlelight their transparency is clearly higher and the colour is like that of pyrope or staurolite from St. Gotthard, [and] one cannot see any trace of green colour. As far as I know, there is no mineral with such a distinct phenomenon described above; there is no way to measure it. Peroffsky also sent me his specimens for investigation; the crystals were exceptionally beautiful in appearance, with some formerly unknown faces, which I have drawn. I also received some less magnificent specimens […].

The events surrounding the discovery of phenakite (kokovinite) and similar trouble related to chrysoberyl (alexandrite) increased the already-existing tension between Perovskii and Kokovin, and contributed to Kokovin's tragic arrest and imprisonment in 1835 (see Schmetzer 2010).

Subsequently, several specimens of 'Siberian' chrysoberyl—*Siberian* being a commonly used geographic designation for Uralian chrysoberyl and alexandrite in the 19th century—were sent by Nordenskiöld to Berzelius for examination between 1834 and 1837. As far as can be ascertained from the sequence of letters edited by Söderbaum (1927), their main interest was the

evaluation of the cause of the colour change. In the full correspondence between Nordenskiöld and Berzelius written between 1834 and 1841, both used the names *cymophane* and *chrysoberyl* to describe the variety that was subsequently referred to as *alexandrite* in 1842 within the 25th anniversary volume of the Russian Imperial Mineralogical Society. Prior to 1842, the terms *cymophane* and *chrysoberyl* were also used in the few scientific descriptions of colour-change chrysoberyl, especially those by Brewster (1835), Sokolov (1838) and Rose (1839; Figures 15 and 16).

A letter written by Nordenskiöld to Berzelius from St Petersburg on 23 April 1842 indicated that Nordenskiöld was in St Petersburg at the time the manuscript for the 25th anniversary volume was prepared (it passed censor on 17 April 1842), which possibly explains why there

Figure 16: This alexandrite trilling in matrix (8.5 × 7.0 cm) was presented by the St Petersburg Mining Institute to Gustav Rose. The morphology of this trilling is also consistent with the crystal drawing shown at the bottom of Figure 15. Specimen courtesy of the Museum für Naturkunde, Berlin, Germany; photo by K. Schmetzer.
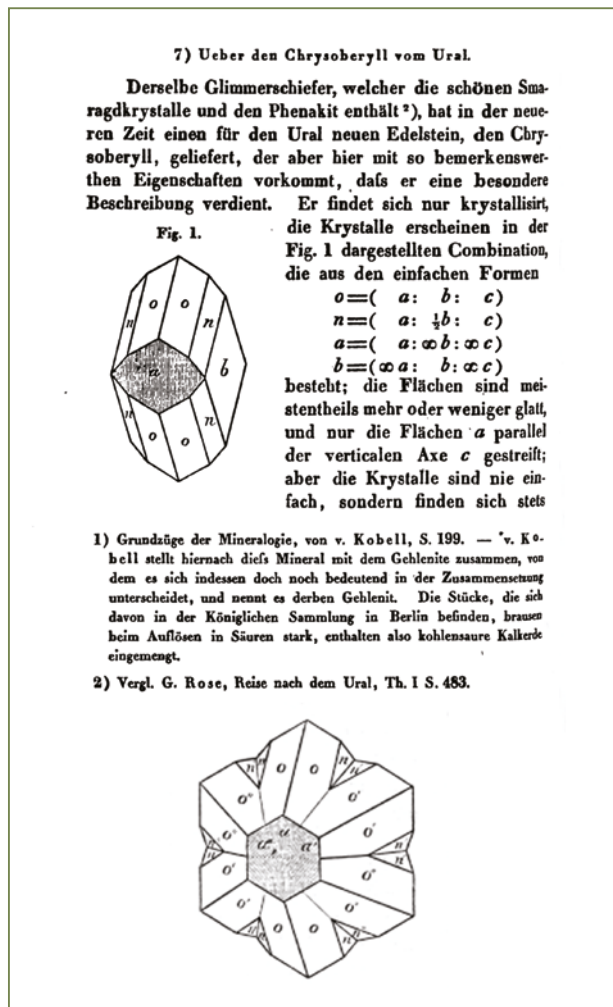
Figure 15: The first detailed description of the crystallographic properties of alexandrite from the Ural Mountains was published by Gustav Rose in 1839 in *Annalen der Physik und Chemie*. The top of this figure shows the first page of the publication (p. 570), which contains a drawing of a chrysoberyl single crystal. Below it is a drawing of a trilling from page 571; its morphology is nicely represented by the specimen shown in Figure 1.

is no written communication about any arrangement or suggestion for the naming of alexandrite. All such discussions, and possible input by Perovskii or others, could have been done verbally so no written correspondence was necessary.

LOCATION OF THE PHENAKITE AND ALEXANDRITE FINDS

In the documents cited above, the exact locations of the various finds within the large emerald mining area were rarely given. Some information is available from Zerrenner[19] (1869), who visited the emerald mines in the 1840s but did not perform a systematic study. Information is also found in a report by Weitz[20] (written in 1842 and published by Fersman in 1923), the successor of Kokovin as head of the Ekaterinburg lapidary factory. The first detailed study of the area was published by

---

[19] The German Carl Michael Zerrenner (1818–1878) worked from 1842 to 1851 as a mining engineer and mining superintendent in various areas of the Ural Mountains. During this period he published several books (e.g. about gold, platinum and diamond mining in the Urals in 1851), as well as descriptions of mineral occurrences (e.g. for uvarovite in 1848). From 1852 onwards he worked in various high positions in Germany and Austria.

[20] Ivan Ivanovich Weitz (1794–1858) was a mining engineer who served as the director of the Ekaterinburg lapidary plant from 1836 to 1858, after Kokovin had been dismissed.

Grewingk[21] (1854a, b), who documented the geology of the emerald mines in mid-1853 for several months. Such activity was initiated by Perovskii because the yield of the emerald mines was steadily declining. The first geological map of the area (Figure 2) was attached to Grewingk's publication. In the following years the problems responsible for the low yield of the emerald mines were not solved. A new examination of the mines was initiated at the end of the 1850s, and a detailed report of this work, which took several years, was published by Miklashevskii[22] (1862). This report eventually led to the end of mining operations under governmental control and to the lease of the mines.

Zerrenner (1869) mentioned that phenakite occurred in the Stretensky mining area and that alexandrite was found in the Sarewtinsky mines (later also named Krasno-bolotsky mines). Weitz (1842, included in Fersman 1923) reported that both phenakite and chrysoberyl were mined at the Stretensky and Marinsky deposits. Grewingk (1854a, b) mentioned that both phenakite and alexandrite (Figure 17) were found in most of the

Figure 17: Occasionally, the two new gem materials discovered in the early 1830s in the Uralian emerald mines—phenakite and alexandrite—are intergrown and found in the same rock sample. The specimen shown here measures about 3.0 × 2.5 × 2.5 cm. Private collection; photo by E. V. Burlakov.

six mining areas he described, with the best phenakite occurring in the Starsky mining area and beautiful alexandrite coming from the Sarewtinsky mines. Miklashevskii (1862) also mentioned various localities where phenakite and chrysoberyl were found. He only used the term *alexandrite* in reporting finds from the Sarewtinsky (Krasnobolotsky) mines, and *chrysoberyl* for samples from the other localities.

A second occurrence of phenakite in Russia was described by Hermann[23] (1846) and Rose (1846). These samples were found in the topaz mines near Miask (now Miass, south of Ekaterinburg) in the Ural Mountains. Compared to those from the emerald deposits, the crystals were of better quality, but smaller.

DISCUSSION

The documents presented in this article for the first time in a detailed context provide a logical chronology of the events from 1832 to 1842 related to the discovery and naming of phenakite and alexandrite. A schematic sketch of the distribution of samples in the 1830s from the emerald mines to the scientists who examined and identified them is given in Figure 18.

It is unknown which individual miners discovered the first phenakite samples in 1832 and first alexandrites in 1833. However, all primary sources and circumstances indicate that the first samples of both gem materials were found under Kokovin's supervision of the mining activities at the Uralian emerald mines, although Kokovin was not mentioned in either the 1842 anniversary volume or in the letters between Perovskii, Nordenskiöld and Berzelius. There is no doubt that Kokovin was the first to realise that in both cases something new had been discovered, and that he was the person who submitted samples to Perovskii and others in Ekaterinburg and St Petersburg.

Perovskii's 1832 trip to the Ural Mountains supplied interesting new materials. Most interest was given to a new mineral which was, according to the correspondence

---

[21] Caspar Andreas Constantin Grewingk (1819–1887) was born in Estonia, at the time part of the Russian Empire, and studied geology in Dorpat (now Tartu), Estonia, and later in Berlin, Freiberg and Jena in Germany. He worked in St Petersburg (1846–1854) and in 1853 was sent to the Ural Mountains to study the emerald deposits. In 1854 he became professor of mineralogy and geology at Dorpat University.

[22] Petr Ivanovich Miklashevskii (1825–1889) was a mining engineer and the successor of Weitz as the director of the Ekaterinburg lapidary factory from 1859 to 1866.

[23] Hans Rudolph Hermann (1805–1879) was born in Dresden, Germany, where he learned chemistry from Friedrich Adolph August Struve. In 1827 he was sent to Moscow to lead a company for mineral waters. Hermann remained in Russia and died in 1879 in Moscow. He published numerous investigations in the field of mineralogy, especially mineral chemistry.
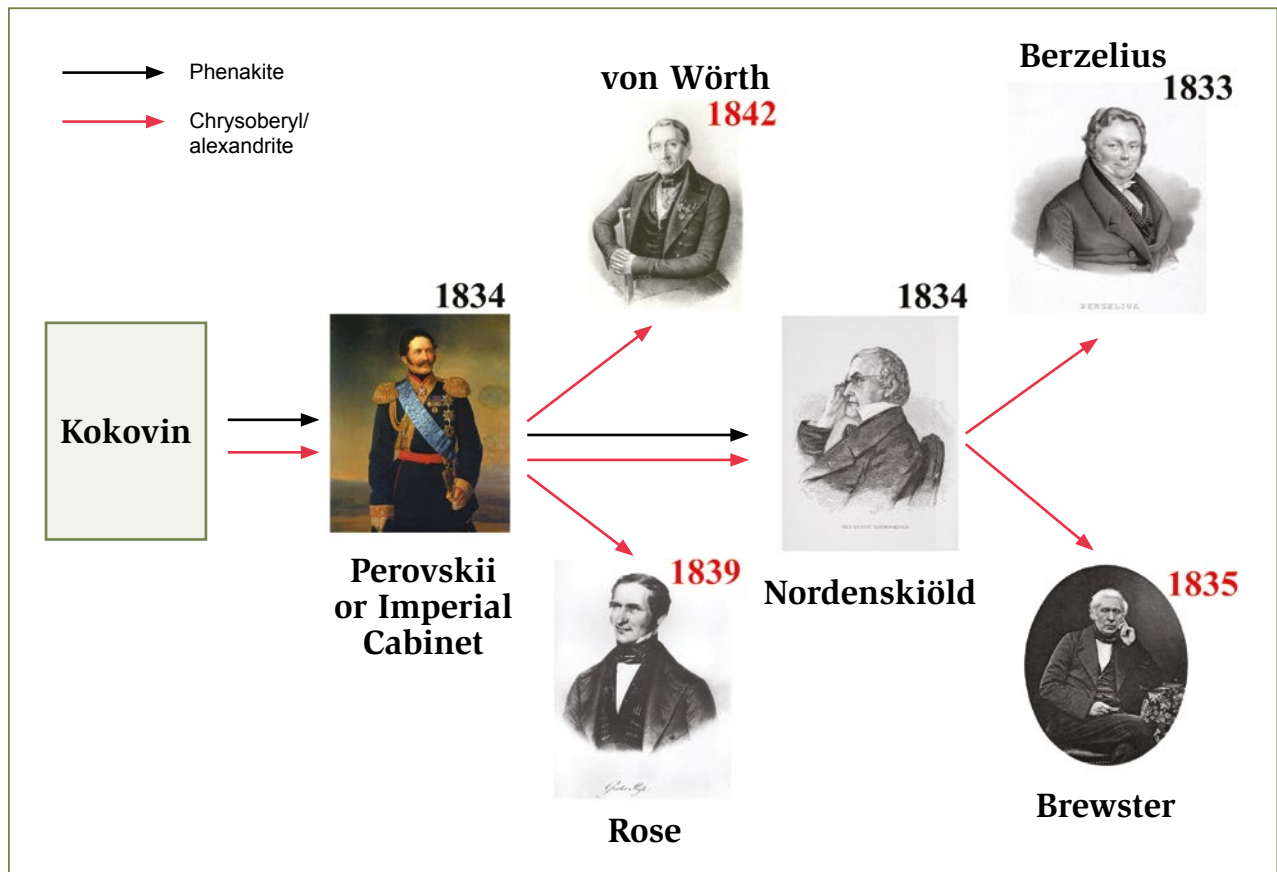
Figure 18: This diagram shows the distribution of the first samples of phenakite, chrysoberyl and the alexandrite variety of chrysoberyl from the Uralian emerald mines in the 1830s. Also given are the years of the resulting publications by the various persons depicted. The brief note on chrysoberyl by Sokolov (1832) is not indicated in the diagram. For Perovskii, see Anonymous (1934); von Wörth's findings were published in von Pott (1842).

between Perovskii and Nordenskiöld, named phenakite in late 1832 or early 1833. This mineral was also mined later in larger quantities and was found to be a new facetable gem material. The first name given to the mineral—*kokovinite*—was intended to honour its discoverer but was ignored by Perovskii, and it seems that this local terminology never reached Nordenskiöld before he had finished his examinations and prepared the final draft of his description to be published in Swedish and German. All this turmoil over its naming might have been the reason that phenakite—which was both a new mineral and a new gem material—and the circumstances of its discovery were not mentioned in the 1842 anniversary treatise.

In contrast to the attention devoted to phenakite, the initial find of chrysoberyl in 1832 attracted little interest. Perovskii did not refer to its discovery when he sent the first samples to Nordenskiöld in 1834, and neither did Sokolov (1838) when he described the properties of the new chrysoberyl variety that later became known as alexandrite. This chrysoberyl find was also not mentioned in the 1842 anniversary

volume of the Russian Imperial Mineralogical Society. Based on the descriptions, we can only assume that this material, found at some distance from the main emerald deposits mined in 1832, was 'simply' yellow or yellowish brown chrysoberyl, which was identified in St Petersburg without any problem according to its mineralogical properties. Yellow chrysoberyl, also in the form of large untwinned single crystals, is typically found in the Uralian emerald deposits in plagioclase-quartz veins or bodies within mica schist (Burlakov *et al.* 1997; Zhernakov 2009). Most likely, such a crystal was mentioned in Perovskii's letter in 1832 and described briefly by Sokolov (1832). Given the high position and influence of Perovskii, the discovery of a first colour-change variety of this mineral during his 1832 inspection trip would definitely have been mentioned later, and especially in the 1842 treatise.

The first alexandrite samples were found in 1833 as small pieces that were difficult to identify. Later, in 1834, larger samples, mainly cyclic twins, were obtained that showed the characteristic colour change between daylight and incandescent light. The sources quoted

above, mostly letters written by Perovskii or Norden-skiöld, are consistent with the dates and events given in the 1842 anniversary volume. Kokovin's letter of June 1834 also supports the details given there.

Both persons involved—Perovskii and Kokovin—spoke about the astonishing optical properties of the new gem variety, and both their letters clearly describe the effect which we now call *colour change*, but they do not indicate who first documented this colour behaviour nor present further circumstances of the samples' discovery.

It is a matter of speculation why Nordenskiöld never published his findings about the colour-change variety of chrysoberyl during the time between 1834 and 1842. If we compare the sequence of publications dealing with phenakite and alexandrite, we observe a major discrepancy. For the new mineral phenakite, it seems that there was a concerted effort by Berzelius, Perovskii and Nordenskiöld to publish articles as soon as possible in 1833 and 1834. Brewster reacted in the same way after he received the colour-change chrysoberyl sample from Nordenskiöld, posted from Helsingfors to Edinburgh in December 1834. As editor of the *London, Edinburgh, and Dublin Philosophical Magazine and Journal of Science*, he was able to publish his article right away in the February 1835 issue, which might have been an unexpected surprise for Nordenskiöld and the scientists in St Petersburg. This early publication on the colour-change variety of chrysoberyl, as well as the competition involved in describing phenakite, the displacement of the name *kokovinite* and the downfall of Kokovin, may have delayed the first detailed description of the new chrysoberyl variety for several years until the article by Rose (1839), who was not involved in the first examinations in 1833 and 1834. Rose had obtained his research samples from Perovskii.

Although we are not aware of any document concerning the naming of alexandrite before the 1842 publication, it is possible that Perovskii and Nordenskiöld discussed this in the early 1840s or even before, when Kokovin was still alive. The actual roles of both Perovskii and Nordenskiöld—the latter of whom suggested the name *alexandrite* in honour of the Tsarevich, the future Alexander II—are also a complete matter of speculation, because more detailed documentation is missing.

The only fact that proves the details given in the 1842 book is the presence of Nordenskiöld in St Petersburg in the spring of 1842, when the book was prepared by a number of geologists and mineralogists who submitted individual contributions for the volume. Therefore, Nordenskiöld's suggestion about the naming might have been given verbally, so no written documentation about

this event needed take place. Furthermore, we could not find any records after 1842 in which Nordenskiöld referred to the discovery and naming of phenakite or alexandrite (e.g. in his correspondence with his son Adolf Erik in Sweden or with other scientists).

No new documents are available to the present authors about the role and intentions of Kokovin, and especially the problem of the magnificent emerald crystal that was stolen in 1835, most likely in St Petersburg. Kokovin's contribution to the developments of the Uralian emerald mines, followed by his tragic downfall, was discussed at length in the literature, but this portion of Russian mineralogical history is not the focus of the present article.

CONCLUSIONS

Undoubtedly, Kokovin was the first to discover the new colour-change variety of chrysoberyl and to realise that he had found something different. However, because he was unable to perform the mineralogical examination according to the standard techniques of the era, the samples were given to the appanage department and came into the hands of Perovskii, who distributed them to various scientists but refrained from mentioning Kokovin's role.

A nearly identical series of events was connected with the discovery of phenakite, in the year before the first pieces of alexandrite were found. Kokovin was also the discoverer of these quartz-like samples and recognised them as another new gem material. Moreover, the mineral was even initially named *kokovinite* in his honour, which was mentioned in the leading Russian mining journal of the time and used locally in the Ural Mountains region, even in official documents. In this case, Perovskii brought samples back from his trip to the Urals and distributed them for scientific study. But Perovskii not only tried to hide Kokovin's contribution, he even submitted Nordenskiöld's results for publication without mentioning either Kokovin or Nordenskiöld.

Later, after Kokovin's downfall, his role was no longer mentioned by any of the numerous researchers in the 19th and 20th centuries (e.g. Sokolov, Kokscharow and Fersman). Nonetheless, we do not really know which facts were known to these scientists and what had been successfully hidden, particularly during the first half of the 19th century. However, new research that commenced in the 1980s by Russian authors led to a rediscovery of Kokovin's role, and restored the honour of the discovery of alexandrite and phenakite to Kokovin.

REFERENCES

Anonymous (presented by L.A. Perovskii, transl. by A.D. Osersky) 1834. Description of phenakite. *Gornyi Zhurnal*, **1834**, Part 3, No. 7, 1–4 (in Russian).

Bautsch, H.-J. 2014. Mineralogische Ergebnisse der Reise von Christian Gottfried Ehrenberg, Alexander von Humboldt und Gustav Rose. *In*: Aranda, K., Förster, A. & Suckow, C. (eds) *Alexander von Humboldt und Russland. Beiträge zur Alexander-von-Humboldt-Forschung*. Akademie Verlag, Berlin, Germany, **31**, 133–145.

Beirich, E. 1835. Nähere Bestimmung des Phenakit nach einem neuen Vorkommen. *Annalen der Physik und Chemie*, **34**(3), 519–525, https://doi.org/10.1002/andp.18351100313.

Berzelius, J.J. 1833. Phenakit. *Årsberättelse om Framstegen i Fysik och Kemi*, **13**, 160 (in Swedish); German translation by Wöhler, F., in *Jahres-Bericht über die Fortschritte der physischen Wissenschaften*, **13**(1834), 156–157; reviewed in *Annalen der Physik und Chemie*, **28**(1833), 420 (in German); which was translated into Russian in *Gornyi Zhurnal*, **1833**, Part 3, No. 9, 429–430.

Brewster, D. 1835. Notice of the optical properties of a new mineral supposed to be a variety of cymophane. *London, Edinburgh, and Dublin Philosophical Magazine and Journal of Science*, **6**(32), 133–134, https://doi.org/10.1080/14786443508648548; reviewed in *Annalen der Physik und Chemie*, **35**(1835), Farberscheinungen bei chromhaltigen Salzen, 383–384, and *Neues Jahrbuch für Mineralogie, Geognosie, Geologie und Petrefaktenkunde*, **1836**, 209.

Burlakov, A. & Burlakov, E. 2018. Emeralds of the Urals. *InColor*, No. 40, 88–94.

Burlakov, E.V. & Burlakov, A. 2019. Alexandrite of the Urals. *InColor*, No. 44, 23–34.

Burlakov, J.V., Polenov, J.A., Gernakov, V.J. & Samsonov, A.V. 1997. Tokowaya-Malyshevo: Die Smaragdgruben des Urals. *Lapis*, **22**(7/8), 44–55.

Damaschun, F. 2019. Ein Smaragd von 2.691 Karat – ein großzügiges Geschenk des Zaren. *In*: Damaschun, F. & Schmitt, R.T. (eds) *Alexander von Humboldt. Minerale und Gesteine im Museum für Naturkunde Berlin*. Wallstein Verlag, Göttingen, Germany, 300–305.

Fersman, A.E. 1923. Archive materials on emerald mines. *In*: Fersman, A.E. (ed) *Emerald Mines in Ural. Materials for Research of Natural Minerals of Russia*. Sbornik Statei I Materialov, Petrograd, Russia, **44**, 5–22 (in Russian).

Grewingk, C.C. 1854a. Die Smaragd-Gruben des Ural und ihre Umgebung. *Verhandlungen der Russisch-Kaiserlichen Mineralogischen Gesellschaft*, **1854**, 206–233.

Grewingk, C.C. 1854b. *Die Smaragd-Gruben des Ural und ihre Umgebung*. Gedruckt bei Carl Kray, St Petersburg, Russia, 30 pp. + map.

Haidinger, W. 1849. Ueber den Pleochroismus des Chrysoberylls. *Annalen der Physik und Chemie*, **77**(2), 228–236, https://doi.org/10.1002/andp.18491530605.

Hermann, R. 1846. Untersuchungen russischer Mineralien. Ueber ein neues Vorkommen von Phenakit. *Journal für Praktische Chemie*, **37**(3+4), 186–188.

Kozlov, Y.S. (transl. by M. Pitskhelauri) 2005. *Alexandrite*. Nauka, Moscow, Russia, 144 pp.

Krasnikova, Y.N. 2010. Corruption in the department of appanages and the fight against in the first third of the XIX century. *Bulletin of the Leningrad State University Named After A.S. Pushkin*, **4**(1), 54–65 (in Russian).

Miklashevskii, P.I. 1862. Description of the Uralian emerald mines and their surroundings. *Gornyi Zhurnal*, **1862**, Part 3, No. 7, 1–57 (in Russian).

Nordenskjöld, N. 1834a. Beschreibung des Phenakits, eines neuen Minerals aus dem Ural. *Annalen der Physik und Chemie*, **31**(4), 57–62, https://doi.org/10.1002/andp.18341070404.

Nordenskjöld, N. 1834b. Beskrifning på Phenakit, ett nytt Mineral från Ural. *Kongliga Vetenskaps-Academiens Handlingar, för År 1833*, 160–165.

Planer, D.I. 1840. Perovskite. *Gornyi Zhurnal*, **1840**, Part 3, No. 7, 419 (in Russian).

Rose, G. 1837. *Mineralogisch-geognostische Reise nach dem Ural, dem Altai und dem Kaspischen Meere*, Vol. 1. Verlag der Sanderschen Buchhandlung, Berlin, Germany, 641 pp.

Rose, G. 1839. Ueber den Chrysoberyll vom Ural. *Annalen der Physik und Chemie*, **48**(4), 570–573; Russian translation in *Gornyi Zhurnal*, **1840**, Part 1, No. 3, 387–392.

Rose, G. 1842. *Mineralogisch-geognostische Reise nach dem Ural, dem Altai und dem Kaspischen Meere*, Vol. 2. Verlag der Sanderschen Buchhandlung, Berlin, Germany, 606 pp.

Rose, G. 1846. Ueber den Phenakit vom Ilmengebirge, einem neuen Fundorte desselben. *Annalen der Physik und Chemie*, **69**(1), 143–150, https://doi.org/10.1002/andp.18461450913.

Schmetzer, K. 2010. *Russian Alexandrites*. Schweizerbart Science Publishers, Stuttgart, Germany, 141 pp., www.ciando.com/ebook/bid-2877614-russian-alexandrites.

Semyonov, V.B. & Timofeev, N.I. 2005. *Emeralds of Russia*. Timofeev Foundation, IGEMMO 'Lithica', Ekaterinburg, Russia, 49–51 (in Russian).

Söderbaum, H.G. (ed.) 1927. *Jac. Berzelius brev. XI, Brewäxling mellan Berzelius och Nils Nordenskiöld (1817–1847)*. Utgivna av Kungl. Svenska Vetmnskapsakademten, Uppsala, Sweden, 331 pp.

Sokolov, D.I. 1832. Appendix. *In*: *Guideline to Mineralogy*, Vol. 2. Pechataio v Tipografii A. Iliuoshchara, St Petersburg, Russia, 1107–1109 (in Russian).

Sokolov, D.I. 1838. *Supplements to Mineralogy Published in 1832*. Pechatano V Tipografii Imperatorskoi | Akademii Nauk, St Petersburg, Russia, 126 pp. (see pp. 49 and 56) (in Russian).

Tankow, A.D. 1842. Phenakite. *Trudy Mineralogiceskogo Obscestva v Sanktpeterburge*, **1842**, Part 2, 400–402 (in Russian).

von Kokscharow, N. 1859. Ueber den russischen Phenakit. *Mémoires de l'Acadèmie Impériale des Sciences de St.-Pétersbourg, VI^E Série*, **VII et Dernier**, 175–198.

von Kokscharow, N. 1862. Beschreibung des Alexandrits. *Mémoires de l'Acadèmie Impériale des Sciences de St.-Pétersbourg, VIIE Série*, **V**(2), 1–19 + 3 plates.

von Pott, H.A.G. (ed) 1842. Ueber den Alexandrit, oder Uralischen Chrysoberyll, dessen Dichroismus und über die ungewöhnlich Grösse seiner Krystalle. Geschichte und wissenschaftliche Beschäftigungen der in St Petersburg gestifteten Russisch-Kaiserlichen Gesellschaft für die gesammte Mineralogie von 1817 bis 1842. *Schriften der in St Petersburg gestifteten Russisch-Kaiserlichen Gesellschaft für die gesammte Mineralogie*, **1**(1), 116–126.

Zerrenner, C. 1869. Nachricht über eine Anzahl aus verschiedenen Gegenden der Erde bei mir eingegangener interessanter Mineralien. *Berg- und huettenmaennische Zeitung*, **28**(1) 10–11.

Zhernakov, V.I. 2009. Ural emerald mines (Izumrudnye Kopi): Notes on mineralogy. *Mineralogical Almanac*, **14**(2), 1–125.

The Authors

Dr Karl Schmetzer
Taubenweg 16, 85238 Petershausen, Germany
Email: SchmetzerKarl@hotmail.com

Dr Evgenii Vladimirovich Burlakov
Ural Geological Museum, Ulitsa Kuybysheva, 39, Yekaterinburg, Sverdlovsk Oblast, Russia, 620014
Email: bevgeny2@mail.ru

Colour Enhancement of Pink Tourmaline from Nigeria by Electron-Beam and Gamma Irradiation

Waratchanok Suwanmanee, Bhuwadol Wanthanachaisaeng, Teerawat Utapong and Chakkaphan Sutthirat

ABSTRACT: Saturated pink-to-red tourmaline is a desirable gem material and therefore pale stones are commonly enhanced by gamma irradiation to intensify the red colour. For this study, 20 tourmalines from Nigeria ranging from near-colourless to pale pink, pink and pale orangey pink were subjected to electron-beam and gamma irradiation. Each sample was cut into two pieces for irradiation by each treatment method at three dose levels (i.e. 400, 800 and 1200 kilograys). During treatment, the samples turned pink to intense pink and orangey pink to pinkish orange or yellowish orange, with more intense colouration produced by electron-beam irradiation. The UV-Vis spectra of the irradiated tourmalines showed a maximum absorption feature centred at around 510–520 nm (due to Mn^{3+}) and a minor band at about 395 nm also attributed to Mn (probably Mn^{3+}), which caused the pink colouration. Yellow colouration seen in some samples after irradiation was probably contributed by the O^- hole centre. Features associated with both the O^- hole centre and H^0 electron centre were present in the EPR spectra of the irradiated samples.

Among the various tourmaline colour varieties, pink-to-red material (commonly known as rubellite in redder shades) is a popular gem material and is highly valued on the current market (Lucas 2015). Pale-coloured tourmaline is commonly enhanced by laboratory irradiation to produce deeper pink-to-red colouration (Pezzotta & Laurs 2011; e.g. Figure 1). For more than two decades, Nigeria has been a major source of gem tourmaline—particularly in pink shades—and this study focuses on the treatment of this material to intensify pink colouration. While gamma irradiation has commonly been applied to strengthen pink or red colour (Bunnag & Sripoonjan 2019) and induce a rubellite-like appearance, the electron-beam technique provides higher energy and is here investigated as an alternative treatment method for tourmaline.

Tourmaline is a boron-aluminium silicate that forms in the trigonal crystal system. Its structure consists of a six-membered cyclosilicate ring having the complicated chemical formula $XY_3Z_6[T_6O_{18}][BO_3]_3V_3W$ (Henry *et al.* 2011; Bosi 2018), in which:

X = Na^+, K^+, Ca^{2+}, □ (vacancy)

Y = Li^+, Mg^{2+}, Fe^{2+}, Mn^{2+}, Cu^{2+}, Al^{3+}, V^{3+}, Cr^{3+}, Fe^{3+}, Mn^{3+}, Ti^{4+}

Z = Mg^{2+}, Fe^{2+}, Al^{3+}, V^{3+}, Cr^{3+}, Fe^{3+}

T = Si^{4+}, Al^{3+}, B^{3+}

V = OH^-, O^{2-}

W = OH^-, F^-, O^{2-}

Depending on the chromophoric elements present in the Y site, gem tourmaline may show a wide range of colours from colourless to pink, red and purple-red, yellow,

Figure 1: These gem-quality tourmalines from Nigeria (left, 5.40 ct natural colour; right, 4.45 ct gamma-irradiated colour) are representative of the material described in this article. Photo by T. Sripoonjan.

green, and blue to violet. The colouring mechanism is generally explained on the basis of absorption spectral information combined with crystal-field theory (as reviewed by Pezzotta & Laurs 2011 and Rossman 2019).

Irradiation of colourless or pale-coloured tourmaline most commonly produces pink or yellow colouration (or combinations thereof, resulting in orangey hues), and the treated stones are typically stable to light and heat (generally up to at least 400°C; Nassau 1994). The mechanisms for the colour changes that occur with irradiation have been ascribed to various causes in the literature. Pink elbaite displays a significant absorption band centred at about 515 nm, which was attributed by Bershov *et al.* (1969) to a hole centre of the Al-O⁻-Al type. Nassau (1975) reported that gamma irradiation can change tourmaline from colourless to pink, pink to yellow, and colourless to yellow. He concluded that irradiation potentially induces an electron colour centre or hole colour centre related to the Mn component, causing the pink colour. Additionally, Reinitz and Rossman (1988) suggested that natural ionising radiation from minerals in the pegmatite host may produce deep pink to reddish colour in tourmaline due to $Mn^{2+} \rightarrow Mn^{3+}$ transformation. According to Petrov (1990), pink colouration in elbaite is due to absorptions related to O⁻ centres, Mn-related electron centres and Mn intra-defects. In addition, Krambrock *et al.*

(2002, 2004b) suggested that the change from colourless to yellow in elbaite subjected to gamma irradiation is associated with O⁻ centres (hole trap centres) and H^0 centres (electron centres). Both defects were detected by those authors using electron paramagnetic resonance (EPR) spectroscopy, and the O⁻ centre was postulated as a cause of yellow colouration in tourmaline.

In addition to those studies mentioned above, various publications have described the effects of irradiation treatment on the pink colour of tourmaline. For instance, de Camargo and Isotani (1988) intensified the pink colour of tourmaline from Brazil using gamma rays. Krambrock *et al.* (2004a) annealed brownish pink tourmaline from Brazil at 600°C to remove colour prior to gamma ray irradiation at 400 kilograys (kGy, an SI unit for the absorbed dose of radiation), which turned the sample pure pink. Ahn *et al.* (2013) applied 10 MeV electron irradiation to intensify the pink colour of tourmaline from Madagascar, which then became colourless after subsequent heating to 550°C. Maneewong *et al.* (2016a) performed electron-irradiation experiments on tourmalines from Afghanistan, changing them from colourless to yellow or deep pink. In addition, Maneewong *et al.* (2016b) heated two pink tourmalines from Nigeria to turn them colourless and then changed their colour to yellow or deep pink using electron irradiation. Bunnag and Sripoonjan (2019) experimented with

gamma-irradiation treatment of pink tourmaline from Afghanistan, Mozambique and Nigeria. The Afghanistan samples turned dark pink to red, whereas those from Mozambique and Nigeria changed to darker brown hues. Most recently, Kurtz *et al.* (2020) used gamma irradiation (total dose of 9410 kGy) to produce very deep pink colour in tourmaline, followed by heating experiments at 200–500°C to investigate decolourising the samples.

The present study compares the effects of treating 20 Nigerian tourmalines using both electron-beam and gamma-ray sources. Three different radiation doses were used, and changes in their colouration and their optical and EPR spectra were documented.

MATERIALS AND METHODS

Twenty rough tourmalines (e.g. Figure 2) from Nigeria were obtained for this study from a Nigerian gem trader. The samples ranged from near-colourless to pale pink, pink and pale orangey pink, and weighed 0.06–0.40 g. All of them were cut and polished into rectangular tablets, with the *c*-axis in the plane of the slabs, and then each sample was sliced into two portions—one each for the electron-beam and gamma irradiation experiments. The colouration of each sample was observed in two directions, parallel and perpendicular to the *c*-axis (e.g. Figure 2c).

The gemmological properties of all samples were investigated at the College of Creative Industry, Srinakharinwirot University, using standard gem-testing equipment. Fluorescence to UV radiation was checked using 4 W long-wave (365 nm) and short-wave (254 nm) UV lamps.

Chemical analyses of 12 representative samples were obtained using a JEOL JXA-8100 electron probe microanalyser (EPMA) at the Department of Geology, Faculty of Science, Chulalongkorn University. The analyses were carried out with an accelerating voltage of 15 kV and a beam current of 25 nA. Measurement times were set at 10 seconds for both the peak and background counts of all analysed elements, leading to an empirical detection limit of about 0.005 wt.%. Natural minerals and pure oxide standards were selected for calibration, and automatic ZAF corrections were applied before the results were reported in oxide form. The atomic
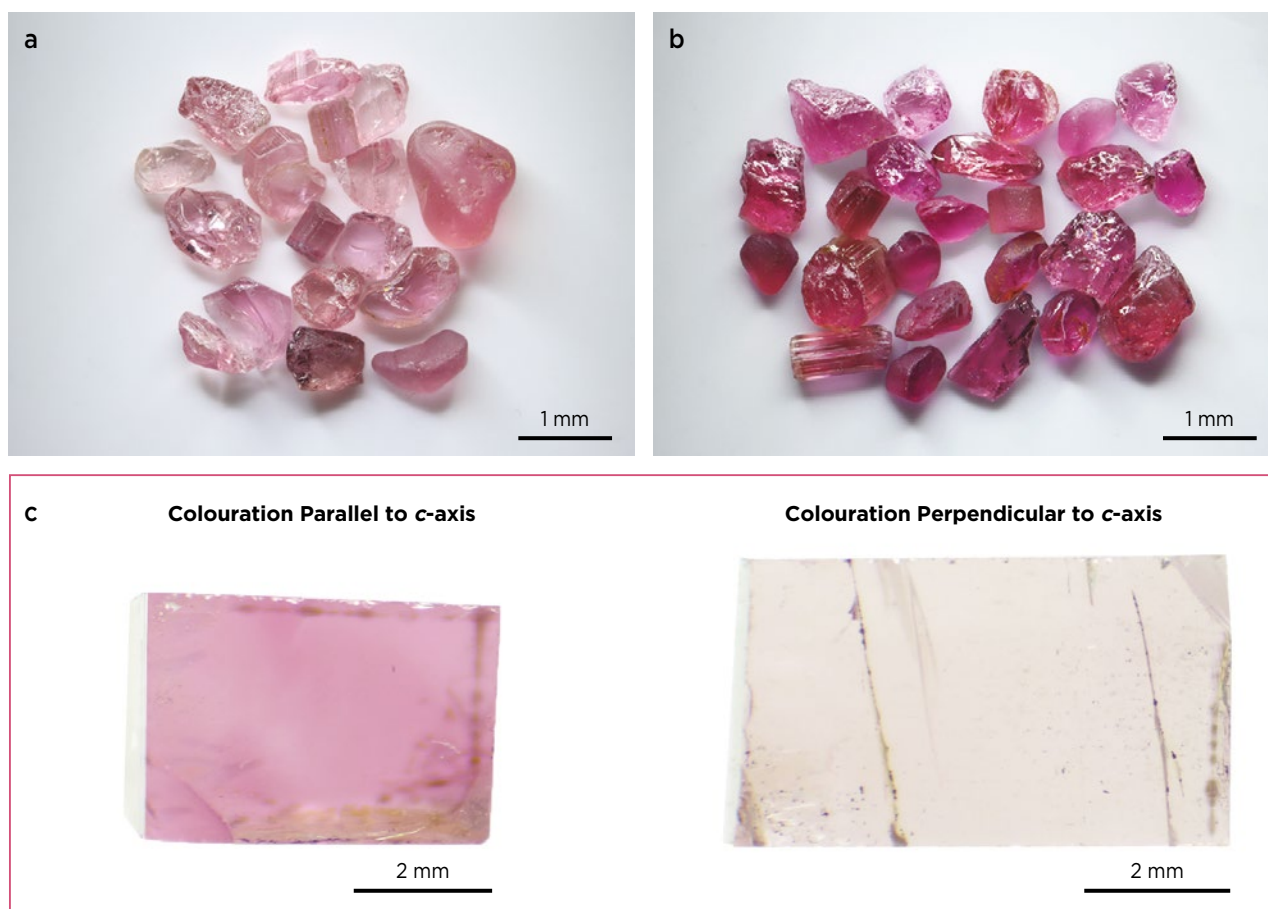
Figure 2: Twenty Nigerian tourmalines were selected from the two groups of samples shown here before irradiation: (**a**) those exhibiting pale colouration and (**b**) those showing a deeper pink appearance. (**c**) The colouration of the same block cut from sample Pk06 are shown in directions parallel (left) and perpendicular (right) to the *c*-axis. Photos by W. Suwanmanee.

proportions were recalculated on the basis of 31 anions (Clark 2007; Henry *et al.* 2011; Okrusch *et al.* 2016) assuming O^{2-}, F^- and OH^- to be allocated proportionally in the V site and W site. Although Li and O cannot be detected by EPMA, they can be estimated from the ideal formula for elbaite. In the Y site, Li^+ was assumed to be the main cation, along with Al^{3+} and some other cations (e.g. Ti, Mn, Fe, Mg, Zn and Pb) filling this site fully, which is based on a total of 15 atoms per formula unit (apfu) allocated in the T site, Y site and Z site (Shirose & Uehara 2013). Moreover, OH was calculated according to the formula OH + F = 4 apfu, as suggested by Clark (2007), Henry *et al.* (2011) and Okrusch *et al.* (2016). The content of B_2O_3 was recalculated by assuming stoichiometry with B = 3 apfu (Henry *et al.* 2011).

Radiation treatment of the samples was performed using three doses—400, 800 and 1200 kGy—by employing an electron beam and gamma rays. Electron-beam irradiation was carried out using a Mevex MB16-20 high-energy electron accelerator operated at 10 MeV with a power of 10 MW. No significant residual radioactivity was produced due to the low radiation dose, small sample size and chemical composition. Gamma irradiation was performed using six columns of cobalt-60 sources (produced by Paul Stephens Consultancy Ltd) at an approximate energy of 1.17 MeV and 1.33 MeV in each column. Both irradiation facilities are based at the Gem Irradiation Center, Thailand Institute of Nuclear Technology (Public Organisation).

Ultraviolet-visible (UV-Vis) absorption spectra in the 250–850 nm range were obtained for all samples before treatment and after each radiation dose using a Perkin-Elmer Lambda 900 spectrophotometer at the Department of Earth Sciences, Faculty of Science, Kasetsart University. The samples were orientated and marked for both directions (parallel and perpendicular to the *c*-axis) before the analyses. After recording the spectrum for the first orientation, each sample was rotated manually to analyse the second direction.

To investigate the presence of colour centres, one sample (Pk03) was analysed before and after irradiation (400 kGy) by each treatment technique using EPR spectroscopy with a Bruker EMXmicro instrument at the Scientific and Technological Research Equipment Centre, Chulalongkorn University. A small portion of the sample (about 2–3 mm) was placed in a glass tube for the analyses, which were done with a microwave frequency of 9.849 GHz, power at 1.051 mW and a sweep time of 150 seconds per scan. The measurements were conducted at room temperature within a magnetic field ranging from 50 to 650 mT.

RESULTS AND DISCUSSION

Physical Properties

The 20 samples (numbered Pk01–Pk20) were separated into four groups (near-colourless, pale pink, pink and pale orangey pink; see Table I) based on the colour seen before treatment in the direction parallel to the *c*-axis. During irradiation most of them turned pink to intense pink, and some turned orangey pink to pinkish orange or yellowish orange.

The gemmological properties of the samples are summarised in Table I. Their RIs ranged from 1.616 to 1.645 (birefringence 0.013–0.022) and SGs were 3.03–3.09. These properties mostly fall within the general ranges reported for gem tourmaline, although the lowest RI and birefringence values may result from measurement error.

Table I: Gemmological properties of the Nigerian tourmaline samples.

Colour before irradiation (‖C)	**Near-colourless:** Pk07, Pk08, Pk11 **Pale pink:** Pk01, Pk09, Pk16 **Pink:** Pk03, Pk06, Pk12, Pk13, Pk15, Pk18, Pk19, Pk20 **Pale orangey pink:** Pk02, Pk04, Pk05, Pk10, Pk14, Pk17
Colour after irradiation (‖C)	**Pink:** Pk11, Pk17 **Intense pink:** Pk01, Pk03, Pk07, Pk08, Pk13, Pk15, Pk16, Pk18 (partially with orangey tint) Pk19, Pk20 **Orangey pink:** Pk06, Pk09, Pk10, Pk12 **Pinkish or yellowish orange:** Pk02, Pk04, Pk05, Pk14
Pleochroism	Moderate dichroism, in pink to orangey pink, pink to orange or orangey pink to orange
Optic character	Doubly refractive, uniaxial negative
RIs	n_o = 1.632–1.645 n_e = 1.616–1.628
Birefringence	0.013–0.022
SG	3.03–3.09
Fluorescence	Inert to long- and short-wave UV radiation

Chemical Composition

All samples were mainly composed of the elbaite end member (cf. Henry *et al.* 2011), with 0.82–0.89 atoms per formula unit (apfu) Na, as well as subordinate Ca (≤0.1 apfu) and vacancies (≤0.15 apfu) in the X site (Table II). A triangular plot of (Na + K) vs Ca vs vacancies shows that all samples fall within the alkali tourmaline field, as expected for elbaite (Figure 3).

Table II: Representative EPMA analyses of tourmaline samples from Nigeria.*

Colour ‖C before irradiation	Near-colourless			Pale pink			Pink			Pale orangey pink		
Sample no.	Pk07	Pk08	Pk11	Pk01	Pk09	Pk16	Pk03	Pk13	Pk20	Pk02	Pk05	Pk14
Oxides (wt.%)												
SiO_2	38.43	38.50	38.63	38.23	38.45	38.00	38.39	38.03	38.24	37.46	38.34	37.98
TiO_2	nd	nd	nd	nd	nd	nd	nd	nd	nd	nd	nd	nd
B_2O_3	11.01	11.00	10.99	10.99	10.98	10.95	10.95	10.86	10.86	10.91	10.91	10.94
Al_2O_3	41.90	41.65	41.55	41.93	41.56	41.26	41.27	41.16	41.03	42.28	41.27	42.06
FeO	0.04	0.03	nd	0.03	nd	nd	0.03	nd	nd	nd	0.05	0.03
MnO	0.29	0.29	0.14	0.12	0.04	0.92	0.19	0.16	0.28	nd	0.05	nd
MgO	0.03	nd	nd	nd	nd	nd	nd	nd	nd	nd	nd	nd
ZnO	0.12	0.07	0.03	0.05	0.06	0.04	0.05	nd	0.09	0.06	0.03	0.05
PbO	nd	nd	0.06	0.17	0.04	0.06	0.05	0.15	0.06	0.17	0.05	0.08
CaO	0.17	0.41	0.18	0.21	0.35	0.76	0.71	0.18	0.04	0.13	0.19	nd
Li_2O	1.79	1.88	1.93	1.81	1.93	1.79	1.95	1.88	1.88	1.64	1.92	1.74
Na_2O	2.76	2.68	2.67	2.79	2.83	2.68	2.77	2.82	2.81	2.83	2.83	2.88
K_2O	0.03	nd	nd	nd	nd	nd	nd	nd	nd	nd	nd	nd
H_2O	3.70	3.66	3.62	3.63	3.63	3.65	3.68	3.59	3.63	3.42	3.27	3.67
F	0.60	0.68	0.75	0.74	0.72	0.67	0.60	0.73	0.64	0.73	0.65	0.62
Subtotal	100.87	100.85	100.55	100.70	100.59	100.78	100.64	99.56	99.56	99.63	99.56	100.05
–O=F	0.25	0.29	0.32	0.31	0.30	0.25	0.27	0.31	0.33	0.31	0.27	0.26
Total	100.62	100.56	100.23	100.39	100.29	100.53	100.37	99.25	99.23	99.32	99.29	99.79
Ions on the basis of 31 (O,OH,F)												
Si	6.068	6.082	6.112	6.047	6.088	6.034	6.091	6.085	6.118	5.966	6.108	6.033
Al	0.000	0.000	0.000	0.000	0.000	0.000	0.000	0.000	0.000	0.000	0.000	0.000
Tet. sum	6.068	6.082	6.112	6.047	6.088	6.034	6.091	6.085	6.118	5.966	6.108	6.033
B	3.000	3.000	3.000	3.000	3.000	3.000	3.000	3.000	3.000	3.000	3.000	3.000
Al (Z site)	6.000	6.000	6.000	6.000	6.000	6.000	6.000	6.000	6.000	6.000	6.000	6.000
Al	1.797	1.755	1.747	1.817	1.756	1.722	1.719	1.761	1.737	1.935	1.749	1.875
Ti	nd	nd	nd	nd	nd	nd	nd	nd	nd	nd	nd	nd
Fe^{2+}	0.005	0.003	nd	0.004	nd	nd	0.004	nd	nd	nd	0.007	0.004
Mn	0.039	0.038	0.018	0.016	0.006	0.124	0.025	0.021	0.038	nd	0.007	nd
Mg	0.006	nd	nd	nd	nd	nd	nd	nd	nd	nd	nd	nd
Li	1.138	1.195	1.229	1.152	1.230	1.145	1.241	1.242	1.211	1.051	1.231	1.111
Zn	0.014	0.008	0.003	0.005	0.007	0.004	0.007	0.006	0.011	0.007	0.004	0.006
Pb	nd	nd	0.003	0.007	0.002	0.003	0.006	nd	0.003	0.007	0.002	0.003
Y sum	2.999	2.999	3.000	3.000	3.000	3.000	3.000	3.000	3.000	3.000	3.000	2.999
Ca	0.028	0.070	0.031	0.035	0.060	0.129	0.120	0.031	0.007	0.022	0.032	nd
Na	0.846	0.821	0.820	0.856	0.869	0.826	0.852	0.876	0.872	0.874	0.874	0.887
K	0.005	nd	nd	nd	nd	nd	nd	nd	nd	nd	nd	nd
Vacancy	0.121	0.109	0.149	0.109	0.071	0.045	0.028	0.093	0.121	0.104	0.094	0.113
X sum	1.000	1.000	1.000	1.000	1.000	1.000	1.000	1.000	1.000	1.000	1.000	1.000
F	0.301	0.338	0.377	0.370	0.359	0.335	0.299	0.367	0.324	0.369	0.326	0.310
OH	3.699	3.662	3.623	3.630	3.641	3.665	3.701	3.633	3.676	3.631	3.674	3.690
W sum	4.000	4.000	4.000	4.000	4.000	4.000	4.000	4.000	4.000	4.000	4.000	4.000
Mn/Fe ratio	7.8	12.7	—	4.0	—	—	6.3	—	—	—	1.0	—

* B_2O_3, Li_2O, vacancies, Li and OH were calculated as reported in the text. Abbreviations: nd = not detected, Tet. = tetrahedral.
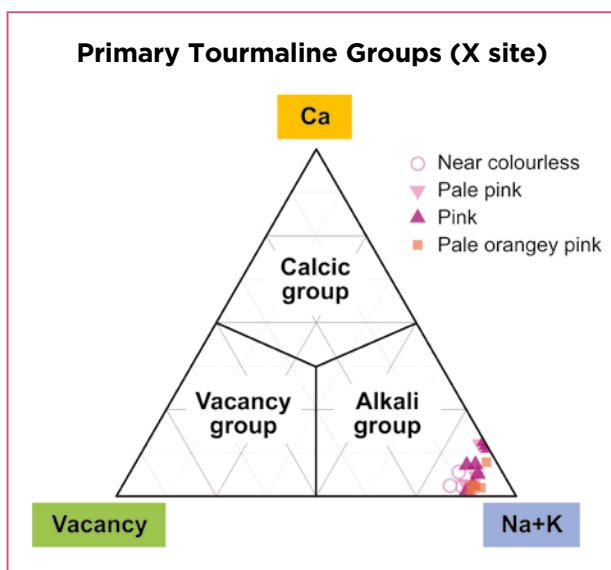
Figure 3: A ternary diagram of (Na + K) vs Ca vs vacancies (after Henry *et al.* 2011) indicates that all the tourmaline study samples belong to the alkali group.

Among the Y-site cations, Mn was the main trace element present that influences tourmaline colour (again, see Table II). Nevertheless, Mn contents were low overall (mostly less than 1 wt.% MnO, equivalent to ≤0.06 apfu Mn). Only sample Pk16 contained 0.92 wt.% MnO (equivalent to about 0.12 apfu Mn). Iron is also important for colouring tourmaline, but the samples showed very low contents of this element. The remaining trace elements, such as Mg and Ti, were mostly below the detection limit, whereas Zn and Pb were present in very small amounts (mostly <0.2 wt.% or ≤0.01 apfu).

Colour Modification by Irradiation

Photos of four specimens before and after treatment are shown in Figures 4 and 5, with the blocks rotated in the direction parallel to the *c*-axis (||C) and perpendicular to the *c*-axis (⊥C), respectively. Images of the other 16 samples are available in *The Journal*'s online data depository. In general, after irradiation most samples turned an intense pink colour, although some became orangey pink to pinkish or yellowish orange. The more intense colours resulted from higher radiation doses. In addition, electron-beam irradiation produced somewhat more intense colours than those resulting from gamma irradiation at equivalent doses. Consistent with the pleochroism exhibited by tourmaline, the colouration was significantly stronger when viewed in the ||C rather than ⊥C direction, for both the untreated and irradiated samples (see Figures 4 and 5, respectively). Aside from the changes in colour, other properties of the samples remained unchanged after irradiation.

Regarding those tourmalines shown in Figures 4 and 5, the untreated colour of sample Pk11 was near-colourless for both ||C and ⊥C directions. After irradiation, the sample was pink ||C and pale pink ⊥C. The untreated colours of Pk13 and Pk16 were pink and pale pink in the ||C direction, respectively, but were pale orangey pink ⊥C. After they were irradiated, both Pk16 and Pk13 changed to intense pink ||C (with slightly stronger colouration shown by Pk13) and appeared orangey pink ⊥C (with slightly stronger colouration shown by Pk16). Sample Pk14 showed a very different colour behaviour, changing from pale orangey pink ||C and pale pinkish orange ⊥C before treatment to pinkish orange ||C and yellowish orange ⊥C after being irradiated.

UV-Vis Spectroscopy

The UV-Vis absorption spectra of the same four tourmaline samples shown in Figures 4 and 5 are presented in Figures 6 and 7.

The spectra of three of the irradiated pink tourmalines (Pk11, Pk16 and Pk13) measured in the direction parallel to the *c*-axis direction (Figure 6) displayed a prominent band with maximum absorption centred around 510–520 nm attributed to Mn^{3+} (Taran *et al.* 1993; Ahn *et al.* 2013; Kurtz *et al.* 2020), as well as two subordinate narrower peaks at 450 and 458 nm that are spin-forbidden bands of Mn^{3+} (Kurtz *et al.* 2020; G. Rossman, pers. comm. 2021). These absorptions in the blue-to-green region are responsible for the pink colour. The position of the Mn^{3+} absorption band in pinkish orange sample Pk14 was between 480 and 560 nm (mostly ~505 nm), and was of much lower intensity than the other three samples. The spectra of all of the above-mentioned samples contained an additional band at around 390–395 nm that relates to Mn. Its exact oxidation state has not yet been assigned (da Silva *et al.* 2018), although Liu *et al.* (2011) suggested this band relates to Mn^{3+}. This absorption in the violet region may produce a slight yellow hue in the pink tourmalines, but it was typically imperceptible because it was obscured by the overall pink colour. Also present in most of the spectra was a relatively weak absorption band centred at around 670–680 nm that relates to Fe^{2+} (Taran *et al.* 1993; Ahn *et al.* 2013; Kurtz *et al.* 2020).

The absorption spectra of sample Pk11 obtained in the direction perpendicular to the *c*-axis (Figure 7) displayed a broad absorption band centred at 510–515 nm with the two small peaks at 450 and 458 nm that can also be seen in Figure 6. The main broad band in sample Pk16 consisted of four overlapping peaks at 450, 458, 478 and 505 nm that were usually present before and after irradiation with a dose of 400 kGy.
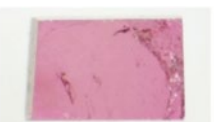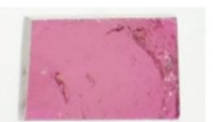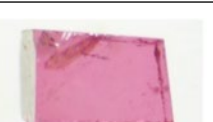
Figure 4: Colour modifications are shown in the direction parallel to the *c*-axis for four representative samples after three radiation doses from electron-beam and gamma-ray treatments. Photos by W. Suwanmanee.

Figure 5: The same tourmaline samples and treatment parameters as in Figure 4 are shown here in the direction perpendicular to the *c*-axis. Photos by W. Suwanmanee.

UV-Vis Spectra Parallel to *c*-axis
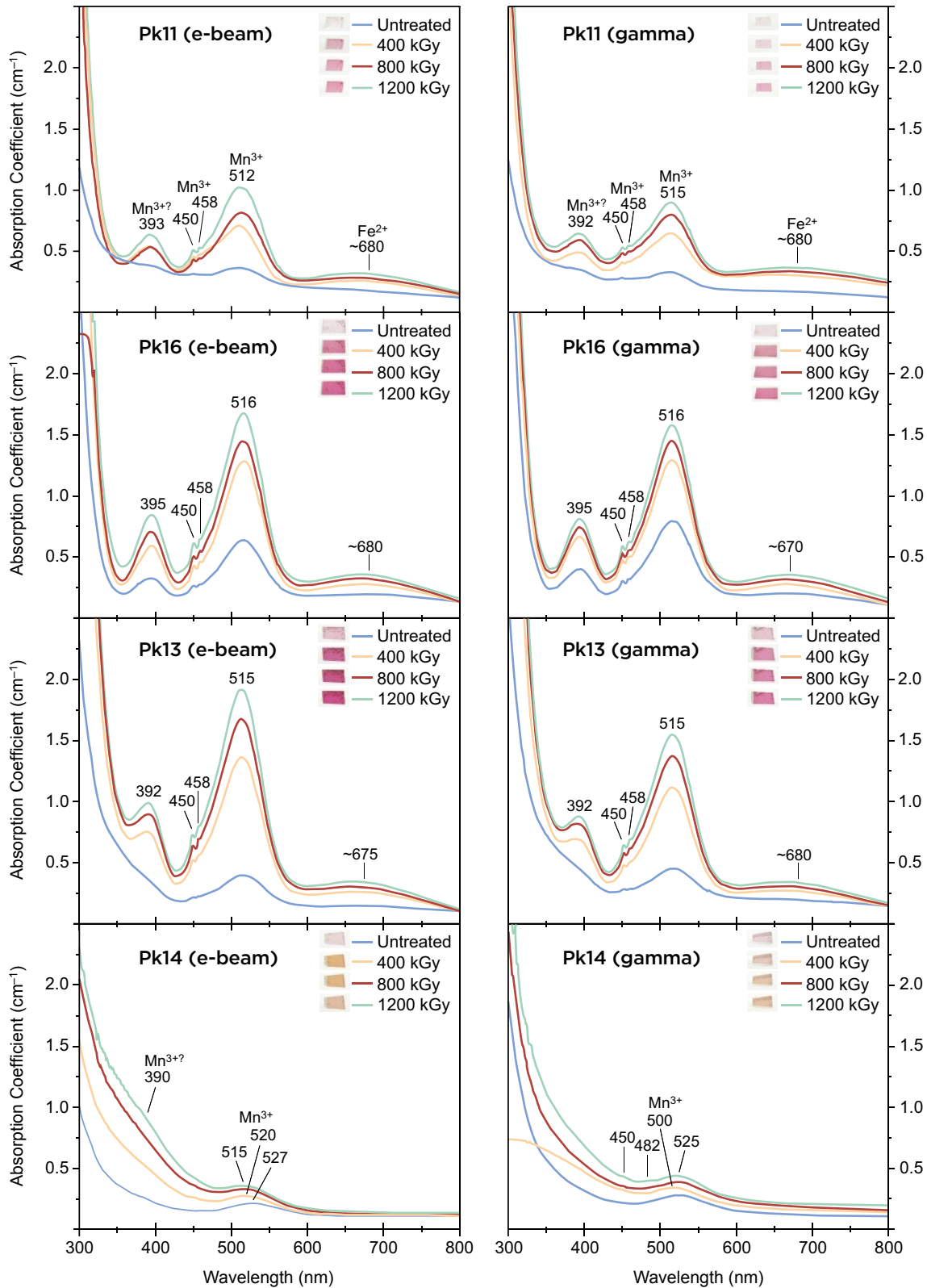
Figure 6: UV-Vis absorption spectra obtained parallel to the *c*-axis for the same tourmaline samples shown in Figures 4 and 5 display relatively weak features before treatment and progressively stronger absorptions with increasing radiation doses.
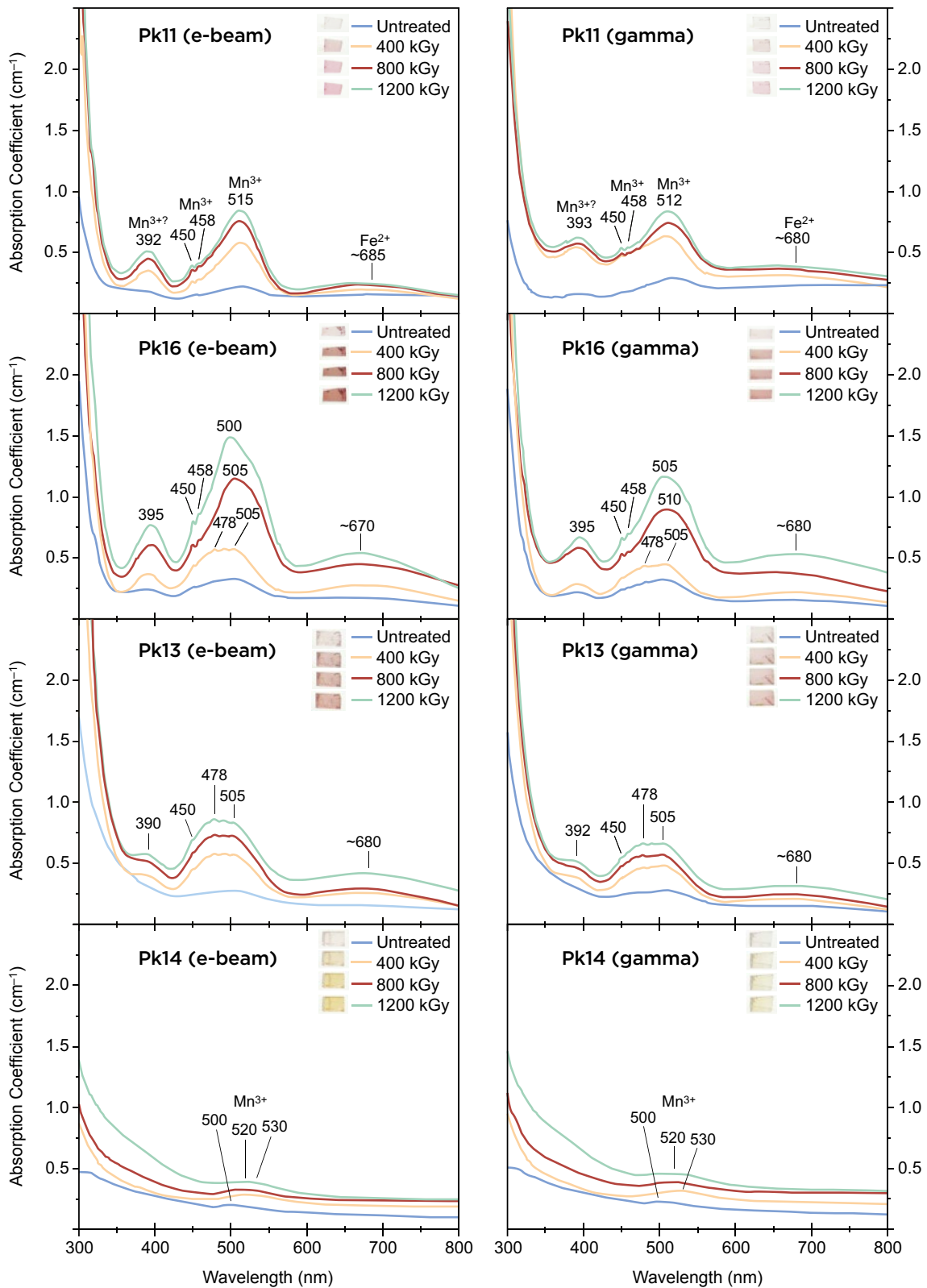
Figure 7: UV-Vis absorption spectra obtained perpendicular to the *c*-axis are shown for the same samples and treatment parameters as in Figure 6.

After irradiation at doses of 800 and 1200 kGy, the maximum absorption was centred at 500–510 nm and was associated with the two small peaks at 450 and 458 nm. Sample Pk13 showed the same primary broad band superimposed with small peaks at 450, 478 and 505 nm. Taran *et al.* (1993) suggested these bands are related to Mn^{3+}. Sample Pk14 displayed a Mn^{3+} absorption band at around 480–530 nm. Other features (observed in three of the four samples) included the minor band centred at about 390–395 nm that is probably related to Mn^{3+} and the weak broad band at around 670–685 nm related to Fe^{2+}.

In general, the irradiated pink samples displayed absorptions that were slightly greater after electron-beam irradiation than after gamma irradiation (Figures 6 and 7), consistent with the more intense colour produced by the electron beam (Figures 4 and 5).

EPR Spectroscopy

EPR spectra of sample Pk03 in the ⊥C direction, which changed from pink to orangey pink when viewed in this orientation after irradiation, are shown in Figure 8. The most important parameter of an EPR signal is the g-factor, which is a constant of proportionality used to calculate the magnetic moment of electron spin. The g-factors presented in Table III were calculated using the equation $h\nu = g\mu_B B$, where h is Planck's constant $(6.6262 \times 10^{-34} \text{ J·s})$, ν is microwave frequency (controlled by experimental conditions), μ_B is the Bohr magneton constant $(9.274 \times 10^{-24} \text{ J/T})$ and B is the magnetic field.

Before treatment, the EPR spectrum contained three resonance signals at 264, 283 and 302 mT (Figure 8a). These signals appear to be caused by manganese (possibly Mn^{2+}; Babińska *et al.* 2008). After irradiation at 400 kGy by both techniques, the EPR spectra presented a series of paramagnetic signals—particularly in the range 320–380 mT—that have been ascribed to defects related to two colour centres: the O^- hole centre (responsible for yellow colouration) and the H^0 electron centre (the local charge compensator for the hole trap; Krambrock *et al.* 2002, 2004b). The H^0 centre is indicated by two relatively sharp signals at 324 and 375 mT, while the O^- centre is represented by the broad signal at about 339–343 mT (Figure 8b, c). The electron-beam irradiation produced stronger signals for these colour centres.
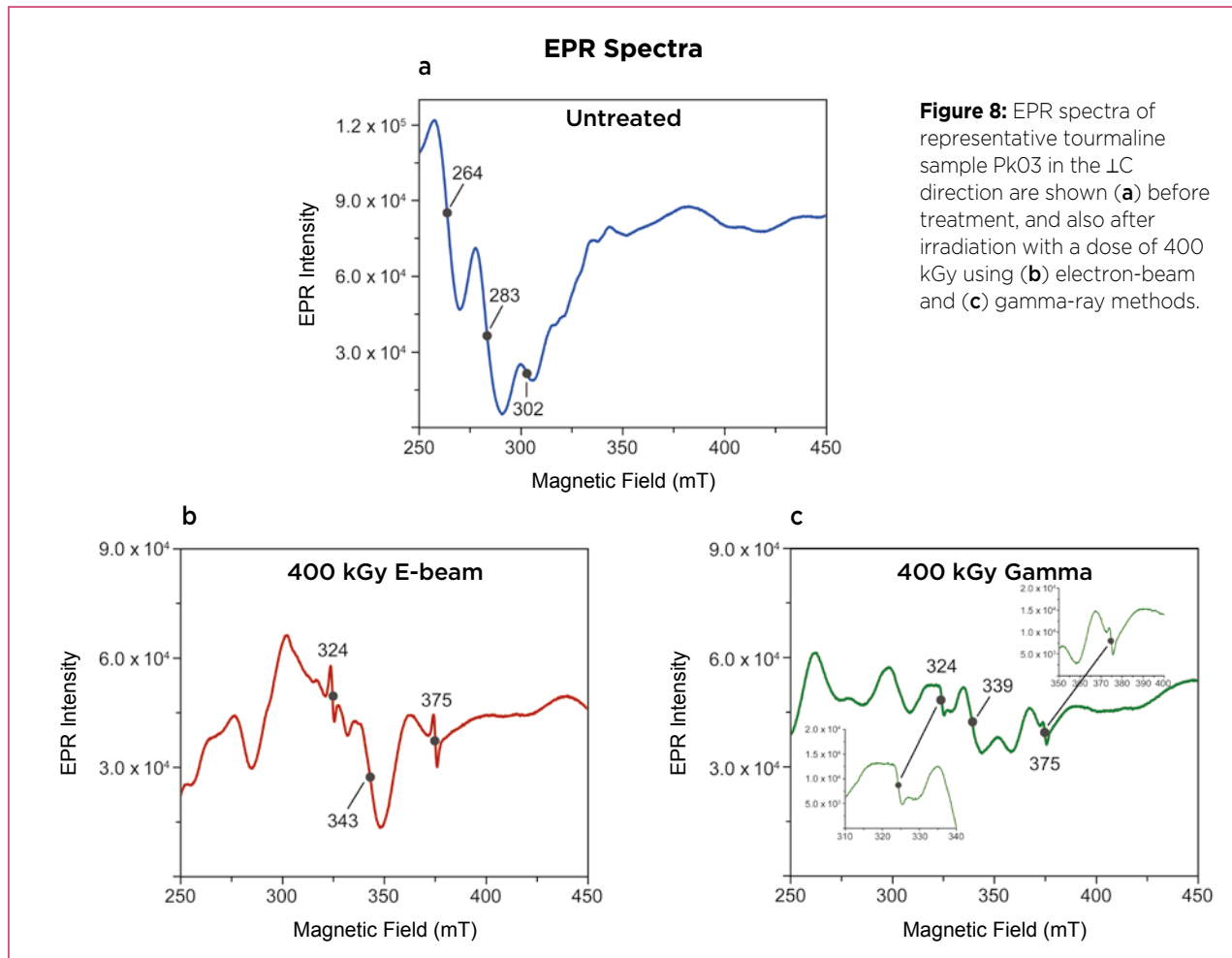
Figure 8: EPR spectra of representative tourmaline sample Pk03 in the ⊥C direction are shown (**a**) before treatment, and also after irradiation with a dose of 400 kGy using (**b**) electron-beam and (**c**) gamma-ray methods.

Table III: Calculated *g*-factor values from EPR signals.

Environment	*g*-factor	Magnetic field (mT)
Mn ions	2.66	264
	2.48	283
	2.33	302
H⁰ centre	2.17	324
	1.88	375
O⁻ centre	2.05	343
	2.07	339

be related to Mn^{3+} was present in most samples. Therefore, the colouration of these elbaite samples before treatment was mainly caused by Mn^{3+}, which produced the dominant pink colour.

Both electron and gamma irradiation can produce intense pink colour with variable yellow modification. In our experiments, these treatments enhanced Mn^{3+} absorptions, and also added a yellow colour component to some samples that was probably due to the O^- hole centre. A more intense pink colour after irradiation was seen in tourmalines containing higher Mn contents. At equivalent dosages, electron-beam irradiation tended to yield a more intense colouration in our samples than gamma irradiation.

CONCLUSIONS

Pink-to-red tourmaline is an important and attractive gem material in the global gem trade (e.g. Figure 9). The samples from Nigeria studied for this report were elbaite that ranged from near-colourless to pale pink, pink and pale orangey pink before treatment. With either electron-beam or gamma irradiation, the samples turned pink to intense pink and orangey pink to pinkish orange or yellowish orange. EPMA analysis indicated that the samples showing a more orangey colour after irradiation contained less Mn compared to the pinker samples. UV-Vis spectra revealed absorption mainly related to Mn^{3+} centred at around 510–520 nm (for the direction parallel to the *c*-axis) or composed of overlapping peaks centred at 478 and 500–510 nm (for the direction perpendicular to the *c*-axis). In addition, a minor band centred at 390–395 nm that may also

Figure 9: These untreated rubellite tourmalines from Mozambique (3.85–5.75 ct) show an appealing deep purplish pink colouration. Photo by T. Sripoonjan.

REFERENCES

Ahn, Y., Seo, J. & Park, J. 2013. Electronic and vibrational spectra of tourmaline – The impact of electron beam irradiation and heat treatment. *Vibrational Spectroscopy*, **65**, 165–175, https://doi.org/10.1016/j.vibspec.2013.01.002.

Babińska, J., Dyrek, K., Pieczka, A. & Sojka, Z. 2008. X and Q band EPR studies of paramagnetic centres in natural and heated tourmaline. *European Journal of Mineralogy*, **20**(2), 233–240, https://doi.org/10.1127/0935-1221/2008/0020-1790.

Bershov, L.V., Martirosyan, V.O., Marfunin, A.S., Platonov, A.N. & Tarashchan, A.N. 1969. Colour centres in lithium tourmaline (elbaite). *Soviet Physics and Chemistry*, **13**, 629–630.

Bosi, F. 2018. Tourmaline crystal chemistry. *American Mineralogist*, **103**(2), 298–306, https://doi.org/10.2138/am-2018-6289.

Bunnag, N. & Sripoonjan, T. 2019. Gamma irradiation on rubellite tourmaline. *Chiang Mai Journal of Science*, **46**(6), 1249–1255.

Clark, C.M. 2007. Tourmaline: Structural formula calculations. *Canadian Mineralogist*, **45**(2), 229–237, https://doi.org/10.2113/gscanmin.45.2.229.

da Silva, F.S., Moura, M.A., Queiroz, H.A. & Ardisson, J.D. 2018. Chemical and spectroscopic characterization of tourmalines from the Mata Azul pegmatitic field, central Brazil. *Journal of Geosciences*, **63**(2), 155–165, https://doi.org/10.3190/jgeosci.258.

de Camargo, M.B. & Isotani, S. 1988. Optical absorption spectroscopy of natural and irradiated pink tourmaline. *American Mineralogist*, **73**(1–2), 172–180.

Henry, D.J., Novak, M., Hawthorne, F.C., Ertl, A., Dutrow, B.L., Uher, P. & Pezzotta, F. 2011. Nomenclature of the tourmaline-supergroup minerals. *American Mineralogist*, **96**(5–6), 895–913, https://doi.org/10.2138/am.2011.3636.

Krambrock, K., Pinheiro, M.V.B., Medeiros, S.M., Guedes, K.J., Schweizer, S. & Spaeth, J.M. 2002. Investigation of radiation-induced yellow color in tourmaline by magnetic resonance. *Nuclear Instruments and Methods in Physics Research Section B: Beam Interactions with Materials and Atoms*, **191**(1–4), 241–245, https://doi.org/10.1016/s0168-583x(02)00568-2.

Krambrock, K., Medeiros, S.M., Guedes, K.J., Pinheiro, M.V.B. & Spaeth, J.-M. 2004a. Pink tourmaline studied by optical detection of magnetic resonance. *In*: Pecchio, M. *et al.* (eds), *Applied Mineralogy: Developments in Science and Technology*, International Council for Applied Mineralogy do [*sic*] Brasil, São Paulo, 567–570.

Krambrock, K., Pinheiro, M.V.B., Guedes, K.J., Medeiros, S.M., Schweizer, S. & Spaeth, J.M. 2004b. Correlation of irradiation-induced yellow color with the O⁻ hole center in tourmaline. *Physics and Chemistry of Minerals*, **31**(3), 168–175, https://doi.org/10.1007/s00269-003-0378-3.

Kurtz, D.A., Rossman, G.R. & Hunter, B.M. 2020. The nature of the Mn(III) color centers in elbaite tourmalines. *Inorganic Chemistry*, **59**(14), 9618–9626, https://doi.org/10.1021/acs.inorgchem.0c00722.

Liu, X., Feng, X., Fan, J. & Guo, S. 2011. Optical absorption spectra of tourmaline crystals from Altay, China. *Chinese Optics Letters*, **9**(8), 1–4, https://doi.org/10.3788/COL201109.083001.

Lucas, A. 2015. From Brazil to China: The journey of rubellite tourmaline. Gemological Institute of America, www.gia.edu/gia-news-research-miranda-journey-of-rubellite-tourmaline, 27 March, accessed 6 January 2021.

Maneewong, A., Pangza, K., Jangsawang, N. & Charoennam, T. 2016a. Effect of heat treatment and electron beam irradiation [*sic*] tourmaline: UV-visible, EPR, and mid-IR spectroscopic analyses. *Walailak Journal of Science & Technology*, **13**(12), 993–1003.

Maneewong, A., Seong, B.S., Shin, E.J., Kim, J.S. & Kajornrith, V. 2016b. Color change of tourmaline by heat treatment and electron beam irradiation: UV-visible, EPR, and mid-IR spectroscopic analyses. *Journal of the Korean Physical Society*, **68**(1), 83–92, https://doi.org/10.3938/jkps.68.83.

Nassau, K. 1975. Gamma ray irradiation induced changes in the color of tourmalines. *American Mineralogist*, **60**(7–8), 710–713.

Nassau, K. 1994. *Gemstone Enhancement: History, Science and State of the Art*, 2nd edn. Butterworth Heinemann, Oxford, 194–197.

Okrusch, M., Ertl, A., Schüssler, U., Tillmanns, E., Brätz, H. & Bank, H. 2016. Major- and trace-element composition of Paraíba-type tourmaline from Brazil, Mozambique and Nigeria. *Journal of Gemmology*, **35**(2), 120–139, https://doi.org/10.15506/JoG.2016.35.2.120.

Petrov, I. 1990. Role of natural radiation in tourmaline coloration: Discussion. *American Mineralogist*, **75**(1–2), 237–239.

Pezzotta, F. & Laurs, B.M. 2011. Tourmaline: The kaleidoscopic gemstone. *Elements*, **7**(5), 333–338, https://doi.org/10.2113/gselements.7.5.333.

Reinitz, I.M. & Rossman, G.R. 1988. Role of natural radiation in tourmaline coloration. *American Mineralogist*, **73**(7–8), 822–825.

Rossman, G.R. 2019. Color in tourmaline. *In*: Simmons, W.B. & Staebler, G.A. (eds), *Rubellite—Tourmaline Rouge*. Lithographie Ltd, Arvada, Colorado, USA, 28–33.

Shirose, Y. & Uehara, S. 2013. Li tourmaline from Nagatare, Fukuoka Prefecture, Japan. *Journal of Mineralogical and Petrological Sciences*, **108**(4), 238–243, https://doi.org/10.2465/jmps.121022e.

Taran, M.N., Lebedev, A.S. & Platonov, A.N. 1993. Optical absorption spectroscopy of synthetic tourmalines. *Physics and Chemistry of Minerals*, **20**(3), 209–220, https://doi.org/10.1007/bf00200123.

The Authors

Waratchanok Suwanmanee and Prof. Dr Chakkaphan Sutthirat
Department of Geology, Faculty of Science, Chulalongkorn University, 254 Phayathai Road, Pathumwan, Bangkok 10330, Thailand, and The Gem and Jewelry Institute of Thailand, 140 ITF Tower, Silom Road, Bangkok 10500, Thailand
Email: chakkaphan.s@chula.ac.th

Dr Bhuwadol Wanthanachaisaeng
College of Creative Industry, Srinakharinwirot University, 114 Sukhumvit 23, Wattana District, Bangkok 10110, Thailand

Teerawat Utapong
Thailand Institute of Nuclear Technology, 9/9 Moo 7, Sai Mun, Ongkharak, Nakorn Nayok 26120, Thailand

Revealing the Formation Secrets of the Matryoshka Diamond

Emmanuel Fritsch

ABSTRACT: The so-called Matryoshka diamond from Siberia, Russia, consists of a 0.62 ct pale green specimen that contains a small, flat diamond crystal which can freely move within an internal cavity in the stone. The cavity is connected to the surface by two small channels. This rare specimen is here proposed to result from an unusual succession of layered growth (octahedral–fibrous–octahedral), which was followed by the etching of two surface-reaching dislocations that penetrated the fibrous layer, allowing circulating etch solutions to entirely resorb the fibrous portion of the crystal. This freed the core (composed of octahedral growth) so that it became loose inside the outer octahedral growth layer of the crystal. This scenario is supported by some lesser-known facts about diamond growth and dissolution, as described here. At least two similar diamonds have been described in the literature previously, so the Matryoshka diamond is not unique.

In October 2019, an inclusion of diamond freely moving inside another diamond was the subject of many announcements (see, e.g., Quick 2019), including YouTube videos (CGTN 2019; Siberian Times 2019) and its own Wikipedia page (Anonymous 2019). This 0.62 ct curiosity was named the Matryoshka diamond (Wang *et al.* 2020; see Figure 1), by analogy with the Russian nesting dolls. The stone was discovered during the sorting process at the Alrosa-owned Nyurba diamond mine in the Nakynskoye field, Siberia,
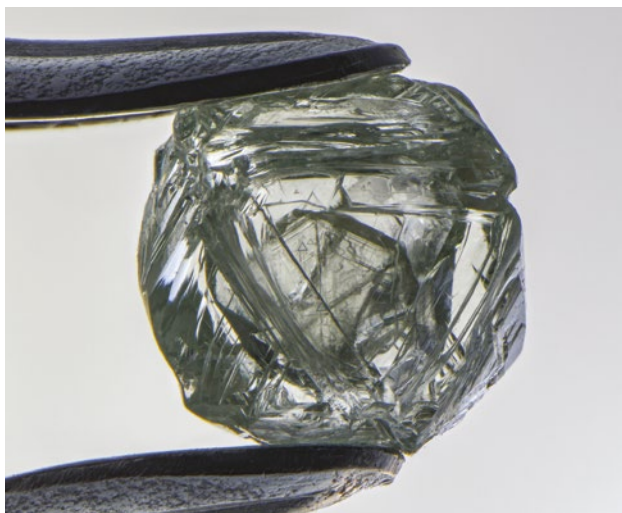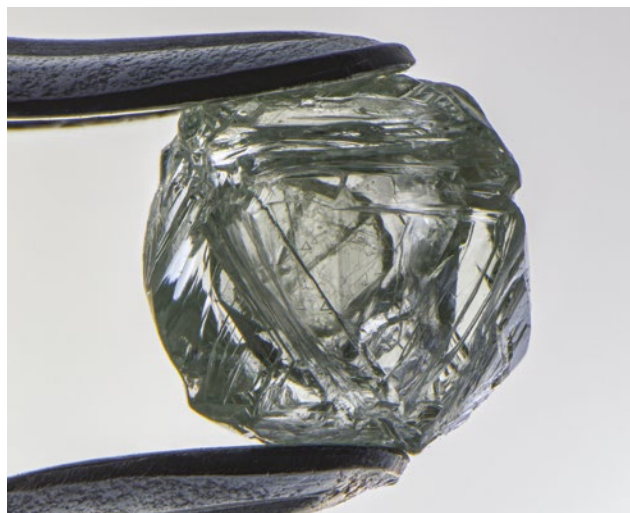

Figure 1: These two images of the Matryoshka diamond clearly illustrate how the smaller diamond can move around inside a cavity within the stone. The pale green specimen weighs 0.62 ct and measures 4.8 × 4.9 × 2.8 mm. Sample courtesy of Alrosa; photos by Nathan D. Renfro, © GIA.

eastern Russia. It is purported to be 800 million years old (Quick 2019). Some reports claim this is the first time such a diamond has been observed and that it is unique. However, a similar diamond-within-a-diamond was previously described in some detail (Kammerling *et al.* 1995; Koivula 2000). It was a flat, triangular, 1.09 ct slightly brownish grey twinned crystal (macle) with a sliding triangular diamond inclusion that had the same properties as the host diamond. In addition, a 0.87 ct diamond crystal with a green diamond freely moving inside was recently documented in the same issue of *Gems & Gemology* that described the Matryoshka stone (Renfro & Koivula 2020).

The Matryoshka diamond was characterised in detail using X-ray tomography to measure and image both of its components separately, as illustrated in a well-made video (Morisseau 2020; Wang *et al.* 2020). The question remains: how is it possible for a diamond to be captive within a cavity of another (apparently) octahedral diamond? One hypothesis was proposed by Alrosa scientists (Quick 2019):

> …[A] layer of porous polycrystalline diamond substance was formed inside the diamond because of ultra-fast growth, and more aggressive mantle processes subsequently dissolved it. Due to the presence of the dissolved zone, one diamond began to move freely inside another on the principle of matryoshka nesting dolls.

Wang *et al.* (2020, p. 129) further proposed that:

> Due to chemical heterogeneity in trace element chemistry or sub-micro inclusions/structure (such as those [of] fibrous diamonds), the middle part of the diamond crystal (now represented by the void) was selectively dissolved during interactions with special type(s) of melt/fluid after its crystallization.

These two hypotheses are very similar but not very detailed. Further, the explanations are very brief and they do not cite any published literature. The lack of a step-by-step scientific explanation leaves the reader's curiosity unsatisfied, and this article offers a more detailed proposal for the Matryoshka diamond's formation, supported by references to existing literature. The scenario described here is based on the author's observations of many normal and unusual diamond morphologies over the years, as well as characteristics of their dissolution. It is at the very least consistent with what is known (although not necessarily published) from some rare and extreme cases of growth and etching in diamonds.

INFERRED MECHANISM OF FORMATION

The following sequence of events leading to the formation of the Matryoshka diamond is first based on a succession of octahedral and fibrous growth events, followed by dissolution, and also considers that the internal crystal is actually a twin. Finally, the timing of the diamond's dissolution and staining events relative to its transport to the earth's surface is discussed.

Octahedral–Fibrous–Octahedral Growth Succession

During the initial crystallisation of the diamond, a 'regular' phase of octahedral growth occurred. This is the most common growth condition for diamond and, thus, the most likely. Subsequently, fibrous growth created a layer composed of diamond fibres oriented perpendicular to the octahedral faces. This has been observed fairly often and results in what is called a *coated* diamond (Boyd *et al.* 1994; Fritsch *et al.* 2005; Tappert & Tappert 2011).

The next growth event is less common, and is essentially the reverse of the previous step, with gem-quality octahedral growth developing on top of the fibrous growth layer. Although this may be surprising, fibrous growth is actually only a type of fast octahedral growth (Sunagawa 2005), so it can act as a template—on rare occasions—for the start of octahedral growth. This is best illustrated by so-called *sugar cube* diamonds (Rondeau *et al.* 2007), which start as a fibrous cubic crystal (actually a diamond dendrite) that is then overgrown by an octahedral layer. These typically appear white due to the scattering of light by the 'fibres' (thus, the 'sugar cube' nickname). They demonstrate the possibility of gem octahedral growth over relatively flat faces of fibrous diamond. For brevity, this succession is indicated here as OFO—for octahedral–fibrous–octahedral. Ultimately, this OFO sequence of growth events produces an octahedron with an internal layer of fibrous growth (Figure 2a).

This progression of events might seem contradictory to observations of diamonds in some Siberian kimberlite pipes, where fibrous growth is believed to have taken place shortly before kimberlite eruption (e.g. Gubanov *et al.* 2019). However, different behaviours have been noted elsewhere, for example in the Democratic Republic of the Congo (DRC), which is well known for producing diamonds with an abundance of fibrous growth events. In fact, the passage of growth from octahedral to fibrous and back to octahedral could simply be due to a slight oscillation in the conditions that govern the start of
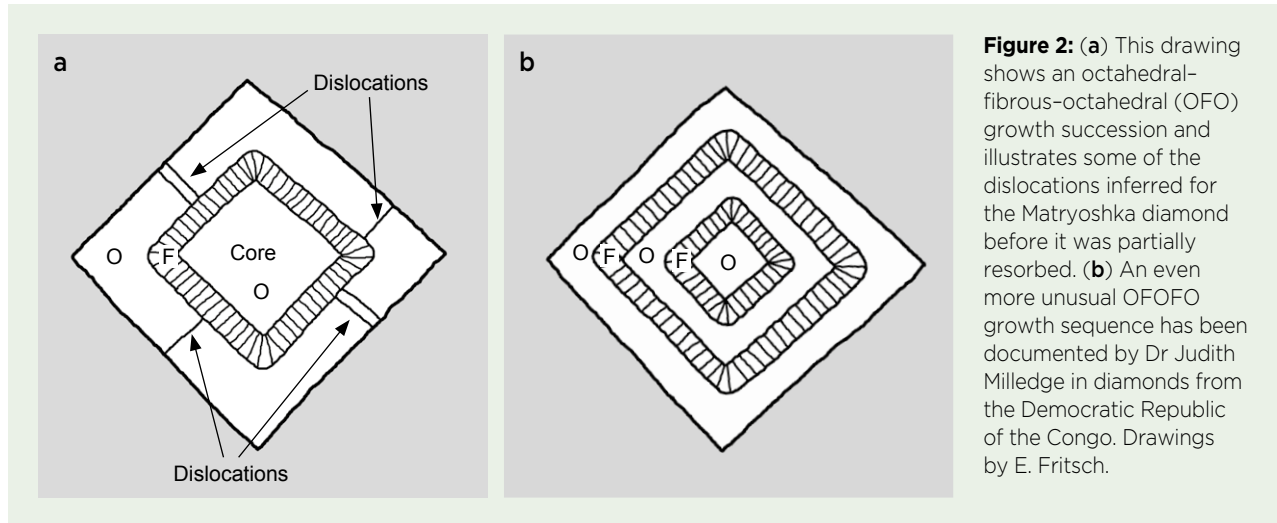
Figure 2: (**a**) This drawing shows an octahedral–fibrous–octahedral (OFO) growth succession and illustrates some of the dislocations inferred for the Matryoshka diamond before it was partially resorbed. (**b**) An even more unusual OFOFO growth sequence has been documented by Dr Judith Milledge in diamonds from the Democratic Republic of the Congo. Drawings by E. Fritsch.

fibrous growth; it does not need to be a dramatic change. Dr Judith Milledge, a well-known diamond scientist who paid special attention to natural diamond morphology, reported having seen a succession of octahedral–fibrous–octahedral–fibrous–octahedral (OFOFO) growth habits in several diamonds from the DRC (J. Milledge, pers. comm., about 2003). At that time, the present author drew a sketch similar to that shown in Figure 2b, and Dr Milledge confirmed unambiguously that this was what she had observed. This OFOFO succession is even less probable than the one we propose here to explain the Matryoshka diamond formation.

Dissolution

Varying amounts of dissolution (often referred to as resorption) follow growth for almost all natural gem diamonds (Bari & Fritsch 2001; Fedortchouk *et al.* 2011; Tappert & Tappert 2011). This is simply an inversion of the growth driving force (e.g. the end of carbon supersaturation). While an internal fibrous layer might be expected to be protected from resorption by the octahedral overgrowth, this external layer might not be perfectly crystallised. Crystal growth commonly includes dislocations—linear defects that are the main factors behind the slow growth of gem crystals. Dislocations can act as preferential zones of dissolution, with very rapid etching rates. To our knowledge, this rate has been measured only on synthetic quartz, where it was established that dissolution along a screw dislocation was up to 1,000 times faster than on a flat crystal surface (Nielsen & Foster 1960). Such a localised, incredibly heightened rate of dissolution may take place in many different gem minerals and not just quartz. In diamond, for example, etch channels may cross an entire crystal (Philippe & Fritsch 2017a, b). Moreover,

numerous spectacular long, large, dissolved dislocations were recently documented in a gem diamond (Delaunay & Fritsch 2018). These observations imply that although these channels may have openings that are quite small, they are extremely efficient at channelling fluids capable of resorbing diamond (even within a gem-quality octahedral crystal).

As reported by Quick (2019) and Morisseau (2020) for the Matryoshka diamond, two obvious tubes connect its surface with its interior (shown diagrammatically in Figure 3), and Wang *et al.* (2020) indicated that one of the channels measures 200 µm (0.2 mm) wide at
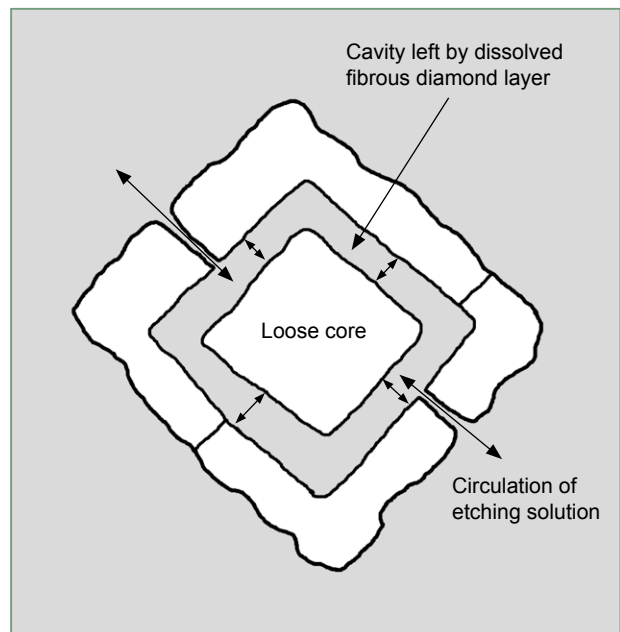
Figure 3: Fluids entered the diamond through channels provided by two dissolved dislocations and etched away the intermediate fibrous growth layer. This liberated the core, which was able to move freely within the cavity formed by the resorbed layer. Drawing by E. Fritsch.

the crystal's surface. Two dislocations apparently were preferentially dissolved all the way to the diamond's fibrous layer. Dissolved dislocations first take on a funnel shape and then may turn into large tubes (Philippe & Fritsch 2017a, b), with their cross-sections increasing over time during dissolution. This means they can allow etching solutions to carry away surprisingly large amounts of dissolved diamond. Only one such tube was necessary to reach the fibrous layer in order to become a major channel for the etching fluids to penetrate the diamond, but in this case the presence of two channels further enhanced the circulation of the fluids.

Fibrous growth dissolves (etches or resorbs) much faster than octahedral growth for two main reasons. First, fibrous growth is very finely divided, and the interfibrous spaces are likely connected, increasing the interaction surface, which directly correlates to the rate of mineral dissolution. Second, the spaces between fibres contain numerous micro-inclusions, which dissolve more easily than diamond and make further room for the etching solutions to take away dissolved carbon. Khokhryakov and Palyanov (2015) explained how the presence of any available surface 'along the cracks and boundaries between the crystal blocks' increases etching. This would be especially true of grain boundaries between the fibres.

Thus, the intermediate (fibrous) layer of the diamond was progressively eaten away with very little effect on the adjacent gem (octahedral) layers, where etching was slow in the absence of dislocations (again, see Figure 3). This initiated the release of the core octahedral diamond from its fibrous diamond matrix. Thus, the two crystals—host and inclusion—in the Matryoshka diamond were initially one and the same crystal,

and they became separate through dissolution of the intervening fibrous layer. Note that the surface of the Matryoshka diamond crystal is far more irregular than the internal surfaces of the host diamond forming the cavity, which are comparatively smooth. This can be seen clearly in the X-ray tomography video mentioned above (Morisseau 2020), and is consistent with the scenario proposed here, because the exterior surface of the crystal would have been subjected to etching for a longer period of time.

An analogous partial dissolution process may be inferred for the 'roof' diamond crystal in Figure 4. This specimen probably originated from the same OFO growth succession. The OFO crystal was broken after growth, freeing a fragment with fibrous growth exposed (Figure 5). This part of the diamond then dissolved in the presence of etching fluids, liberating the 'roof' and, possibly, a small piece of underlying octahedral growth.

Diamond Core as a Macle

The proposed growth model thus far has deliberately treated the diamond crystal as being mainly formed by octahedral growth zones, but the core inclusion is flattened, with a near-hexagonal outline (Quick 2019; Wang *et al.* 2020). Wang further stated that this 'flat octahedral diamond is a twinned macle'. Typically, macles are flattened by preferential growth along the twin plane (Sunagawa 2005). So, how would the presence of a twin affect the growth scenario of the Matryoshka diamond? Very little. Coated twins are known to occur (Fritsch *et al.* 2005), and the formation mechanism proposed here can take place in the presence of a twinned diamond core rather than a regular octahedron with no significant differences.
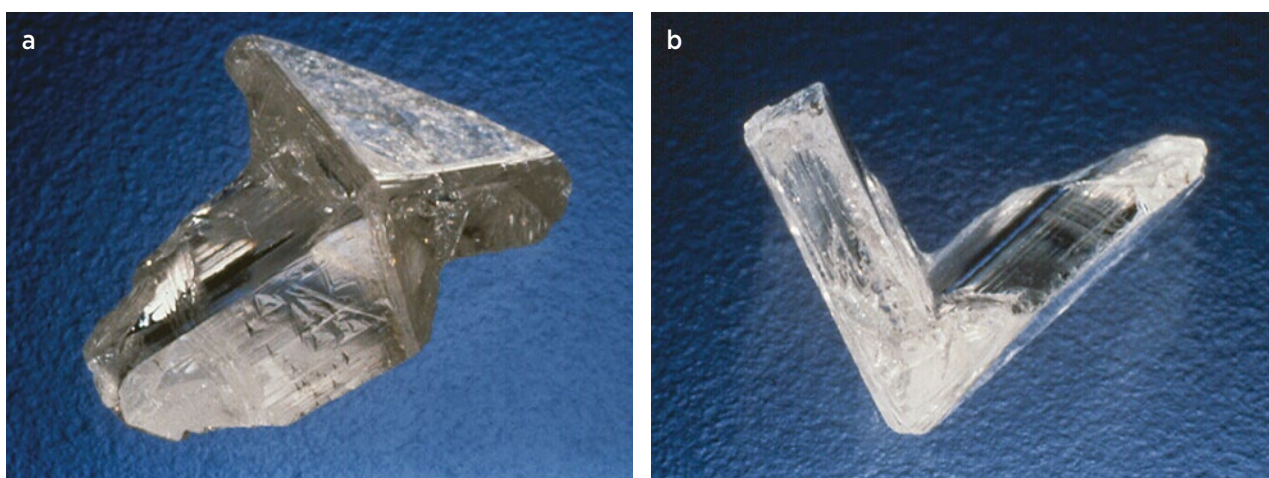
Figure 4: The 'roof' diamond crystal from the De Beers Special Crystals Collection consists of four adjacent octahedral faces of equivalent thickness. It is photographed here in two different orientations: (**a**) from above and (**b**) from the side. It is approximately 1 cm in maximum dimension. Specimen courtesy of De Beers; photos by Mike Crowder.
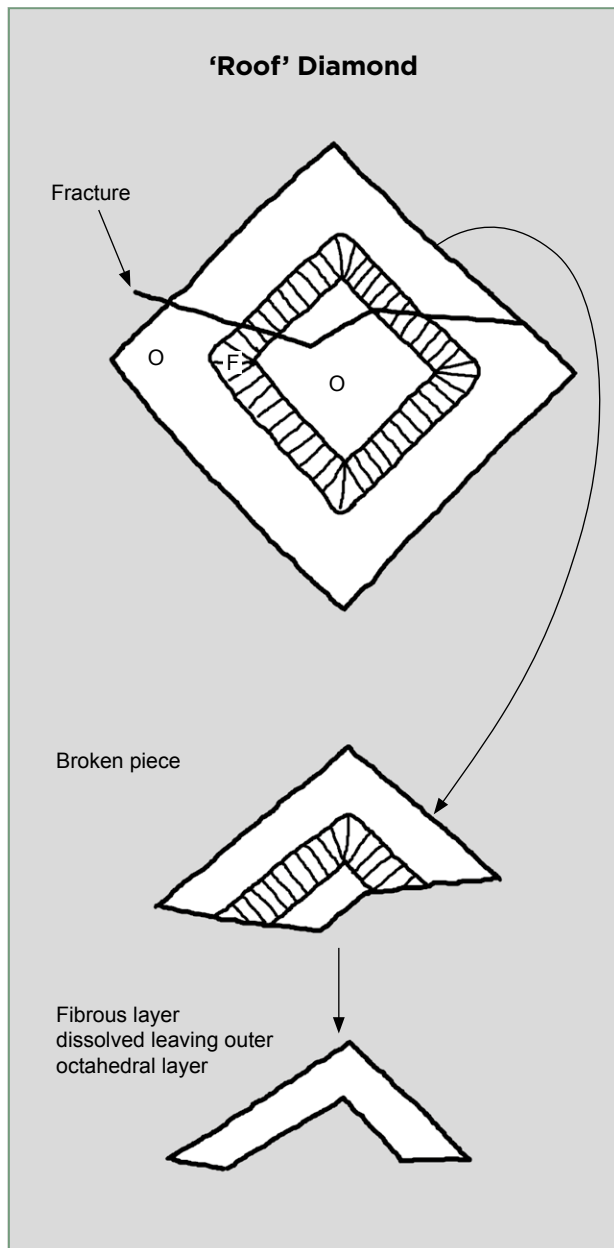
Figure 5: This diagram shows how OFO growth followed by fracturing and etching of a fibrous layer could have led to the unique morphology of the 'roof' diamond in Figure 4. Drawing by E. Fritsch.

Interestingly, two of the three Matryoshka-type diamonds described in the literature are flattened pseudo-triangular twins. One might wonder why. If twins are less frequent than regular octahedra, then this complex scenario might also be less frequently encountered with twins. However, Matryoshka-type diamonds appear to *preferentially* develop on twinned crystals, as those would be expected to permit greater dissolution through the presence of more abundant dissolved dislocations. Therefore, the 'Matryoshka' scenario should be more likely to occur on twinned diamonds because the twin plane commonly hosts a greater number of dissolved dislocations than the faces of a regular octahedron.

Timing of Dissolution and Staining

The chronology of events related to the Matryoshka diamond's transport to the earth's surface remains unclear. Dissolution is often associated with diamond transport from the mantle to the surface, although some examples show indications that dissolution occurred before uplift to the surface (Bulanova 1995). Such pre-transport timing of the resorption could strengthen the proposal put forward in this article.

After the selectively resorbed—now 'Matryoshka' diamond—reached the surface, radioactive solutions penetrated the same voids that were created by the etching fluids. Such solutions turned all diamond surfaces slightly green by imparting radiation stains caused by uranium alpha particles. This is the most common cause of green colour in diamond rough (Fritsch 1997). Dissolved dislocations with radiation stains have been previously recorded in diamond (see, e.g., Koivula 2000), so this final staining event in the Matryoshka diamond's history is not surprising.

CONCLUSION

This article proposes an OFO growth sequence followed by dissolution through two dissolved dislocations as mechanisms for the formation of the Matryoshka diamond. Through reference to detailed scientific work, each stage in the formation of this type of specimen has already been documented to some extent. What is truly unusual is that they happened in a certain sequence, as described and illustrated here in detail for the first time. Moreover, there are now three documented diamonds to which this scenario might apply, supporting this proposal. Such exceptional specimens demonstrate how highly unusual formation processes are useful for furthering our understanding of the science of diamond growth and dissolution.

Dedication: This article is dedicated to Dr H. Judith Milledge, who sadly passed away on 21 January 2021, during the final stages of this article's preparation. She was Emeritus Reader in Crystallography at University College London, and much of her work was devoted to studying the external morphology and internal zoning of natural diamond crystals. She is fondly remembered by her many colleagues and former students as both an insightful scientist and a kind and engaging personality with a sometimes dry sense of humour.

REFERENCES

Anonymous 2019. Matryoshka (diamond). Wikipedia, https://en.wikipedia.org/wiki/Matryoshka_(diamond), accessed 5 February 2021.

Bari, H. & Fritsch, E. 2001. The natural history of diamond. *In*: Bari, H. & Sautter, V. (eds) *Diamonds*. Vilo International, Adam Biro Books, Paris, France, 20–43.

Boyd, S.R., Pineau, F. & Javoy, M. 1994. Modelling the growth of natural diamonds. *Chemical Geology*, **116**(1–2), 29–42, https://doi.org/10.1016/0009-2541(94)90156-2.

Bulanova, G.P. 1995. The formation of diamond. *Journal of Geochemical Exploration*, **53**(1–3), 1–23, https://doi.org/10.1016/0375-6742(94)00016-5.

CGTN 2019. Matryoshka diamond found in Russia with another gem trapped inside. YouTube, www.youtube.com/watch?v=8ofV3FUCxuI, accessed 5 February 2021.

Delaunay, A. & Fritsch, E. 2018. *G&G* Micro-World: Type IIa diamond with extraordinary etch channels. *Gems & Gemology*, **54**(1), 66–67.

Fedortchouk, Y., Manghnani, M.H., Hushur, A., Shiryaev, A. & Nestola, F. 2011. An atomic force microscopy study of diamond dissolution features: The effect of H_2O and CO_2 in the fluid on diamond morphology. *American Mineralogist*, **96**(11–12), 1768–1775, https://doi.org/10.2138/am.2011.3828.

Fritsch, E. 1997. The nature of color in diamonds. *In*: Harlow, G.E. (ed) *The Nature of Diamonds*. Cambridge University Press, Cambridge, 23–47.

Fritsch, E., Moore, M., Rondeau, B. & Waggett, R.G. 2005. X-ray topography of a natural twinned diamond of unusual pseudo-tetrahedral morphology. *Journal of Crystal Growth*, **280**(1–2), 279–285, https://doi.org/10.1016/j.jcrysgro.2005.02.058.

Gubanov, N., Zedgenizov, D., Sharygin, I. & Ragozin, A. 2019. Origin and evolution of high-Mg carbonatitic and low-Mg carbonatitic to silicic high-density fluids in coated diamonds from Udachnaya kimberlite pipe. *Minerals*, **9**(12), article 734 (17 pp.), https://doi.org/10.3390/min9120734.

Kammerling, R.C., Koivula, J.I., Johnson, M.L. & Fritsch, E. (eds) 1995. Gem News: Diamond with mobile diamond inclusion. *Gems & Gemology*, **31**(3), 204.

Khokhryakov, A.F. & Palyanov, Y.N. 2015. Effect of crystal defects on diamond morphology during dissolution in the mantle. *American Mineralogist*, **100**(7), 1528–1532, https://doi.org/10.2138/am-2015-5131.

Koivula, J.I. 2000. *The Microworld of Diamonds*. Gemworld International, Northbrook, Illinois, USA, 157 pp.

Morisseau, S. 2020. GIA researchers reveal the secrets to diamond-in-a-diamond mystery. Gemological Institute of America, www.gia.edu/gia-news-research/gia-researchers-reveal-secrets-diamond-in-diamond-mystery, accessed 15 December 2020.

Nielsen, J.W. & Foster, F.G. 1960. Unusual etch pits in quartz crystals. *American Mineralogist*, **45**(3–4), 299–310.

Philippe, M. & Fritsch, E. 2017a. Les dislocations dissoutes : des inclusions pas toujours faciles à identifier – 1er partie. *Revue de Gemmologie A.F.G.*, No. 200, 11–22.

Philippe, M. & Fritsch, E. 2017b. Les dislocations dissoutes : des inclusions pas toujours faciles à identifier – 2ème partie. *Revue de Gemmologie A.F.G.*, No. 201, 12–16.

Quick, D. 2019. World-first "Matryoshka diamond" found in Russia. New Atlas, https://newatlas.com/materials/matroyoshka-diamond-inside-diamond-discovered-russia, accessed 15 December 2020.

Renfro, N. & Koivula, J.I. 2020. *G&G* Micro-World: Diamond with mobile green diamond inclusion. *Gems & Gemology*, **56**(1), 141.

Rondeau, B., Fritsch, E., Moore, M., Thomassot, E. & Sirakian, J.-F. 2007. On the growth of natural octahedral diamond upon a fibrous core. *Journal of Crystal Growth*, **304**(1), 287–293, https://doi.org/10.1016/j.jcrysgro.2007.03.004.

Siberian Times 2019. Matryoshka diamond. YouTube, www.youtube.com/watch?v=YKbP0i3bWu0, accessed 5 February 2021.

Sunagawa, I. 2005. Crystals: *Growth, Morphology and Perfection*. Cambridge University Press, Cambridge, 308 pp.

Tappert, R. & Tappert, M.C. 2011. *Diamonds in Nature: A Guide to Rough Diamonds*. Springer, Berlin, Germany, 154 pp.

Wang, W., Persaud, S., Myagkaya, E., D'Haenens-Johansson, U. & Moses, T.M. 2020. Lab Notes: Formation of the "Matryoshka" diamond from Siberia. *Gems & Gemology*, **56**(1), 127–129.

The Author

Dr Emmanuel Fritsch FGA
Institut des Matériaux Jean Rouxel (IMN),
UMR CNRS 6502, 2 rue de la Houssinière,
BP 32229, F 44322 Nantes Cedex 3, France
Email: emmanuel.fritsch@cnrs-imn.fr

Gem-A Notices

COVID-19 NOTICE FROM GEM-A CEO ALAN HART

We continue to see the unprecedented impact of the COVID-19 pandemic on our lives across the world, with new variants presenting additional challenges in our fight against the virus. But we have renewed hope with the successful development and rapid implementation of vaccination programmes globally, so we hope to return to some normality soon. For the UK, 2021 started with another hard lockdown, and while our London office has once again been temporarily closed, our staff continue to work from home on the delivery of our Education and Membership programs. Although we had to cancel our January exams in some areas affected by COVID rules, we successfully delivered examinations in many other locations. As the pandemic and related changes in business and society have accelerated, the need for digital transformation has become more evident, and the Association has moved rapidly to support the delivery of its core functions through technology. In February 2021, Gem-A's Accredited Teaching Centre (ATC) in London started delivering its first on-site blended teaching programme. We also continue to grow our Online and Distance Learning (ODL) programme globally, with a new term starting in April 2021. In addition, we are providing support to our global ATCs toward delivering Gem-A education during the pandemic through the blended-learning approach.

We have successfully run our 2021 Membership renewals, and I would like to thank all our Members for their support of our great Association. It is still not too late to renew your Membership for the year 2021 to continue enjoying Gem-A's Membership benefits, including being part of a highly regarded and well-respected global network of gemmology professionals. When the Association comes out of the pandemic, we have many exciting initiatives in the pipeline that I will share with our global Membership in due course. Gem-A has a culture of shared success and a continued commitment to make a positive difference to the gem and jewellery industry together with our staff, global Membership, students, partners and communities.

Throughout its history, Gem-A has embraced constant change, and this pandemic is no different. I want to take this opportunity to thank all our Gem-A staff for their incredible dedication, perseverance and commitment as we face a new reality and new ways to work. I also want to thank all our Members, partners and communities for their continued trust and support. As an Association, we have never been more committed to creating shared success for all, as we look to the future with hope and continued aspirations.

GEM-A DIPLOMA PASSES AND AWARDS

For the September 2020 examinations, 71 students passed our Gemmology and Diamond Diploma examinations, and four of them passed with Distinction. Due to the postponement of the Gem-A June examinations until September 2020, the 2020 Prize and Medal winners were not announced last year. We are very pleased to announce the 2020 award winners along with the list of September Graduates. Later this year, we look forward to holding a combined 2020/2021 Gem-A Graduation and Presentation of Awards at London's historic Church House.

GEMMOLOGY DIPLOMA PASSES

Masahide Deepak Aoyama, Japan

Karin Bartha, The Netherlands

Christopher Blacklock, United Kingdom

Zheng Bowen, P.R. China

Thanh Nhan Bui, Belgium

Justine Buscail, France

Marie Sabine Anne Callies, France

Giulio Carpenito, Italy

Fabiola Chambriard, France

Da Chang, P.R. China

Ke-Ning Chen, Taiwan (R.O.C.)

Jyun-Yi Chih, Taiwan (R.O.C.)

Elodie Crochon, France

Sherril Dixon, United Kingdom

Latifa Mohamed Hasan Falamarzi, Bahrain

Xia Fengwang, P.R. China

Nicole Fix, Australia

Satoru Funami, Japan

Zuleika Florence Rosa Gerrish, United Kingdom

Emilie Grimonprez, France

Melody Hsu, Taiwan (R.O.C.)

Peng Huang (Paul), P.R. China

Laura Jalabert, France

Li Jingwen, P.R. China

Xiaona Ju, P.R. China

Lei Li, P.R. China

Ying Li, P.R. China

Chia-Hsien Lin, Taiwan (R.O.C.)

Yi-Hsuan Ma, Taiwan (R.O.C.)

Elizabeth Marshall, United Kingdom

Zhong Menghan, P.R. China

Rachel Sarah Nield, United Kingdom

Saki Okawa, Japan

Julie Olivier, France

Elia Omegna, Italy

Machiko Ota, Japan

Yiwen Pan, P.R. China

Marion Stephanie Paule Protteau Lambert, France

Sicheng Qin, P.R. China

Henk Rijneveld, The Netherlands

Chiemi Sasajima, Italy

Tadashi Sato, Japan

Katie Smith, United Kingdom

Kazuyoshi Takahashi, Japan

Takayuki Tanaka, Japan

Floriane Van Den Brande, United Kingdom

Paul Villié, France

Danielle J M Wallace, New Zealand

Xinhong Wang, P.R. China

Di Wei, France

Linying Wu, P.R. China

Pei Chu Wu, Taiwan (R.O.C.)

Li Xiaoran, P.R. China

Rika Yamagiwa, Japan

Lan Ye, P.R. China

Wang Yiding, P.R. China

Sakuragi Yoko, Japan

Shuqi Zhang, P.R. China

Jiequn Zhong, New Zealand

Min Zhu, P.R. China

Liu Zicong, P.R. China

GEMMOLOGY DIPLOMA PASSES WITH MERIT

Yun-Wen Chen, Taiwan (R.O.C.)

Taïs Gobeaux, Belgium

Alistair McCallum, United Kingdom

Misono Nishihara, Japan

GEMMOLOGY DIPLOMA PASSES WITH DISTINCTION

Côme Guérin, France

Zhenhui Liu, P.R. China

DIAMOND DIPLOMA PASSES

Chen Min, Hong Kong (S.A.R.)

DIAMOND DIPLOMA PASSES WITH MERIT

Abigail Haslett, United Kingdom

DIAMOND DIPLOMA PASSES WITH DISTINCTION

Kate Bliss, United Kingdom

Sarah Elizabeth Bromfield, United Kingdom

PRIZE AND MEDAL WINNERS

Awards and prizes are presented to the best candidates of the year, selected from our students worldwide.

GEMMOLOGY FOUNDATION CERTIFICATE

Anderson Medal

Awarded to the candidate submitting best papers of the year in the Gemmology Foundation examination.

This medal was established in 1981 in honour of Basil W. Anderson FGA, former Director of the Gem Testing Laboratory, London.

2020 Winner: Léa Juglair, a student from Tencin, France

GEMMOLOGY DIPLOMA

The Christie's Prize for Gemmology

Awarded to the candidate submitting the best papers of the year in the Gemmology Diploma examination.

This prize was established in 1954 as the Rayner Prize, renamed the Diploma Trade Prize in 1991, replaced and sponsored from 2001 by Christie's London.

2020 Winner: Côme Guérin, a student from Fontaine lès Dijon, France

The Read Practical Prize for Gemmology

Awarded to the candidate submitting the best practical papers of the year in the Gemmology Diploma examination.

First awarded in 2009 and named in memory of Peter Read FGA, author and former tutor for Gem-A. In 2020, the prize was sponsored by Richard Drucker FGA (Hons) of Gemworld International.

2020 Winner: Renping Cheng, a student from Beijing, P.R. China

DIAMOND DIPLOMA

The Bruton Medal

Awarded to the overall best candidate of the year in the Diamond Diploma examination.

This silver medal was established in 1996 in honour of Eric Bruton FGA to recognise his work in the field of diamonds.

2020 Winner: Stacie Tayler, a student from Northampton, UK

The Deeks Diamond Prize

Awarded to the candidate submitting the best theory papers of the year in the Diamond Diploma examination.

First awarded in 2001, the prize is sponsored by Noel W. Deeks FGA DGA, a Vice President of the Association who taught the diamond course for many years.

2020 Winner: Ceylan Ismail, a student from Purley, Surrey, UK

The Mok Diamond Practical Prize

Awarded to the best candidate in the Diamond Practical examination.

First awarded in 2009 and sponsored by Dr Dominic Mok FGA DGA, AGIL, Hong Kong.

2020 Winner: Oliver Webb, a student from Holt, Norfolk, UK

> *Gem-A would like to congratulate all of our students who achieved such fantastic results!*

MEMBERSHIP RENEWAL NOTICE

At the end of October 2020, Gem-A started its annual Membership renewal run, and the support of our Membership has never been more important than now. If you haven't already done so, it is still not too late to renew your Membership. Head over to the Gem-A website to securely pay for your annual Membership. We have streamlined our payment options by introducing GoCardless and PayPal subscription services. We also still accept bank transfers, but due to the current pandemic we kindly discourage you from sending cheques, and we are unable to take payments over the phone. If you need assistance with your renewal, Gem-A's Membership Secretary is available via email at membership@gem-a.com.

GEM-A ANNUAL GENERAL MEETING 2020

Gem-A successfully delivered its first online AGM on 16 December 2020 at 17:00 GMT. The meeting was held via GoToWebinar, and more than 50 Members attended online. Voting on the AGM resolutions also took place online, and a total of 280 Members securely submitted their votes through the Civica Election Services voting platform.
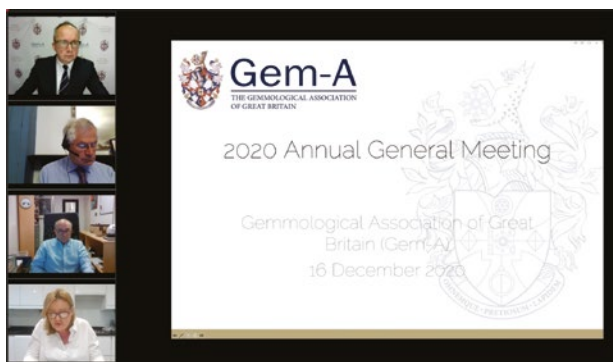
During the AGM, Justine L. Carmody FGA, Philip Sadler FGA DGA and Louise Goldring were reappointed to the Gem-A Board of Trustees. Maggie Campbell Pedersen FGA ABIPP was re-elected Gem-A President. Several Members submitted their questions in advance, and Gem-A's CEO Alan Hart FGA DGA responded to them during the online AGM. For those who missed it, a recording of the AGM is available in the Members area of the Gem-A website (log in and go to https://gem-a.com/agm-2020).

A WEBINAR WITH THE EDITOR

Go behind the scenes at *The Journal of Gemmology* by tuning in to our ongoing webinar series with Editor-in-Chief Brendan Laurs FGA, on 15 April 2021 at 17:00 GMT. Join us as we hear Brendan discuss the current issue of *The Journal* with Gem-A's CEO Alan Hart FGA DGA, explaining how the issue was developed and focusing in greater detail on some of the fascinating feature articles and Gem Notes. To register for the webinar, head to https://linktr.ee/

gemaofgb. Did you miss our previous sessions of Gem-A Live with Brendan? Head to Gem-A's YouTube Channel and watch them now: www.youtube.com/c/GemAOfficialChannel.

OBITUARIES

Dr Walter William (Bill) Hanneman
1934–2020

Bill with the Hanneman/Hodgkinson refractometer (photo by A. Hodgkinson).

The name *Bill Hanneman* has become something of a household word in the field of gemmology, but not from any conventional approach to the field. He saw that the traditional routes of analysing gems were expensive, so he devised gem-testing tools and techniques at a fraction of the cost, while providing fun in the process. In fact, Peter Read described Bill as 'a pioneer in the production of inexpensive gemmological test equipment'.

From his Californian niche as chief analytical chemist for Kaiser Aluminum, Bill was always on the lookout for anything new. At the time he got started in gemmology, there was a rapid growth of gem fairs. Visiting some of these events, he realised that many sellers had little idea of exactly what they were selling. He developed a series of filters that could screen a whole array of gem materials, mainly in bead necklaces, and so was born the 'Hanneman Bead Buyer's & Parcel Picker's Filter Set'. More filters were to follow, including those for ruby, aquamarine, tanzanite and synthetic emerald (the last one developed with this author and named the Hanneman/Hodgkinson Synthetic Emerald Filter).

As new developments in gemmology appeared, they would often induce ideas for new instruments, some born on the lathe in Bill's garage: the Mini-cube, Jeweler's Eye (based on the concept of Sarasota Instruments' Gemeter), Diamond Eye and others. The birth of each was usually accompanied by an article in a gemmological journal. For example, Bill's article titled 'The role of reflectivity in gemmology' (*The Journal* 1978) escorted the Jeweler's Eye, and in 'Magnetic properties of synthetic diamond' (*Gems & Gemology* 1996) he cited the usefulness of his 'Magnetic Wand' for separating synthetic diamond from its natural equivalent.

In 1978, Bill visited the Gem Testing Laboratory in Hatton Garden, where he met and began a friendship with its director, Basil Anderson. It was there that Bill also met the present author and we became lifelong friends. Bill became captivated by 'visual optics' and authored a paper on the subject, 'Educating the eyeball – The Hodgkinson method' (*Lapidary Journal* 1980). Following some criticism of visual optics, Bill responded with 'Understanding the Hodgkinson method' (*The Journal* 1982).

Of particular interest to the gemmologist was the development of the Hanneman/Hodgkinson refractometer (see photo), which required no contact liquid. A bonus was that for the first time the dispersion of a gemstone could be measured. A further benefit was that the B/D ratio could be derived—birefringence divided by dispersion. The B/D ratio represented a completely new optical index that a gemmologist could use without any instruments whatsoever—provided the moon was out or a penlight was handy. The penlight yielded another of Bill's pocket aids: a simple plastic cap with a slit to provide an ideal light source for visual optics.

Bill's published works are far too numerous to be given here in their entirety, but following are some of his articles:

- L_H—A new gemological property (*Gems & Gemology* 1977)
- A practical approach to the characterization of simulated diamonds (*Lapidary Journal* 1977)
- Gemological instruments—Which should I buy? (*Lapidary Journal* 1978)
- The role of reflectivity in gemmology (*The Journal* 1978)
- The first tool of gemmology won't cost you a penny (*Australian Gemmologist* 1978)
- Water as a gemological tool (*Lapidary Journal* 1978)
- Refractive index determination by the method of B. W. Anderson (*Lapidary Journal* 1979)
- A new classification for red-to-violet garnets (*Gems & Gemology* 1983)

- Art of gemology (a three-part series in *Lapidary Journal* starting in September 1991)
- Sodium polytungstate as a gemmological tool (*The Journal* 1991)
- Determination of dispersion using a refractometer (*The Journal* 1992)
- More on misnomers in gemology (*Gems & Gemology* 1992)
- A unified system for classifying garnets (*The Journal* 1997)
- The Hodgkinson method, a.k.a. the eye and prism method: Clarifying the records (*Australian Gemmologist* 1998)
- L_H—An 'old' gemmological property (*Australian Gemmologist* 1999)
- The Hanneman refractometer (*The Journal* 2000)
- Dispersion, birefringence, and the critical angle refractometer (*Australian Gemmologist* 2001)
- The magnetic index (*Australian Gemmologist* 2002)

Bill was in his element if he could find someone or something gemmological to argue with or about. However, his letters to gemmological journals often contained significant contributions to the gemmological literature. A good example was the subject of garnet classification (*The Journal* 1997), followed by his booklet *A Unified System for Classifying Garnets*. It included pull-out pages which could be folded and taped to form a three-dimensional model he christened 'the Rosetta Stone of garnets'. Bill also authored several books, including *Guide to Affordable Gemology, Naming Gem Garnets* and *Determinative Gemology*. Then there was *What Trout Actually See* to mark angling as another lifelong interest.

As his name continued to gain prominence in the literature, Bill was invited to give talks and demonstrations at numerous events, from local lapidary club meetings to the Tucson gem shows and further afield. Bill delivered a new, laid-back style for disseminating gemmological information (often with tongue in cheek). In 2018, Bill was awarded the Antonio C. Bonanno award for his contributions to gemmological education and tools.

For all his scientific bent, Bill was also a stickler for the English language and the use of English in written or spoken form. This led to his establishment of the Hanneman Trophy, awarded for important contributions to the gemmological literature. Early recipients were Basil Anderson's *Gem Testing* and Richard Liddicoat's *Handbook of Gem Identification*.

All of the above was undertaken by Bill for the sheer satisfaction of promoting gemmology with little thought of reward. Just as the Rosetta Stone has lasted 5,000 years, so Hanneman's gemmological legacy will live on after his passing at the age of 93. For how long, we shall have to wait and see!

Alan Hodgkinson FGA DGA
Ayrshire, Scotland

Syed Iftikhar Hussain
1952–2020

Syed Iftikhar Hussain, a Pakistani gem and mineral specimen trader, and a prospector of the Hindu Kush and Karakorum mountains, passed away on 25th November 2020 due to COVID-19.

Born in 1952 in Pakistan's then Federally Administered Tribal Areas, Iftikhar trained as a geologist at the University of Balochistan (Quetta, Pakistan) and studied gemmology at Bangkok's Asian Institute of Gemological Sciences under the tutelage of Richard W. Hughes in the 1980s. He went on to join the Gemstone Corporation of Pakistan, a state-sponsored agency mandated to explore and market the gem wealth of Pakistan's mountains. It was then that he discovered the potential of Pakistan's gem industry, made key contacts and acquired his love of emeralds.

After leaving the Gemstone Corporation of Pakistan in the late 1980s, Iftikhar's work as a gem dealer rose to prominence in the cauldron of intrigue that was Afghanistan in the mid-to-late 1990s. In the absence of international backers, Afghanistan's tenacious Northern Alliance militia coalition was largely funded by its sales of Panjshir
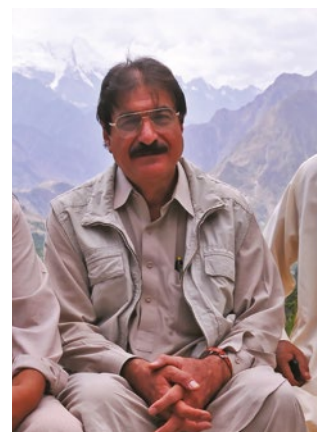
Iftikhar in Pakistan's mountains (photo by Vincent Pardieu, © GIA).

emeralds, with Iftikhar becoming a key player in the movement of the stones to markets in Idar-Oberstein and Bangkok. This work cemented his reputation in the field, and he became instrumental in bringing more of the region's valuable gems and minerals to international markets. With his keen ability to trace emerging gem deposits, Iftikhar became an important international supplier of Iranian demantoid, spinel from the Pamir Mountains in Tajikistan, tourmaline from Nuristan in Afghanistan, sphene from the Karakoram Mountains in Pakistan, and emerald from Pakistan's Swat Valley, as well as numerous other gem and mineral rarities.

Iftikhar enjoyed sharing his knowledge of the region's stones with global gemmologists and dealers during the annual Tucson gem shows, where from his showroom he would provide gifts of numerous samples to dealers and institutions (including Gem-A) for research and enjoyment. Iftikhar's work and knowledge was mentioned in *Gems & Gemology* and *The Journal of Gemmology* nearly a dozen times, and he invited and guided numerous international dealers and gemmologists through Pakistan's gem markets and mountainous gem deposits.

A proud aficionado of his country's mountains, culture, people and food, Iftikhar would frequently share with his international friends such regional bounty as Hunza Valley apricots and Balochistan pomegranates. He was always hospitable, kind and loyal, with never a bad word to say about anyone, and his friends perceived him as an old-fashioned gentleman. Ultimately, his character was underpinned by being the very embodiment of Pashtunwali, the code of life and character-trait aspirations for Pashtun people.

Survived by his wife and three children, Iftikhar was a diplomatic, charming and sometimes shy man, and the gem industry has lost one of its most interesting and original characters.

Simon Bruce-Lockhart FGA DGA
Chanthaburi, Thailand

Evelyne Stern FGA
1924–2021

Evelyne in Dresden, Germany (photo by Marion Stern).

Evelyne Stern, beloved daughter, wife, mother and friend, passed away on 3 January 2021 at the age of 96. Evelyne was a well-known Fellow of Gem-A, an international personality in diamond and gem circles, and possessed a boundless knowledge of almost everything connected to the trade, which she was more than happy to share with anyone. She supported the Gemmological Association of Great Britain for many decades in varying capacities, including serving on the Board of Trustees, being an Associate Editor of *The Journal of Gemmology* and acting as an examiner for the Diamond Diploma, until she was diagnosed with cancer in spring 2019.

Evelyne's life was shaped by her incredible energy, her insatiable appetite for life and her infectious sense of humour, always seeing the happiest side of things. Her life was so unassuming, considering her many achievements.

She was born Evelyne Steindorff in Berlin in 1924. When Hitler came to power in 1933 she was sent to Karlsbad to stay with her mother's brother and was subsequently joined there by her parents, Rosl and Jerome. They lived in Karlsbad until Hitler annexed the Sudetenland in 1938. The family escaped, along with many other Jews from the region, to Prague. After the Nazi invasion of Czechoslovakia and occupation of Prague, it was clear that it was time to flee again. Evelyne's parents managed to secure a space for her on a Kindertransport organised by the Scottish church. After a long, tumultuous journey, she arrived at a children's home in Selkirk. Evelyne's parents managed, through a combination of good luck and fate, to secure exit visas so that they too were able to escape to England. Initially, her mother found a position as a live-in housekeeper in Worthing, and her father found accommodation nearby while Evelyne went to a boarding school.

The family was eventually reunited, and her father found employment in London so the family moved to Belsize Park. Evelyne started her professional career with a job in a chemical laboratory near Angel. The director suggested that she would be better employed doing chemical translations for him at the Patent Office, so she moved to that role. After two years at the Patent Office, in 1944 she was recruited by the Diamond Trading Company of De Beers (at a salary of £4 per week). She worked in the Diamond Research department, where she met her husband-to-be Werner. They married in 1947 and a year later their daughter, Marion (this author), was born.

When, after the war, the Diamond Trading Company decided to supply the German diamond manufacturing industry, De Beers approached Werner to become a broker looking after German clients, and Evelyne joined him in the brokerage firm. In addition, they worked with industrial diamonds, leveraging their research work and forming a close business and personal relationship with Diamant Gesellschaft Tesch in Ludwigsburg.

Werner introduced Evelyne to gemstones, and her fascination with gems developed over her many trips to Idar-Oberstein. She became a frequent visitor to the Gemmological Association of Great Britain in London. She studied for her Gemmology Diploma under Keith Mitchell and received one of the first Diamond Diplomas that Eric Bruton taught. She was an enthusiastic participant at Alan Jobbins' post-Gemmology Diploma classes and their later incarnations, and she greatly enjoyed the meetings of the Society of Jewellery Historians.

Werner worked as a De Beers broker until his death in 1971, and then Evelyne took over his role. After the brokerage business dwindled she continued working with industrial diamonds and pursuing her interests in gemmology.

Despite the many forced relocations of her childhood and youth, Evelyne had a great love for travel. With her daughter Marion she was an adventurous and intrepid traveller to South America, Asia, the Middle East and Europe. Latterly, her travels focused on places she loved, such as the Maldives, Italy, Turkey and, of course, Ireland, to which Evelyne and Marion went every year for the last 13 years accompanied by Maxie, Marion's lurcher dog. She enjoyed visiting Berlin and was delighted to celebrate her 91st birthday while staying at the Hotel Adlon. She kept fit by regularly practicing Tai Chi, which also provided an important social component for her.

Evelyne always seemed younger than she was, as if she would be around forever. A dear friend of Evelyne, Rosemary Ross, has a lovely mug given to her by Evelyne, with three horses looking over a stone wall, with *Nag, Nag, Nag* inscribed inside, which always brings a smile to her face while enjoying her morning tea.

Despite the health challenges that cancer presented, Evelyne remained astute right until the end, totally clear about what she desired and how she wanted things to be done. It was important for her to return to her beloved bungalow with its large, beautiful garden for her last few months, and she was granted her wish to die in her own home.

We will miss her sense of humour, her happy disposition, and her willingness to talk to so many old and new friends. A wonderful lady, she will be sorely missed.

Marion Stern FGA DGA
Hampstead, London

Learning Opportunities

CONFERENCES AND SEMINARS

10th National Opal Symposium
31 March–1 April 2021 (to be confirmed)
Coober Pedy, Australia
www.opalsymposium.org

**17th Annual Sinkankas Symposium –
Agate & Chalcedony**
24 April–8 May 2021
Online (pre-recorded presentations
available on demand)
https://sinkankassymposium.net

Swiss Gemmological Society Conference
30 May–1 June 2021
St Gallen, Switzerland
https://gemmologie.ch/en/current

**14th International Conference on New Diamond
and Nano Carbons (NDNC)**
7–9 June 2021
Online
www.ndnc2020.org

Diamonds – Source to Use 2021
9–11 June 2021
Johannesburg, South Africa (hybrid online)
www.saimm.co.za/saimm-events/upcoming-events/
diamonds-source-to-use-2020

Jewellery in Texts: Texts in Jewellery
19 June 2021
London
www.societyofjewelleryhistorians.ac.uk/news

Sainte-Marie-aux-Mines Mineral & Gem Show
24–27 June 2021
Sainte-Marie-aux-Mines, France
www.sainte-marie-mineral.com
Note: Includes a seminar programme

**Association for the Study of Jewelry and
Related Arts Conference**
26–27 June 2021
Online
www.jewelryconference.com

6th Mediterranean Gem and Jewellery Conference
9–11 July 2021
Thessaloniki, Greece
www.gemconference.com
Note: Includes workshops and mine tours

MJSA Expo
8–10 August 2021
New York, New York, USA
https://mjsa.org/eventsprograms/mjsa_expo
Note: Includes a seminar programme

NAJA 56th Ace© It Mid-Year Conference
14–17 August 2021
Location TBA
www.najaappraisers.com/html/conferences.html

**9th International Conference Mineralogy
and Museums**
24–26 August 2021
Sofia, Bulgaria
www.bgminsoc.bg
Note: Gem minerals and archaeogemmology are
among the topics that will be covered.

JCK Las Vegas
27–30 August 2021
Las Vegas, Nevada, USA
https://lasvegas.jckonline.com
Note: Includes a seminar programme

3rd European Mineralogical Conference (emc2020)
29 August–2 September 2021

Krakow, Poland (or online)
https://emc2020.ptmin.eu
Sessions of interest: The Geology of Gem Deposits:
A Session in Honour of Gaston Giuliani; Materials
Sciences and Archaeometry for Cultural Heritage

**31st International Conference on Diamond
and Carbon Materials**
6–9 September 2021
Online
www.elsevier.com/events/conferences/international-
conference-on-diamond-and-carbon-materials

**3rd International Conference on Tourmaline
(TUR2021)**
9–11 September 2021
Elba Island, Italy
www.tur2021.com

JVA Registered Valuer Conference 2021
10–12 September 2021
Loughborough
https://thejva.org/jewellery-watch-valuer-conference

NAJ Summit
11–13 September 2021
Northampton, East Midlands
www.naj.co.uk/summit

American Gem Society Conclave
12–14 September 2021
Dallas, Texas, USA
www.conclave2021.americangemsociety.org

HardRock Summit 2021
16–19 September 2021
Denver, Colorado, USA
https://hardrocksummit.com
Note: Includes a seminar programme

Jewellery & Gem WORLD Hong Kong
17–23 September 2021
Hong Kong
https://exhibitions.jewellerynet.com/9jg
Note: Includes a seminar programme

13th Annual Portland Jewelry Symposium
September 2021 (exact dates TBA)
Portland, Oregon, USA
https://portlandjewelrysymposium.com

Canadian Gemmological Association Conference
22–24 October 2021

Vancouver, British Columbia, Canada
https://canadiangemmological.com

The Munich Show
22–24 October 2021
Munich, Germany
https://munichshow.de/?lang = en
Note: Includes a seminar programme

**GAC-MAC London 2021 Joint
Annual Meeting**
1–3 November 2021
London, Ontario, Canada
https://gacmac2021.ca
Session of interest: Diamonds in Cratons,
Diamond-bearing Rocks and Mantle Xenoliths

**2021 International Gems & Jewelry
Academic Conference**
Mid-November 2021 (exact dates TBA)
Beijing, China
Email: ngtcyjb@ngtc.com.cn

**NAJA 57th Ace© It Annual
Winter Conference**
30–31 January 2022
Tucson, Arizona, USA
www.najaappraisers.com/html/conferences.html

AGTA Gemfair Tucson
1–6 February 2022
Tucson, Arizona, USA
https://agta.org/agta-gem-fair-tucson
Note: Includes a seminar programme

Tucson Gem and Mineral Show
10–13 February 2022
Tucson, Arizona, USA
www.tgms.org/show
Note: Includes a seminar programme

Inhorgenta Munich
11–14 February 2022
Munich, Germany
www.inhorgenta.com/en
Note: Includes a seminar programme

12th International Kimberlite Conference
15–19 August 2022
Yellowknife, Northwest Territories, Canada
https://12ikc.ca

OTHER EDUCATIONAL OPPORTUNITIES

Gem-A Workshops and Courses
Gem-A, London
https://gem-a.com/education

Gemstone Safari to Tanzania
7–24 July 2021 and 12–29 January 2022
www.free-form.ch/tanzania/gemstonesafari.html

Lectures with Gem-A's Midlands Branch
Fellows Auctioneers, Augusta House, Birmingham
Email Louise Ludlam-Snook at
gemamidlands@gmail.com

- Charles Evans—Minberly Mines & Diamonds
  26 March 2021 (online)

- Peter Buckie—The Treasures Seen by an
  Expert Valuer
  30 April 2021 (online)

Lectures with The Society of Jewellery Historians
Society of Antiquaries of London, Burlington House
www.societyofjewelleryhistorians.ac.uk/current_lectures

- Carol Michaelson—Chinese Jade Jewellery and
  Ornaments from the Neolithic to the Present
  27 April 2021

- Gonçalo de Vasconclo e Sousa—
  Portuguese Jewellery
  25 May 2021

- Karl Schmetzer—The Late 14th-Century
  Royal Crown of Blanche of Lancaster
  22 June 2021

- Charlotte Gere—Colour in Victorian Jewellery
  28 September 2021

- Three Speakers TBA—New Research
  on Jewellery
  26 October 2021

- Ute Decker—Sculptural Minimalism
  & Fairtrade Gold – Philosophy, Provenance
  and Process
  23 November 2021

New Media
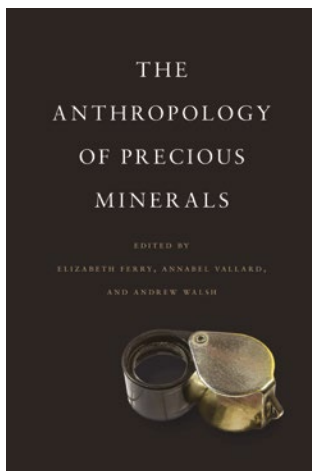
The Anthropology of Precious Minerals

Ed. by Elizabeth Ferry, Annabel Vallard and Andrew Walsh, 2020. University of Toronto Press, Toronto, Ontario, Canada, https://utorontopress.com/us/the-anthropology-of-precious-minerals-3, 216 pages, illus., ISBN 978-1487503178 (hardcover) or ISBN 978-1487517342 (eBook). USD57.00 hardcover or eBook.

I have always loved gemstones that exhibit asterism, and star sapphires and rubies are my favourites. Traders know this and keep them aside for me, but I keenly remember being chastised by a dealer in Bangkok's Jewelry Trade Center: 'We Thais love these stones not just because they are beautiful, but because they give us the power to see things more sharply, better and differently. They give us an animal eye.' I took this to mean, as we say, 'an eagle eye' or *oeil de linx* (French for *lynx's eye*). I wondered if the gem term *cat's-eye* links to this belief in the supernatural power of gems.

I thought of this when I read *The Anthropology of Precious Minerals*, because this edited collection of essays challenges us to rethink the way humans interact with things non-human—in this case minerals—and to look at the familiar as if it were unfamiliar, precious and strange. The authors and editors are anthropologists whose life's work is to study humanity—its institutions, beliefs, and social and cultural forms, and semiotics (the study of signs and meanings of words and other things).

To the gemmologist and the metallurgist, the book offers a loupe to examine different attributes of precious materials, their stories and meanings—looking beyond physical properties to what makes a stone or metal valuable. The editors argue that minerals '…are especially good [for thinking] about how value becomes solidified in the material world'. The various authors investigate the ways in which value is contextually determined across the 'biography' of the mineral and the world views of those who handle it, none of which is apparent from a superficial inspection. They draw upon a sophisticated and eclectic mix of philosophy, literature, history and anthropology to examine minerals through time, suggesting a stone is not simply inert inorganic matter, but has a vitality that can be analysed to better understand not only the origin of the earth, but also more metaphorical quests, such as the search for life's meaning and enhancement.

Minerals draw the human eye through 'shine, iridescence and brilliance', and these factors often contribute to the estimation of their preciousness. However, it is the extraction, exchange and valuation of minerals that provides complex opportunities for storytelling and meaning making. An example is the connection that gems, precious metals and jewellery have with marital and sexual exchanges across time and history, embodied in engagement and wedding rings. The valuation of preciousness is not limited to physical characteristics, rareness and value on the market, but also involves, in the words of Richard Hughes, the valuer's 'educated attention and emotion'.

The first part of the book, 'Engaging Mineral Sources', focuses on the artisanal extraction of minerals through three very different studies: the scrapping of mobile phones in North America to obtain gold and other precious metals (by Joshua Bell), the sapphire trade in Madagascar (by Andrew Walsh) and the hunters of Alpine crystals (by Gilles Raveneau). These studies illustrate the ways in which interactions with precious minerals shape the lives of artisanal miners.

Bell analyses a scrapper's YouTube channel where personal accounts show the real and potential value of the minerals found in e-waste and the employment opportunities such scavenging provides, particularly when the price of gold is high. The disassembling and scrapping of mobile phones also reveals the complex supply chain of the minerals used to create them. It tells the story of the relationship between minerals and those whose lives are engaged with and touch them at every point in the value chain.

Walsh's chapter on the mining of sapphires in

Madagascar draws upon his extensive research in the field and challenges the reader to go beyond the usual image of artisanal and small-scale mining as 'crude and backward'. He argues that a consideration of the vocation, skill and dedication implicit in the word 'artisan' (as in artisanal mining) provides a reframing of the miner's work and a contribution beyond the realm of straightforward human-mineral engagements. In this way, he argues, miners' paths both above ground and underground mark our current geological era, the Anthropocene, and reveal processes of 'being and becoming' human, which are unique to this age.

The central idea of Raveneau's chapter, 'The Value and Social Lives of Alpine Crystals', is that crystals, like people, have biographical trajectories and that these intertwine in the stories of crystal 'hunters' in the Alps. Pursuing collectible Alpine minerals is risky and competitive, but the rewards of discovering a new crystal 'virgin oven' are great, both commercially and symbolically. Such treasures are inextricably linked to the hunters' economic and social value, and even their lives. This is the case with 'Laurent', a red fluorite and smoky quartz crystal specimen discovered on Mt Blanc: 'six centimetre octahedrons of an intense red fluorite arranged like a lava flow on the tip of a twenty centimetre smoky quartz'. The piece is named for the hunter's climbing partner, who died in the Alps the year before its discovery.

The second part of the book, titled 'Mineral Connections', focuses on what makes particular minerals—diamond, emerald, jade, corundum, gold and very few others—precious. It contains three essays, careful ethnographies that map the patterns and variations of preciousness that come 'into being through the social actions in which they engage or are engaged'. The stories are of gems and goldwork in Thailand (by Annabel Vallard), the challenges of diamond valuation (by Filipe Calvão), and a final piece on gold and its value and power across history (by Les W. Field).

The chapter on Thailand, a detailed and well-researched piece, unveils the ritual and power enshrined in the Emerald Buddha (actually green jasper), which give it a spiritual value independent of the quality of the mineral it is crafted from. The exquisite detail seen in the gem-studded gold 'garments' that adorn the Buddha is testament to Thai lapidary and jewellery-making skills, as well as to the handing down of such skills across generations of Thai craftspeople. But Vallard refocuses our attention beyond this to consider the intimate relationship between the stones and the cutter, an intimacy which permits the emergence of balance, symmetry and play-of-light in a gem that might have been 'invisible or unperceived at first'. In this intimacy, it is as if the mineral has taken on a life of its own.

The chapter on diamonds tackles the complex topic of their valuation, and the roles of place of origin and traceability. Diamonds, the author argues, especially internally flawless stones of unverifiable origins, are hard to value. Calvão contrasts the sales milieu of elite auctioneers, such as those at Sotheby's in Geneva with the work of Angolan traders and diamond miners who wear dirt under their fingernails as a sign of the authenticity of their stones. In both places, trading in diamonds involves performative exchanges of words, and Calvão argues that the stone's origin in both contexts is significant in determining the value.

The final chapter takes a philosophical orientation to the way gold has been viewed by society across the centuries. Field first presents the dominant Western view of gold as money or as a symbol of wealth and prestige, which does not tarnish or decay. He notes, however, that the image of gold is tainted by the damage done to the environment through the use of mercury in its extraction at some sites, a process thousands of years old. Gold is unique and timeless in the sense that 'all the gold that has ever been mined...is still bouncing around today'. The view of gold held by pre-Columbian Amerindians, by contrast with the dominant Western view, could not be starker. Sixteenth-century raiders from Spain, full of lust for gold, neither cared about nor understood the Amerindian worldview, where raw gold sold for the same price as salt and yet, when worked and shaped, became a priceless powerful symbol of the sun and all its potency.

The Anthropology of Precious Minerals is not an easy read; it is a sophisticated and carefully built collection. It is deeply grounded in the language and theory of knowledge and anthropology, which are not always readily accessible to the layperson. Yet with diligence and attention, reading these chapters brings its own rewards, with fabulous stories from across space and time that illuminate the fascinating world of precious minerals and how they can create social, political and spiritual meaning. We are left enriched by these scholars' views of how the value of precious minerals is constructed, and the symbiotic relationship between the mineral and its admirer. There are layers of meaning to be uncovered. All is not what we see and can put a monetary value to, as is attested by my encounter with a Thai trader of star sapphire and ruby.

Dr Lynda Lawson
Sustainable Minerals Institute
The University of Queensland, Australia
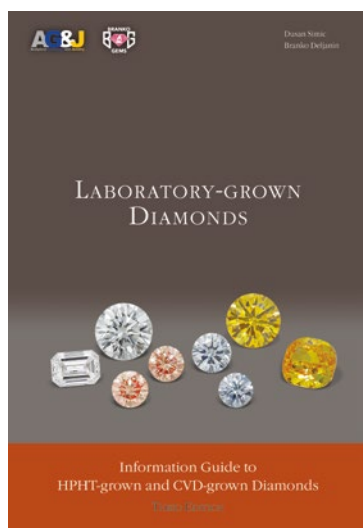
Laboratory-grown Diamonds: Information Guide to HPHT-grown and CVD-grown Diamonds, 3rd edn.

By Dusan Simic and Branko Deljanin, 2020. Gemmological Research Industries Inc., Vancouver, British Columbia, Canada, www.brankogems.com/shop/books/laboratory-grown-diamonds-information-guide-to-hpht-and-cvd-grown-diamonds, 188 pages, illus., ISBN 978-177369200. USD39.95 (or USD49.95 including shipping to USA or Canada) softcover.

This is the third edition of a book on the synthesis and identification of synthetic diamonds by Dusan Simic and Branko Deljanin, two leading experts in gem diamond identification. The first edition, titled *Laboratory-created Diamonds* (2004), was written by Sharrie Woodring and Branko Deljanin, and it was followed by the second edition in 2007 (by the current authors). The third edition is presented in four main parts with added contributions from innovators in their respective fields, and consists of content from the 2007 edition together with 2020 updates—all of which are clearly labelled with colour-coded headings.

The first part of the book gives a historical background and review of the two methods used to produce laboratory-grown diamonds, namely, high-pressure, high-temperature (HPHT) synthesis and chemical vapour deposition (CVD). The authors set the scene well by reviewing the development of HPHT and CVD techniques by pioneers such as Dr Tracy Hall and Dr William G. Eversole, respectively. This is followed by a useful overview on diamond 'types' (I and II) and the treatments—irradiation and annealing—required to induce a permanent colour change in diamond.

The book's second part explores existing methods to produce synthetic diamonds in more detail, with review articles from Dr Boris Feigelson and Malay Hirani being major highlights. Their explanations of the various technologies are thorough, well articulated and will be particularly appreciated by those who have some technical, scientific or engineering background.

A review of the carbon phase diagram and the key parameters required to turn graphite into diamond (mind-boggling pressures of around 50,000 atmospheres and temperatures of >1000°C) attest to the engineering challenges faced. The different forms of HPHT growth are then explained, including molten metal-film and temperature-gradient types, as well as the available presses, such as belt, split anvil, toroid and cubic.

Hirani then brings a pragmatic approach to CVD synthesis and describes in detail the various types of CVD chambers developed over the years, from hot-filament to state-of-the-art microwave-plasma CVD reactors, and the challenges of producing synthetic diamond at low pressures. He explains the various pros and cons of the microwaves used and the technology available for producing them. He even goes one step further for those interested in setting up a synthetic diamond production facility by taking us through the logistics and costs involved.

This part ends with a useful list of the current major producers of synthetic diamonds and includes the present state of the industry in China (extracted from a contribution by Dr Taijin Lu to be published in an upcoming book by co-author Branko Deljanin). The might of China's industrial and gem-quality synthetic diamond production is astounding and puts the reader in good stead for the third and largest section of the book.

First, however, the authors provide a brief section on the slightly off-beat topic of 'memorial diamonds'. This is the business of growing synthetic diamonds from the carboniferous remains (<2%) of cremated relatives and/ or their hair. The article is authored by Frank Ripka, CEO of Algordanza (Switzerland), a leader in the production of 'memorial diamonds', and it addresses (convincingly) the technical feasibility of such an enterprise while also delving into the emotional implications.

The book's third part covers identification of synthetic diamond. The authors discuss the unique features that can be observed in both HPHT- and CVD-grown synthetics, and the types of equipment that can be used, ranging from standard gemmological instruments to the more advanced methods present in a well-equipped gemmological laboratory. Some of the characteristics of natural and synthetic diamonds discussed are photoluminescence,

fluorescence, inclusions (including a section by Sharrie Woodring, who co-authored the first edition of the book), anomalous birefringence and growth patterns. Images, spectra and diagrams provide good examples of what typically can be observed, as well as a useful overview and point of reference.

The following section on the detection of melee-size synthetic diamonds (<0.1 ct) in yellow, blue and pink colours is particularly useful, given the challenges of screening such small stones and the reported risk of encountering undisclosed synthetic melee in parcels or jewellery in recent years.

The identification section concludes with a useful set of observations that, using standard equipment, a gemmologist can employ to determine whether a diamond is natural or synthetic, or should be submitted for further analysis by a gem laboratory using advanced equipment.

The last part of the book is an overview of the grading and nomenclature used for synthetic diamonds, as developed by the authors. They make it clear that much more must be done to protect consumers and jewellers from fraudulent purveyors of synthetic diamonds. To this end, Dusan Simic outlines his patent for tracking synthetic diamonds by labelling them with an intrinsic pink fluorescence marker (by doping with NV centres via post-growth treatment) that can be excited with a standard gemmological UV lamp. This sounds ideal, but the industry is far from adopting a single overarching system, with many synthetic producers currently using their own methods for marking their products. Loose and mounted gemstones in melee sizes usually require close scrutiny, not just to identify synthetics but also to detect the (albeit lesser) presence of diamond simulants. In any case, it is unlikely that the plethora of screening instruments and training in the identification of synthetics will fall by the wayside any time soon.

Overall, the book is well written, has many useful illustrations and is quite readable. It feels more like a handbook than a textbook or compilation of scientific articles, and therefore has appeal to a layperson as well as a technical audience. Perhaps the book is a little repetitive at times, with some overlap across chapters, although this might be seen as a helpful recap. Overall the text has a reasonable flow and the book can be read cover-to-cover in just a few days. In short, this is an extremely useful reference guide for anyone working in the gem diamond industry or having a specific interest in the growth and identification of diamond.

Dr Peter M. P. Lanigan and Dr Colin D. McGuinness
De Beers Ignite
Maidenhead, Berkshire

Other Book Titles

GENERAL REFERENCE

Edelsteine: Bestimmung, Eigenschaften und Behandlung [Gemstones: Determination, Properties and Treatment]
Tobias Häger and Ursula Wehrmeister, 2020. Springer Spektrum, Germany, 238 pages, ISBN 978-3662613047 or e-ISBN 978-3662613054 (in German). EUR36.93 hardcover or EUR29.99 eBook.

JEWELLERY HISTORY

The Althorp Leopard: The Celebrated Life of a Renaissance Cameo
By Sandra Hindman, 2020. Les Enluminures, Paris, France, 88 pages, ISBN 978-2956702436. USD18.00 softcover.

Art & Court of James VI & I: Bright Star of the North
By Kate Anderson, Jemma Field, Catriona Murray, Anna Groundwater and Karen Hearn, 2021. National Galleries of Scotland, Edinburgh, 160 pages, ISBN 978-1911054412. GBP29.95 hardcover.

The Art of Medieval Jewelry: An Illustrated History
By T. N. Pollio, 2021. McFarland & Co., Jefferson, North Carolina, USA, 91 pages, ISBN 978-1476681757 or e-ISBN 978-1476640471. USD55.00 hardcover.

JEWELLERY AND *OBJETS D'ART*

At the Bench Vol. 2: Tips, Techniques, and Step-by-Step Projects for Jewelers of All Skill Levels
Ed. by Joel McFadden, 2020. MJSA Press, Attleborough, Massachusetts, USA, 150 pages, ISBN 978-0979996245. USD34.95 softcover.

BBeyond Jewellery: Spectacular and Collectible Pieces
Ed. by Caroline Brand, 2021. Beyond Black, London, 161 pages, ISBN 978-1905904785 (print) or ASIN B08MXY3X58 (Kindle edn). GBP200.00 loose-leaf,

GBP9.99 Kindle edn or free digital edition at http://beyondblack.org/b-beyond-jewellery.

Berber Memories: Women and Jewelry in Morocco
By Michel Drauget, 2020. Yale University Press, New Haven, Connecticut, USA, 600 pages, ISBN 978-0300253955. USD90.00 hardcover.

Beyond Fabergé: Imperial Russian Jewelry
By Marie Betteley and David Schimmelpennick van der Oye, 2020. Schiffer Publishing, Atglen, Pennsylvania, USA, 384 pages, ISBN 978-0764360435. USD75.00 hardcover.

In Flux: American Jewelry and the Counterculture
By Susan Cummins, Damian Skinner and Cindi Strauss, 2020. Arnoldsche Art Publishers, Stuttgart, Germany, 184 pages, ISBN 978-3897905979. EUR28.00 softcover.

Jewelry Stories: Highlights from the Collection 1947–2019
Ed. by Barbara Paris Gifford, 2021. Arnoldsche Art Publishers, Stuttgart, Germany, 160 pages, ISBN 978-3897906020. USD65.00 hardcover.

Jewels of the Nile: Ancient Egyptian Treasures from the Worcester Art Museum
By Yvonne Markowitz and Peter Locavera, 2021. D. Giles Ltd, London, 96 pages, ISBN 978-1911282792. GBP39.95 hardcover.

Jewels that Made History: 101 Stones, Myths, and Legends
By Stellene Volandes, 2020. Rizzoli, New York, New York, USA, 224 pages, ISBN 978-0847868544. USD45.00 hardcover.

Karl Fritsch: Ruby Gold
By Galerie Zink, 2020. Arnoldsche Art Publishers, Stuttgart, Germany, 168 pages, ISBN 978-3897906143. EUR28.00 hardcover.

Once Upon a Diamond: A Family Tradition of Royal Jewels
By Lavinia Branca Snyder and Prince Dimitri, 2020. Rizzoli, New York, New York, USA, 288 pages, ISBN 978-0847866915. USD85.00 hardcover.

Ornament in Transition: Silke Trekel Jewellery 1995–2020
By Ellen Maurer Zilioli and Monika Fahn, 2021. Arnoldsche Art Publishers, Stuttgart, Germany, 112 pages, ISBN 978-3897906136 (in German and English). USD50.00 softcover.

Quiet Elegance: The Jewelry of Eleanor Moty
By Helen W. Drutt English, Matthew Drutt and Bruce Pepich, 2020. Arnoldsche Art Publishers, Stuttgart, Germany, 176 pages, ISBN 978-3897906082. EUR38.00 hardcover.

Reinhold Ziegler: Transgression
By Heike Endter and Reinhold Ziegler, 2020. Arnoldsche Art Publishers, Stuttgart, Germany, 72 pages, ISBN 978-3897906044. EUR28.00 hardcover.

Simply Brilliant: Artist-Jewelers of the 1960s and 1970s
By Adam MacPhàrlain, Amanda Triossi, Cynthia Amnéus, Rosemary Ransome Wallis and Ruth Peltason, 2020. D. Giles Ltd, London, 256 pages, ISBN 978-1911282525. GBP40.00 hardcover.

Stone Setting
By Scott McIntyre, 2020. The Crowood Press, Marlborough, Wiltshire, 96 pages, ISBN 978-1785006913. GBP12.99 softcover.

[Sur]Naturel Cartier: Haute Joaillerie et Objets Précieux ([Sur]Naturel Cartier: High Jewelry and Precious Objects)
By François Chaille and Hélène Kelmachter, 2020. Flammarion, Paris, France, 256 pages, ISBN 978-2081521360 (French) or 978-2080204820 (English). EUR95.00 hardcover.

Thinking Jewelry 2
By Wilhelm Lindemann and Theo Smeets, 2020. Arnoldsche Art Publishers, Stuttgart, Germany, 184 pages, ISBN 978-3897905399. EUR15.00 softcover.

MISCELLANEOUS

Enchantment: Ashes, Diamonds and the Transformation of Funeral Culture
By Thorsten Benkel, Thomas Klie, Matthias Meitzler, 2020. Vandenhoeck & Ruprecht, Göttingen, Germany, 239 pages, ISBN 978-3525670217. EUR30.00 softcover.

PEARLS

In the Search of the Lost Pearl: Rediscovery of Southern Populations of *Margaritifera margaritifera* (L.) in Russia as a Model of Conservation Research
By Igor Popov (transl. by N. Lentsman), 2021. Springer Nature, Switzerland, 246 pages, ISBN 978-3030662547 or e-ISBN 978-3030662554, https://doi.org/10.1007/978-3-030-66255-4. EUR145.59 hardcover or EUR117.69 eBook.

Literature of Interest

COLOURED STONES

Characterization of the fluorescent hyalite of San Luis Potosí, Mexico. F. Butini, G.L. Cattaneo, N. Precisvalle, A. Sodo and F. Zorzi, *Rivista Italiana di Gemmologia/Italian Gemological Review*, No. 47, 2020, 65–74.

10

Deep Purple – Vesuvianit (Idokras) aus Pakistan [Deep purple – Vesuvianite (idocrase) from Pakistan]. H.A. Hänni, L. Franz and H. Wang, *Gemmologie: Zeitschrift der Deutschen Gemmologischen Gesellschaft*, **69**(1/2), 2020, 59–64 (in German with English abstract).

Electron microprobe study of turquoise-group solid solutions in the Neyshabour and Meydook mines, northeast and southern Iran. E.M. Gandomani, N. Rashidnejad-Omran, A. Emamjomeh, P. Vignola and T. Hashemzadeh, *Canadian Mineralogist*, **58**(1), 2020, 71–83, https://doi.org/10.3749/canmin.1900004.

FTIR investigation of garnet: Indication for specific species and coloration: A case study of a yellow garnet. J. Wang, Y. Wang, D. Zhang, Z. Liu, C. Wang, K. Yin, X. Gao and Y. Xu, *Journal of Gems & Gemmology*, **22**(1), 2020, 20–25 (in Chinese with English abstract).

Gemmological analysis on a meionite. R. Liao and J. Guo, *Journal of Gems & Gemmology*, **22**(2), 2020, 20–28 (in Chinese with English abstract).

Gemmological characteristic of colour-changed [*sic*] sapphire from Tanzania. C. Chen, T. Shao, W. Huang, C. Shen, Z. Li and A.H. Shen, *Journal of Gems & Gemmology*, **22**(3), 2020, 19–25 (in Chinese with English abstract).

Gemmological characteristic of green kyanite. S. Tian, C. Chen, W. Huang, Z. Li and A.H. Shen, *Journal of Gems & Gemmology*, **22**(2), 2020, 12–19 (in Chinese with English abstract).

Gemological classification and identification characteristics of agate. Y. Xia, S. Dai, D. Chen, H. Chen, W. Qu, S. Xu and J. Liao, *Journal of Mineralogy and Petrology*, **40**(2), 2020, 1–14 (in Chinese with English abstract).

Hetian jade: The original stone of heaven. Zhou Zhengyu and Liu Yicen, *InColor*, No. 47, 2020, 18–25, www.incolormagazine.org/books/vehz/#p=18.*

Imperial jadeite the divine green. I. Alexandris, *InColor*, No. 47, 2020, 34–39, www.incolormagazine.org/books/vehz/#p=34.*

Inclusion and trace element characteristics of emeralds from Swat Valley, Pakistan. H. Guo, X. Yu, Y. Zheng, Z. Sun and M.F.-Y. Ng, *Gems & Gemology*, **56**(3), 2020, 336–355, https://doi.org/10.5741/gems.56.3.336.*

Jade: A lifetime in search of heaven. R. Hughes, *InColor*, No. 47, 2020, 60–65, www.incolormagazine.org/books/vehz/#p=60.*

Jadeite jade: Appreciating the king of jade. Geng Li, *InColor*, No. 47, 2020, 10–17, www.incolormagazine.org/books/vehz/#p=10.*

Judging the quality of Burmese jadeite jade. R. Schluessel and J. Mason, *InColor*, No. 47, 2020, 68–75, www.incolormagazine.org/books/vehz/#p=68.*

Our friends the inclusions. The detective at the party of inclusions. Eighth episode. L. Costantini and C. Russo, *Rivista Italiana di Gemmologia/Italian Gemological Review*, No. 10, 2020, 7–14.

Relishing jadeite from rough to remarkable. C. Unninayar, *InColor*, No. 47, 2020, 40–44, www.incolormagazine.org/books/vehz/#p=40.*

La scapolite marialite : Origine de sa luminescence orange et possible mécanisme de son photo-chromisme [Marialite scapolite: Origin of its orange luminescence and possible mechanism of its photochromism]. F. Blumentritt, E. Fritsch, C. Latouche, Y. Morizet and S. Jobic, *Revue de Gemmologie A.F.G.*, No. 210, 2020, 12–19 (in French with English abstract).

Spectral characteristics of Qinghai nephrite with different colors. H. Song, H. Tan and E. Zu, *Bulletin of the Chinese Ceramic Society*, **39**(1), 2020, 242–246 (in Chinese with English abstract).

Testing green jadeite jade. D. Mok, *InColor*, No. 47, 2020, 76–83, www.incolormagazine.org/books/vehz/#p=76.*

Twinkle, twinkle little star [star gemstones]. L. Langeslag, *Gemmology Today*, December 2020, 90–92, https://tinyurl.com/1py6hebu.*

Unique raindrop pattern of turquoise from Hubei, China. L. Liu, M. Yang and Y. Li, *Gems & Gemology*, **56**(3), 2020, 380–400, https://doi.org/10.5741/gems.56.3.380.*

UV-Vis spectral characteristic and colour characterization of turquoise from Tongling, Anhui Province. R. Zuo, H. Dai, W. Huang, L. Yu and W. Deng, *Journal of Gems & Gemmology*, **22**(1), 2020, 13–19 (in Chinese with English abstract).

CULTURAL HERITAGE

Historical jewels in the museums of the world. J. Romanenkova, I. Bratus and A. Gunka, *Agathos*, **11**(1), 2020, 131–144.

Nondestructive analysis of alterations of Chinese jade artifacts from Jinsha, Sichuan Province, China. Y. Bao, X. Yun, C. Zhao, F. Wang and Y. Li, *Scientific Reports*, **10**(1), 2020, article 18476 (10 pp.), https://doi.org/10.1038/s41598-020-73290-y.*

Royal jewelry exchange in sixteenth century Anglo-Scottish politics. C. Auble, *Explorations in Renaissance Culture*, **46**(1), 2020, 70–82, https://doi.org/10.1163/23526963-04601002.

DIAMONDS

Comparison of gemological and spectroscopic features in type IIa and Ia natural pink diamonds. S. Eaton-Magaña, G. McElhenny, C.M. Breeding and T. Ardon, *Diamond and Related Materials*, **105**, 2020, article 107784 (13 pp.), https://doi.org/10.1016/j.diamond.2020.107784.

Correlation between EPR spectra and coloration of natural diamonds. C.W.Y. Lee, J. Cheng, Y.C. Yiu, K. Chan, D. Lau, W.C. Tang, K.W. Cheng, T. Kong *et al.*, *Diamond and Related Materials*, **103**, 2020, article 107728 (5 pp.), https://doi.org/10.1016/j.diamond.2020.107728.*

The enigma of cuboid diamonds: The causes of inverse distribution of optical centers within the growth zones. E.A. Vasilev, D.A. Zedgenizov and I.V. Klepikov, *Journal of Geosciences*, **65**(1), 2020, 59–70, https://doi.org/10.3190/jgeosci.301.*

Fancy ideas [grading fancy-shaped diamonds]. R. Evans, *Gems&Jewellery*, **29**(4), 2020, 31.

Inside the Hope diamond. E. Chung, *Gems&Jewellery*, **29**(4), 2020, 32–35.

Natural-color D-to-Z diamonds: A crystal-clear perspective. S. Eaton-Magaña, T. Ardon, C.M. Breeding and J.E. Shigley, *Gems & Gemology*, **56**(3), 2020, 318–335, https://doi.org/10.5741/gems.56.3.335.*

Putting a price on colour [coloured diamonds]. K. Hughes, *Gems&Jewellery*, **29**(4), 2020, 36–37.

Yellow diamonds with colourless cores – Evidence for episodic diamond growth beneath Chidliak and the Ekati mine, Canada. M.Y. Lai, T. Stachel, C.M. Breeding and R.A. Stern, *Mineralogy and Petrology*, **114**(2), 2020, 91–103, https://doi.org/10.1007/s00710-020-00693-0.

Wrestling with radiation [origin-of-colour determination of yellow-green to greenish blue diamonds]. T. Hainschwang, *Gems&Jewellery*, **29**(4), 2020, 28–30.

FAIR TRADE

Blood diamonds: An analysis of the state of affairs and the effectiveness of the Kimberley Process. M. Schulte and C.M. Paris, *International Journal of Sustainable Society*, **12**(1), 2020, 51–75, https://doi.org/10.1504/ijssoc.2020.105017.

Cultured pearl and precious coral jewellery, as symbols of a sustainable and responsible jewellery industry. G. Cavalieri, *Taiwan Gemmological Association Annual Publication*, 2020, 17–20.

Good news: In 2020, sustainable jewellery is finally top of the agenda. R. Garrahan, *British Vogue*, 19 September 2020, www.vogue.co.uk/fashion/article/sustainable-jewellery-technology.*

Women's work in the gemstone supply chain: Africa, India and Thailand. L. Lawson, *Australian Gemmologist*, **27**(4), 2020, 190–198.

GEM LOCALITIES

Casual continental conversation – A road trip of USA gem mines. D. Nini, *Australian Gemmologist*, **27**(4), 2020, 225–231.

Les gemmes du Gondwana [Gems of Gondwana]. G. Giuliani, *Le Règne Minéral*, No. 152, 2020, 6–18 (in French with English abstract).

Gemstones of eastern Kazakhstan. J. Chlachula, *Geologos*, **26**(2), 2020, 139–162, https://doi. org/10.2478/logos-2020-0013.*

In search of Mayan jade. H. Serras-Herman, *InColor*, No. 47, 2020, 26–33, www.incolormagazine.org/ books/vehz/#p=26.*

The mining mind-set [BlueRock Diamonds plc, miner in South Africa]. Anonymous, *Gems&Jewellery*, **29**(4), 2020, 18–21.

Ocean origins [South African diamond divers]. Anonymous, *Gems&Jewellery*, **29**(4), 2020, 14–16.

Pedogenic origin of Mezezo opal hosted in Ethiopian Miocene rhyolites. D. Ayalew, R. Pik, S. Gibson, G. Yirgu, S. Ali and D. Assefa, *Canadian Mineralogist*, **58**(2), 2020, 231–246, https://doi.org/ 10.3749/canmin.1900059.

Research status of emerald in Zimbabwe. Y. Wang, *Superhard Material Engineering*, **32**(1), 2020, 47–52 (in Chinese with English abstract).

Sapphire deposit of Sri Lanka. G. Zoysa, *Taiwan Gemmological Association Annual Publication*, 2020, 27–29.

Smaragde aus Kolumbien [Emeralds from Colombia]. T. Häger, Y. Rojas-Agramonte, F. Charris-Leal, J.D. Villalobos-Basler, M.A. Gonzalez-Pinzon and C. Hauzenberger, *Gemmologie: Zeitschrift der Deutschen Gemmologischen Gesellschaft*, **69**(1/2), 2020, 47–58 (in German with English abstract).

Smaragde aus Kolumbien – die Geschichte der Smaragdmine von Chivor 1880 – 1970 [Emeralds from Colombia – History of the Chivor emerald mine 1880 – 1970]. K. Schmetzer, G. Martayan, J.G. Ortiz and A.R. Blake, *Gemmologie: Zeitschrift der Deutschen Gemmologischen Gesellschaft*, **69**(1/2), 2020, 3–46 (in German with English abstract).

Travels around Britain with the gemstone detective. K. Rix, *Gemmology Today*, December 2020, 25–31, https://tinyurl.com/3v5ezq7t.*

Types and metallogenic mechanism of jade deposits in southern Hunan. D. Chen, S. Hu and X. Chen, *Resource Information and Engineering*, **35**(2), 2020, 1–3 (in Chinese with English abstract).

U–Pb dating of zircon and zirconolite inclusions in marble-hosted gem-quality ruby and spinel from Mogok, Myanmar. M.M. Phyo, H.A.O. Wang, M. Guillong, A. Berger, L. Franz, W.A. Balmer and M.S. Krzemnicki, *Minerals*, **10**(2), 2020, article 195 (18 pp.), https://doi.org/10.3390/min10020195.*

Update on Australian sapphires. I.T. Graham, N. Raffan, R. Bottrill, D.M. Duncan, W.D. Birch, P.J. Downes, S.M. Stocklmayer and G. Giuliani, *Australian Gemmologist*, **27**(4), 2020, 175–189.

A visit to the Indonesian opal fields in 2019 – Opal types, mining and treatments: Part 1. T. Coldham and J. Ivey, *Australian Gemmologist*, **27**(4), 2020, 199–213.

INSTRUMENTATION AND TECHNOLOGY

Application of 3D printing on design and manufacture of baroque pearl jewelry. J. Hua, Y. Li, H. Mu, J. Du, X. Zheng, L. Hao and F. Ma, *Journal of Gems & Gemmology*, **22**(1), 2020, 51–60 (in Chinese with English abstract).

Coding Python machine learning to help in Cr-corundum pink/red boundary evaluation. J.-M. Arlabosse and G. Arlabosse, *Gemmology Today*, December 2020, 66–71, https://tinyurl.com/5rygbktu.*

How to enter the 'micro world'. N. Zolotukhina, *Gemmology Today*, December 2020, 82–89, https:// tinyurl.com/2bdreynu.*

Nondestructive identification of gemstones by using a portable XRF–XRD system: An illuminating study for expanding its application in museums. J. Shen, *SN Applied Sciences*, **2**(3), 2020, article 372 (18 pp.), https://doi.org/10.1007/s42452-020-2183-8.*

JEWELLERY HISTORY

An aquamarine fit for a queen. J. Ogden, *Taiwan Gemmological Association Annual Publication*, 2020, 21–23.

A brief history of Australian jewellery till World War 1. R. Bauer, *Taiwan Gemmological Association Annual Publication*, 2020, 24–26.

A history of European royal jewel sales, including Sotheby's 2018 auction of Marie Antoinette's jewels. R. Shor, *Gems & Gemology*, **56**(3), 2020, 356–379, https://doi.org/10.5741/gems.56.3.356.*

El Libertador – La Medella Presidencial [diamond and gold medal made for Simón Bolívar]. G. Quintin, *Gemmology Today*, December 2020, 5–21, https://tinyurl.com/1vatbvyh.*

Si ce bijou m'était conté…**Un cadeau de la Reine Victoria [If this jewel could talk…A gift from Queen Victoria].** F. de Montjoye, *Revue de Gemmologie A.F.G.*, No. 210, 2020, 20–23 (in French).

LAPIDARY TOPICS

Contemporary jade carving in China. A. Shaw, *InColor*, No. 47, 2020, 52–58, www.incolormagazine.org/books/vehz/#p=52.*

A piece of Greenland? Making marketable and artisan gemstones. N. Brichet, *Anthropological Journal of European Cultures*, **29**(1), 2020, 80–100, https://doi.org/10.3167/ajec.2020.290106.*

MISCELLANEOUS

The evolution of gem-testing laboratories. C.P. Smith and M. Furuya, *InColor*, No. 47, 2020, 84–92, www.incolormagazine.org/books/vehz/#p=84.*

The 'gems' of thrones [diamond and ruby characteristics]. D. Marchiori, *Gemmology Today*, December 2020, 74–81, https://tinyurl.com/a5efn5fw.*

Hunting for 100 point ratings: A comparison between gemstone and wine ratings. R. Schluessel, *GemGuide*, **40**(1), 2021, 4–11.

Why is a gem precious? O. Segura, *InColor*, No. 47, 2020, 94–96, www.incolormagazine.org/books/vehz/#p=94.*

NEWS PRESS

Letter from the U.K.: The curse of the buried treasure. R. Mead, *New Yorker*, 16 November 2020, www.newyorker.com/magazine/2020/11/16/the-curse-of-the-buried-treasure.*

The world's most glamorous quarantine project [diamond replicas]. G. Fabrikant, *New York Times*, 28 November 2020, www.nytimes.com/2020/11/28/style/hope-diamond-story-smithsonian-copy.html.*

ORGANIC/BIOGENIC GEMS

Fluorescence spectral characteristic of amber from Baltic Sea region, Dominican Republic, Mexico, Myanmar and Fushun, China. Z. Zhang, X. Jiang, Y. Wang, A.H. Shen and F. Kong, *Journal of Gems & Gemmology*, **22**(3), 2020, 1–11 (in Chinese with English abstract).

Gemmological characteristic of root amber from Myanmar. C. Tu, Qian, C. and T. Chen, *Journal of Gems & Gemmology*, **22**(4), 2020, 13–22 (in Chinese with English abstract).

Precious coral in jewelry: New discoveries. L.E. Cartier, *GemGuide*, **39**(6), 2020, 4–7.

A review of amber and copal occurrences in Africa and their paleontological significance. V. Bouju and V. Perrichot, *Bulletin de la Société Géologique de France*, **191**(1), 2020, article 17 (11 pp.), https://doi.org/10.1051/bsgf/2020018.*

PEARLS

Effect of number of nuclei and nucleus position on shell growth and mabé pearl coating in *Pteria penguin* cultured in coastal waters of southeast Sulawesi, Indonesia. I. Nur, W.O. Mushaffa and M. Hamzah, *Journal of Shellfish Research*, **39**(2), 2020, 345–351, https://doi.org/10.2983/035.039.0216.

From coque de perle to Osmeña pearl: A short documentary history. K. Kennedy, *Journal of Jewellery Research*, **3**, 2020, 22–40.*

Perles de la mer de Cortez [Pearls of the Sea of Cortez]. S. Leblan, A. Delaunay and E. Fritsch, *Revue de Gemmologie A.F.G.*, No. 210, 2020, 8–11 (in French).

Shark Bay [Australia], pearl shell and family heirlooms. L.J. Rennie, *Australian Gemmologist*, **27**(4), 2020, 216–224.

Vietnam: Shell nuclei, pearl hatcheries, and pearl farming. N. Sturman, K. Lawanwong, N. Kitdee and D. Chodhry, *Gems & Gemology*, **56**(3), 2020, 402–415, https://doi.org/10.5741/gems.56.3.402.*

SYNTHETICS

A breath of fresh air [Aether Diamonds, producer of CVD synthetics]. R. Shearman, *Gems&Jewellery*, **29**(4), 2020, 22–23.

Growth characteristics of type IIa large single crystal diamond with Ti/Cu as nitrogen getter in FeNi–C system. M.-M. Guo, S.-S. Li, M.-H. Hu, T.-C. Su, J.-Z. Wang, G.-J. Gao, Y. You and Y. Nie, *Chinese Physics B*, **29**(1), 2020, article 018101 (6 pp.), https://doi.org/10.1088/1674-1056/ab592f.

Patterns of note [CVD synthetic diamonds]. N. DelRe and A. Inns, *Gems&Jewellery*, **29**(4), 2020, 46.

Spectroscopic properties of Lightbox CVD-grown diamonds. H. Choi, Y. Kim and S. Kim, *Taiwan Gemmological Association Annual Publication*, 2020, 30–33.

TREATMENTS

Discrimination of HPHT-treated type Ia cape diamonds using optical and photoluminescence spectroscopic techniques. Z. Song, T. Lu, S. Tang, B. Gao, J. Su and J. Ke, *Rock and Mineral Analysis*, **39**(1), 2020, 85–91 (in Chinese with English abstract).

Discussion on optimization of emerald purity [clarity enhancement with oil]. Z. Mo and W. Hu, *Superhard Material Engineering*, **32**(2), 2020, 55–58 (in Chinese with English abstract).

FAAS, FT-IR and XRD identification of natural and heat treated opals located in Wadla Woreda, north Wello, Ethiopia. G.Y. Abate, A.N. Alene, S.D. Mekonnen and A.T. Habte, *Asian Journal of Applied Chemistry Research*, **7**(1), 2020, 1–8, https://doi.org/10.9734/ajacr/2020/v7i130171.*

Growth-sector dependence of irradiated defects in high-temperature and high-pressure synthetic boron-doped diamond. K. Wang and S. Ding, *Journal of Synthetic Crystals*, **49**(2), 2020, 217–221 (in Chinese with English abstract).

An overview of emerald enhancements. Fillers, oil, resins and gem lab reports. J. Bergman, *Rivista Italiana di Gemmologia/Italian Gemological Review*, No. 10, 2020, 25–44.

Potential development of green and purple colors in colorless natural quartz from geodes in rhyodacites, Serra Geral Group, Brazil. L.L. Tononi, L. da Cunha Duarte, P.L. Juchem, F.S. Lameiras, J. Schnellrath and M.T. Fenilli de Menezes, *Brazilian Journal of Geology*, **50**(3), 2020, 11 pp., https://doi.org/10.1590/2317-488920202020190114.*

Research on heat treatment of yellowish-green apatite. F. Lyu, J. Zhang and A.H. Shen, *Journal of Gems & Gemmology*, **22**(2), 2020, 29–37 (in Chinese with English abstract).

Study on the effect of heat treatment on amethyst color and the cause of coloration. R. Cheng and Y. Guo, *Scientific Reports*, **10**(1), 2020, article 14927 (12 pp.), https://doi.org/10.1038/s41598-020-71786-1.*

COMPILATIONS

G&G **Micro-World.** Cloth fibre in resin-filled cavity in emerald • Manufactured inclusions in quartz • Egg-like epigenetic residue surrounding a rutile needle in quartz • Blue inclusion in quartz • Tree-shaped metal sulfide inclusion in quartz • Dendritic inclusions in sapphire • Spinel crystals on a sapphire crystal • Staurolite in ruby from Mozambique • Ferrocolumbite in topaz. *Gems & Gemology*, **56**(3), 2020, 426–435, www.gia.edu/gg-issue-search?ggissueid=1495322050124&articlesubtype=microworld.*

Gem News International. Embedded device in bead-cultured pearls • Trapiche-type emerald from Swat Valley, Pakistan • Unusual violet Maxixe beryl • Rutilated quartz spheres with epoxy resin 'matrix' • Black star sapphire filled with glass and dopping varnish • Oiled spinel • Report on GSA Annual Meeting. *Gems & Gemology*, **56**(3), 2020, 436–445, www.gia.edu/gg-issue-search?ggissueid=1495322050124&articlesubtype=gni.*

Lab Notes. Color-zoned alexandrite • Novelty-cut yellowish brown diamond with blue and yellow fluorescence • Color-change cat's-eye diaspore • Emerald with large quartz inclusion • 15.53 ct pearl from edible oyster • Magnetite inclusions in star peridot • Faceted light blue spodumene • Synthetic moissanite with fraudulent GIA inscription. *Gems & Gemology*, **56**(3), 2020, 416–425, www.gia.edu/gg-issue-search?ggissueid=1495322050124&articlesubtype=labnotes.*

*Article freely downloadable or readable online, as of press time